



UNIL | Université de Lausanne

Unicentre

CH-1015 Lausanne

<http://serval.unil.ch>

Year : 2023

Novel combinatorial gene-engineering approaches for improving T-cellbased cancer immunotherapy against solid tumors

Ouchen Khaoula

Ouchen Khaoula, 2023, Novel combinatorial gene-engineering approaches for improving T-cellbased cancer immunotherapy against solid tumors

Originally published at : Thesis, University of Lausanne

Posted at the University of Lausanne Open Archive <http://serval.unil.ch>

Document URN : urn:nbn:ch:serval-BIB_F7A40B8297B67

Droits d'auteur

L'Université de Lausanne attire expressément l'attention des utilisateurs sur le fait que tous les documents publiés dans l'Archive SERVAL sont protégés par le droit d'auteur, conformément à la loi fédérale sur le droit d'auteur et les droits voisins (LDA). A ce titre, il est indispensable d'obtenir le consentement préalable de l'auteur et/ou de l'éditeur avant toute utilisation d'une oeuvre ou d'une partie d'une oeuvre ne relevant pas d'une utilisation à des fins personnelles au sens de la LDA (art. 19, al. 1 lettre a). A défaut, tout contrevenant s'expose aux sanctions prévues par cette loi. Nous déclinons toute responsabilité en la matière.

Copyright

The University of Lausanne expressly draws the attention of users to the fact that all documents published in the SERVAL Archive are protected by copyright in accordance with federal law on copyright and similar rights (LDA). Accordingly it is indispensable to obtain prior consent from the author and/or publisher before any use of a work or part of a work for purposes other than personal use within the meaning of LDA (art. 19, para. 1 letter a). Failure to do so will expose offenders to the sanctions laid down by this law. We accept no liability in this respect.



UNIL | Université de Lausanne

Faculté de biologie
et de médecine

Université de Lausanne (UNIL)
Département de l'Oncologie UNIL
Ludwig Institute for Cancer Research (LICR) Lausanne Branch

Novel combinatorial gene-engineering approaches for improving T-cell-based cancer immunotherapy against solid tumors

Thèse de doctorat ès sciences de la vie (PhD)

Présentée à la

Faculté de biologie et de médecine de l'Université de Lausanne

Par

Khaoula Ouchen

Master en Bio-Engineering de l'Université de Hassan I^{er},
Faculté des Sciences et Techniques.

Jury

Prof. Fabio Martinon

Prof. George Coukos

Dr. Melita Irving

Dr. Jesus Corria Osorio

Prof. Alexandre Harari

Prof. Michele De Palma

Président

Directeur de thèse

Co-directrice de thèse

Co-directeur de thèse

Expert

Expert

Lausanne 2023

Imprimatur

Vu le rapport présenté par le jury d'examen, composé de

Président·e	Monsieur	Prof.	Fabio	Martinon
Directeur·trice de thèse	Monsieur	Prof.	George	Coukos
Co-directeurs·trices	Madame	Dre	Melita	Irving
	Monsieur	Dr	Jesus	Corria-Osorio
Expert·e·s	Monsieur	Prof.	Alexandre	Harari
	Monsieur	Prof.	Michele	De Palma

le Conseil de Faculté autorise l'impression de la thèse de

Khaoula Ouchen

Master in bioengineering, Université Hassan 1er, Maroc

intitulée

Novel combinatorial gene-engineering approaches for improving T-cell-based cancer immunotherapy against solid tumors

Lausanne, le 25 septembre 2023

pour le Doyen
de la Faculté de biologie et de médecine

Prof. Fabio Martinon



Acknowledgements

I would like to express my profound gratitude to my thesis director, **Prof. George Coukos**, for granting me the invaluable opportunity to work in his esteemed laboratory on these exciting projects and for providing me with exceptional scientific guidance and support.

I am sincerely thankful to my supervisor and mentor, **Dr. Melita Irving**, for her continuous encouragement, constant trust, and numerous opportunities to explore new fields. I am sincerely thankful, Melita, for your limitless kindness throughout the entire journey of my Ph.D.

I am deeply thankful to my mentor, **Dr. Jesus Corria**, for his support during challenging times in the laboratory. Many thanks, Jesus, for your guidance and valuable scientific input that have been instrumental to my research progress.

I would also like to extend my gratitude to the president of the jury, **Prof. Fabio Martinon**, and the esteemed committee members, namely **Prof. Alexandre Harari** and **Prof. Michele De Palma**, for generously devoting their time and providing valuable feedback. I eagerly look forward to our forthcoming and stimulating discussions. I am also grateful to the formal committee member, **Prof. Werner Held**, for dedicating his time to follow my work and offering insightful scientific input.

I convey my deep appreciation to the entire Coukos Lab for sharing their scientific enthusiasm and for being such a compassionate group of people throughout the years. They have not only been colleagues but also become my friends and extended family during my Ph.D. journey. I am particularly grateful to **Catherine Ronet**, who has been an exceptional scientific mentor, teaching me invaluable lessons beyond the realm of science. I sincerely thank you, Cat, for the fond memories we shared during late nights spent in the lab and cell culture. I would also like to thank **Greta Giordano-Attianese and Elisabetta Cribioli** for their treasured friendship, which brought me many joyful memories while enriching my learning process. Special thanks to my "Guru" in Molecular Biology, **Patrick Reichenbach**, for his humorous jokes, incredible experimental tricks, and memorable moments. I am immensely grateful to **Romain Vuillefroy de Silly** for his kindness, scientific input, and willingness to share knowledge, as well as to **Bili Seijo** for his help and great ideas. I sincerely thank **Aodrenn Spill** for her incredible assistance, especially during the most demanding and hectic days, and **Mélanie Triboulet** for her aid and kindness. Thank you, **Kirsten Scholten** and **Jennifer Murray**, for your positive energy and support. Many thanks, **Arthur Mulvey**, for your encouraging spirit and the memories we created with our team. My sincere thanks also to my former coworkers, **Cristina Jimenez Luna** and **Dimitrios Alatzoglou**, for their friendship, encouragement, and positive attitude.

I am profoundly grateful to all my supportive friends. Thank you, **Jan Rath**, for being an incredible friend, offering priceless advice, and being a companion with whom I have shared unforgettable memories filled with laughter, jokes, and funny moments. Our friendship holds a special and significant position in my life. Thank you, **Danisha Bhugowon**, for being a precious presence in my life, offering love and positive energy.

To my dear friends **Jenny, Tamila, Dhabersee**, and **Aurélie**, you have been my extraordinary and exemplary second family here in Lausanne, accompanying me on this thrilling Ph.D. adventure. I am grateful for your understanding, advice, and friendship, which I will always cherish. I extend my thanks to my mentor and friend, **Prof. O. Maria**, for being a guiding light during challenging times and leading me through difficult periods. Getting to know you has been a blessing, and I am grateful for the circumstances that allowed me to meet such a wise and wonderful person.

Finally, I would like to express my heartfelt thanks to my beloved family, who have lavished me with love throughout my life. I am grateful to my mother, **Amina EL Ammari**, for her tenderness and guidance and for instilling strength, resilience, patience, and good values in me. Mother, without your sacrifices, wisdom, and vision, I would not be in the privileged position I am in today. In memory of my father, **Abdallah Ouchen**, I express my gratitude for his unconditional love, unwavering support, and belief in me and for teaching me the importance of determination and motivation in pursuing my dreams and overcoming life's challenges. Our extensive debates and conversations encompassing various intellectual subjects have nurtured my rational and analytical thinking. The years we spent together were undoubtedly my life's most enjoyable and valuable time. You will forever remain my source of inspiration and my idol!

Thank you, my little beloved sister, **Oumaima Ouchen**, and my little cherished brother, **Amine Ouchen**, for your unwavering love and consistent support throughout this academic journey. Your encouragement, patience, and understanding have sustained me during the countless hours of research and writing. Your belief in me has been a source of inspiration, and I am truly blessed to have such incredible siblings by my side.

Soufiane Bel Rhali, I am infinitely thankful for your love, limitless support, patience, and our joyous moments. Words cannot fully express the depth of my sincere feelings and gratitude to life for granting me the privilege of having you as my spouse.

Summary

Cancer immunotherapy has emerged as a promising therapeutic approach for cancer treatment, specifically through adoptive cell transfer (ACT), which involves the utilization of engineered tumor-specific T-cells. Gene therapy, involving modifying T-cells to express chimeric antigen receptors (CARs) or T-cell receptors (TCRs), holds significant potential for addressing the limitations of T-cell-based therapies for solid tumors. Ongoing research endeavors are dedicated to enhancing the specificity of engineered T-cells to effectively recognize tumor cells. Efforts are also focused on optimizing TCR activation and increasing overall antitumor activity to overcome the immunosuppressive tumor microenvironment (TME). Furthermore, diverse engineering strategies are being explored to mitigate the potential adverse effects associated with T-cell adoptive therapy, including TCR T-cell cross-reactivities, cytokine release syndrome, and on-target/off-tumor toxicities. The precise regulation of gene expression and the refinement of vector design play a pivotal role in advancing gene engineering approaches and ensuring their efficacy in clinical settings.

This thesis addresses the challenges associated with treating solid tumors by employing innovative combinatorial T-cell engineering strategies. The first part of the study introduces a novel lentiviral vector design incorporating two genes of interest, notably, an inducible or constitutive microRNA (miRNA) for instance, to induce a gene knockdown (KD) explicitly targeting hematopoietic progenitor kinase 1 (HPK1), which is an intracellular negative regulator of the TCR, in addition to a constitutive CAR targeting prostate-specific membrane antigen (PSMA) in prostate cancer or a TCR targeting New York esophageal squamous cell carcinoma 1 (NY-ESO1) which is a cancer-testis antigen expressed in various solid tumors, including melanoma and sarcoma. Furthermore, we have developed an optimized protocol for high-titer viral particle production to mediate efficient genetic modification in T-cells while ensuring its suitability for clinical translation. The second part of the thesis investigates a novel combinatorial approach that targets multiple negative regulators of TCR signaling, focusing primarily on HPK1 as the primary target while also considering other selected genes.

In this regard, we have conducted a comprehensive overview of various negative regulators within the TCR signaling pathway and identified the most relevant targets for our specific study. We have also investigated the impact of downregulating these genes on T-cell antitumor activity using a retroviral vector designed to incorporate single, dual, or multiple miRNAs for inducing single or concomitant perturbations downstream of the TCR pathway. After screening over twelve genes for their upregulation upon antigen stimulation, casitas B-lineage lymphoma b (Cbl-b) and neural precursor cell-expressed developmentally downregulated protein 4 (NEDD4), both belonging to the ubiquitin-protein ligases family, were selected for constitutive downregulation alongside HPK1. The impact of their downregulation on *in vivo* antitumor activity and *in vitro* cytotoxicity, proliferation, and cytokine secretion was assessed. While downregulating NEDD4 in addition to HPK1 KD or in combination with HPK1-Cbl-b KD did not yield significant advantageous outcomes, while the combination of HPK1-Cbl-b KD showed promising potential. It notably resulted in a significant delay in tumor growth *in vivo* and increased cytokine secretion *in vitro* upon antigen engagement. This work also revealed the advantages of high-affinity TCR T-cells over low-affinity TCR T-cells. It highlighted the importance of removing intracellular TCR checkpoints to enhance T-cell activation, particularly in high-affinity TCR. Furthermore, a clustered regularly interrupted short palindromic repeats (CRISPR) screening approach, utilizing a small TCR signaling library comprising twenty-seven negative regulators, along with positive and negative controls, underscored the necessity of adopting a combinatorial KD approach as individual negative regulator genes alone failed to improve T-cell persistence *in vivo*.

Taken together, this thesis contributes to the development of effective gene therapy strategies by addressing the challenges faced in T-cell-based immunotherapy through innovative combinatorial T-cell engineering approaches aiming to enhance the efficacy of treatments against solid tumors.

Résumé

L'immunothérapie du cancer s'est imposée comme une approche thérapeutique prometteuse pour le traitement du cancer, notamment par le transfert adoptif des cellules T génétiquement modifiées pour reconnaître spécifiquement les cellules cancéreuses. La thérapie génique, qui consiste à modifier les cellules T pour qu'elles expriment des récepteurs d'antigènes chimériques (CAR) ou des récepteurs des cellules T (TCR), offre un potentiel significatif pour surmonter les limites des thérapies à base de cellules T contre les tumeurs solides. Des recherches en cours visent à améliorer la spécificité des lymphocytes T génétiquement modifiés pour une reconnaissance efficace des cellules tumorales. Les efforts sont également axés sur l'optimisation de l'activation des TCR et l'augmentation de l'activité antitumorale globale afin de surmonter les obstacles rencontrés dans le microenvironnement immunosuppresseur des tumeurs (TME). En outre, différentes stratégies de génie génétique sont explorées pour atténuer les effets indésirables potentiels liés à la thérapie adoptive des cellules T, tels que les réactions croisées des TCR, le syndrome de libération de cytokines et les toxicités ciblées ou non tumorales. La régulation précise de l'expression des gènes et le raffinement de la conception des vecteurs jouent un rôle crucial dans le développement des approches de génie génétique et dans la garantie de leur efficacité dans les contextes cliniques.

Cette thèse aborde les défis associés au traitement des tumeurs solides en utilisant des stratégies combinatoires novatrices de la modification génétique des cellules T. La première partie de l'étude présente une nouvelle conception de vecteur lentiviral incorporant deux gènes d'intérêt. Il s'agit notamment d'un microARN (miARN), par exemple, soit inducible ou constitutif pour l'inhibition génique ciblant spécifiquement la kinase 1 du progéniteur hématopoïétique (HPK1) comme étant un régulateur négatif intracellulaire du TCR, en plus d'un CAR constitutif ciblant l'antigène membranaire spécifique de la prostate (AMSP) du cancer de la prostate ou d'un TCR ciblant l'antigène NYESO1 (New York esophageal squamous cell carcinoma 1) qui est un antigène du cancer-testicule exprimé dans diverses tumeurs solides, y compris le mélanome et le sarcome. De plus, nous avons développé un protocole optimisé pour la production de particules virales à haut titre, permettant une modification génétique efficace des cellules T tout en garantissant son adaptation à l'utilisation clinique. La deuxième partie de la thèse explore une nouvelle approche combinatoire ciblant multiples régulateurs négatifs du signal TCR, en se focalisant principalement sur HPK1 en tant que cible principale, tout en considérant également d'autres gènes sélectionnés.

À cet égard, nous avons réalisé une revue complète des différents régulateurs négatifs de la voie de signalisation du TCR et avons identifié les cibles les plus pertinentes pour notre spécifique étude. Nous avons également étudié l'impact de l'inhibition de ces gènes sur l'activité antitumorale des cellules T en utilisant un vecteur rétroviral conçu pour incorporer un, deux ou plusieurs miARNs afin d'induire des perturbations individuels ou concomitantes en aval de la voie du TCR. Après avoir examiné plus de douze gènes pour leur expression lors de la stimulation antigénique, le lymphome à lignée B de casitas b (Cbl-b) et la protéine 4 régulée au cours du développement exprimée par les cellules précurseurs neuronales (NEDD4) qui appartiennent tous deux à la famille des ligases de l'ubiquitine, ont été sélectionnées pour une inhibition constitutive parallèlement à HPK1. L'impact de leur répression sur l'activité antitumorale *in vivo*, ainsi que sur la cytotoxicité, la prolifération et la sécrétion de cytokines *in vitro*, a été évalué. Bien que la répression de NEDD4 en plus de celle du HPK1 ou en combinaison avec l'inactivation de HPK1-Cbl-b n'ait pas conduit à des résultats significativement avantageux, il est important de souligner que la combinaison de HPK1-Cbl-b KD a montré un potentiel prometteur. Elle a notamment entraîné un retard significatif de la croissance tumorale *in vivo* et une augmentation de la sécrétion de cytokines *in vitro* lors de la stimulation antigénique. Cette étude a également mis en évidence les avantages des lymphocytes T à TCR à haute affinité par rapport à ceux à faible affinité, soulignant l'importance de l'élimination des points de contrôle intracellulaires du TCR pour renforcer l'activation des lymphocytes T, en particulier dans le cas des TCR à haute affinité.

De plus, une approche de criblage CRISPR (clustered regularly interrupted short palindromic repeats) utilisant une petite librairie comprenant vingt-sept régulateurs négatifs de signalisation du TCR a souligné la nécessité d'adopter une approche combinatoire d'inhibition, car l'inactivation individuelle des gènes régulateurs négatifs n'a pas amélioré la persistance des lymphocytes T *in vivo*.

Dans l'ensemble, cette thèse contribue au développement de stratégies efficaces de thérapie génique en s'attaquant aux défis rencontrés dans l'immunothérapie à base de lymphocytes T, en utilisant des approches innovantes et combinatoire de génie génétique visant à améliorer l'efficacité des traitements contre les tumeurs solides.

Résumé (large public)

Au cours des dernières décennies, une approche de traitement contre le cancer appelée immunothérapie a été développée, comprenant différentes stratégies visant à éliminer les cellules cancéreuses. L'une de ces stratégies est le transfert adoptif de lymphocytes T modifiés génétiquement, qui consiste à prélever des lymphocytes T du patient ou de donneurs sains et à les modifier en laboratoire pour qu'ils puissent reconnaître spécifiquement les tumeurs et les éliminer. Cela peut être réalisé en introduisant des récepteurs antigéniques chimériques (CAR) ou des récepteurs de cellules T (TCR) dans les lymphocytes T. Bien que cette approche ait montré une efficacité significative dans le traitement de certains cancers du sang, elle est limitée pour les tumeurs solides en raison des obstacles présents dans le microenvironnement immunosuppresseur des tumeurs (TME).

Cette thèse propose des stratégies innovantes de modification génétique des lymphocytes T pour surmonter ces obstacles.

Dans la première partie de l'étude, un nouveau type de vecteur lentiviral est présenté étant un des moyens utilisés en génie génétique pour introduire du matériel génétique spécifique dans les cellules. Ce nouveau vecteur contient deux gènes d'intérêt. Le premier gène introduit un CAR, de manière constitutive, spécifique de l'antigène membranaire spécifique de la prostate (AMSP) pour cibler le cancer de la prostate, ou un TCR spécifique du NYESO1 (antigène du carcinome épidermoïde de l'œsophage de New York 1) exprimé dans diverses tumeurs solides. Le deuxième gène est, par exemple, un microARN (miARN) qui réduit l'expression d'un gène inhibiteur de l'activation des lymphocytes T. Ce gène peut être exprimé de manière constitutive ou induite pour éviter une suractivation indésirable des lymphocytes T dans le TME. De plus, un protocole optimisé de production de particules virales à haute concentration a été développé pour permettre une modification génétique efficace des lymphocytes T tout en garantissant son utilisation clinique.

La deuxième partie de la thèse explore de nouvelles approches combinatoires ciblant plusieurs régulateurs négatifs du signal TCR, en mettant l'accent sur la kinase des progéniteurs hématopoïétiques 1 (HPK1) en tant que cible principale. Après avoir identifié les cibles les plus pertinentes pour cette étude, les effets de l'inhibition de ces gènes sur l'activité antitumorale des lymphocytes T ont été étudiés en utilisant un vecteur rétroviral conçu pour introduire un, deux ou plusieurs miARNs.

Par conséquent, des perturbations individuelles ou concomitantes de la voie du TCR sont générées. L'examen de l'expression de plus de douze gènes lors de la stimulation antigénique a permis la sélection de deux gènes appartenant à la famille des ligases de l'ubiquitine, notamment le lymphome à lignée B de casitas b (Cbl-b) et le neural precursor cell-expressed developmentally downregulated protein 4 (NEDD4), pour une inhibition constitutive. La stratégie combinée d'inactivation de HPK1 et Cbl-b a montré des résultats prometteurs retardant significativement la croissance tumorale *in vivo* et augmentant la sécrétion de cytokines *in vitro* lors de la stimulation antigénique. De plus, une approche de criblage utilisant la technologie CRISPR (clustered regularly interspaced short palindromic repeats) et une librairie comprenant vingt-sept régulateurs négatifs de la signalisation du TCR a souligné la nécessité d'adopter une approche combinatoire d'inhibition, car l'inactivation individuelle de ces gènes n'a pas amélioré la persistance des lymphocytes T *in vivo*.

Dans l'ensemble, cette thèse contribue au développement de stratégies efficaces de thérapie génique pour les tumeurs solides en utilisant des approches innovantes de génie cellulaire combinatoire visant à améliorer l'efficacité des traitements contre ces types de cancer.

Table of content:

ACKNOWLEDGEMENTS	II
SUMMARY	IV
RÉSUMÉ	V
RÉSUMÉ (LARGE PUBLIC)	VII
LIST OF FIGURES:	X
LIST OF SUPPLEMENTARY FIGURES:	X
LIST OF TABLES:	X
LIST OF ABBREVIATIONS	XI
I. INTRODUCTION	1
1. The Immune System	1
1.1. The Innate Immune Response:	1
1.2. The Adaptive Immune Response:.....	2
1.3. Crosstalk Between The Innate And Adaptive Immune Responses:	3
2. Cancer	5
2.1. Solid Tumors:	5
2.2. Solid Tumor Immunosuppressive Microenvironment:.....	7
2.2.1.1. T-cell exhaustion.....	8
3. Cancer Immunotherapy:	10
3.1. Adoptive Cell Therapy (ACT).....	10
3.1.1. Tumor-infiltrating lymphocyte (TIL) therapy:	11
3.1.2. Genetically engineered T-cell therapy:.....	11
3.1.2.1. CAR-T-cell therapy:	13
3.1.2.2. TCR-T-cell therapy:.....	15
3.1.2.3. Gene editing technologies.....	16
3.1.2.4. Gene editing delivery methods	18
3.1.2.5. Gene inhibitory strategies	20
4. Intracellular negative regulators downstream of the TCR signaling pathways.	25
4.1. TCR signaling pathway:	25
4.2. TCR signaling intracellular checkpoints:	26
II. PH.D. PROJECT AIM:	37
III. RESULTS:	39
1. Development of novel approaches and vector constructs comprising inducible or constitutive miRNA for CAR and TCR-based T-cell therapies.	39
1.1. Co-author contribution:.....	39
1.2. Summary:.....	40
1.3. Article	41
2. Evaluation of the antitumor activity of CAR/TCR T-cell expressing miRNAs for HPK1 downregulation:	68
2.1. Summary:.....	68
2.2. Material and Methods:	69
2.3. Results:.....	73
2.3.1. In the context of Pz1-CAR T-cells:	73
2.3.2. In the context of NYESO-1 TCR T-cells:.....	77
3. A combinatorial gene-engineering approach targeting multiple TCR intracellular negative regulators for enhanced T-cell persistence and functionality.	85
3.1. Summary	85
3.2. Material and Methods:	86

3.3. Results.....	90
3.3.1. Identification of relevant intracellular negative regulators for miRNA targeting downstream the TCR signaling pathway.....	90
3.3.2. Evaluation of gene expression of the selected negative regulators in high-affinity CD8+ cells:	90
3.3.3. miRNA screening for achieving a high knockdown level of the selected targets using the single-miRNA vector in high-affinity CD8+ cells.....	92
3.3.4. Vector design for dual and multiple targeting of the selected TCR intracellular inhibitory checkpoints:	94
3.3.5. Evaluation of <i>in vitro</i> and <i>in vivo</i> T-cell antitumor activity upon multiple perturbations targeting the TCR negative regulators in high and low-affinity CD8+ cells:	97
3.3.6. Development of an unbiased high throughput screening approach for identifying inhibitory genes in the context of high versus low-affinity CD8+ cells.	105
3.4. Extended data:.....	107
IV. GENERAL DISCUSSION AND PERSPECTIVES:.....	110
1. Optimizing lentiviral vector design for dual gene insertion and inducible gene knockdown in engineered T-cells for enhanced antitumor activity.	110
2. Enhancing primary human T-cell function and antitumor response through HPK1 downregulation....	111
3. Combinatorial strategies targeting TCR negative regulators for enhanced functionality in high-affinity TCR T-cells	112
V. REFERENCES:	116

List of Figures:

FIGURE 1: SCHEMATIC OVERVIEW OF INNATE AND ADAPTIVE IMMUNE RESPONSES.	4
FIGURE 2: COMPARATIVE CHARACTERISTICS OF COLD AND HOT TUMORS IN TME.	6
FIGURE 3: MECHANISMS OF TUMOR REJECTION AND ESCAPE.....	9
FIGURE 4: STRATEGIES FOR ACT THERAPY: TIL VERSUS GENE THERAPY.	13
FIGURE 5: CAR STRUCTURE, GENERATION, AND NOVEL DESIGNS.	14
FIGURE 6: ENGINEERING STRATEGIES FOR TCR-T-CELL THERAPY.....	16
FIGURE 7: COMPARATIVE OVERVIEW OF MAJOR GENE EDITING TECHNOLOGIES.	18
FIGURE 8: GENE EDITING DELIVERY METHODS	20
FIGURE 9: CELLULAR PROCESSING MACHINERY OF miRNA VERSUS shRNA VERSUS siRNA.....	22
FIGURE 10: TCR INTRACELLULAR NEGATIVE REGULATORS	35
FIGURE 11: CHARACTERIZATION OF HPK1 KNOCKDOWN IN TRANSDUCED JURKAT CELLS AND ANTI-PSMA-CAR PRIMARY CD4+ AND CD8+ T-CELLS.	74
FIGURE 12: FUNCTIONAL EFFECT OF HPK1 DOWNREGULATION ON HUMAN PRIMARY Pz1-CAR T-CELLS.	76
FIGURE 13: EVALUATION OF KNOCKDOWN LEVELS USING miRS TARGETING HPK1 IN TRANSDUCED NYESO-1-TCR CD4+ AND CD8+ T-CELLS.	78
FIGURE 14: <i>IN VITRO</i> CHARACTERIZATION OF NYESO-1+ T-CELLS DOWNREGULATING HPK1 USING miR A AND B COMPARED TO CTRL NYESO-1+ T-CELLS.	80
FIGURE 15: <i>IN VIVO</i> EVALUATION OF HPK1 KD IMPACT ON NYESO-1+ T-CELLS' ANTITUMOR ACTIVITY.....	82
FIGURE 16: ASSESSMENT OF CYTOTOXICITY AND INHIBITORY CHECKPOINTS EXPRESSION UPON HPK1 KNOCKDOWN IN NYESO-1 T-CELLS.	84
FIGURE 17: EVALUATION OF SELECTED NEGATIVE REGULATORS' EXPRESSION LEVELS IN THE CONTEXT OF <i>IN VITRO</i> EXHAUSTION ASSAY USING HIGH-AFFINITY TCR OTI CELLS.	91
FIGURE 18: DOWNREGULATION OF SELECTED TCR NEGATIVE REGULATORS IN TRANSDUCED OTI CELLS WITH SINGLE miRNA RETROVIRAL VECTOR	93
FIGURE 19: GENERATION AND EVALUATION OF DUAL AND MULTIPLE miR RETROVIRAL VECTORS FOR KNOCKING DOWN HPK1, CBL-B, AND NEDD4 IN OTI AND OT3 CELLS.	96
FIGURE 20: <i>IN VIVO</i> STUDY IN THE B16 OVA TUMOR MODEL TO EVALUATE THE ANTITUMOR ACTIVITY OF OTI CELLS DOWNREGULATING HPK1, CBL-B, AND NEDD4 AS SINGLE AND COMBINATORIAL PERTURBATIONS.	98
FIGURE 21: <i>IN VITRO</i> EVALUATION OF CELLULAR CYTOKINE EXPRESSION AND CYTOTOXICITY UPON DOWNREGULATING HPK1 AS SINGLE OR IN COMBINATION WITH CBL-B KD AND/OR NEDD4 KD IN OTI CELLS.	100
FIGURE 22: <i>IN VIVO</i> EVALUATION OF OT3 CELL ANTITUMOR ACTIVITY BEARING SINGLE AND COMBINED HPK1, CBL-B, AND NEDD4 DOWNREGULATION.....	101
FIGURE 24: FUNCTIONAL CHARACTERIZATION AND EVALUATION OF TCR SIGNALING SUPPRESSIVE MOLECULES IN OT1 AND OT3 CELLS IN THE CONTEXT OF THE B16 OVA TUMOR MODEL.....	104
FIGURE 25: IDENTIFICATION OF TCR SUPPRESSOR AND ESSENTIAL GENES FOR <i>IN VIVO</i> T-CELL PERSISTENCE USING A SMALL TCR CRISPR LIBRARY.....	106

List of Supplementary Figures:

SUPPLEMENTARY FIGURE 1: EVALUATION OF SELECTED TCR CHECKPOINT INHIBITORS' EXPRESSION LEVELS AND THEIR DOWNREGULATION BY miRS.	107
SUPPLEMENTARY FIGURE 2: ASSESSMENT OF HPK1, CBL-B, AND NEDD4 KNOCKDOWN LEVELS IN OTI CELLS	108
SUPPLEMENTARY FIGURE 3: FLOW CYTOMETRIC ANALYSIS OF HPK1, CBL-B, AND NEDD4 EXPRESSION IN OTI CELLS STIMULATED WITH aCD8/aCD28 DYNABEADS AND SIINFEKL PEPTIDE.....	109
SUPPLEMENTARY FIGURE 4: DESIGN, IMPLEMENTATION, AND <i>IN VITRO</i> EVALUATION OF GENERATED SMALL TCR CRISPR LIBRARY USING OTI CELLS.	109

List of Tables:

TABLE 1: COMPARISON OF siRNA, shRNA, AND miRNA CHARACTERISTICS.....	24
TABLE 2: TARGETING TCR INTRACELLULAR NEGATIVE REGULATORS FOR CANCER IMMUNOTHERAPY.	36

List of Abbreviations

Ab = antibody
ACT = adoptive cell transfer
ADAP = adhesion and degranulation-promoting adapter protein
ADCC = antibody-dependent-cellular cytotoxicity
ADCP = antibody-dependent cellular phagocytosis
AGO2 = argonaute 2
AKAP5 = A-kinase anchoring protein 5
Akt = Ak strain transforming
AML = acute myeloid leukemia
AMP = adenosine monophosphate
AP-1 = activator protein 1
APCs = antigen-presenting cells
AR = androgen receptors
Arp2/3 = actin-related protein 2/3
ATCC = american type culture collection
B-ALL = B- cell-precursor acute lymphoblastic leukemia
BATF = basic leucine zipper ATF-like transcription factor
BCL10 = B-cell lymphoma/leukemia 10
BCR = B cell receptor
BiKE = Bispecific Killer cell Engager
BiTE = bispecific T-cell engager
BRAF = v-raf murine sarcoma viral oncogene homolog B1
BSA= bovine serum albumin
BV=brilliant violet
Bv8 = bombina variegata peptide 8
C-X-C = chemokine receptor type 4 (CXCR-4)
Ca²⁺ =calcium
Cabin1 = calcineurin binding protein 1
CAFs = cancer associated fibroblasts
CAR = chimeric antigen receptor
Cas9= CRISPR-associated protein 9
Cbl-b = casitas B-lineage lymphoma b
CCL = The chemokine C-C motif ligand
CCR=chemokine receptor
CD=cluster of differentiation
CDC = complement-mediated cytotoxicity
CEA=carcinoembryonic antigen
CFSE=carboxyfluorescein succinimidyl ester
cGAS = cyclic GMP-AMP Synthase
CISH = chromogenic in situ hybridization
CiTEs = checkpoint-inhibitory T-cell engagers
CRISPR = clustered regularly interrupted short palindromic repeats
CRS = cytokine release syndrome
CSF-1 = colony-stimulating factor 1
Csk = C-terminal Src kinase
CTC = circulating tumor cells
CTL(s) = cytotoxic T lymphocytes
CTLA-4 = cytotoxic T-lymphocyte antigen-4

CXCL = C-X-C motif chemokine ligand
CXCR = C-X-C motif chemokine receptor
CYLD = cylindromatosis
DAG = diacylglycerol
DAMPs = danger-associated molecular patterns
DC(s)=dendritic cell(s)
DGCR8=droscha-DiGeorge critical region-8
DGKs = diacylglycerol kinases
DNA=deoxyribonucleic acid
DOK = downstream of kinases
DP=double positive
DSB = double-strand break
DUBs = deubiquitination enzymes
DUSPs = dual specificity phosphatases
eADO = extracellular adenosine
ECM = extracellular matrix
EGFR=epidermal growth factor receptor
ELISA = enzyme-linked immunosorbent assay
ELISpot = enzyme-linked immunosorbent spot
ER=endoplasmic reticulum
ERK = extracellular signal-regulated kinase
ESI-MS = electrospray ionization mass spectrometry
ETS = erythroblast transformation specific
EVs = extracellular vesicles
Facs = fluorescence activated cell sorting
FAK = focal adhesion kinase
FAs = fatty acids
FasL = Fas ligand
FBS = fetal bovine serum
Fc=fragment crystallizable
FDA = food and drug administration
FITC=Fluorescein isothiocyanate
FOXP3 = forkhead box P3
GMP = guanosine monophosphate
GPR = G-protein-coupled receptor
GRAIL = gene related to anergy in lymphocytes
Grb2 = growth factor receptor-bound protein 2
GTP = nucleotide guanosine triphosphate
h=hour/s
HCC = hepatocellular carcinoma
HECT = homologous to the E6-AP carboxyl terminus
HEK = human embryonic kidney
HI = Heat-Inactivated
hi= high
HIF-1 α = hypoxia-inducible factor 1-alpha
HLA = human leukocyte antigen
HPK1= hematopoietic progenitor kinase 1
HR = homologous recombination
HSCs = hematopoietic stem cells
i.v.=intravenous

ICB = immune checkpoint blockade
 ICOSL = immune checkpoint molecules such as inducible T-cell costimulator ligand
 IDO = indoleamine 2,3 deoxygenase
 Ig=Immunoglobulin
 iICPs = intracellular immune checkpoints
 IKK = IkappaB kinase
 IL = interleukin
 lncRNAs = long non-coding RNAs
 int = intermediate
 IP3 = inositol 1,4,5-trisphosphate
 IR = immune response
 IRES = internal ribosome entry site
 IRF4 = Interferon regulatory factor 4
 IS = immunological synapse
 ITAM = immunoreceptor tyrosine-based activation motifs
 ITIMs = immunoreceptor tyrosine-based inhibition motifs
 ITSMs = immunoreceptor tyrosine-based switch motifs
 JNK = c-Jun N-terminal kinase
 KD = knockdown
 KI = knockin
 KO = knockout
 LAG-3 = lymphocyte-activation gene 3
 LAT=linker of activation of T-cells
 Lck = lymphocyte-specific protein tyrosine kinase
 lo= low
 LS = leader sequence
 LTR= long terminal repeat
 mAb= monoclonal antibody
 MAC = membrane attack complex
 MACS = magnetic-activated cell sorting
 MAGEs = melanoma antigen-encoding genes
 MALT1 = Mucosa-associated lymphoid tissue 1
 MAP4K1 = mitogen-activated protein kinase 1
 MAPK = mitogen-activated protein kinase
 MART-1 = melanoma-associated antigen recognized by T-cells-1
 MB = mitochondrial biogenesis
 mbIL-15 = membrane-bound IL-15
 MDM2 = murine double minute 2
 MDSCs=myeloid derived suppressor cells
 MFI = mean fluorescence intensity
 MHC = major histocompatibility complex
 MICA = major histocompatibility complex class I chain-related gene a
 MICB = major histocompatibility complex class I chain-related gene b
 min=minute/s
 miRNA=microRNA
 ml= milliliter
 MM = multiple myeloma
 MMPs = matrix metalloproteinases
 MOI=multiplicity of infection
 mPD-L1 = membrane PD-L1
 mRNA = messenger RNA

MSCs = mesenchymal stem cells
mTOR = mammalian target of rapamycin
mTORC1=mammalian target of rapamycin complex 1
NEDD4 = neural precursor cell-expressed developmentally downregulated protein 4
neg = negative
NF- κ B= nuclear factor κ light chain enhancer of B cells activation
NFAT = nuclear factor of activated T-cells
ng=nanogram
NGS = next-generation sequencing
NHEJ = nonhomologous end joining
NK Cells = natural killer cells
nm=nanometer
NOD = nucleotide-binding oligomerization domain
NRAS=Neuroblastoma-RAS
NSCLC = non-small cell lung cancer
NY-ESO-1 = New York esophageal squamous cell carcinoma 1
O₂=oxygen
ON=over night
OS = overall survival
OSCC = oral squamous cell carcinoma
OTUD7B = OTU deubiquitinase 7B
OV = oncolytic virus
OVA = Ovalbumin
OXPHOS=oxidative phosphorylation
P2A = picornavirus 2A
p53= tumor protein 53
PA = phosphatidic acid
PAG = phosphoprotein associated with glycosphingolipid-enriched microdomains
PAMPs = pathogen-associated molecular patterns
PBMCs = peripheral blood mononuclear cells
PCK1 = phosphoenolpyruvate carboxykinase 1
PD-L1 = programmed cell death ligand 1
PD-1 = Programmed cell death protein 1
pDCs = plasmacytoid dendritic cells
PEI=Polyethyleneimine
Peli1 = Pellino E3 ubiquitin protein ligase 1
PEP = PEST-domain enriched tyrosine phosphatase
Percp=Peridinin chlorophyll protein
PGC-1a=PPAR-gamma coactivator 1a
PGE2 = prostaglandin E2
PGK=phosphoglycerate kinase
PI3K = Phosphoinositide 3-kinase
PIP2=phosphatidylinositol-4,5-bisphosphate
PKA = protein kinase A
PKC- θ =protein kinase θ
PLC γ 1=Phospholipase C γ 1
pMHC = peptide–major histocompatibility complex
PPAR = peroxisome proliferator-activated receptor
pri-miRNA = primary precursor miRNA
PRRs = Pattern recognition receptors

PSA = prostate-specific antigen
 PSMA = prostate-specific membrane antigen
 PTEN=phosphatase and TENsin homolog
 PTKs = protein tyrosine kinases
 PTPN(s) = protein tyrosine phosphatase non-receptor type
 PTPs = protein tyrosine phosphatases
 qPCR = quantitative polymerase chain reaction
 Rap1 = Ras-proximate-1
 RAS = neuroblastoma rat sarcoma
 RASA2 = RAS p21 protein activator 2
 RASGRP1 = RAS guanyl nucleotide-releasing protein 1
 REP = rapid expansion procedure
 RhoGDI = Rho guanine dissociation inhibitor
 RING = really interesting new gene
 RISC = RNA-induced silencing complex
 RNA = ribonucleic acid
 RNAi = RNA interference
 RNPs = ribonucleoprotein complexes
 rpm=rotation per minutes
 RPMI=roswell park memorial institute medium
 RT-qPCR = reverse transcription quantitative polymerase chain reaction
 RT=room temperature
 Runx2 = runt-related transcription factor 2
 s.c.=subcutaneous
 s.e.m=standard error of mean
 SARS-CoV-2 = severe acute respiratory syndrome coronavirus 2
 SB = sleeping beauty
 scFv=single chain fragment variable
 SD=standard deviation
 sec=second/s
 sgRNA(s) = single guide RNA (s)
 SHP = Src homology 2 (SH2) domain-containing tyrosine phosphatase
 shRNA=short hairpin RNA
 Siglec(s)=sialic acid-binding immunoglobulin-like lectins
 siRNA=small interference RNA
 SLP-76 = leukocyte protein of 76 kDa
 SMITEs = simultaneous multiple interaction T-cell engagers
 SOCS = suppressor of cytokine signaling
 SOPF = specific and opportunistic pathogen-free animal facility
 sPD-L1 = soluble programmed cell death-ligand 1
 STAT3 = signal transducer and activator of transcription 3
 STING = stimulator of interferon genes
 STS = suppressor of T-cell receptor signaling
 T-bet=T-box transcription factor
 TAAs = tumor-associated antigens
 TACs = T-cell-activating conjugates
 TALENs = transcription activator-like effector nucleases
 TALEs = transcription activator-like effectors
 TAMs = tumor-associated macrophages
 TBI = total body irradiation

TCR(s)= T-cell receptor(s)
TE = transduction efficiency
TEM= effector memory T-cells
TER = terminal
TERT = Telomerase reverse transcriptase
Tex cells = exhausted T-cells
TGF- β = transforming growth factor-beta
Th= T helper
TIGIT = T cell immunoreceptor with Ig and ITIM domains
TIL(s) = tumor-infiltrating lymphocyte(s)
TIM-3 = T-cells immunoglobulin and mucin domain-containing-3
TIRs = terminal inverted repeats
TM = transmembrane
TME = tumor microenvironment
TMG = tandem minigenes
TNF = tumor necrosis factor
TNFAIP3 = tumor necrosis factor- α -induced gene 3
tNGFR = truncated nerve growth factor receptor
TOX = thymocyte selection-associated HMG BOX
TRAF3 = TNF receptor-associated factor
TRAIL = TNF-related apoptosis-inducing ligand
TRBP= transactivation response element RNA-binding protein
Treg(s)= regulatory T-cell(s)
TriKEs = trispecific killer cell engagers
TRuC(s) = T-cell receptor fusion construct (s)
TRUCKs = T-cell redirected for universal cytokine-mediated killing
TSA(s) = tumor-specific antigen(s)
TSC = tumor suppressor tuberous sclerosis complex
UBASH = ubiquitin-associated and SH3 domain-containing protein
USP12 = ubiquitin specific peptidase 12
UTD = untransduced
UTRs=untranslated regions
VEGF = vascular endothelial growth factor
VS. = versus
WASP = wiskott-aldrich syndrome protein
WES = whole-exome sequencing
WHO = world health organization
WT = wild type
WT1 = wilms tumor protein 1
XBP1 = X-box-binding protein 1
Zap70=zeta-chain-associated protein kinase 70
ZFNs = zinc-finger nucleases
 μ g = microgram
 μ l=microliter

I. Introduction

1. The Immune System

The immune system comprises a complex network of cells, tissues, and soluble molecules working together to defend the body against infectious agents, such as bacteria, viruses, fungi, parasites, and tumor cells. The mechanisms of immune protection have become increasingly complex as species adapt to combat evolving pathogens. It primarily discriminates between "self" and "non-self" molecules and cells, eliminating the latter while leaving the former intact ¹. Two main types of responses are adaptive and innate immunity. Innate immunity, or natural non-specific immunity of immediate action, is the first line of defense involving cells and molecules responsible for phagocytosis of a wide range of invading pathogens and, in some cases, killing infected cells. On the other hand, adaptive immunity involves the specific recognition of the foreign substance, which will be neutralized and destroyed ² (**Figure 1**). While the innate immune response (IR) exists in all multicellular organisms, the adaptive IR is found only in vertebrates ³.

1.1. The Innate Immune Response:

The innate immune system plays a critical role in maintaining homeostasis and is the first line of defense against infectious and pathogenic agents. It is activated by danger signals resulting from interactions between self-receptors on various cells and non-self-molecules on microorganisms. Dysregulation of the innate immune system can lead to immunodeficiencies ⁴, autoimmune disorders ⁵, and chronic diseases such as diabetes ⁶, Alzheimer ⁷, and atherosclerosis ⁸.

The innate immune response involves different defense modules (**Figure 1**). These include physical and chemical barriers, such as the skin and mucous membranes, that prevent pathogen entry into the body ⁹. Induced modules, including the inflammatory response and phagocytosis, involve phagocytic cells, soluble molecules, and cytokines ¹⁰. Pattern recognition receptors (PRRs) are key components of this response as they recognize pathogen-associated molecular patterns (PAMPs) and danger-associated molecular patterns (DAMPs), initiating immune responses¹¹. Examples of key PRRs are Toll-like, nucleotide-binding oligomerization domain (NOD-like), RIG-I-like, C-type lectin, STING (stimulator of interferon genes) and cyclic guanosine monophosphate (GMP)-adenosine monophosphate (AMP) synthase (cGAS), which detect cytosolic deoxyribonucleic acid (DNA) and trigger antiviral immune responses ^{12,13}. Phagocytic cells, such as macrophages and dendritic cells (DCs), engulf and destroy invading pathogens (phagocytosis) and function as antigen-presenting cells (APCs) by presenting antigens via class I and II major histocompatibility complex (MHC) molecules ^{14,15}. Dendritic cells can originate either from myeloid or lymphoid (for some subsets, e.g., Ly6D⁺, Interleukin (IL)-7R alpha (α)⁺, a cluster of differentiation (CD) 81⁺ and CD2⁺ plasmacytoid DCs ¹⁶) progenitors. DCs can either present the antigen at the site of infection or migrate to secondary lymphoid organs to trigger the adaptive immune response ¹⁷.

Natural killer (NK) cells are derived from CD34+CD38-CD7+ common lymphoid progenitors in the bone marrow ¹⁸. However, they do not present the CD3 differentiation cluster; instead, they are characterized by the CD56 and CD16 differentiation clusters ¹⁹⁻²². NK cells can spontaneously recognize and destroy virus-infected or tumor cells without prior activation ²³⁻²⁶. Moreover, they exhibit tight regulation through activating and inhibitory receptors, allowing them to target abnormal cells while sparing healthy ones ^{27,28}.

Lastly, gut microbiota, such as *Lactobacillus reuteri*, also shapes the innate immune system and affects susceptibility to infectious diseases ²⁹⁻³².

1.2. The Adaptive Immune Response:

The adaptive immune system was first described through observations of protection against subsequent infections. Animals were found to be shielded by exposure to a weakened form of the pathogen or by receiving serum from previously infected animals³³⁻³⁵. In the early twentieth century, Ehrlich introduced the concept of "horror autotoxicus," suggesting that the immune system can distinguish between self and non-self³⁶⁻³⁹. Landsteiner expanded on this idea by discovering the ABO blood group system and showing its ability to trigger antibody (Ab) responses to foreign antigens^{38,40}. Medawar and Burnet later proposed the clonal selection theory, providing a framework for understanding how the immune system generates specific responses to antigens⁴¹⁻⁴⁴. These outlined discoveries paved the way for understanding the role of the adaptive immune system.

The adaptive immune response serves as the second line of defense against infectious agents and involves lymphocytes playing a significant role. It is distinguished by self/non-self-discrimination, specificity, diversity, and memory, leading to long-term protection against various pathogens³ (**Figure 1**). Lymphocytes are the major cell type of the adaptive immune response characterized by a unique process of dual differentiation modulated by antigenic influences. Depending on their maturity, they are found in different locations, including secondary lymphoid organs, blood, and spleen¹. Lymphocytes can be categorized into B lymphocytes, responsible for the humoral response and possessing B Cell Receptors (BCR), and T lymphocytes, responsible for the cellular response and presenting TCR⁴⁵. B- and T-cells acquire their unique antigen specificity through V(D)J recombination, mediated by the V(D)J recombinase enzyme complex, which recognizes specific DNA sequences flanking the variable (V), diversity (D), and joining (J) gene segments that encode for the BCR.

1.2.1. B lymphocytes:

B cells originate from hematopoietic stem cells (HSCs) in the bone marrow and undergo a series of maturation phases, including gene rearrangement and positive and negative selection, to finally migrate to secondary lymphoid organs such as the spleen and lymph nodes for further development. B cells are characterized by the expression of the CD19 and a BCR complex comprising a signaling Ig α -Ig β dimer that enables specific recognition of antigenic peptide fragments derived from pathogens. Additionally, B cells function as APCs, presenting both MHC class I and class II molecules^{2,46}. V(D)J recombination allows B cells to acquire unique antigen specificity, generating a variety of BCRs for recognizing numerous pathogens^{46,47}. On exposure to pathogenic antigens, B cells proliferate and differentiate into plasma cells secreting antibodies for pathogen neutralization or long-lived memory B cells for faster subsequent infection responses⁴⁶.

Antibodies are heterotetrameric structures composed of two disulfide-connected heavy (H) bonds and two light chains (L), each featuring variable (V) and constant (C) regions. Heavy chains exhibit isotypes (IgM, IgD, IgG, IgA, and IgE) with specific functions. Antibodies can undergo fragmentation via enzymes such as papain (producing Fab and Fc fragments) or pepsin (resulting in F(ab)₂ and pFc' fragments)².

B cells use several mechanisms for direct or indirect target cell killing, including i) Antibody-dependent cellular phagocytosis (ADCP) or antibody-dependent cellular cytotoxicity (ADCC)^{48,49}, ii) Complement-mediated cytotoxicity (CDC), involving the membrane attack complex (MAC)⁴⁹, iii) Cytokine-mediated cell death, by releasing cytokines, such as tumor necrosis factor-alpha (TNF- α) and iv) Direct cell-mediated cytotoxicity via Fas ligand (FasL) capable of inducing apoptosis or programmed cell death in target cells⁵⁰.

1.2.2. T lymphocytes:

T-cells play a vital role in mediating specific cellular immunity. They acquire their antigen specificity through the TCR, which specifically recognizes antigenic fragments presented on the cell surface by MHC molecules. Upon activation, T-cells target infected cells, cancer cells, and cells that are damaged or malfunctioning^{1,2}. HSCs in the bone marrow give rise to T-cells, which then migrate to the thymus. In the thymus, immature T-cells, known as thymocytes, undergo a selection process that determines their antigen specificity and functional characteristics. Similar to B cells, thymocytes undergo V(D)J recombination, involving gene rearrangements responsible for TCR encoding⁴⁷.

Positive and negative selection mechanisms occur during T-cell development to ensure that T-cells can recognize foreign antigens while avoiding attacks on the body's own cells⁵¹. A study led by Kathryn M. et al. demonstrated that T-cells can recognize antigens through conformational changes in response to antigen binding⁵², enabling the recognition of a broad range of antigens, including highly variable ones found on viruses. T-cells are characterized by the CD3 along with either the CD4+ or CD8+ differentiation clusters. Based on surface markers, T lymphocytes can be classified into various types. Still, the main types are cytotoxic CD8+ T-cells characterized by the presence of the CD8+ coreceptor and recognition of MHC I and II, and CD4+ T-cells characterized by the presence of the CD4+ coreceptor and recognition of MHC II. CD4+ T-cells can further differentiate into helper T-cells, which regulate the adaptive immune response. Both CD8+ and CD4+ T-cells can develop into "memory" cells after encountering the antigen, enabling a faster and more robust response upon subsequent encounters with the same antigen^{1,2}.

T-cells possess diverse mechanisms to eliminate target cells, including i) Direct cell-mediated cytotoxicity, whereby T-cells induce cell death in target cells via FasL and by releasing toxic molecules such as perforin and granzymes. Encased within granules, these molecules are released by T-cells upon TCR engagement with the antigen. T-cells form nanotubes that establish a direct connection with target cells, facilitating the transportation of perforin directly to the target cell membrane. Consequently, pores are formed, enabling the entry of granzymes. This sequence of events sets in motion a cascade that ultimately results in the demise of the target cell^{53,54}. ii) Cytokine secretion: T-cells produce cytokines, including interferon-gamma (IFN- γ) and TNF- α /beta (β), capable of inducing cell death in target cells². iii) Activation of other immune cells represents another essential mechanism employed by T-cells to eliminate target cells. For example, T-cells can secrete IFN- γ which stimulates other immune cells, including macrophages, for enhanced antigen presentation and bactericidal function⁵⁵. Furthermore, T-cells contribute to Th1 differentiation, cytotoxic T lymphocyte (CTL) function, as well as the activation of neutrophils and NK cells^{56,57}.

1.3. Crosstalk Between The Innate And Adaptive Immune Responses:

The activation of the adaptive immune system is facilitated by the innate immune response through the recruitment of immune cells to the infection site and antigen presentation to T and B cells, which then mount a specific response to the invading pathogen. This process, known as antigen presentation, is crucial for the initiation of adaptive immunity (**Figure 1**). Notably, APCs play a dual role in innate and adaptive immunity by activating lymphocytes, which are the principal cells of adaptive immunity. Among these lymphocytes, B cells, considered APCs, also contribute to adaptive immunity. Consequently, it can be inferred that innate immunity serves as the instigator of adaptive immunity, establishing a significant connection between humoral and cellular-mediated immunity. The integrity of this interface is of utmost importance in maintaining the body's defense, as a disruption in even a single mechanism can lead to severe or even fatal diseases and syndromes⁵⁸.

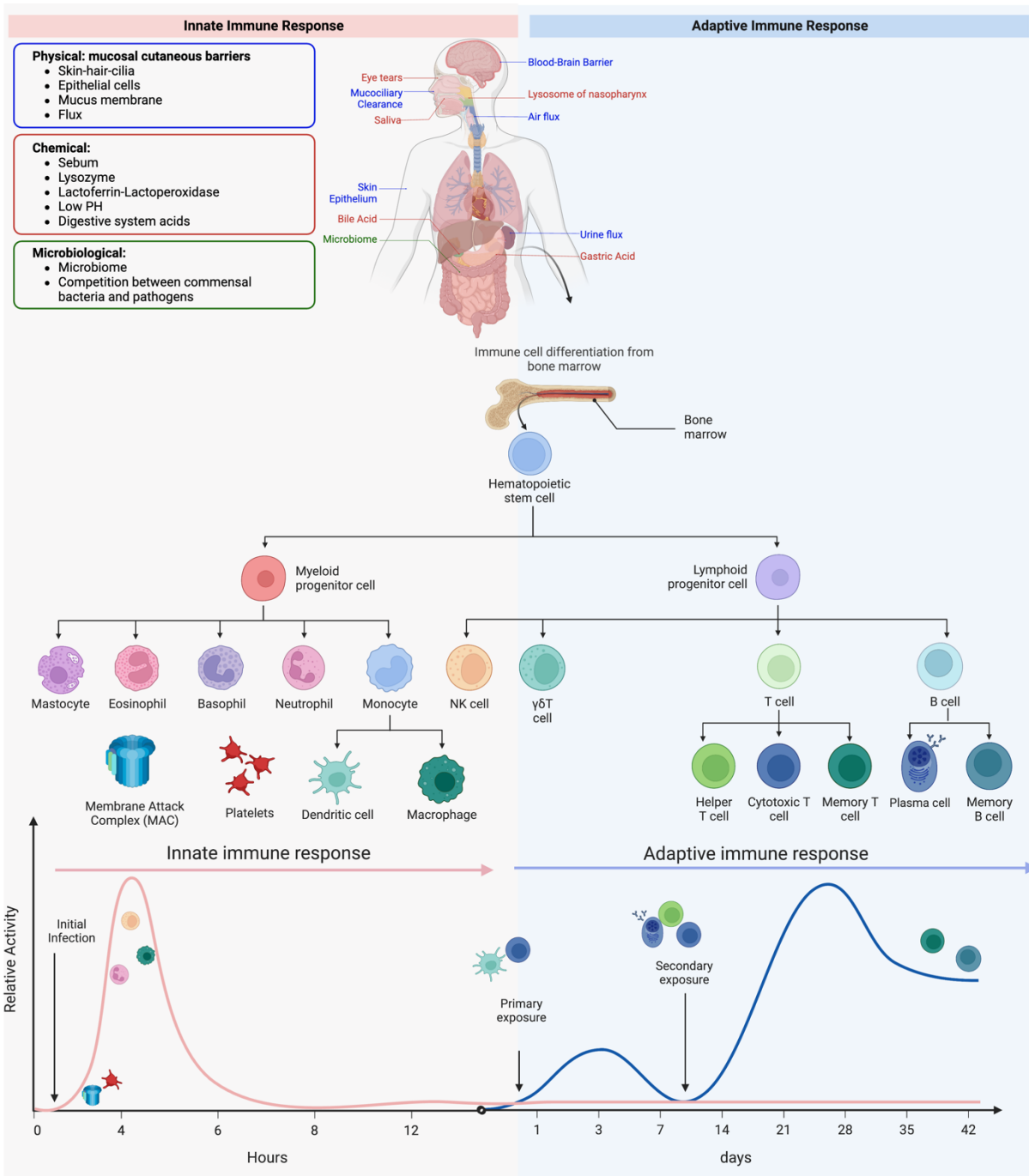


Figure 1: Schematic overview of innate and adaptive immune responses.

top; the innate immune system is the first line of defense against infection, including physical, chemical, and microbiological mechanisms. middle; genesis and differentiation of immune cells from hematopoietic stem cells to various innate and adaptive immune cells. bottom; timeline of immune responses, from the rapid innate response to the gradual and highly specific adaptive response, highlighting the establishment of memory T and B cells in generating long-term immunity.

2. Cancer

Cancer is the leading cause of death globally, accounting for an estimated 10 million deaths in 2020, according to the world health organization (WHO)⁵⁹. Cancer incidence is also on the rise, with nearly 19 million reported in 2020 and an estimated 29 million expected by 2040 based on Globocan data⁶⁰. Cancer is considered a genetic and, more recently, also a metabolic disorder that can be inherited or sporadic⁶¹. It involves qualitative and quantitative changes in gene expression and function, resulting in the uncontrolled growth and spread of abnormal cells in the body. Cancer cells arise and proliferate in different body sites, forming tissue masses (i.e., tumors).

Cancers are usually named based on the type of cell or organ from which they originate. Malignant tumors, unlike benign ones, have the ability to spread to adjacent organs or tissues, forming new tumors in distant locations (metastasis) through the blood or the lymph system^{62,63}. Tumors may consist of different clonal types with distinct genetic mutations, responses to treatment, and the potential for recurrence⁶⁴.

Advancements in genome sequencing have revealed chromosomal rearrangements, epigenetic changes, and alterations in DNA repair mechanisms as novel genetic alterations and pathways involved in cancer initiation and progression^{65,66}. For instance, epigenetic modifications such as DNA methylation and histone modifications can alter gene expression and contribute to cancer development^{67,68}. Moreover, the TME, including immune cells, blood vessels, and extracellular matrix (ECM) components, plays a critical role in cancer initiation, progression, and metastasis through interaction with cancer cells and their microenvironment⁶⁹⁻⁷¹. In addition, non-coding ribonucleic acid (RNA), such as miRNAs and long non-coding RNAs (lncRNAs), are deregulated in various cancer types and implicated in multiple aspects of cancer growth, migration, and invasion⁷²⁻⁷⁴. Emerging evidence also highlights the role of the gut microbiome in cancer development and progression by influencing immune responses and metabolic pathways through various mechanisms, including the secretion of bacterial toxins, molecules that damage DNA, and cytokines such as interleukin (IL)-1 and IL-12⁷⁵⁻⁷⁸.

2.1. Solid Tumors:

Solid and liquid malignancies are two main types of tumors that differ in their physical and structural characteristics. Liquid tumors consist of either white blood cells that circulate in the bloodstream and bone marrow (leukemias) or abnormal lymphocytes circulating in the lymphatic system (lymphomas) without forming masses. In contrast, solid tumors, which can be classified as either "cold" or "hot" tumors (**Figure 2**), comprise cells that form a lump in a particular body area and can spread to other organs or tissues. Cold tumors are characterized by a lack of immune cell infiltration and an immunosuppressive tumor microenvironment, which hinders the immune system's ability to recognize and attack cancer cells. On the other hand, hot tumors exhibit significant immune cell infiltration and an inflamed tumor microenvironment, promoting an active immune response against cancer cells. Solid tumors are a significant contributor to the burden of cancer worldwide⁷⁹⁻⁸¹.

The National Cancer Institute estimated that solid tumors accounted for 90% of all adult human cancers in 2023, with breast, lung, prostate, colorectal, and melanoma being the most common types of solid tumors^{82,83}. The prognosis for patients with solid tumors varies depending on the type and stage of cancer, as well as other factors such as age and overall health. Treatment options for solid tumors may include surgery, radiation therapy, chemotherapy, targeted therapies, and more recently, immunotherapy.

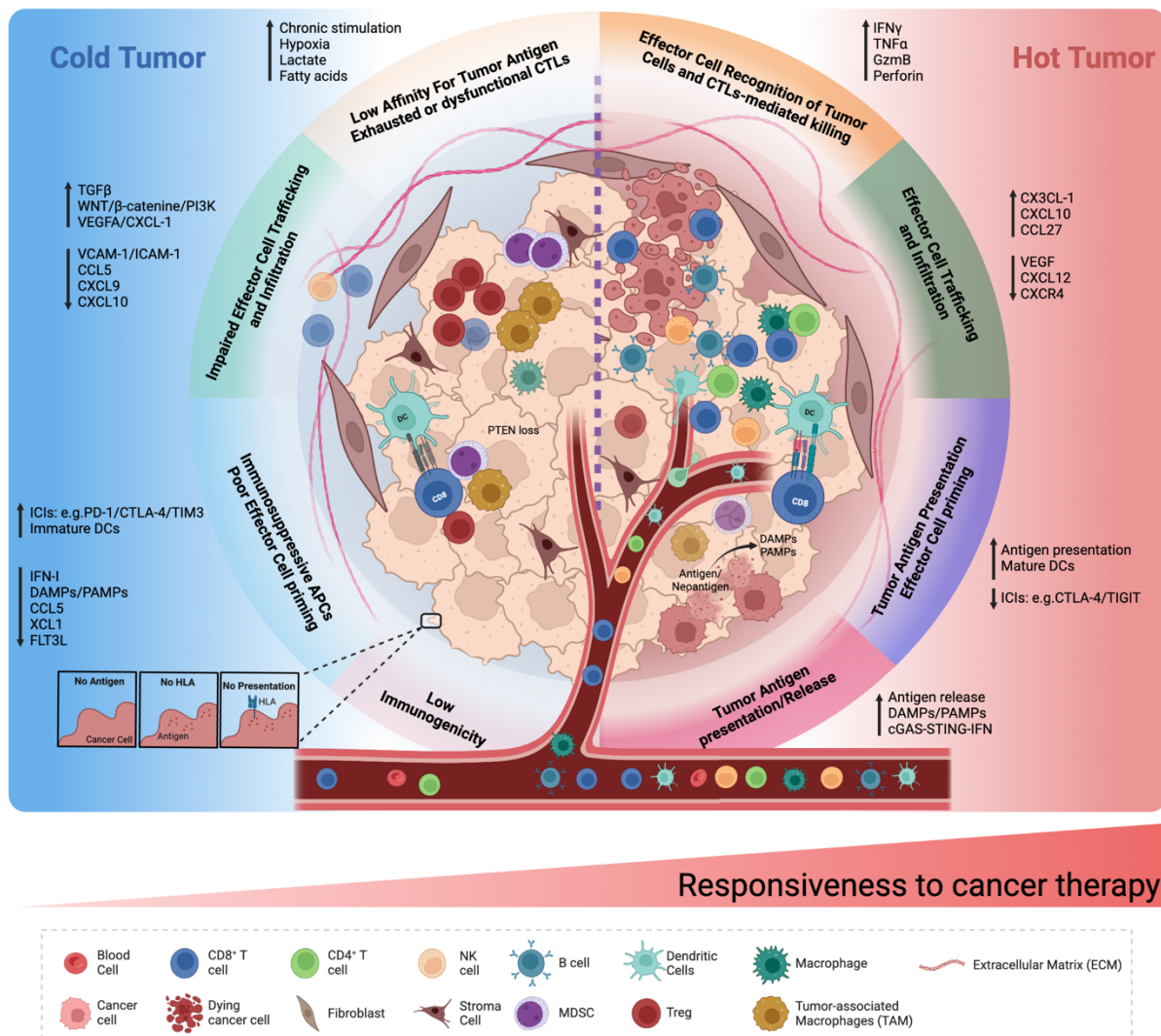


Figure 2: Comparative characteristics of cold and hot tumors in TME.

left; cold tumors are characterized by low immunogenicity, inadequate effector cell priming, and limited infiltration of effector immune cells. These tumors harbor a high proportion of immunosuppressive components and cells, which collectively hinder the immune system's ability to detect and eliminate cancer cells, leading to CTL cell dysfunction and a reduced response to cancer therapies. right; hot tumors are distinguished by an efficient release of tumor antigens, successful priming of effector cells, particularly CTL cells, and a significant presence of infiltrating effector immune cells within an inflamed TME. These characteristics result in a more efficient eradication of cancer cells and an increased responsiveness to cancer therapies.

2.1.1. Melanoma:

Melanoma is the most aggressive type of skin cancer that emerges from malignant melanocytes⁸⁴, which are specialized cells that make melanin. It can be caused by genetic alterations, such as mutations in v-raf murine sarcoma viral oncogene homolog B1 (BRAF), telomerase reverse transcriptase (TERT), neuroblastoma-RAS (NRAS), and phosphatase and TENsin homolog (PTEN) genes, as well as chromosomal rearrangements and gene fusions⁸⁵⁻⁸⁷. Research has identified key signaling pathways involved in melanoma, including the mitogen-activated protein kinase (MAPK) and Phosphoinositide 3-kinase (PI3K)/Akt strain transforming (AKT)/mammalian target of rapamycin (mTOR) complex pathways. Dysregulation of these pathways is observed in a significant number of melanomas, opening up new targets for therapy^{87,88}. Moreover, recent studies have identified specific components, such as tumor-associated macrophages (TAMs), ECM proteins, and growth factors, within the melanoma microenvironment. Combinatorial therapies, including immunotherapies targeting multiple pathways and components, have shown promise in both preclinical and clinical studies⁸⁹⁻⁹⁵. Furthermore, emerging evidence suggests that the gut and skin microbiomes contribute to melanoma development and progression. They may affect the immune system and DNA damage repair.

Specific microbial species and metabolites associated with melanoma risk and outcomes have been identified, presenting new avenues for prevention and treatment⁹⁶⁻⁹⁹. Melanoma can be clinically stratified into different subtypes based on histopathological features. Common subtypes include superficial spreading melanoma, nodular melanoma, lentigo maligna melanoma, and acral lentiginous melanoma^{100,101}.

2.1.2. Prostate cancer:

The most common type of prostate cancer is adenocarcinoma, which accounts for over 90% of cases^{102,103}. It arises from glandular cells producing prostate fluid and is characterized by prostate-specific antigen (PSA) expression and abundant androgen receptors (AR), as well as mutations in the erythroblast transformation specific (ETS) gene family. Additionally, it exhibits enhanced oxidative phosphorylation (OXPHOS) and lipogenesis^{104,105}. Recent studies have identified biomarkers associated with adenocarcinoma¹⁰⁶⁻¹⁰⁹, as well as genes linked to more aggressive disease and resistance to androgen deprivation therapy in certain subtypes of adenocarcinoma¹¹⁰⁻¹¹². There are other less frequent and aggressive types of prostate cancer. One example is prostatic acinar adenocarcinoma with ductal differentiation, which is characterized by the presence of glandular and ductal structures. This subtype is associated with a higher risk of biochemical recurrence and a poorer prognosis¹¹³. Another type is prostatic urothelial carcinoma, which originates from the urothelial cells lining the bladder, neck, and prostatic urethra. This subtype is known for its high frequency of genetic alterations and poor prognosis¹¹⁴.

2.2. Solid Tumor Immunosuppressive Microenvironment:

TME is a complex network of highly heterogeneous cellular, non-cellular, and molecular components. Different regions exhibit different physical, cellular, and metabolic barriers that significantly influence cancer progression, invasion, metastasis, and resistance to therapy (including immunotherapies). These barriers inhibit the activity of effector immune cells, including cytotoxic T-cells, NK cells, and DCs¹¹⁵⁻¹¹⁸ (**Figure 3**).

Upregulation of immune checkpoint molecules such as programmed cell death 1 (PD-1), cytotoxic T-lymphocyte antigen-4 (CTLA-4), and lymphocyte-activation gene 3 (LAG-3) in the TME dampen T-cell activation and promote exhaustion (discussed below in this section)^{119,120}. For instance, patients with advanced non-small cell lung cancer (NSCLC) expressing programmed cell death ligand 1 (PD-L1) on circulating tumor cells (CTC) showed improved survival with anti-PD-1/PD-L1 therapy, highlighting the role of PD-L1 in immune suppression and drug resistance¹²¹.

Another challenge faced by T-cells in the TME is the presence of cytokines, chemokines, and growth factors that mediate communication between immune cells and components within the TME. For instance, IL-6, transforming growth factor- β (TGF- β), and IL-10 can inhibit T-cell function and promote the differentiation of immunosuppressive cells¹²²⁻¹²⁴. Moreover, the vascular endothelial growth factor (VEGF) present in TME can promote cancer angiogenesis and limit T-cell infiltration^{125,126}. Furthermore, specific chemokines such as chemokine C-C motif ligand 2 and 5 (CCL2, CCL5), C-X-C motif chemokine ligand 12 (CXCL12), and C-X-C motif chemokine receptor 4 and 7 (CXCR4, CXCR7) attract immunosuppressive cells to the TME and contribute to cancer progression^{123,127-129}.

The TME also recruits immunosuppressive cells, namely regulatory T-cells (Tregs) and myeloid-derived suppressor cells (MDSCs). Tregs have the ability to inhibit the activation and differentiation of T-cells¹³⁰⁻¹³³. They induce tumor immune escape through various mechanisms, such as the high consumption of IL-2 due to the expression of high-affinity IL-2 receptors, the inhibition of CD80/CD86 expression on DCs through their interaction with CTLA-4 on their surface with CD80/CD86 on DCs, the production of inhibitory metabolites as prostaglandin E2 (PGE-2), IL-10 and transforming growth factor-beta (TGF- β) within the TME, and even by directly killing anti-tumor effector cells^{132,134-136}. Hence, depleting Tregs has enhanced immune checkpoint blockade (ICB) effectiveness in preclinical models^{132,136-141}, with efficacy depending on the tumor burden and

the specific antibody used for Treg depletion¹³⁹. On the other hand, MDSCs are a heterogeneous population of immature myeloid cells that can suppress T-cell function by secreting IL-10 and IL-12 and promote angiogenesis via, for instance, bombina variegata peptide 8 (Bv8) and matrix metalloproteinases 9 (MMP-9) production^{133,142-145}. Additionally, plasmacytoid dendritic cells (pDCs) expressing IFN- α also exert an immunosuppressive role within the TME¹⁴⁶⁻¹⁴⁸. These pDCs promote cancer cell invasion through the TNF- α / nuclear factor κ light chain enhancer of B cells activation (NF- κ B)/CXCR-4 pathway in oral squamous cell carcinoma (OSCC) and hepatocellular carcinoma (HCC) contexts¹⁴⁹. This is due to their role in the upregulation of ectonucleotidases CD39 and CD73, which are essential for extracellular adenosine (eADO) production. This upregulation is induced by hypoxia-inducible factor 1-alpha (HIF-1 α) and leads to the recruitment and the differentiation of CD4⁺ CD25⁺ Foxp3⁺ Tregs^{147,150,151}. pDCs induce immunotolerance by expressing certain immune checkpoint molecules, including inducible T-cell costimulator ligand (ICOSL)¹⁵² and indoleamine 2,3 deoxygenase 1 (IDO1)^{147,153}. Targeting these cells has shown promise in improving immunotherapy response in preclinical models¹⁵⁴. TME can also promote the differentiation of cancer-associated fibroblasts (CAFs) located in the stroma. CAFs can originate from various cell types, including myofibroblasts, fibroblasts, adipocytes, and cancer-associated mesenchymal stem cells (MSCs)¹⁵⁵. They create a favorable environment for tumor growth, impair T-cell function, and play a role in drug resistance. For instance, the CD10⁺ G-protein-coupled receptor 77 (GPR77)⁺ CAF subset, secreting IL-6 and IL-8, directly promotes human breast and lung cancer cell formation¹⁵⁶. In addition, CAFs limit T-cell function either directly by releasing TGF- β , CXCL12 and by forming a physical barrier through ECM deposition^{133,157-159} or indirectly by recruiting immunosuppressive Tregs and myeloid cells through the secretion of IL-1 β , IL-6, VEGF, colony-stimulating factor 1 (CSF-1), CCL2, and Chitinase 3-like1¹⁶⁰⁻¹⁶⁴. Furthermore, CAFs contribute to drug resistance and chemotherapy resistance in certain cancers^{155,165}.

A study led by Li et al. has identified the release and transfer of immunosuppressive bioactive lncRNA from cancer cells to MSCs via exosomes, resulting in the inhibition of MSC osteogenesis in the multiple myeloma (MM) model. Inhibition of exosome release has correlated with efficient bone formation and prevention of bone loss¹⁶⁶. Moreover, the TME induces immune evasion through the modulation of the ECM, which acts as a physical barrier to immune cell infiltration and hinders their activity. High levels of collagen, fibronectin, hyaluronan proteoglycan, and ECM receptors, such as integrins and CD44, are often present in the TME and contribute to T-cell exhaustion and inhibition of their cytotoxic activity^{133,167-169}. Targeting these molecules can enhance T-cell activity and cytotoxicity, reduce T-cell exhaustion, and improve the response to immunotherapy, particularly when combined with ICB¹⁷⁰⁻¹⁷⁵.

2.2.1.1. T-cell exhaustion

T-cell exhaustion is a state of functional impairment and dysfunction observed during chronic infections, including viral and tumor infections. Exhausted T-cells (Tex cells) form a distinct T-cell subset distinct from naïve, memory, and effector cells¹⁷⁶. Tex exhibits a progressive decline in effector function and cytotoxicity along with sustained expression of inhibitory receptors, including PD-1, T-cells immunoglobulin and mucin domain-containing-3 (TIM-3), LAG-3, CTLA-4, and T cell immunoreceptor with Ig and ITIM domains (TIGIT)^{177,178}. These cells also experience reduced production of cytokines and metabolic impairments¹⁷⁹. Despite their exhausted state, exhausted T-cells (Tex cells) retain the ability to proliferate *in vivo* and generate effector molecules, allowing them to exert some control over pathogens or tumors^{178,180}. T-cell exhaustion, although limiting clearance of virus-infected or tumor cells, plays a vital role in protecting against excessive immunopathology¹⁷⁹. Reversal of T-cell exhaustion is possible to some extent, but a threshold of high exhaustion may exist, beyond which reversal becomes unlikely, particularly in PD-1^{hi} CD8⁺ Tex cells¹⁸¹.

Chronic TCR signaling plays a pivotal role in driving T-cell exhaustion, as evidenced by the involvement of the calcineurin-dependent transcription factor NFAT (nuclear factor of activated T-cells)¹⁸² and other TCR-responsive transcription factors (e.g., Interferon regulatory factor 4 (IRF4), basic leucine zipper ATF-like

3. Cancer Immunotherapy:

Cancer immunotherapy is a type of cancer treatment that harnesses the power of the body's immune system to target and fight cancer cells. It relies on understanding the complex interaction between the immune system and cancer cells. Cancer immunotherapy has proven its efficacy in treating many patients with different types of tumors. Moreover, it represents an essential milestone in the development of cancer treatments and has the potential to revolutionize cancer care¹⁹³⁻¹⁹⁵. Cancer immunotherapy has a long history dating back to the late 19th century. Two German physicians, Fehleisen and Busch, independently observed tumor regression after erysipelas infection, and then Fehleisen identified *Streptococcus pyogenes* as the cause. In 1891, William Bradley Coley, a bone surgeon famously known as the “father of immunotherapy”, attempted to use the immune system to target bone cancer and developed a mixture of bacteria known as Coley's toxins. Although some patients experienced tumor regression, inconsistent and variable data, along with the risk of infecting patients, led to the decline of Coley's treatment, ultimately falling out of favor with the advent of radiation and chemotherapy^{193,196-198}. Around the same time, Paul Ehrlich proposed the theory of "side chain" or "receptor," suggesting that T-cells have specific proteins that recognize and bind to “antigens”.

Emil von Behring and Shibasaburo Kitasato substantiated his theory by later discovering, in 1890, antibodies. In 1907, Ehrlich introduced the concept of a "magic bullet," involving a targeted therapy aimed at selectively eliminating cancer cells while preserving normal cells in the patient's body. Subsequently, he confirmed Coley's observations in 1908, and significant discoveries in immunology followed¹⁹⁹. Later in 1950, researchers found that the immune system can distinguish between self and non-self-antigens, including unique antigens expressed by cancer cells. The role of T-cells in cancer immunotherapy was revealed in 1967, leading to the exploration of cytokines, monoclonal antibodies, and cancer vaccines. However, these approaches had limited success until the late 20th century when advances in molecular biology and immunology sparked interest again. Checkpoint inhibitors, which remove breaks from immune cells and allow T-cells to effectively recognize and kill cancer cells, revolutionized cancer immunotherapy. The food and drug administration (FDA) approved the first drug, ipilimumab (anti-CTLA-4), against advanced melanoma in 2010, and James Allison and Tasuku Honjo were awarded the Nobel Prize in 2018 for their work on checkpoint blockade molecules²⁰⁰. Other immunotherapy drugs like pembrolizumab (anti-PD-L1) and nivolumab (anti-PD-1) have been approved for various cancers, shaping cancer immunotherapy as it stands nowadays^{201,202}. Several strategies have been developed to enhance T-cell activity and overcome immunosuppression, each with its own advantages and limitations. The choice of treatment depends on factors such as cancer type, stage, patient health, and availability. Immunotherapy strategies include ICB, the introduction of immunomodulatory cytokines, cancer vaccines, and ACT.

3.1. Adoptive Cell Therapy (ACT)

Adoptive cell therapy is a targeted form of cancer immunotherapy treatment involving the isolation of immune cells, specifically tumor-infiltrating lymphocytes (TILs) from a cancer patient or from peripheral blood mononuclear cells (PBMCs) of a healthy donor (particularly T-cells) (**Figure 4**). These cells can be subject to laboratory-based engineering and expansion processes on a large scale. Subsequently, the modified or unmodified T-cells (in the case of TILs) are then reintroduced into the patient via transfer or reinfusion, with the primary objective of eradicating cancerous cells. Genetic modification of immune cells can include, for instance, CARs or TCRs²⁰³⁻²⁰⁵. Unlike non-specific treatments like chemotherapy and radiotherapy, which can affect healthy cells, ACT is a personalized and targeted approach against cancer cells. Chemotherapy uses drugs to kill cancer cells, while radiotherapy damages cancer cell DNA to impede their division and growth. However, both treatments can have significant side effects, impacting healthy cells and causing nausea, hair loss, and a weakened immune system²⁰⁶. The concept of ACT originated in the 1980s when Steven Rosenberg and colleagues first demonstrated that TILs isolated from melanoma patients could be expanded *in vitro* and reinfused into patients for enhanced antitumor efficacy^{207,208}.

In 1994, the first successful clinical application of ACT was reported, showing a 34% objective response rate and complete responses in many patients with metastatic melanoma²⁰⁹. Since then, ACT has expanded to include various immune cells, such as dendritic cells and natural killer cells in multiple cancer types. Moreover, a breakthrough in ACT occurred in 2010 with the development of CAR-T-cells. CAR-T-cell therapy has demonstrated remarkable clinical responses against certain blood cancers, leading to the approval of CD19 CAR-T-cells by the FDA in 2017 for treating relapsed or refractory acute lymphoblastic leukemia in children and young adults²¹⁰⁻²¹³. While ACT has shown promising clinical results, it faces challenges related to technical complexity, cost, cell selection, target antigen identification, toxicity, and tumor immune escape mechanisms^{214,215}.

Ongoing research projects aim to enhance the efficacy and safety of ACT through novel T-cell engineering approaches, gene editing technologies, and the combination of ACT with checkpoint inhibitors, low-dose radiotherapy, or combinatorial engineering to improve T-cell persistence and immunomodulation^{214,215}.

3.1.1. Tumor-infiltrating lymphocyte (TIL) therapy:

TIL therapy involves the isolation and big-scale *in vitro* expansion of lymphocytes, particularly T-cells, from a patient's tumor using high doses of IL-2. These expanded TILs are then either directly reinfused or engineered before being transferred back into the patient. TILs possess the advantage of specifically recognizing and attacking tumor cells upon encountering tumor antigens. However, ongoing efforts aim to enhance TIL reactivity toward tumor antigen recognition, specifically neoantigens^{216,217}. To identify tumor neoantigens during TIL preparation, Rosenberg and colleagues developed a protocol that involves spotting mutant proteins specific to tumor cells using whole-exome sequencing (WES) technology and RNA-seq (**Figure 6**). These mutant proteins are synthesized as peptides or tandem minigenes (TMG)²¹⁸. Subsequently, MHC-matched APCs process these neoantigens for coculture with TILs to evaluate antigen presentation and recognition based on IFN- γ production measured through enzyme-linked immunosorbent spot (ELISPOT) assays. Neoantigen-specific TILs are then purified via fluorescence-activated cell sorting (FACS) or magnetic-activated cell sorting MACS, using activation markers like CD137, and are exposed to the "rapid expansion procedure" (REP) before reinfusion into the patient receiving lymphodepletion, along with IL-2²¹⁹.

A pre-REP step may be included, where tumor fragments containing TILs are cultured *in vitro* with IL-2 to expand "young TILs" or perform IFN- γ -ELISPOT for detecting antigen-specific TILs, prior to the REP protocol. These methods have shown promising results in certain patients with melanoma and other solid tumors, such as colorectal cancer, breast cancer, and ovarian cancer²²⁰.

3.1.2. Genetically engineered T-cell therapy:

Gene therapy is a modern approach that involves altering the genetic material of the cells to treat or prevent diseases. There are several types of gene therapy for cancer, which can be broadly classified into two categories: gene addition therapy and gene editing therapy. Gene addition therapy introduces new genetic material into cells, while gene editing therapy modifies existing genetic material in cells.

Gene therapy originated in the 1970s and gained momentum in 1990 with the successful treatment of a patient with adenosine deficiency by receiving genetically modified white blood cells that produced the missing enzyme²²¹. Since then, numerous clinical trials have been conducted to optimize gene therapy for various conditions, including cancer.

One approach involves manipulating genes related to tumor development and progression. Additionally, gene therapy can also modify immune cells, such as T-cells, to specifically recognize and eliminate cancer cells. In particular, T-cell-based gene therapy has shown promise in treating blood cancers, although challenges remain in its effectiveness against solid tumors²²².

Different strategies can be employed for enhancing the ability of genetically modified T-cells to target cancer cells in the TME. These include targeting tumor-associated antigens, overcoming immune suppression in the TME, and improving T-cell migration, infiltration, and persistence. For this, various T-cell-based gene therapy approaches are available, such as the following (**Figure 4**):

- **Targeting tumor-associated and tumor-specific antigens:** Genetic modification of T-cells can be used to target tumor-specific antigens (TSAs) that are expressed only by cancer cells in the TME but not in healthy tissues such as neoantigens induced by cancer cell genetic mutations. Unlike targeting tumor-associated antigens (TAAs), or shared antigens, selective TSA targeting reduces the risk of “on-target, off-tumor” toxicity²²³. TAAs include cancer/testis (CT) antigens²²⁴ (involving melanoma antigen-encoding genes (MAGEs) and NY-ESO1 antigens), differentiation antigens (such as melanoma-associated antigen recognized by T cells-1 (MART-1) and carcinoembryonic antigen (CEA)), as well as overexpressed antigens (such as mesothelin)^{223,225}.
- **Overcoming immunosuppression:** This involves expressing molecules such as checkpoint inhibitors²²⁶⁻²²⁸, a dominant-negative form of transforming growth factor beta receptor II (TGF- β RII)²²⁹, optimized forms of activation molecules such as high-affinity activation receptors/ligands or TCR adapter Zeta-chain-associated protein kinase 70 (Zap70)²³⁰, or knocking out (KO)/KD inhibitory genes downstream of signaling pathways to prevent T-cell exhaustion.

T-cell homing and infiltration can also be enhanced by modifying T-cells to secrete chemokines or express chemokine receptors, such as the CXCR2 receptor that improved T-cell migration and antitumor activity^{231,232}.

Improving T-cell persistence within the TME can be achieved, for instance, through the genetic engineering of T-cells to secrete cytokines such as IL-2, IL-7, IL-15, IL-12, IL-18, and IL-21, which have been investigated for their potential to boost T-cell antitumor function^{203,228}. Additionally, modified CAR-T-cells expressing both the 4-1BB costimulatory endodomain and the CD28 signaling endodomain have shown improved persistence and killing capacity^{228,233}.

Moreover, metabolic reprogramming of T-cells can also enhance their function within the TME^{92,118}. This includes, for example, modulating glycolysis by genetically engineering T-cells to overexpress phosphoenolpyruvate carboxykinase 1 (PCK1), which was demonstrated to enhance T-cell antitumor function in melanoma model²³⁴ or by favoring alternative metabolic pathways such as fatty acid oxidation^{235,236} and modulating mitochondrial biogenesis (MB). This later is illustrated by the overexpression of the proliferator-activated receptor gamma coactivator 1-alpha (PGC-1 α) in CD8+ T-cell that pushes toward a central memory phenotype, resulting in a robust antitumor response against melanoma tumors. This is accompanied by an increased expansion and a higher mitochondrial activity in TILs upon rechallenge in a tumor-free host *in vivo*²³⁵.

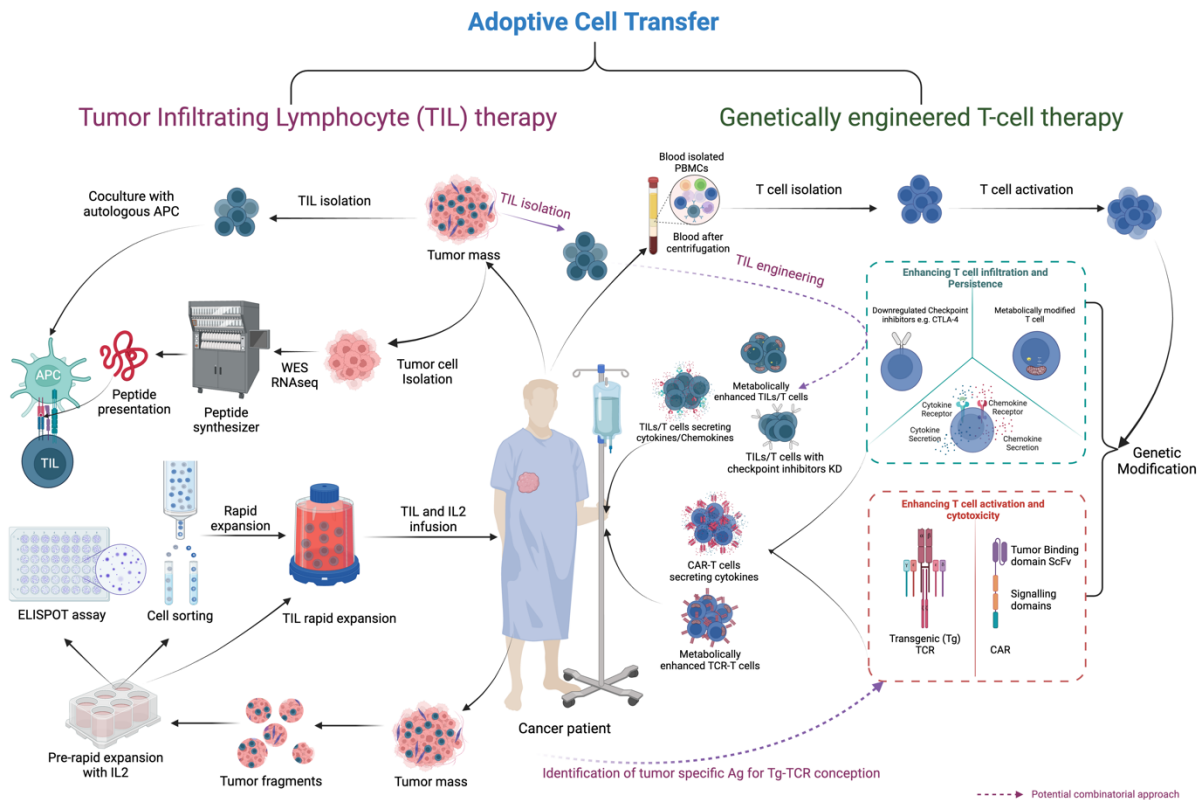


Figure 4: Strategies for ACT therapy: TIL versus gene therapy.

Left; TIL therapy englobes TIL extraction followed by their *in vitro* expansion using both pre-rapid and rapid expansion methods. TILs can also be primed through autologous APCs presenting peptides derived from tumor cells. right; Gene therapy includes strategies to augment T-cell infiltration and persistence as well as activation and cytotoxicity. These include engineering T-cells to express cytokines, enhancing their metabolic fitness, and downregulating checkpoint inhibitors. To specifically target cancer cells, T-cells can be engineered to express CARs or TCRs. Combinatorial methods are also used to further enhance T-cell fitness and tumor-killing capacity. (Adapted from ²²⁰).

3.1.2.1. CAR-T-cell therapy:

CAR-T-cell therapy employs genetically engineered T-cells to express chimeric antigen receptors, thereby specifically targeting cancer cells. The CAR comprises an antigen-binding domain specific for a tumor-associated antigen and a signaling domain that activates the T-cell when the antigen is encountered. This innovative treatment has shown impressive clinical success, particularly in treating hematological malignancies, and has also shown progressive clinical improvements against solid tumors ²¹⁴. This success is attributed to precise targeting that spares healthy cells, long-lasting antitumor activity, and a possible "bystander effect" resulting in the extended elimination of even untargeted cancer cells ²³⁷. Gross, Eshhar, et al. first proposed CAR-T-cell therapy in the late 1980s ²³⁸. This study led to its successful clinical trial in 2010, targeting CD19+ B cell leukemia and lymphomas with a complete remission rate of 90% ²¹¹. Since then, subsequent CAR-T-cell therapies targeting various antigens have demonstrated promising outcomes.

CAR-T-cells are differentiated into various generations according to the composition and signaling domains of the CAR. The first-generation CARs have a single signaling domain, typically the CD3 zeta (CD3ζ) chain, that triggers T-cell activation upon antigen detection, albeit with restricted efficacy and susceptibility to T-cell exhaustion *in vivo*. Overcoming these limitations involved the incorporation of extra costimulatory domains like CD28 or 4-1BB into the CAR structure or integrating inhibitory domains to thwart T-cell exhaustion, leading to the creation of second-generation CARs. These second-generation CARs facilitate both T-cell activation and costimulation upon antigen detection, improving CAR-T-cell function and persistence *in vivo* ^{214,222,239}. Despite this, T-cell exhaustion remains an issue, impeding their long-term effectiveness.

Consequently, third-generation CARs emerged from augmenting the second-generation models with additional costimulatory domains, modifying the relative signaling strength, or incorporating novel signaling domains. The third-generation CARs, with typically two costimulatory domains and the CD3 ζ chain, enhance T-cell activation and persistence *in vivo* compared to their predecessors. A recent study has demonstrated that a CAR with a CD28 costimulatory domain and a 4-1BBL signaling domain effectively treated relapsed or refractory MM²¹¹. Further, a third-generation CAR with a 4-1BB and an ICOS costimulatory domain displayed enhanced antitumor activity against solid tumor models²⁴⁰. The fourth-generation or TRUCKs (T-cells redirected for universal cytokine killing) are engineered to boost CAR-T-cell function by promoting cytokine secretion or other effector molecules (Perforin, granzyme, Fas-L, and TNF-related apoptosis-inducing ligand (TRAIL)) upon antigen recognition besides providing potent T-cell activation and costimulation^{241,242}. Fifth-generation CARs, currently under development, are based on the second-generation but include a truncated cytoplasmic IL-2 receptor β -chain domain and a binding site for the transcription factor signal transducer and activator of transcription 3 (STAT3)²⁴¹ (**Figure 5**).

While CAR-T-cell therapy has shown promising results, it also introduces several complexities. These include refining the CAR structure to augment its function and curtail off-target toxicity, managing risks associated with insertional mutagenesis during the viral vector delivery of the CAR, identifying cancer cell-specific target antigens, and formulating strategies for efficient and stable CAR expression in T-cells^{239,243,244}. The potential side effects, such as cytokine release syndrome (CRS) and neurotoxicity, also pose significant issues²⁴⁵.

To address the emerging challenges, contemporary research endeavors include the development of dual-targeting CAR-T-cells, universal CAR-T-cells, innovative CAR designs for enhanced safety, and integration of CAR-T cells into other cancer therapies (**Figure 5**). For example, CAR-T-cells that concurrently target CD19 and CD22 effectively addressed refractory B-cell acute lymphoblastic leukemia²⁴². Meanwhile, 'switchable' CAR-T-cells, such as Stop-CARs, On Switch-CARs, or Split CARs, can be toggled on or off using a small molecule, providing superior therapeutic control²⁴⁵⁻²⁴⁷. Additionally, research has underscored the advantages of combining CAR-T therapies with other treatments like radiotherapy, chemotherapy, or checkpoint inhibitors, leading to improved patient outcomes²⁴⁸.

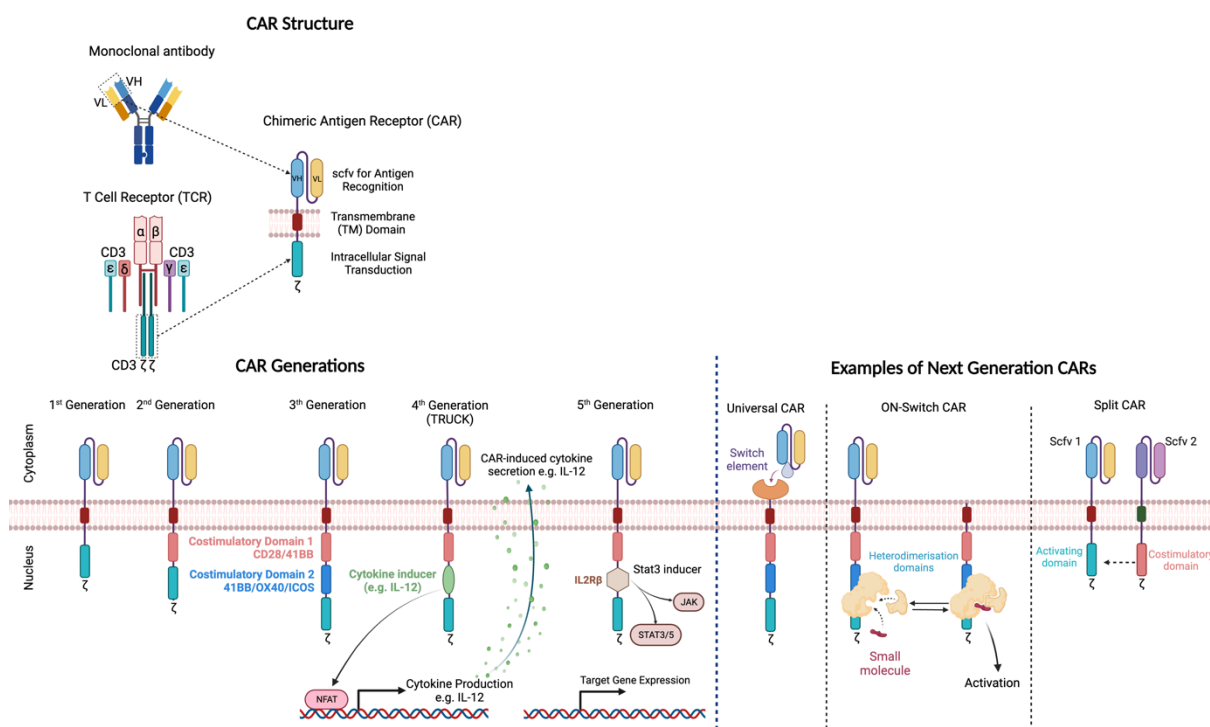


Figure 5: CAR structure, generation, and novel designs.

Top; CAR general structure displays key components, including the antigen-binding domain, hinge, transmembrane domain, and intracellular signaling domain. Bottom left; CAR generations, namely 1st, 2nd, 3rd, 4th, and 5th generations, outline the progression and distinct features regarding costimulatory domains and signaling modules. Bottom right; Next-generation CAR designs provide examples of advanced designs for CARs aimed at enhancing T-cell activation and safety of CAR-T-cell therapies.

3.1.2.2. TCR-T-cell therapy:

TCR-T-cell therapy involves engineering a patient's T-cells to recognize and bind to cancer-specific peptide-MHC (pMHC) complexes, thereby enabling T-cells to eliminate cancer cells. Several types of TCRs are used for gene engineering TCR-T-cell therapy, including primarily natural TCRs and affinity-optimized (or transgenic) TCRs. Naturally occurring TCRs can be obtained and cloned for gene-engineering methodologies. These include TCRs targeting NY-ESO-1 and MAGE-A3, both are cancer-testis antigens present in numerous solid tumors and hematological malignancies. These TCRs have been applied in clinical trials to treat advanced cancers, such as melanoma^{225,249-251}. Another example is the Wilms tumor protein 1 (WT1), a TAA that is displayed in multiple malignancies but is minimally expressed in normal cells. Preliminary studies indicate the efficacy of WT1-targeted TCR-T-cell therapy in treating acute myeloid leukemia (AML) and solid tumors, including ovarian cancer²⁵²⁻²⁵⁴.

Conversely, transgenic TCRs are designed or altered TCRs to recognize TSAs with high affinity and a reduced risk of cross-reactivity. These TCRs recognize exclusively tumor-expressed antigens, such as neoantigens or viral-derived oncoproteins²⁵⁵. Cancer neoantigens make the target antigen highly patient-specific since they arise from cancer-specific genetic alterations²⁵⁶⁻²⁵⁸. Nevertheless, some neoantigens, shaped by prevalent oncogenic mutations, may be common across individuals. Moreover, since conventional $\alpha\beta$ -TCR-based T-cell therapies are MHC/human leukocyte antigen (HLA) restricted, this can limit their applicability to a small pool of patients with the matching HLA allele. Nonetheless, TCR-T-cell therapies targeting these neoantigens are advantageous due to their specific tumor targeting, superior TCR affinity, diminished likelihood of tumor evasion, and reduced "off-tumor" effects and associated toxicity. However, the process of identifying these neoantigen TCRs is intricate and necessitates the utilization of high-throughput screening methods.

Engineered TCR-T-cells can also encounter a major challenge of MHC expression reduction or loss on tumor cells, serving as an evasion strategy from T-cell targeting^{259,260}. To address this, research has shifted toward creating T-cells with MHC-independent TCRs, such as gamma-delta ($\gamma\delta$) TCRs and natural killer T (NKT) cell TCRs, aiming for more precise and safer cancer immunotherapy. $\Gamma\delta$ TCRs are unique for their broad antigen recognition, including those that are not MHC-presented. For instance, V δ 1-J δ 1 TCR can detect the stress-responsive major histocompatibility complex class I chain-related gene a and b (MICA/B) protein present in various tumor cells. Conversely, NKT-cell TCRs, which are semi-invariant in nature, recognize glycolipid antigens presented by the non-polymorphic MHC class I-like molecule CD1d. These TCRs have been harnessed for TCR-T-cell engineering, either by modifying the TCR structure or incorporating additional signaling domains.

T-cell-activating conjugates (TACs) and T-cell receptor fusion constructs (TRuCs) also present alternative strategies for mitigating MHC restriction and leveraging physiologic $\alpha\beta$ -TCR signaling for improved tumor-targeting. TACs are bispecific antibodies facilitating tumor cell destruction by linking T-cells to tumor cells through simultaneous recognition of a specific tumor antigen and activation of the TCR complex on T-cells. TRuCs, however, are engineered TCRs that combine a TCR's tumor antigen specificity with the signaling domains of a costimulatory receptor such as CD28 and 4-1BB, thereby enabling T-cell direct activation and eliminating the requirement for additional signals from antigen-presenting cells (**Figure 6**). Despite their early development phase, both approaches have exhibited potential in preclinical studies to effectively redirect T-cells toward tumor cells.

Engineering transgenic TCR-T-cells for ACT demands careful consideration of TCR affinity and avidity, which define the binding strength between the TCR and the antigen. TCR affinity, denoted by the dissociation constant (K_d), measures the interaction's strength between a T-cell and a corresponding site on a cancer cell's MHC molecule²⁶¹. Avidity, on the other hand, accounts for the collective interaction strength among multiple binding sites. In the genetic engineering of TCR-based T-cells, affinity can be enhanced and tuned to meet specific needs^{262,263}. Additional techniques to improve TCR-T-cell therapy include avoiding mispairing of α and β chains of endogenous and transgenic TCRs^{262,264,265} (**Figure 6**), co-transferring the entire CD3 signaling domain with the transgenic TCR²⁶⁶, and exploring methods for developing MHC II-restricted TCR expressing CD4+ T-cells. Consistent with this approach, CD4+ T-cells redirected with a class I-restricted TCR and transgenic CD8 $\alpha\beta$ (TCR8) have shown cytotoxic activity while preserving their CD4+ lineage features²⁶⁷⁻²⁶⁹.

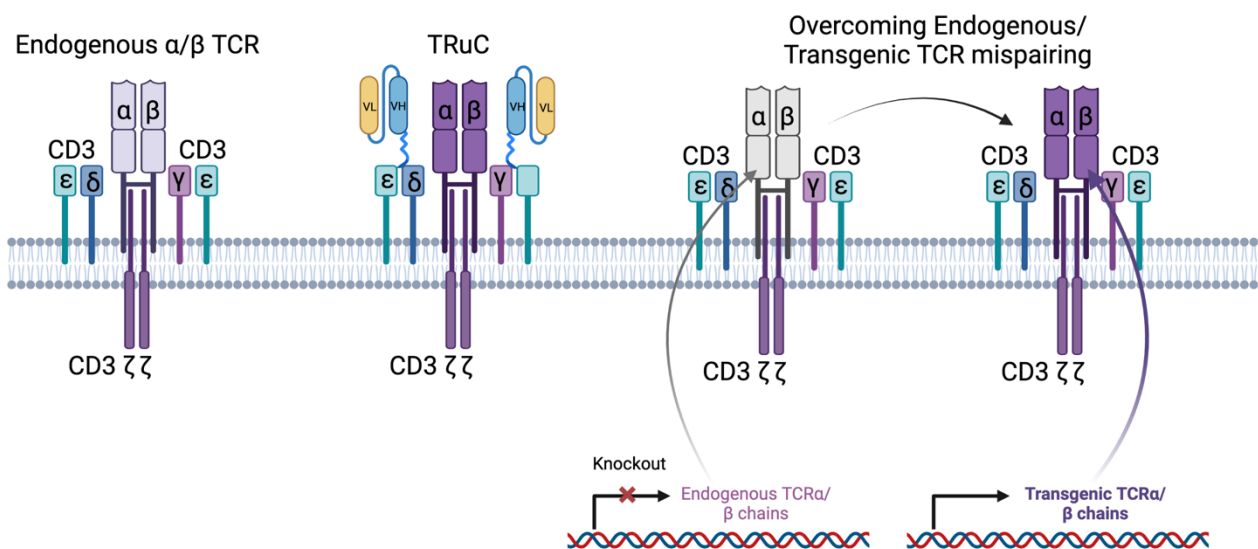


Figure 6: Engineering strategies for TCR-T-cell therapy.

TCR signaling mediated by the interaction of the alpha and beta chain of endogenous TCR with MHC complex can be further enhanced by engineering T-cell with T-cell receptor fusion construct (TRuC) harboring tumor antigen specificity and costimulatory receptor signaling domains. The strategy of knockout deployed to delete the endogenous alpha and beta chains of the endogenous TCR is an efficient method to prevent chain mispairing between endogenous and transgenic TCRs, thereby ensuring the efficacy and safety of TCR gene therapy.

3.1.2.3. Gene editing technologies

Genome-editing technologies have been widely used to modify the DNA sequence of specific genes in a precise and targeted manner. Each tool has its own mechanism and advantages for gene editing. Transposons, movable DNA sequences within the genome, facilitate site-specific integration in non-viral cellular engineering enabling stable gene cargo delivery^{270,271}, including co-delivery of multiple genes²⁷² with minimal genotoxicity²⁷³. This system involves a transposase enzyme binding to terminal inverted repeats (TIRs) to mobilize flanked DNA²⁷⁴.

- **Transposons:** Transposon-modified human T-cells, specifically using a sleeping beauty (SB) DNA transposon, have been assessed in preliminary clinical trials for CAR T-cell therapy^{275,276}. However, this method's effectiveness is constrained by the low efficiency of plasmid DNA delivery into human cells²⁷⁷ and its limitation to only introducing and adding a transgene into a cell (**Figure 7**).
- **Zinc-finger nucleases (ZFNs):** They consist of engineered proteins that comprise a zinc-finger DNA-binding domain recognizing a specific DNA sequence and a FokI endonuclease domain that functions as a dimer; thus, a pair of ZFN is required to cleave the DNA at the target site²⁷⁸. The break is repaired by

endogenous nonhomologous end joining (NHEJ) or homologous recombination (HR) mechanisms²⁷⁹. An NHEJ can result in small insertions (knockin (KI)) or deletions (KO) in the form of indels, while an HR can replace a gene²⁸⁰. ZFNs have the advantage of being highly efficient and specific, which can minimize off-target effects^{281,282}. Moreover, due to their small size, ZFNs can ensure effective transgene delivery for successful cancer therapy²⁸³. However, the design and production of ZFNs can be laborious and costly as proteins must be engineered specifically for each target in the genome²⁷⁹. In addition, they can be immunogenic and may trigger immune responses in the host (**Figure 7**).

- **Transcription activator-like effector nucleases (TALENs):** Similar to ZFNs, they consist of a non-specific FokI endonuclease domain and a DNA-binding domain that contains a highly conserved repeat sequence from transcription activator-like effectors (TALEs)²⁸⁰. TALEs are modular protein domains designed to recognize specific DNA sequences²⁸⁴. TALENs have the advantage of being highly specific and efficient and can be used to target a wide range of DNA sequences. Unlike ZFNs, TALENs can be easier to design and optimize, but their large size renders the delivery of gene cargo difficult²⁸⁰. They can still have off-target effects and may not work in some cell types or organisms. Still, clinical trials have used the TALEN platform to develop universal allogeneic T-cells that can be used for cancer treatment²⁸⁵ (**Figure 7**).
- **CRISPR/CRISPR-associated protein 9 (Cas9):** CRISPR/Cas9 is a revolutionary genome-editing technology that uses the bacterial immune system to target and cleave specific DNA sequences. The CRISPR system consists of a small single-stranded guide RNA (sgRNA) to direct the Cas9 nuclease to a specific DNA sequence, creating a double-strand break that can be repaired by the cell's endogenous DNA repair machinery²⁸⁶. The sgRNA can be easily designed and synthesized to target virtually any gene of interest, either for gene KO, KI, or regulation. By targeting control elements such as promoters or enhancers, CRISPR/Cas9 allows gene modulation without fully disabling it. Additionally, it can increase gene expression by introducing a transcriptional activator to the gene's promoter region. CRISPR/Cas9 can be delivered in diverse formats such as plasmid DNA, ribonucleoprotein complexes (RNPs), or messenger RNA (mRNA)^{287,288}. The sgRNA is typically delivered separately via lentiviral vectors for stable expression^{285,286}. However, it can also introduce off-target effects, anti-Cas9 responses, and unwanted mutations, which raise concerns of potential tumor malignancy promotion²⁷⁴, and renders *in vivo* delivery complicated due to the simultaneous introduction of several components²⁸⁵. Nevertheless, because of its simplicity, efficiency, specificity, and versatility, CRISPR/Cas9 system has been preferred for T-cell engineering in clinical trials^{285,289}, and has become the most widely used gene editor in various organisms, including humans²⁸⁰ (**Figure 7**).

Overall, each genome-editing technology possesses unique strengths and weaknesses, and the selection depends on the required precision, efficiency, and specificity for different applications (**Figure 7**).

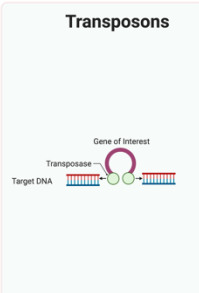
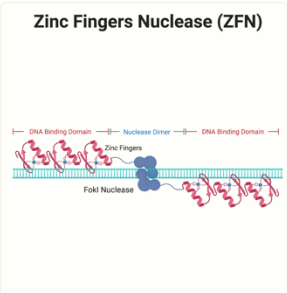
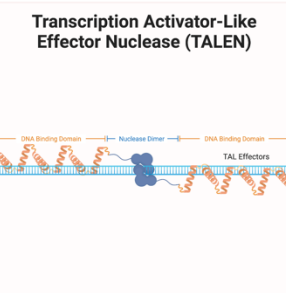
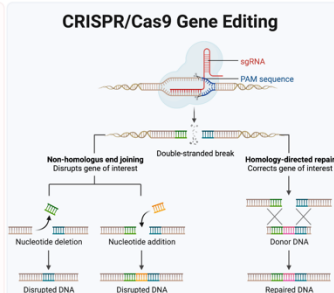
	 Transposons	 Zinc Fingers Nuclease (ZFN)	 Transcription Activator-Like Effector Nuclease (TALEN)	 CRISPR/Cas9 Gene Editing
Efficiency	Moderate	High, Moderate	Low	Low
Integration	Yes, random	Yes, site specific	Yes, site specific	Yes, site specific (less than ZNF and TALEN)
Stability of gene expression	Stable	Stable	Stable	Moderate
Cargo	High capacity, Suitable for co-delivery of multiple genes	Specific protein design required for each gene target	Specific protein design required for each gene target	High capacity
Toxicity/Off-target effect	Low genotoxicity Less toxic than viral transduction	Few off-target effects	Few off-target effects	Risk off-target effects mutagenesis and immunogenicity
Manufacturing	Not for human delivery, Moderate cost	High cost	High cost	Suitable for large-scale manufacturing High Cost

Figure 7: Comparative overview of major gene editing technologies.

Evaluation of four major gene editing technologies, namely transposons, ZFNs, TALENs, and CRISPR/Cas9 systems, for key parameters including efficacy, integration, and stability of gene insertion, toxicity, cargo capacity, and manufacturing process. Each technology is represented by a separate column along with its characteristics. (Adapted from ^{280,286}).

3.1.2.4. Gene editing delivery methods

T-cell gene engineering is a promising approach to cancer therapy. There are two main approaches to T-cell gene engineering: non-viral and viral ²⁷⁶. Viral approaches, such as CAR T-cell therapy, have shown success in clinical trials, while non-viral approaches offer a simpler and safer alternative for gene editing.

- Non-Viral approaches involve chemical or physical methods to deliver genes into T-cells without viral vectors. Transfection and electroporation are the most common methods to introduce DNA into T-cells. Transfection entails using chemical agents, such as lipids, to facilitate the entry of exogenous DNA used to deliver genes into T-cells. Conversely, electroporation requires exposing T-cells to pulsed high-voltage electrical currents, which creates small pores in the cell membrane that allow nanometer-sized plasmid DNA or mRNA to enter the cell transiently. These techniques enable gene replacement or disruption in T-cells, providing a means for delivering genes. ^{280,286}. Unlike viral transduction, this method offers distinct advantages, including a large cargo capacity to facilitate multiple genes or nucleic acid delivery ²⁹⁰. Although electroporation is broadly used, for instance in CRISPR-Cas9 system delivery and has entered phase I clinical trial to evaluate DNA vaccine against SARS-CoV-2 ²⁹¹, it is still not well validated for *in vivo* T-cell delivery because of its limited penetration depth and localized administration ²⁹². In addition, the high voltage used for electroporation could cause a loss of cytoplasmic content and raise the risk of cytotoxicity when used for *ex vivo* studies in addition to affecting the expression profile in the cell ²⁹³⁻²⁹⁵. Among the significant constraints faced when using this delivery method is the need for more commercial machines designed for large-scale manufacturing rather than for research and development. One of the developed techniques for electroporation is nucleofection which can deliver the transgene directly into the nucleus without disrupting the nuclear envelope. Similar to conventional electroporation, nucleofection still faces the same challenges regarding *in vivo* use. However, it holds promise for *ex vivo* T-cell gene engineering ²⁹⁶ (**Figure 8**).

- Viral transduction is an adopted method to efficiently deliver the transgene in T-cells using viral vectors derived from engineered viruses that are naturally able to deliver their genetic material into host cells efficiently²⁸⁰. Viral vectors are a common tool used for gene engineering T-cells to redirect them against cancer cells or deliver therapeutic genes to tumor cells for their destruction²⁹⁷. While adenoviruses and adeno-associated viruses can introduce transient expression of the transgene, gamma-retroviruses and lentiviruses can integrate into the host genome to enable stable gene expression and are the most common vectors for T-cell gene delivery due to their high transduction efficiencies leading to long-term gene expression, notably for CAR/TCR-T-cells or cytokine secretion^{280,285,286}. To this date, this tool has also been developed to make it suitable for applications beyond conventional systems as it has expanded to include other gene editing systems such as CRISPR-Cas9 and ZFN for *ex vivo* studies to inhibit specific genes for enhanced T-cell function^{287,298} (**Figure 8**).

Lentiviruses and retroviruses are types of RNA viruses exploited for gene engineering in T-cells to develop cancer therapies. Despite their similarities, they harbor significant differences that can influence their effectiveness and safety for gene therapy. Their primary disparity lies in tropism, or the types of cells they can infect. Lentiviruses, including HIV, can infect dividing and non-dividing cells, facilitating long-term gene expression^{286,299}. However, their safety profile is a concern, as lentiviruses, especially HIV, carry a higher risk of adverse effects due to potential reactivation and the risk of insertional mutagenesis. This occurs when the viral vector integrates into a gene and disrupts its normal function, potentially leading to cancer, viral replication, and dissemination²⁴⁵.

Conversely, retroviruses only infect dividing cells, posing limitations for certain uses such as TIL engineering^{285,300}. Transitioning from the limitations of viral vectors, the intricacies of gene engineering are further complicated when introducing two separate genes into T-cells. Gene delivery and expression in T-cells containing two different genes entail challenges around gene elements' size, regulation, and compatibility. Difficulties also arise when delivering large DNA constructs with multiple genes in a single vector, potentially reducing transduction efficiency (TE) and gene expression levels³⁰¹. Additionally, co-expression of several genes may cause off-target effects and toxicity, including insertional mutagenesis²³⁹.

Moreover, cross-regulation of different gene cargos may complicate the tight regulation necessary for optimal therapeutic outcomes. For example, the expression of certain cytokines or checkpoint inhibitors may need to be temporally regulated to prevent excessive T-cell activation and potential toxicities, as well as potentially affecting the efficacy of the CAR^{245,247,297,302}. Thus, balancing the expression levels of the gene cargo is essential to amplify synergistic effects and prevent adverse interactions. Furthermore, overexpression of multiple gene cargos may exhaust or impair T-cells due to increased metabolic demands, reducing the *in vivo* persistence and efficacy of the engineered T-cells³⁰³.

To address these issues, strategies have been developed, such as optimizing DNA constructs for dual gene expression, using smaller gene elements to decrease the DNA construct size, and incorporating costimulatory domains in the CAR. The application of inducible promoters and gene switches can help regulate gene cargo expression based on the T-cell activation state³⁰⁴⁻³⁰⁶.

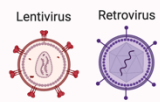
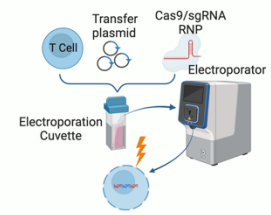
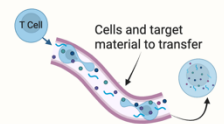
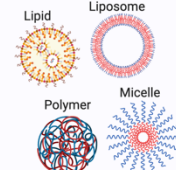
	Viral transduction 	Electroporation 	Cell squeezing 	Nanoparticles 
Efficiency	High	High, Moderate	Moderate, low	Moderate, low
Integration	Yes, random	Yes, random Limited penetration depth in vivo	No	No
Stability of gene expression	Stable or transient (Constitutive or inducible expression)	Stable or transient (Constitutive or inducible expression)	Minimal effect on transcriptional responses	Moderate
Cargo	Limited, Not suitable for co-delivery of multiple genes	Suitable for delivering multiple genes or nucleic acids	Suitable for delivering multiple genes or nucleic acids	Highly customizable, Can be designed for targeted delivery
Toxicity	Risks of genotoxicity due to mutagenesis Safety concerns for clinical applications	Risk of cytotoxicity due to high voltage	Risk of cytotoxicity Not suitable for in vivo applications	Low cytotoxicity, Risks of liver and spleen toxicity Suitable for ex vivo and in vivo applications
Manufacturing	Suitable for large-scale manufacturing High cost	Not suitable for large-scale manufacturing Moderate cost	Not suitable for large-scale manufacturing Moderate cost	Not suitable for large-scale manufacturing Low Cost

Figure 8: Gene editing delivery methods

Overview of major gene editing delivery tools, both viral and non-viral. Viral delivery tools involve the usage of lentiviruses or retroviruses, while non-viral approaches include electroporation, cell squeezing, and nanoparticles. Key parameters for comparison are highlighted, such as efficacy, integration, stability of gene insertion, toxicity, cargo capacity, and manufacturing complexity. Each technique is represented by a separate column along with its characteristics. (Adapted from ^{280,286}).

3.1.2.5. Gene inhibitory strategies

Suppressing the activity of inhibitory molecules or receptors on effector immune cells, such as PD-1/PD-L1, CTLA-4, TIM-3, and LAG-3, has emerged as a promising strategy to enhance T-cell-mediated cancer therapy that has shown promising results in preclinical and clinical studies ^{280,298}. Similar to ZFN and TALEN, there are other gene editing approaches for disrupting or knocking down the expression of a gene in T-cells for cancer treatment, including RNA interference (RNAi) and CRISPR/Cas9 ^{239,280,307}.

siRNA, shRNA, and miRNA for gene knockdown:

RNAi is a powerful gene silencing mechanism that targets and degrades specific mRNA transcripts of the gene of interest, thereby knocking down a gene expression in T-cells for cancer treatment ^{308,309}. There are different RNAi technologies, including small interfering RNA (siRNA), short hairpin RNA (shRNA), and miRNA, that involve different cellular machinery, including different RNA polymerases and RNA processing enzymes ³¹⁰ (**Figure 9**).

siRNA are short double-stranded RNA molecules that target a specific mRNA transcript of the corresponding gene expression. This leads to its degradation and subsequent KD mediated by the RNA-induced silencing complex (RISC). siRNA-mediated gene KD is transient, as siRNAs are rapidly degraded by cellular nucleases. Still, siRNAs are easy to design and deliver and have been widely used for gene KD in T-cells and in cancer cells to silence genes known to contribute to cancer development and progression ^{310,311}.

On the other hand, shRNAs are transcribed from a DNA vector using RNA polymerase III (Pol III). They are processed by Drosha machinery in the nucleus to generate a hairpin-shaped precursor miRNA (pre-miRNA),

which is then exported to the cytoplasm and further processed by Dicer to generate the mature siRNA-like molecules. The mature shRNA molecules are then loaded onto the RISC complex for targeting specific mRNA degradation³¹⁰⁻³¹² (**Figure 9**). shRNA-mediated gene KD is more stable than siRNA-mediated KD, as shRNAs are expressed from a plasmid or viral vector and can persist in cells for extended periods of time. However, shRNAs can have off-target effects and may trigger immune responses³¹².

Another approach for gene inhibition involves miRNAs which are small non-coding RNA molecules that regulate gene expression via the cellular machinery. This machinery is responsible for miRNA biogenesis, involving Drosha and Dicer enzymes. Endogenous miRNAs are transcribed from endogenous genes by RNA polymerase II (Pol II). The primary transcript is then processed by Drosha in the nucleus to generate a pre-miRNA hairpin. The pre-miRNA is then exported to the cytoplasm and further processed by Dicer to generate a mature miRNA duplex. One strand of the duplex is loaded onto the RISC complex for target mRNA transcript degradation. The mature miRNA within the RISC guides the complex to target mRNAs by complementary base pairing, usually to the 3' untranslated regions (UTRs). This can result in either translational repression or mRNA degradation, depending on the degree of complementarity between the miRNA and its target. In general, perfect or near-perfect complementarity leads to the cleavage of the target mRNA by the Argonaute 2 (AGO2) protein, which is a key component of RISC with a cleavage activity. On the other hand, imperfect complementarity results in translational repression and, often, subsequent mRNA degradation.^{310,313} (**Figure 9**).

There are several advantages of using miRNA-mediated gene KD over shRNA, including that miRNA can target multiple genes simultaneously, whereas shRNAs typically target a single gene³¹⁰. This feature makes miRNAs more suitable for studying complex biological processes that involve multiple genes or pathways. Furthermore, miRNAs are naturally occurring, and non-coding RNAs are involved in the endogenous regulation of gene expression. Thus, they may better mimic physiological gene regulation than shRNAs, which are artificially introduced. Moreover, miRNAs are generally better tolerated by cells and have fewer off-target effects than shRNAs as they act through partial complementary base pairing with their target mRNA. This results in more specific and controlled gene silencing. miRNAs could also be of low cytotoxicity as they are less likely to trigger an immune response or cause cytotoxicity compared to shRNAs, as they are naturally occurring molecules and part of the cellular machinery. Some miRNAs have tissue-specific or developmentally regulated expression patterns, making them suitable for studying gene function in a specific cellular context or developmental stage^{311,312,314} (**Table 1**).

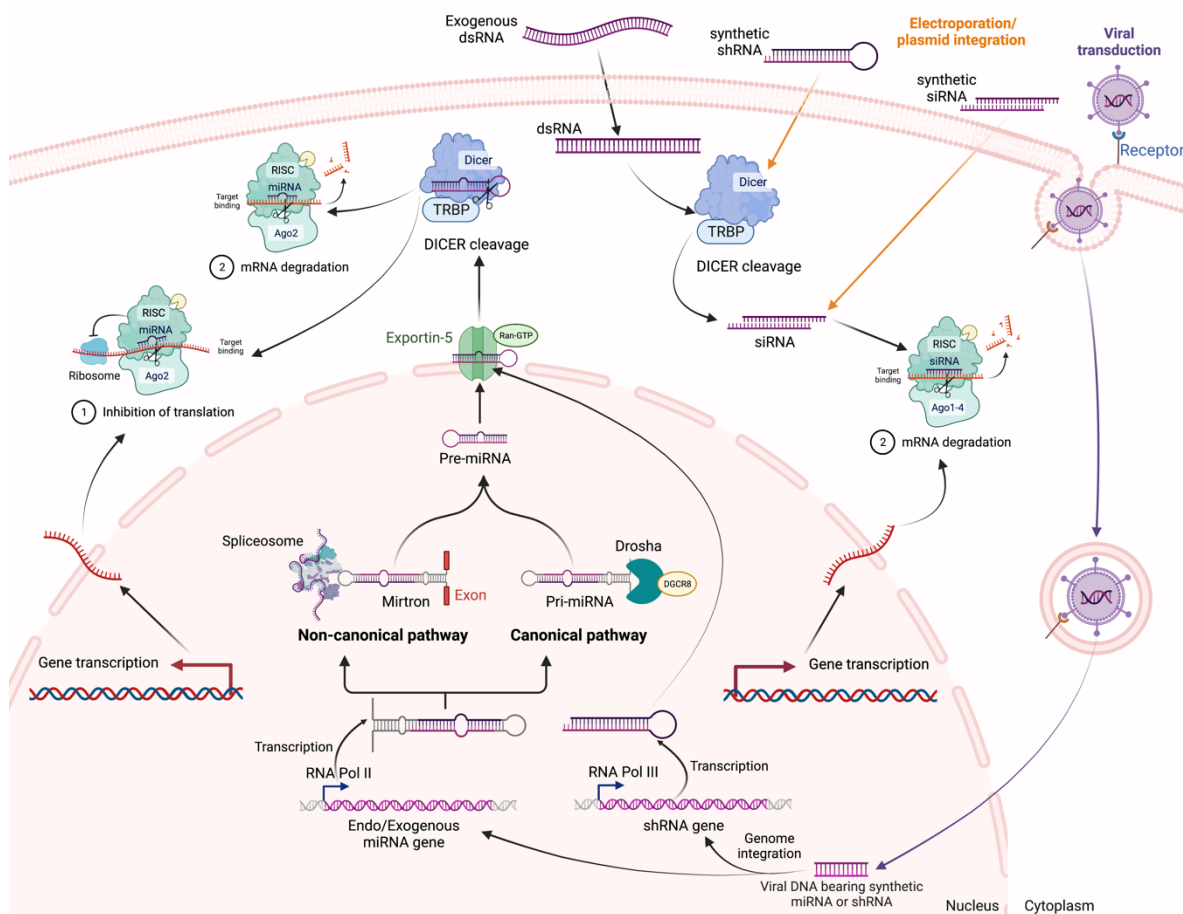


Figure 9: Cellular processing machinery of miRNA versus shRNA versus siRNA.

The transcription of miRNAs, whether from within the cell or transferred through viral vectors, starts with RNA Polymerase II, producing primary miRNAs (pri-miRNAs). The non-canonical pathway involves mirtrons, which are introns mimicking the hairpin structure of pre-miRNAs. Mirtrons skip the Drosha processing step and resemble pre-miRNAs after splicing and debranching. They are then exported to the cytoplasm for further processing by Dicer and incorporation into the RISC complex. In the canonical pathway, pri-miRNAs are cleaved within the nucleus by the Drosha-DiGeorge critical region-8 (DGCR8) complex, creating pre-miRNAs in a hairpin conformation. Exportin-5 translocates the pre-miRNAs into the cytoplasm. In the cytoplasm, the DICER complex, with the help of the transactivation response element RNA-binding protein (TRBP), processes the pre-miRNAs, generating miRNA duplexes. The guide strand integrates into the RISC complex with the Ago2 protein, regulating target mRNAs through degradation or translational inhibition. The passenger strand is usually degraded. Exogenous shRNAs, introduced via viral vectors, undergo a similar biogenesis process to miRNAs, but they are synthesized by RNA Polymerase III, bypassing the Drosha step. Instead, shRNA is directly exported to the cytoplasm by Exportin-5. In the cytoplasm, shRNA is processed by Dicer and incorporated into the RISC complex, resembling miRNA processing stages. Upon cellular introduction, Dicer cleaves exogenous dsRNAs or synthetic shRNAs delivered by non-viral tools, guiding the RISC complex to target mRNAs. On the other hand, synthetic siRNAs, similar to Dicer cleavage products, bypass Dicer processing and load directly into the RISC complex. Although these molecules have distinct processing routes, they converge in utilizing the RISC complex for post-transcriptional gene silencing.

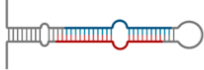
CRISPR/Cas9-mediated gene knockout

CRISPR/Cas9 can be used to create a loss-of-function mutation in the target gene by the KO or by introducing a specific mutation by KI approaches. By designing guide RNAs that target specific sites in the genome, the Cas9 nuclease can be directed to cut the gene of interest resulting in a double-strand break (DSB) at the target site. The DSB can then be repaired by the error-prone NHEJ pathway. Consequently, this leads to a frameshift mutation and a loss of gene function, such as the deletion of PD-1 in T-cells that resulted in enhanced function and tumor clearance^{285,298,307}. CRISPR/Cas9 can also be used to introduce a specific mutation into the target gene, altering its function or expression. This strategy has been used to insert CARs for adoptive T-cell therapy where a specific tumor-targeting domain is introduced into the TCR locus^{285,289,307}.

In summary, these gene editing strategies provide promising opportunities for inhibiting suppressive genes in T-cell-based cancer therapy. The choice of the suitable strategy depends on the specific application and the desired level of KD efficiency, stability, and safety with reduced off-target effects.

Furthermore, building upon these advancements, harnessing gene editing tools such as RNA interference or CRISPR-Cas9 to target and inhibit specific intracellular TCR signaling negative regulators emerges as a potential avenue to selectively modulate and KD the activity or expression of suppressive genes in T-cell-based cancer therapy. This presents a potential approach to fine-tune TCR signaling and amplify the antitumor response of T-cells by relieving the inhibitory checkpoints on T-cells imposed by these regulators. However, selecting the appropriate gene editing strategy must be carefully considered and tailored to the specific application requirements.

Table 1: Comparison of siRNA, shRNA, and miRNA characteristics.

	siRNA 	shRNA 	miRNA 
Full name	Small interfering RNA	Short hairpin RNA	microRNA
Origin	Exogenous, Synthetic	Exogenous, Synthetic	Exogenous and endogenous
Length	21-25nt	60-80nt	19-25nt + flanking sequences
Target site binding	High	Moderate	Moderate-Low
Hairpin structure	Absent	Present	Present
Delivery	Transfection or electroporation	Plasmid, viral vector	Endogenous or vector delivery
Promoter	N/A (Synthetic RNA)	Mainly Pol III (U6, H1), Pol II (CMV, EF1 α)	Pol II (Endogenous miRNA), Pol II/III (Exogenous miRNA)
Processing Machinery	RISC complex	DICER, RISC complex	Drosha, DICER, RISC complex
Stability	Transient	Stable	Stable
Efficiency	Efficient at a high dose	Efficient at a low dose	Efficient at a low dose
Off-target effect	High off-target effect	Moderate off-target effect	Low off-target effect
Gene silencing mode	mRNA Cleavage	mRNA Cleavage	mRNA Cleavage/ translational repression
Toxicity	Moderate	High (Saturation of miRNA biogenesis machinery)	Low

4. Intracellular negative regulators downstream of the TCR signaling pathways.

4.1. TCR signaling pathway:

The TCR signaling system is a complex network of intracellular pathways that are activated when the TCR binds to an antigen presented by the antigen-MHC complex on the surface of an APC. This triggers a series of intracellular signaling events involving tyrosine kinases, phosphatases, and adaptor proteins, leading to the activation of transcription factors and, ultimately, T-cell activation, differentiation, proliferation, and survival.

Dysregulation of this pathway can cause immune-related disorders such as autoimmune diseases and immunodeficiencies. The TCR is a heterodimeric protein complex composed of α and β chains, or γ and δ chains, associated with intracellular signaling proteins. The TCR associates with the CD3 receptor to transmit the signal, forming a functional TCR-CD3 complex^{315,316}. The CD3 receptor consists of CD3 γ and CD3 δ heterodimers and a CD3 ζ homodimer containing immunoreceptor tyrosine-based activation motifs (ITAM) that activate signaling³¹⁷.

An immunological synapse (IS) is triggered upon encountering a specific antigen, causing the TCR complex to change shape and initiate a signaling cascade. This process involves the co-receptor CD4+ or CD8+ interacting with the MHC molecules on the APC to stabilize the TCR-antigen interaction. Costimulatory receptors like CD28 are also activated by ligands on APCs (CD80 (B7-1) or CD86 (B7-2)), providing the necessary co-stimulation for T-cell activation.

The conformational change in the TCR complex activates protein tyrosine kinases (PTKs), such as lymphocyte-specific protein tyrosine kinase (Lck) and Fyn, which phosphorylate ITAMs on CD3 ζ chains. Phosphorylated ITAMs serve as docking sites for downstream kinases ZAP-70 and Syk, which in turn phosphorylate other signaling molecules, including adapter proteins LAT and leukocyte protein of 76 kDa (SLP-76). These proteins form a complex that recruits additional signaling molecules like phospholipase C γ 1 (PLC γ 1), Vav, and Growth Factor Receptor-bound protein 2 (Grb2). PLC γ 1, when activated, cleaves the membrane lipid phosphatidylinositol-4,5-bisphosphate (PIP2) into the second messenger inositol 1,4,5-trisphosphate (IP3) and diacylglycerol (DAG)³¹⁸. IP3 binds to receptors on the endoplasmic reticulum (ER), releasing intracellular calcium ions into the cytoplasm. The calcium influx activates calcineurin, dephosphorylating the transcription factor NFAT, enabling it to translocate to the nucleus and activate target genes. Meanwhile, DAG activates downstream signaling pathways such as protein kinase (PKC), I κ B kinase (IKK) (in a MALT1-CARMA1- B-cell lymphoma/leukemia 10 (BCL10)-dependent pathway³¹⁹, RAS guanyl nucleotide-releasing protein 1 (RasGRP1), Ras-ERK, activator protein-1 (AP-1), and NF- κ B³¹⁹⁻³²².

The Ras/MAPK pathway, along with the PI3K/Akt, NFAT, and the NF- κ B pathways, cooperate to initiate the T-cell activation transcriptional program, resulting in cytokine production and T-cell activation as exhibited by the upregulation of the activation marker CD69^{323,324}. Taking together, TCR engagement leads to intracellular signals that differentiate between antigens with different affinities. Hence, as a counterpart, negative signaling loops are crucial for maintaining a threshold for T-cell activation³²⁵. These loops interact with regulatory molecules to modulate immune activation, allowing tolerance to self-antigens while eliciting a response to foreign antigens³²⁶. TCR negative regulators, including molecules such as phosphatases and inhibitory receptors on the cell membrane (e.g., CTLA-4 and PD-1), downregulate or inhibit TCR signaling pathways, providing feedback control³²⁷. CTLA-4 is a prominent co-inhibitory checkpoint receptor that competes with CD28 for binding with higher affinities to CD80 and CD86 ligands on activated APCs³²⁸.

Post-TCR engagement, CTLA-4 is expressed and translocated to the cell surface, where it downregulates CD28 ligand availability through trans-endocytosis of CD80 and CD86³²⁹⁻³³¹. It also recruits phosphatase Src homology 2 (SH2) domain-containing tyrosine phosphatase1 (SHP1) to inhibit phosphorylation events

downstream of TCR/CD28 signaling³³². Another key co-inhibitory receptor is PD-1, presented on the cell surface after T-cell activation, which binds to ligands PD-L1(CD274; B7-H1) and PD-L2 (CD273; B7-DC) expressed on immune cells and nonlymphoid tissues, including tumors³³³. PD-1 engagement leads to phosphorylation of its intracellular motifs, notably immunoreceptor tyrosine-based inhibition motif (ITIM) and immunoreceptor tyrosine-based switch motifs (ITSM)³³⁴, recruiting SHP2 to dephosphorylate key mediators of TCR and CD28 signaling such as ZAP70, as well as downstream of CD28, in particular PI3K³³⁵. Additional important co-inhibitory receptors in T-cells include TIM-3, which promotes immunosuppression by promoting myeloid suppressor cell expansion and positively regulating the suppressive functions of Tregs^{336,337}, and TIGIT, which binds to CD112, CD113, and CD155 ligands on APCs and cancer cells³³⁸. The stability of receptors and the signalosome at the cell surface is another regulatory layer in T-cell activation, involving the dephosphorylation of LCK by the CD45 phosphatase upon T-cell activation³³⁹.

4.2. TCR signaling intracellular checkpoints:

The balance of internalization, recycling, and degradation of TCR receptors determines the amplitude and duration of TCR signaling. The process of ubiquitination, which is essential for the internalization of TCR/CD3 complexes, has been established^{340,341}. However, the ubiquitin-dependent mechanisms controlling TCR endocytosis and surface stability remain uncovered. Non-optimal T-cell stimulation prevents sustainable T-cell activation³⁴². Indeed, chronic viral infections or cancer can lead to T-cell dysfunction, characterized by hypo-responsiveness illustrated by anergy due to a lack of costimulatory signal 2 induced by CD28/CD80 interaction and signal 3 for cytokine stimulation^{343,344} or T-cell exhaustion³⁴⁴ often accompanied by the co-expression of inhibitory receptors like CTLA-4, PD-1, LAG-3, and TIM-3. In the context of repeated antigen-driven proliferation, T-cells can become senescent and enter a cell cycle arrest³⁴⁵, downregulating costimulatory molecules such as CD28 and CD27³⁴⁶⁻³⁴⁸. Senescent, exhausted, and anergic immune cells are commonly found in the TME and pose challenges to the efficacy of cancer immunotherapy^{349,350}.

Alongside immune checkpoint proteins on the cell surface, certain intracellular proteins contribute to negative feedback loops downstream of the TCR (**Figure 10**). These proteins, known as intracellular immune checkpoints (iICPs), have gained attention as promising targets for cancer immunotherapies³⁵¹⁻³⁵⁴ (**Table 2**). This approach is particularly valuable due to the limitations observed in other cancer immunotherapies, such as CAR-T therapies or protein checkpoint blockade, which can suppress CD8+ T-cell activation due to exposure to multiple immunosuppressive factors in the TME³⁵⁵⁻³⁵⁷. These proteins can be categorized into various groups based on their mechanism of action, including kinases, protein phosphatases, ubiquitin ligases, and deubiquitination enzymes (DUBs).

4.2.1. Kinases:

Various serine/threonine kinases and lipid kinases play a crucial role in regulating intracellular signaling pathways downstream of the TCR³⁵⁸. Unlike protein-targeting kinases, lipid phosphorylation can have both stimulatory effects mediated by PI-3-kinase and inhibitory effects mediated by diacylglycerol kinases (DGKs). Therefore, both serine/threonine and lipid kinases present potential targets for boosting immune responses against tumors.

4.2.1.1. HPK1:

Hematopoietic Progenitor Kinase 1 (HPK1), encoded by the mitogen-activated protein kinase 1 (MAP4K1) gene, is a serine/threonine kinase³⁵⁹. It consists of an N-terminal kinase domain, followed by four SH3-binding proline-rich motifs and a large citron homology domain at its C terminus^{360,361}. HPK1 serves as a negative regulator of TCR signaling by phosphorylating and inhibiting crucial downstream molecules involved in T-cell activation. Dysregulated HPK1 expression or activity can result in impaired T-cell responses and contribute to the development of various diseases. HPK1 exerts its regulatory effects on TCR signaling through interactions with key proteins and signaling pathways. Upon TCR engagement, HPK1 is recruited to the IS in

the plasma membrane³⁶²⁻³⁶⁴. Once activated via Y381 phosphorylation, it associates with essential adaptors like adhesion and degranulation-promoting adapter protein (ADAP) and SLP-76^{359,360}. This interaction activates downstream kinases, including c-Jun N-terminal kinase (JNK) and p38 MAPK, ultimately regulating transcription factors like AP-1 and NFAT. Consequently, HPK1 recruits the negative regulator 14-3-3, inhibiting the phosphorylation of proximal TCR signaling molecules such as ZAP-70 and LAT^{360,365}. The destabilization of SLP-76's interaction with LAT signalosome triggers SLP-76 degradation^{366,367}, negatively impacting the MAPK ERK pathway signaling^{360,364}.

Interestingly, HPK1 expression correlates with T-cell exhaustion³⁵⁴, and dampens Ras-proximate-1 (Rap1) activation, resulting in decreased activity of the adhesion receptor LFA-1. HPK1-deficient T-cells exhibit increased ADAP recruitment to SLP-76 and elevated Rap1 activation, leading to enhanced adhesion and cell spreading³⁶⁸. Additionally, HPK1 is exploited by PGE-2 to suppress T-cell-mediated antitumor responses in a protein kinase A (PKA)-dependent manner³⁶⁹⁻³⁷¹.

Studies employing HPK1 inhibitors or gene silencing techniques have exhibited promising outcomes by augmenting T-cell responses against tumors, leading to increased TCR signaling and enhanced antitumor immune reactions against malignant cells. Downregulation of HPK1 expression or inhibition of its kinase activity augments AP-1-dependent gene transcription³⁶⁴, enhancing TCR signaling, T-cell activation, proliferation, effector function, and cytotoxicity against target cells^{359,365}. Notably, robust immune responses have been observed in HPK1 kinase-dead transgenic mice against various tumor models, including sarcoma, Lewis lung carcinoma, and GL261 glioma which express high amounts of PGE-2 and adenosine³⁵⁹. Devoid of HPK1 expression, both mouse and human CD8⁺ cells, as well as CAR-T-cells, exhibited improved degranulation activity (CD107a), cytokine production, and reduced expression of exhaustion markers such as PD-1, TIM-3, and LAG-3³⁵⁴. In murine xenograft models, adoptive cell transfer of HPK1 KO CAR-T-cells, while in both mice and humans, demonstrated better tumor growth control³⁵⁴. Additionally, several small molecule inhibitors targeting HPK1 are currently undergoing clinical trials for cancer immunotherapy³⁷². Mechanistically, the inhibition of HPK1 lowers the activation threshold of TCR, imparts resistance against suppressive factors like PGE-2, and enhances chemokine/receptor signaling. The absence of HPK1 exposes T-cells to elevated cytotoxic potential, hyperproliferation, and significantly higher secretion of Th1/effector cytokines, namely IL-2, IFN γ , Granzyme B, and TNF- α ^{359,365,369}. Furthermore, HPK1 KO from kinase-dead mice bearing single loss or point mutation in HPK1 improves the functionality of other effector immune cells by enhancing maturation and antigen presentation of DCs and enhancing NK-mediated cytotoxic activity against tumors when compared to their wild-type counterparts³⁵⁹.

4.2.1.2. Csk

The cytoplasmic tyrosine kinase C-terminal Src kinase (Csk) plays a crucial role in inhibiting proximal T-cell activation. Csk is recruited to the plasma membrane through interactions with various scaffolding proteins, including focal adhesion kinase (FAK), downstream of kinases 1/2 (Dok1/2), TNF receptor-associated factor (TRAF3), and the phosphoprotein associated with glycosphingolipid-enriched microdomains (PAG). Upon T-cell activation, PAG undergoes dephosphorylation, resulting in the release of Csk from the plasma membrane and its subsequent distance from potential substrates. This enables Csk to phosphorylate inhibitory tyrosines (Y505 and Y528) within the Src kinases Lck and Fyn³⁷³⁻³⁷⁷. Inhibiting Csk leads to enhanced TCR activation^{378,379}. Moreover, T-cells lacking Csk exhibit spontaneous proximal TCR activation, but the signaling cascade does not extend distally to PLC γ 1 activation without additional signals, such as CD28 costimulation³⁸⁰. Unlike PAG-deficient mice, mice lacking Csk demonstrate severe abnormalities in T-cell development, suggesting that other binding partners redundantly recruit Csk to the plasma membrane³⁸⁰⁻³⁸³.

4.2.1.3. DGKs

Diacylglycerol kinases are enzymes that convert DAG into phosphatidic acid (PA)³⁸⁴. This phosphorylation process by DGKs disrupts the association of DAG with RasGRPs, leading to the inhibition of the RAS/MAPK pathway and the attenuation of TCR function, including cytokine production^{324,384-387}.

Two specific isoforms of DGKs, DGK α , and DGK ζ , regulate DAG downstream of the TCR³⁸⁶. While both isoforms have redundant functions in metabolizing DAG and inducing T-cell anergy, they exhibit distinct structural motifs, expression patterns, and activation modes^{388,389}.

TILs in human tumors upregulate DGK isoforms, resulting in functional inhibition, while DGK-deficient mice show substantial antitumor activity^{390,391}. Interestingly, despite being less abundant in T-cells, DGK ζ plays a dominant role in DAG metabolism and the suppression of Ras signaling due to its increased kinase activity relative to DGK α in naïve T-cells^{392,393}. Single KD of DGK α or ζ does not affect T-cell development or the number of CD4⁺ or CD8⁺ T-cells but can impact the number of activated T-cells in unchallenged mice^{324,387,394}. In contrast, mice lacking both isoforms of DGK demonstrate a significant reduction in the number of peripheral CD4⁺ and CD8⁺ T-cells³⁹⁴. Notably, DGK KO or pharmacological inhibition enhances the cytotoxicity of CAR-T-cells against tumors in mouse and human models, while CRISPR inactivation of both DGK isoforms synergistically improves tumor clearance, cytokine production, proliferation, and the phenotype of CAR-T-cells to effector memory^{352,395}. Furthermore, DGK ζ KO in CD8⁺ mice enhances resistance to tumor growth and improves *in vivo* antitumor responses upon ACT of naïve or primed DGK ζ CD8⁺ T-cells^{385-387,395}.

4.2.2. Protein Phosphatases:

Protein phosphorylation events, including ITAM phosphorylation, generally activate proteins. Conversely, dephosphorylation by phosphatases of signaling proteins attenuates the TCR signaling cascade, leading to decreased activity³⁹⁶. Protein tyrosine phosphatases (PTPs) and protein tyrosine phosphatase non-receptor type (PTPN) are a group of negative regulators involved in TCR signaling. PTPN, specifically, has been associated with T-cell exhaustion³⁹⁷. Among the PTPN family, three members, PTPN2, PTPN6, and PTPN22, are involved in downstream TCR signaling negative feedback loops and have been evaluated in preclinical models for their anticancer activity.

4.2.2.1. PTPN2:

PTPN2 also referred to as TC-PTP, is an important phosphatase primarily expressed in hematopoietic cells. It plays a crucial role in T-cell signaling by directly dephosphorylating Lck and Fyn kinases in CD4⁺ and CD8⁺ T-cells. This activity establishes a threshold for triggering the TCR^{398,399}. T-cells lacking PTPN2 display enhanced T-cell-mediated immunosurveillance, increased numbers of effector memory T-cells (TEM), tumor infiltration, and heightened cytokine production⁴⁰⁰. Deletion of PTPN2 in mouse CAR-T-cells results in acquiring an effector memory phenotype (CD44⁺CD62L) and increased expression of IFN γ , TNF α , and Granzyme B, making them less prone to exhaustion⁴⁰⁰. Furthermore, the use of small molecule inhibitor targeting PTPN2 improves the cytotoxicity of mouse CAR-T-cells and demonstrates similar benefits for human CAR-T-cells *in vitro*^{400,401}.

4.2.2.2. PTPN6 (SHP1):

SHP-1, also known as PTPN6, is a protein tyrosine phosphatase predominantly expressed in hematopoietic cells³⁵⁸. It has been identified as a negative regulator of T-cell activation and interacts with various molecules involved in TCR signaling, including Zap-70, Syk, PI3K, Vav, Lck, CD3 ζ , and SLP-76³⁵⁸. The exact mechanism of SHP-1 function during T-cell activation remains uncertain due to variations in experimental conditions⁴⁰²⁻⁴⁰⁹.

SHP-1 deficiency in mice leads to increased phosphorylation and activation of Lck, Fyn, and other key components of TCR signaling, resulting in T-cells that are hyper-responsive to TCR/CD3 stimulation and produce more IL-2^{410,411}. SHP-1 has also been found to exert its inhibitory effects by mediating inhibitory cytokines, such as IL-10 and TGF β , and by modulating the activation threshold of T-cells as SHP-1 is also upregulated in a TCR affinity-dependent manner^{412,413}. Furthermore, SHP-1 has been shown to inhibit T-cell activation by dephosphorylating casitas B-lineage lymphoma b (Cbl-b), thus protecting it from degradation⁴¹⁴.

Targeting SHP-1 has shown promise in preclinical models, particularly in therapies involving adoptive T-cells⁴¹⁵. Deletion of SHP-1 in CD8+ T-cells enhances their proliferation potential, cytolytic capacity, and cytokine production^{416,417}. Although SHP-1 has been observed to interact with PD-1 in CD4+ T-cells and Jurkat T-cell lines, recent data suggests that their activities do not entirely overlap^{335,418,419}. Interestingly, PD-1 blockade has shown that SHP-1-deficient CD8+ T-cells are more responsive to anti-PD-1 and exhibit improved control of melanoma cell growth⁴²⁰. Pharmacological inhibition of SHP-1 (and partially SHP-2) has also been found to enhance the cytotoxic capacity of human primary CD8+ T-cells against tumors⁴¹⁹.

4.2.2.3. PEP/PTPN22

PEST-domain enriched tyrosine phosphatase (PEP), also known as PTPN22, is a cytoplasmic phosphatase found near the plasma membrane in all hematopoietic cells, including lymphocytes⁴²¹. It forms a tight complex with the negative regulatory kinase Csk, inhibiting T-cell activation by preventing phosphorylation of the TCR receptor complex^{422,423}. PTPN22 can also dephosphorylate Lyn and Fyn, Src-family protein tyrosine kinases, competing with Csk^{423,424}. It regulates Zap-70, TCR ζ , and Vav1 activities, and its absence in T-cells increases T-cell association with antigen-presenting cells through enhanced activation of the small nucleotide guanosine triphosphate hydrolases (GTPase), Rap1^{425,426}. The C1858T mutation in PEP, reducing its association with Csk, is linked to over twenty autoimmune diseases⁴²⁷⁻⁴³¹.

Studies consistently show that targeting PEP enhances TCR signaling while overexpressing it results in the opposite effect⁴³¹. Experimentally, PTPN22 KO CD8+ T-cells demonstrated improved control of tumor growth, increased cytokine production, and resistance to TGF β -mediated immunosuppression⁴³²⁻⁴³⁴. Moreover, multiple successful screening approaches have identified small-molecule inhibitors of this phosphatase, which hold potential for clinical use as cancer immunotherapeutic⁴³⁵⁻⁴³⁸.

4.2.2.4. PTP-PEST/PTPN12

PTPN12, a phosphatase containing a PEST domain, is widely expressed in mammalian cells⁴³⁹. It interacts with Csk⁴⁴⁰ and acts as a potent negative regulator by dephosphorylating important signaling molecules like Grb2, inhibiting Ras activation in B and T-cells^{440,441}. PTPN12 also regulates actin reorganization and the formation of the IS in lymphocytes by targeting the wiskott-aldrich syndrome protein (WASP) and actin-related protein 2/3 (Arp2/3). When conditionally knocked down in T-cells, PTPN12 has been found to induce anergy, secondary T-cell activation, and autoimmunity⁴⁴². In contrast, PTPN12 overexpression decreases IL2 production and inhibits NF- κ B signaling⁴⁴²⁻⁴⁴⁴.

4.2.3. SOCS family:

There are currently eight identified proteins known as SOCS (suppressor of cytokine signaling), including SOCS1-7 and CISH (chromogenic in situ hybridization). These proteins are negative regulators facilitating the degradation of JAKs and STATs⁴⁴⁵⁻⁴⁴⁷. T-cell activation leads to the downregulation of SOCS3, and its depletion enhances T-cell proliferation and IL2 production⁴⁴⁸. Additionally, SOCS6 is believed to act as a negative regulator of TCR signaling by targeting the proximal signaling kinase Lck for degradation⁴⁴⁹.

4.2.3.1. CISH

CISH, a negative regulator of TCR signaling, degrades PLC γ 1 and SLP76, which inhibit NFAT and NF- κ B in CD8⁺ T-cells^{450,451}, NK cells^{452,453}, and DC cells⁴⁵⁴. In mice lacking CISH, CD8⁺ T lymphocytes displayed improved proliferation, Ca²⁺ signaling, and IL-2 production upon TCR engagement. These cells also exhibited increased expression of effector function-associated genes and showed enhanced control of tumor progression when used in ACT³⁵¹.

Ongoing clinical trials are exploring CRISPR-Cas9 targeting of CISH in TILs prior to ACT, which has shown promising effects in improving the efficacy of ICB therapies as combined targeting of CISH^{-/-} TILs isolated from CISH KO mice with anti-PD-1 antibodies has effectively controlled tumor progression³⁵¹. Recent studies have demonstrated the benefits of targeting the intracellular checkpoint SOCS-1, a member of the CISH family, in DCs for treating relapsed acute leukemia⁴⁵⁴. Furthermore, the importance of CISH-expressing DCs in enhancing antitumor immunity and CTL activity has been demonstrated in mouse models⁴⁵⁵.

4.2.4. E3 Ligases

Ubiquitination is a cellular process that involves attaching ubiquitin, a 76 amino acid protein, to substrate proteins, marking them for degradation in the proteasome or endosome. This process serves as a mechanism for removing misfolded or unwanted proteins and regulating the levels of transcription factors and signal transduction mediators. Ubiquitination occurs through three enzymatic steps, with the final step involving the E3 ubiquitin ligase. The E3 ligase recognizes the substrate and facilitates the transfer of ubiquitin from the E2 enzyme to a lysine residue on the substrate protein^{456,457}.

4.2.4.1. CBL Family

The Cbl (Casitas B-lymphoma) proteins, including c-Cbl, Cbl-b, and Cbl-3, are a conserved family of proteins⁴⁵⁸⁻⁴⁶⁰. These proteins play a role in downregulating the TCR signaling cascade by promoting the degradation of multiple targets^{461,462}. While the specific function of Cbl-3 is not yet fully understood, both Cbl-b and c-Cbl have been demonstrated to act as negative regulators of TCR signaling^{463,464}.

1.1.1.1.1 c-Cbl:

c-Cbl plays a crucial role in T-cell signaling by binding and targeting various proteins for degradation. After TCR activation, c-Cbl primarily targets the CD3 ζ chain of the TCR complex for degradation, leading to the downregulation of TCR signaling⁴⁶⁵. Lck, a cytoplasmic tyrosine kinase, and LAT, an adaptor protein necessary for TCR signal transduction, are also important targets for c-Cbl-mediated degradation in activated T-cells⁴⁶⁶. c-Cbl deficiency in immature T-cells results in increased expression of TCR-CD3 ζ complexes and enhanced positive selection⁴⁶⁷. The interaction between c-Cbl and the ζ chain is facilitated by Zap-70, which acts as a scaffold and aids in terminating TCR signaling⁴⁶⁵.

Interestingly, evidence suggests that c-Cbl can promote the degradation of CD3 ζ through ubiquitination and subsequent translocation into lysosomal vesicles, independent of the proteasome^{468,469}. Additionally, depletion of c-Cbl leads to impaired LAT internalization and elevated LAT levels in T-cells⁴⁷⁰. c-Cbl also affects PD-1 by binding to its cytosolic tail and promoting ubiquitination for proteasomal degradation⁴⁷¹. Consequently, genetic reduction of c-Cbl results in increased PD-1 expression in CD8⁺ T-cells and macrophages⁴⁷¹.

1.1.1.1.2 Cbl-b:

The E3 ubiquitin ligase Cbl-b is a crucial regulator of T-cell activation, possessing really interesting new gene (RING) finger catalytic domains responsible for protein ubiquitination and subsequent degradation of target proteins⁴⁷². Cbl-b is prominently expressed and functional in peripheral T-cells⁴⁷³. Upon T-cell activation and clustering at the IS, Cbl-b is recruited to the TCR^{474,475}, where it employs various inhibitory mechanisms downstream of the TCR. Cbl-b interacts with important TCR signalosome molecules, including LCK, SLP76, ZAP70, PLC γ 1, Vav1, and the regulatory subunit p85 of PI3K, to dampen T-cell activation⁴⁷⁶⁻⁴⁷⁹.

Mice lacking Cbl-b display hyperactive T-cells that do not require CD28 for activation, leading to enhanced T-cell antitumor immunity *in vivo*^{480,481}. CD28 activation triggers Cbl-b ubiquitination and degradation via phosphorylation by PKC θ in a negative feedback loop^{482,483}. The homologous to the E6-AP carboxyl terminus (HECT) E3 ligase NEDD is a potential facilitator of Cbl-b degradation⁴⁸²⁻⁴⁸⁴. The binding of CD28 ligands (B7-1 or B7-2) to CTLA-4 on T-cells increases Cbl-b protein levels, suggesting a contribution of Cbl-b to CTLA-4's inhibitory function⁴⁸⁵. Cbl-b represses PTEN inactivation by NEDD4, reducing PI3K activity⁴⁸⁶. Cbl-b, along with ITCH, is involved in TGF- β -mediated regulation of forkhead box P3 (Foxp3). The absence of either E3 ligase impairs the development of TGF- β -induced Foxp3+ Tregs (iTreg), resulting in iTregs with reduced Foxp3 expression and impaired suppressive functions⁴⁸⁷⁻⁴⁹⁰. Cbl-b-deficient mice exhibit fewer exhausted T lymphocytes in the tumor microenvironment, and depletion of Cbl-b through CRISPR/Cas9 can restore the expression of inflammatory cytokines and cytotoxic molecules in exhausted PD-1+TIM-3+ T-cells³⁵³.

CRISPR-Cas9-mediated depletion of Cbl-b in mouse CAR-T-cells promotes tumor regression and resistance to exhaustion³⁵³. Adoptive transfer of Cbl-b-deficient CD8+ T-cells to tumor-bearing mice confers antitumor activity and tumor rejection^{481,491,492}. The loss of Cbl-b upon TCR triggering leads to increased phosphorylation of Akt/Erk, proliferation, activation, cytokine production (IFN γ , TNF α , IL-2), and cytolytic capacity (Granzyme B)^{353,493-495}. Cbl-b-deficient CD4+ and CD8+ T-cells are less susceptible to PD-1 or CTLA-4 inhibition^{485,496} and immune suppression by Tregs, TGF β , and PD-L1^{481,491,493,497}. Of note, combining therapies targeting CTLA-4 with Cbl-b-deficient T-cells synergistically enhances antitumor response and survival in melanoma mouse models⁴⁹³. Cbl-b-deficient mice reject various tumors and exhibit long-term tumor-specific immunological memory^{353,481,491,493-495,497,498}. Although Cbl-b KO mice are more susceptible to T-cell-mediated autoimmunity and type 1 diabetes^{480,499,500}, mild and non-lethal autoimmunity development in Cbl-b-deficient mice contrasts with enhanced antitumor immunity^{491,501}. Wild-type mice receiving Cbl-b KO or KD CD8+ T-cell-based adoptive transfer immunotherapy have not shown any autoimmune injury^{462,481,491,492,494,502}.

1.1.1.1.3 GRAIL:

The gene known as RNF128, or the gene related to anergy in lymphocytes (GRAIL), is a transmembrane RING E3 ligase found in endosomes that negatively regulates T-cell activation and plays a vital role in enforcing T-cell tolerance⁵⁰³. GRAIL achieves this by poly-ubiquitinating and degrading CD3 ζ molecules via the proteasome, leading to the downregulation of the TCR/CD3 complex on the cell surface⁵⁰³. GRAIL directly targets TCR β and CD3 ζ , as evidenced by the significant decrease in CD3 ζ ubiquitination observed in GRAIL-deficient mice⁵⁰³. Furthermore, GRAIL is involved in the ubiquitination of proteins like Rho guanine dissociation inhibitor (RhoGDI), Arp2/3 subunit 5, and coronin 1A, which are associated with regulating the actin cytoskeleton and potentially modulating the anergic state of T-cells^{504,505}. GRAIL's impact extends upstream as well, as its deficiency leads to enhanced phosphorylation of ERK1/2 after T-cell activation, suggesting its role in regulating proteins preceding this signaling node⁵⁰⁶. Absence of GRAIL in T-cells results in increased proliferation and cytokine secretion, independent of CD28 co-stimulation^{503,507}. During anergy induction, GRAIL upregulation correlates with decreased CD40 ligand (CD40L) expression, which is critical for dendritic cell-mediated licensing of T-cells^{508,509}. GRAIL binds to CD40L and promotes its ubiquitination for degradation⁵¹⁰.

GRAIL deficiency in mice confers resistance to anergy induction, hyperactivation of CD4+ T-cells mediated by TCR, and enhanced proliferation and survival of T-cells following activation^{503,507}. Additionally, GRAIL-deficient mice display heightened susceptibility to autoimmune diseases⁵⁰³. Other potential targets of GRAIL have been identified, including CD83, which contributes to CD4+ T-cell costimulation, as well as tetraspanins like CD81 and CD151^{511,512}. Overexpression of GRAIL inhibits IL2 and IL4 production and induces anergy in CD4+ T-cells. It is upregulated in CD8+ T-cells within transplanted EL-4 and EG-7 (EL4-ova) lymphoma

tumors⁵¹³. Remarkably, CD8⁺ TILs lacking GRAIL exhibit improved tumor control, increased production of IFN γ and Granzyme B, and elevated expression of IL-21R.⁵¹³ Furthermore, GRAIL plays a critical role in Treg function, as GRAIL-deficient Treg cells exhibit reduced immunosuppressive capacity and express genes associated with TH17 cells⁵¹⁴.

1.1.1.1.4 Roquin-1 and Roquin-2:

Roquin-1 and Roquin-2 are intriguing mRNA-binding proteins that possess an active RING-E3 ligase domain. They directly reduce ICOS expression by binding to the 3' untranslated region (3'UTR) of ICOS mRNA, aided by the cofactor NUFIP2^{515,516}. Additionally, both Roquin paralogs suppress OX40 levels by repressing OX40 mRNA levels⁵¹⁷. Consequently, T-cells lacking Roquin exhibit heightened levels of ICOS and OX40. Remarkably, the increased ICOS levels in Roquin-deficient mice can override the need for CD28-costimulation in their T-cells⁵¹⁸.

1.1.1.1.5 NRDP1:

NRDP1, an E3 ligase, hinders TCR signaling by participating in ZAP-70 ubiquitination (NRDP1-mediated Lys33-polyubiquitin chains)⁵¹⁹. These Lys33-linked ubiquitin chains facilitate the recruitment of suppressor of T-cell receptor signaling (Sts) 1 and 2 phosphatases, which subsequently dephosphorylate and deactivate ZAP70⁵¹⁹. TCR stimulation of CD8⁺ T-cells derived from *Nrdp1*^{-/-} mice results in augmented proliferation, elevated phosphorylation of signaling proteins (ZAP-70, LAT, PKC, ERK-1/2, and JNK-1/2), increased cytokine production (IFN γ , IL-2), and enhanced expression of critical transcription factors (Prf1, Gzmb, Tbet, Eomes) associated with effector function⁵¹⁹. Additionally, *Nrdp1*-deficient primed CD8⁺ T-cells exhibit improved control over syngeneic tumor development in a mouse model during adoptive cell transfer⁵¹⁹. The inhibitory effects of NRDP1 on T-cells are counteracted by the deubiquitination proteins OTU deubiquitinase 7B (OTUD7B) and ubiquitin specific peptidase 12 (USP12)^{520,521}.

1.1.1.1.6 Peli1:

Peli1 (Pellino E3 ubiquitin protein ligase 1), an E3 ubiquitin ligase, exerts negative control over TCR signaling through two distinct mechanisms. First, upon TCR/CD28 stimulation, Peli1 targets the NF- κ B protein c-Rel, tagging it with Lys48-polyubiquitin chains, leading to proteasomal degradation. This degradation prevents the induction of ICOS and CD40L expression, as well as T-cell activation, proliferation, and cytokine production^{522,523}. Second, following TCR engagement, Peli1 facilitates the ubiquitination of tumor suppressor tuberous sclerosis complex (TSC), a tumor suppressor gene, enhancing TSC1/TSC2 dimerization and inhibiting mammalian target of rapamycin complex 1 (mTORC1), which a protein involved in the PI3K-Akt pathway that regulates metabolism⁵²⁴. Recent studies have shown that Peli1 KO mice exhibit hyper-responsive effector T-cells⁵²⁵. These mice demonstrate improved tumor control in various tumor models, attributed to increased infiltration of CD4⁺ and CD8⁺ T-cells into tumors and enhanced production of IFN γ and granzymes⁵²⁴. Consistent with its biochemical function, Peli1-deficient mice develop autoimmunity due to hyperactivated T-cells resistant to suppression by regulatory T-cells or TGF β ⁵²⁵.

1.1.1.1.7 NEDD4 Family:

The NEDD4 (neural precursor cell expressed developmentally downregulated 4) family consists of nine members, distinct from Cbl E3 ligases, as they use a HECT domain for ubiquitin transfer instead of a RING domain⁵²⁶. Specifically, NEDD4-1 and Itch have been identified as negative regulators of T-cell activation by attenuating NF- κ B-mediated signaling⁵²⁶. They achieve this by ubiquitinating and promoting lysosomal degradation of BCL10, a component of the CARMA1-BCL10-MALT1 (CBM) complex that activates NF- κ B⁵²⁶. NEDD4-1 and Itch also target downstream signaling proteins, PKC θ and PLC- γ 1, for ubiquitination and degradation, leading to reduced AP-1 activation⁵²⁷. NEDD4 has also been found to regulate the expression of the costimulatory receptor GITR, and its degradation diminishes the cytotoxic response of T-cells⁵²⁸.

Furthermore, Itch interacts with and enhances the ubiquitination of CD3 ζ to terminate TCR signaling while regulating NF- κ B activation in conjunction with NEDD4-1. Itch phosphorylation by JNK induces the degradation of c-Jun and JunB transcription factors⁵²⁹⁻⁵³¹. Itch inhibits IL-17 production from Th17 CD4+ T-cells and $\gamma\delta$ T-cells⁵³². Loss of Itch leads to modest increases in T-cell proliferation and IL-2 production, enhanced Th2 differentiation, and elevated IL-4 production. Homozygous Itch mutations can result in urticaria, autoimmune hepatitis, and susceptibility to spontaneous autoimmunity^{533,534}. Treg-specific Itch deficiency in mice causes severe airway inflammation due to increased TH2 cytokine production⁵³⁵. Additionally, double-KO mice lacking Itch in combination with either WWP2 or Cbl-b exhibit stronger autoimmune phenotypes than single-gene deficient mice^{536,537}.

1.1.1.1.8 Deltex1

Upon Notch signaling activation, Deltex1 which is an E3 RING finger ubiquitin ligase, is upregulated during T-cell anergy^{538,539}. The negative regulation of T-cell activation by Deltex1 remains controversial, but it involves both E3-dependent and E3-independent mechanisms. Deltex1 inhibits T-cell activation even without its Notch-binding domain and regulates the expression of anergy-associated molecules, Gadd45b and Cbl-b⁵⁴⁰. The significance of Deltex1-mediated suppression of T-cell activation is uncertain, as deletion of its RING finger domain only moderately affects its inhibitory capacity⁵³⁹. It interacts with Egr-2 for optimal Cbl-b expression, and genes like Gadd45b, Egr2, and Egr3 are upregulated in anergic T-cells⁵⁴¹. A deficiency of Deltex1 increases T-cell activation, impairs anergy induction and enhances inflammation. This makes it a downstream component of calcium-NFAT signaling that regulates T-cell anergy⁵⁴⁰. Additionally, Deltex1 can immunoprecipitate with PKC θ ⁵⁴². Mice lacking Deltex1 exhibit increased mature peripheral lymphocytes, enhanced T-cell activation and proliferation with reduced T-cell tolerance and heightened susceptibility to autoimmune diseases⁵⁴⁰.

1.1.1.1.9 MDM2:

The E3 ligase murine double minute 2 (MDM2) degrades the T-cell activation factor NFATc2 in CD4+ T-cells, independent of the tumor-suppressor, tumor protein 53 (p53)⁵⁴³. This degradation process may lead to a reduction in TCR activity^{543,544}. When MDM2 is knocked out in mice, naïve CD4+ T-cells exhibit increased production of IL-2 and IFN γ upon TCR stimulation. Moreover, the transfer of CD4+ T-cells with MDM2 deficiency resulted in decreased tumor growth in mice with tumors⁵⁴³. Moreover, Zhou J. et al. (2020) found that mice with MDM2 deficiency in T-cells display an accelerated progression of tumors along with reduced survival and functionality of CD8+ TILs. The authors also showed that MDM2 competes with c-Cbl for STAT5 binding, leading to decreased in c-Cbl-mediated STAT5 degradation and enhanced STAT5 stability, specifically in CD8+ TILs.

On the other hand, MDM2 deficiency using pharmacological drugs enhances the production of CD8+ T-cell effector cytokines, such as IFN- γ and IL-2⁵⁴⁵. Furthermore, clinical evidence showed that MDM2 abundance correlates with T-cell function and the interferon- γ signature in cancer patients⁵⁴⁵. Still, the precise molecular mechanisms through which MDM2 modulates CD8+ TCR signaling are being elucidated.

4.2.5. Dual Specificity Phosphatases (DUSPs):

DUSP family members, including DUSP14 and DUSP22, play a role in inhibitory feedback control of TCR-triggered signals. On the other hand, DUSP2 (PAC1) is upregulated in exhausted tumor-infiltrating T lymphocytes, and the absence of DUSP2 in CD8+ TILs from KO mice resulted in reduced exhaustion markers (PD-1, TIM-3, LAG-3), improved production of IFN γ , TNF α , and Granzyme B, enhanced control of tumor growth, and increased survival⁵⁴⁶. However, their inhibitory capacities have not been demonstrated in mouse tumor models.

4.2.6. Deubiquitination enzymes (DUBs):

The deubiquitinases A20 and cylindromatosis (CYLD), known for their role in regulating NF- κ B signaling in innate immune cells, also impact T-cell function. A20, or tumor necrosis factor- α -induced gene 3 (TNFAIP3), removes ubiquitin chains from activated mucosa-associated lymphoid tissue 1 (MALT1) in the Carma1-BCL10-MALT1 (CBM) complex, preventing its interaction with IKK and inhibiting NF- κ B activation upon TCR stimulation⁵⁴⁷. Conditional deletion of A20 in peripheral CD8⁺ T-cells enhances NF- κ B signaling, leading to increased production of IL-2, TNF α , IFN- γ , and cytotoxicity⁵⁴⁸⁻⁵⁵⁰. In a mouse melanoma model, ACT using pre-stimulated A20 KO CD8⁺ T-cells significantly reduces tumor growth^{549,551}. Similarly, the deubiquitinase CYLD disrupts T-cell activation by removing Lys63-ubiquitin chains from the TAK1 kinase downstream of the CBM complex. CYLD deficiency results in colitis, elevated T-cell frequency, and activation, accompanied by spontaneous activation of IKK and NF- κ B⁵⁵².

Other negative regulators, including **RASA2** (RAS p21 protein activator 2) and scaffold proteins of the Dok family, such as Dok1 and Dok2, play important roles in the negative regulation of TCR signaling^{325,553-555}. For instance, RASA2 ablation has been shown to enhance human CD8⁺ T-cell proliferation and improve *in vivo* tumor control during ACT of engineered T-cells in xenograft models⁵⁵⁶. **Dok1 and Dok2** proteins recruit different negative enzymes, such as Csk, SHIP-1, or RasGAP, establishing a platform for these proteins and bringing them close to the LAT signalosome. Furthermore, Ubiquitin-associated and SH3 domain-containing protein3a (**Ubash3a**) acts as a negative regulator of TCR signaling by recruiting and activating phosphatases, including SHP-1 and SHP-2, to the TCR signaling complex³³⁵. These later phosphatases dephosphorylate tyrosine residues on various components of the TCR signaling pathway, which attenuates downstream signaling events. Similarly, **Ubash3b** interacts with the TCR complex and recruits phosphatases, inhibiting the activation of downstream signaling molecules³²⁵.

X-box-binding protein 1 (**XBPI**), specifically the spliced isoform of X-box binding protein 1, serves as a negative regulator of TCR signaling by repressing the expression of key components involved in the pathway⁵⁵⁴. It binds to specific regulatory regions of target genes and inhibits their transcription, resulting in the downregulation of critical signaling molecules. Notably, XBPI also regulates glutamine influx, cholesterol-induced CD8⁺ T-cell exhaustion, and transcriptional reprogramming in T-cells within the metastatic ovarian cancer milieu⁵⁵⁵.

Additionally, **Siglec E, F, and G, members of the Siglec family**, function as negative regulators of TCR signaling by binding to sialic acid residues on cell surface glycoproteins³³⁵. These binding recruits inhibitory signaling molecules, including SHP-1 and SHP-2, to the TCR complex, leading to the attenuation of the TCR signaling and dampening T-cell activation. **Ptpre**, also known as CD45, negatively regulates TCR signaling by dephosphorylating tyrosine residues on key signaling molecules³³⁵. By counteracting the action of protein tyrosine kinases, **Ptpre**, also known as CD45, attenuates TCR signaling and modulates T-cell activation. Moreover, **Rasal1** acts as a negative regulator of TCR signaling by promoting the hydrolysis of the GTP bound to Ras proteins³³⁵. This GTPase-activating activity leads to the inactivation of Ras, a critical component of the TCR signaling pathway. Consequently, Rasal1 attenuates TCR signaling and regulates T-cell activation.

Furthermore, calcineurin binding protein 1 (**Cabin1**) Cabin1 suppresses NFAT activation and dampens TCR signaling through its inhibitory interaction with calcineurin⁵⁵³, while **Akap5** (A-kinase anchoring protein 5) negatively regulates TCR signaling by sequestering PKA away from its downstream targets⁵⁵³. Akap5 acts as a scaffold protein, binding PKA and preventing its interaction with TCR signaling molecules. This sequestration of PKA attenuates TCR signaling and modulates T-cell activation.

Table 2: Targeting TCR intracellular negative regulators for cancer immunotherapy.
(Adapted from ^{559,560}).

Clinical trials targeting intracellular inhibitors in T cells							
Protein (Gene)	Mechanism of targeting	CT ID	Method	Transfer	Phase	Tumor type	Other interventions
SHP-2	Sequestered from dephosphorylating and activating Lck by PD1 binding May facilitate TCR signaling in some instances	NCT05370755	Pharmacological inhibition ICP-189	Systemic	I	Advanced Solid Tumors	In combination with anti-PD-1 monoclonal antibody
Cbl-b	Degradation of TCR critical signaling proteins (e.g., CD3ζ and PI3K regulatory subunit P85) Establishment of anergy	NCT03087591	KD (siRNA) APN401	Adoptive cell transfer (PBMC)	I	Solid Tumors	
		NCT05107674	Pharmacological inhibition NX-1607	Systemic	I	Advanced Solid Tumors	
		NCT05107739	Pharmacological inhibition De-TIL-0255	Adoptive cell transfer (TILs)	I	Gynecological malignancies	
		NCT05169489	MegaTAL enzymatic genetic editing	Adoptive cell transfer (CARS)	I/II	Relapsed / Refractory B	Dual-targeted CAR-T (CD20, CD79a)
CISH	Degradation of TCR key signaling proteins (i.e. PLC	NCT05662397	Pharmacological inhibition HST 1011	Systemic	I/II	Relapsed Solid Tumors	In combination with
		NCT04426669	CRISPR/Cas9	Adoptive cell transfer (TILs)	I/II	Metastatic Gastrointestinal	
HPK-1	Degradation of TCR key signaling proteins (i.e. by recruiting E3 ligase to SLP76)	NCT05566223	CRISPR/Cas9	Adoptive cell transfer (TILs)	I/II	Non-Small Cell	In combination with Pembrolizumab (a-PD1)
		NCT03198052	KD by RNAi	Adoptive cell transfer (CARS)	I	Lung Cancer	KD for PD1
		NCT04037566	CRISPR/Cas9	Adoptive cell transfer (CARS)	I	B cell Lymphomas	XYF19 CAR-T
		NCT03198546	KD by RNAi	Adoptive cell transfer (CARS)	I	Hepatocellular Carcinoma	KD for PD1
		NCT04521413	Pharmacological inhibition CF1.402411	Systemic	I/II	Multiple	In combination with Pembrolizumab (a-PD1)
		NCT04649385	Pharmacological inhibition BGB-15025	Systemic	I	Advanced Solid Tumors	In combination with Tislelizumab (a-PD1)
		NCT05128487	Pharmacological inhibition NOL101150	Systemic	I/II	Solid Tumors	In combination with Pembrolizumab (a-PD1)
		NCT05159700	Pharmacological inhibition PRJ1.3024	Systemic	I	Solid Tumors	
		NCT05233436	Pharmacological inhibition PF-07265028	Systemic	I	Solid Tumors	
		NCT05315167	Pharmacological inhibition PRJ1-3024	Systemic	I/II	Solid Tumors	In combination with Sasanlimab (a-PD1)
Other perspective for clinical development targeting intracellular inhibitors							
Protein	Targeted protein	Mechanism of Action		Evidence of Autoimmunity	Development of Small Molecule Inhibitors	Preclinical Trials	
E3 ubiquitin ligases intracellular checkpoint							
c-Cbl	CD3ζ, LCK	Ubiquitination		Yes	-	No	
		Establishment of anergy					
GRAIL	TCRβ, CD3ζ	Ubiquitination		Yes	-	Yes	
		Establishment of anergy					
NEDD4	PLCy1, PKC, BCL-10	Ubiquitination		Yes	-	No	
Itch	CD3ζ, BCL-10, Jun	Ubiquitination		Yes	++	No	
		Establishment of anergy					
Deltex1	PLCy1, PKG, MEKK	Ubiquitination		Yes	-	No	
		Establishment of anergy					
MDM2	NFATc2	Ubiquitination		No	+++	Yes	
Pel1	c-REL, TSC1, NIK	Ubiquitination		Yes	(not as cancer immunotherapy)		
NRDP1	ZAP-70	Ubiquitination		Not yet determined	-	Yes	
Phosphatase intracellular checkpoints							
SHP1	CD3ζ, LCK, ZAP-70, PI3K	Dephosphorylation		Yes	+++	Yes	
PTEN	PI3K	Inactivation		Yes	-	No	
		Dephosphorylation					
SHIP-1	PI3K	Inactivation		No	+++	Yes	
		Dephosphorylation					
PEP (PTPN22)	FYN, LYN	Dephosphorylation and inactivation		Yes	+	Yes	
PTPN2	LCK, FYN	Dephosphorylation		Yes	+	Yes	
PTP-PEST (PTPN12)	Ras, GRB2, actin reorganisation	Dephosphorylation and inactivation		Yes	-	No	
		Establishment of anergy					
Other intracellular checkpoints							
CSK	LCK, FYN	Phosphorylation		No	-	No	
DGKs	DAG	Phosphorylation		No	++	Yes	
		Establishment of anergy					
SOCS family	LCK, PI3K	Ubiquitination		No	Yes	No	
DUSP2	ERK	Dephosphorylation		No	+++	Yes	
A20	MALT	Deubiquitination		Yes	/+	Yes	
CYLD	TAK1	Deubiquitination		Yes	/+	No	

- None yet developed ; -/+ Proposed; + Early development; ++ Validated in pre-clinical trials; +++ In clinical trials.

II. Ph.D. Project aim:

Adoptive T-cell transfer is a groundbreaking cancer treatment that can generate a strong and long-lasting response against different types of cancer. However, its effectiveness in solid tumors is limited compared to hematological malignancies, leading to modest responses and frequent relapses²¹⁴. This is primarily due to the death or dysfunction of infused T-cells within the TME, which contains factors, immune cells, and physical barriers that prevent T-cells from efficiently infiltrating the tumor and exerting their cytotoxic activity. To improve T-cell persistence and antitumor function in solid tumors, various gene-engineering approaches have been employed to redirect T-cells toward cancer cells expressing specific TAAs^{223,224} (**Figure 4**), as well as addressing the negative signals received by engineered T-cells (**Figure 3**).

Our study focuses on overcoming the obstacles that hinder T-cell activation, persistence, and antitumor activity. We identified suppressive molecules downstream of the TCR signaling pathway that can be targeted and inhibited to enhance T-cell activation and unlock their full antitumor potential. Additionally, we developed gene-engineering tools to target those intracellular negative regulators, either individually or in combination, to enhance T-cell functionality *in vivo*, particularly in human and murine melanoma models. The study is divided into the following aims:

Aim 1: Development of novel vector constructs and a protocol to gene-engineer T-cells with inducible or constitutive miRNA for downregulating targets while expressing a CAR or a transgenic TCR to redirect T-cells into the TME.

To modulate TCR negative regulators and direct engineered T-cells to kill cancer cells, this chapter focuses on the development of a new lentiviral vector design. The design includes two gene cargos under independent promoters, enabling genetic modification of T-cells.

This process involves:

1-Comprehensive examination of existing gene-editing technologies and the development of novel strategies to effectively gene-engineer T-cells, thereby enhancing their antitumor function.

2-Validating the novel vector design by using miRNA to downregulate HPK1, the primary negative regulator target. Recent evidence demonstrates promising results by deleting HPK1, which elevates constraints on T-cell activation and antitumor activity.

Aim 2: A combinatorial approach targeting multiple intracellular TCR negative regulators for enhanced T-cell persistence and functionality *in vivo*.

This section presents a combinatorial strategy to inhibit multiple intracellular checkpoint inhibitors downstream of the TCR network. We also demonstrate the enhanced T-cell function and evasion of TME immunosuppression through the concomitant downregulation of dual intracellular negative regulators of TCR, both *in vitro* and *in vivo*.

This part will cover:

Aim 2.1: Identifying relevant intracellular negative regulators to target downstream TCR signaling pathways.

Here, we will involve an in-depth, comprehensive literature overview and evaluation of currently studied TCR intracellular inhibitory checkpoints and their significance in immune regulation, T-cell activation, as well as their antitumor responses to highlight relevant targets to downregulate for our study.

Aim 2.2: Evaluate the expression of selected negative regulators in high-affinity TCRs:

To achieve our primary goal of downregulating specific negative regulators, our strategy relies on upregulating those genes during the TCR synapse with tumor antigen. This approach is valid only when the target expression is ensured in the context of T-cell activation within the TME. To simulate this antigen encounter in the lab, we employed an experimental method that induces a state resembling T-cell exhaustion. This was achieved by chronically stimulating the T-cells with ovalbumin (OVA) SIINFEKL peptide, using an adapted protocol adapted from Katsikis lab published in 2020⁵⁶¹.

Aim 2.3: Screen miRNAs for achieving a high knockdown level of the selected targets using the single-miRNA vector in high-affinity TCRs.

The main goal of delivering miRNA for gene inhibition is achieving high KD efficiency. However, this outcome is not always guaranteed. Indeed, it depends on various factors such as vector design elements (promoter, spacers, and miRNA backbone) as well as the miRNA biogenesis affecting the potency of targeted gene KD. We will demonstrate an experimental method and resulting data for screening multiple miRNAs using a single miRNA vector to ensure effective gene silencing for all selected TCR intracellular inhibitors.

Aim 2.4: Design vectors for dual and multiple targeting of the selected TCR intracellular inhibitory checkpoints:

One key challenge in gene engineering T-cells for simultaneous multiple gene inhibition is designing and constructing a polycistronic miRNA vector. In our context, the shRNA-based miRNA approach is the tool of choice. Synthetic miRNA minigenes (SMIGs) hold significant potential for molecular therapy. However, their optimal architecture has been the focus of numerous studies aimed at enhancing cloning efficiency, expression, successful delivery, and consistent KD potency. Considering factors such as insert size limitation, miRNA stability, biology, and regulation, we outline the method used to construct a multiple miRNA vector for downregulating multiple genes simultaneously.

Aim 2.5: Evaluate T-cell antitumor activity *in vitro* and *in vivo* when carrying multiple perturbations targeting TCR negative regulators in high and low-affinity TCRs:

To validate our experimental approach, engineered T-cells were assessed for their antitumor activity upon downregulating suppressive molecules downstream of the TCR signaling pathway. This involves evaluating their cytokine secretion, proliferation, and persistence in the immunosuppressive TME, specifically in cold tumors using the B16/B16 OVA syngeneic tumor model in high and low-affinity TCR scenarios for performing ACT.

Aim 2.6: Develop an unbiased, high-throughput screening approach for identifying suitable candidates for gene silencing.

To enlarge our strategy to a broader spectrum, we adopted the CRISPR/Cas 9 system as a high throughput screening method enabling the inclusion of a larger number of potential TCR suppressive regulators and an unbiased screening of all the targets at once based on T-cell persistence. We demonstrated the outcome of silencing 19 targets downstream of the TCR signaling pathway using a small pooled CRISPR library we built and validated in our team.

III. Results:

1. Development of novel approaches and vector constructs comprising inducible or constitutive miRNA for CAR and TCR-based T-cell therapies.

Inverted lentiviral transfer vector comprising independent promoters for on-command gene-cargo delivery by tumor-redirected T-cells

Patrick Reichenbach,^{1,*} Greta Maria Paola Giordano-Attianese^{1,*}, Khaoula Ouchen¹, Elisabetta Cribioli¹, Melanie Triboulet¹, Sarah Ash¹, Margaux Saillard¹, Romain Vuillefroy de Silly¹, George Coukos^{1,†} & Melita Irving^{1,†}

¹Ludwig Institute for Cancer Research, University of Lausanne and Department of Oncology, Lausanne University Hospital (CHUV), Lausanne, Switzerland

*The following authors equally contributed to this paper

†Correspondence to Melita.Irving@unil.ch & George.Coukos@chuv.ch.

Peer-reviewed review article (<https://doi.org/10.1126/sciadv.aaz7809>)

1.1. Co-author contribution:

In this study, Melita Irving and George Coukos directed the overall research, with Melita Irving providing supervision. Patrick Reichenbach and Greta Giordano Attianese were responsible for designing and planning experiments related to the vector configurations while experiments related to HPK1 KD were planned and designed by myself. The following individuals, including myself, contributed to the execution, analysis and interpretation of experiments: Patrick Reichenbach, Greta Giordano Attianese, Elisabetta Cribioli, Melanie Triboulet, Sarah Ash, Margaux Saillard, Romain Vuillefroy de Silly.

My specific contributions to the study are as follows: performing the cloning of the bidirectional configuration vector for transducing Jurkat cells and conducting the flow cytometric analysis (**Figure 1b**); contributing to the execution and analysis of *in vivo* bioluminescence imaging experiments, comparing prostate-specific membrane antigen (PSMA) sCAR/aCAR/aCARNovB2 Tax with untransduced (UTD) and CD19 CAR cells (**Figure 5e**); cloning the miRNAs targeting HPK1 and miRNA CTRL in the pCRRL lentiviral vector for constitutive expression, along with NGFR and the NYESO-1 TCR (**Figure 6e**); planning, performing, analyzing, and interpreting the western blot data for HPK1 downregulation in NYESO TCR transduced Jurkat cells (**Figure 6f**); planning, performing, analyzing, and interpreting the flow cytometric results assessing the transduction efficiency of NGFR and NYESO-1 TCR expression in transduced primary human CD4+ and CD8+ T-cells (**Figure 6g**); planning, performing, analyzing, and interpreting the western blot results evaluating HPK1 KD levels in NYESO-1 TCR-CD4+ and CD8+ T-cells from three different healthy donors (**Figure 6h**); planning, performing, analyzing, and interpreting the cytotoxicity experiments for NYESO-1 T-cells against target cells using IncuCyte (**Figure 6i**), as well as cytokine secretion upon coculture with target cells (**Figure 6j**) and proliferation assay (**Figure 6k**).

Additionally, I evaluated the functionality of the dual antisense configuration vector by planning, performing, analyzing, and interpreting flow cytometric results of Pz1-CAR expression upon transduction of CD4+ and CD8+ primary human T-cells with the pCRRL lentiviral vector containing the inducible miRNA B targeting HPK1 in dual antisense configuration, along with western blot results assessing HPK1 downregulation in Pz1-CAR T-cells (**Figure 7c**). I also analyzed the flow cytometric data for pan-TCR and eGFP expression in T-cells transduced with constitutive miRNA targeting TRAC (**Figure 7d**), along with performing, analyzing, and interpreting the *in vivo* bioluminescence results for the study using the antisense orientation vector comprising the inducible luciferase along with the constitutive aPSMA or aCD19 CAR (**Extended Data Figure 5g, 5h, 5i, and 5j**). Furthermore, I contributed to the writing and editing of the manuscript.

1.2. Summary:

In the quest to bolster the efficacy of T-cell-based immunotherapies for oncological applications, this research endeavor addressed issues linked to the co-expression of genes in engineered T-cells. We combined the benefits of controllable, inducible gene expression in synergy with a perpetually expressed tumor-specific receptor. Meanwhile, we developed a fine-tuned and clinically viable procedure to amplify viral titer during viral synthesis, thereby enhancing transduction efficiency and facilitating the simultaneous expression of the pair of genes.

In fact, gene-engineering T-cells to express tumor-targeting receptors such as CARs or transgenic TCRs along with additional therapeutic genes (i.e., miRNAs, chemokines, or cytokines) has largely been achieved by the co-transduction of two delivery vectors^{562,563}. However, this results in high GMP-grade production costs, cellular stress, decreased viability due to repeated infection, and an increased risk of insertional mutagenesis⁵⁶⁴. Existing approaches involve alternative strategies using bicistronic vectors to express both genes of interest under the same promoter^{565,566} comprising a picornavirus 2A (P2A) peptide sequence^{567,568} or an internal ribosome entry site (IRES)⁵⁶⁹ for separating and constitutively expressing the two genes. However, these gene-separation approaches have limitations, such as reduced gene expression of the downstream gene and potential immunogenicity led by incomplete cleavage at the P2A site, in addition to limiting the size of the inserted “gene-cargo” in case of using, for instance, IRES (about 500bp).

By developing a novel lentiviral vector design with two independent promoters in the antisense orientation, we could demonstrate the successful generation of T-cells expressing the inducible transgene and the constitutively expressed tumor-targeting receptor using Pz1-CAR and NYESO-1-TCR with improved gene expression, transduction efficiency, and T-cell performance. Through *in vitro* and *in vivo* experiments, the engineered T-cells exhibit enhanced tumor cell recognition, resulting in improved tumor cell killing and tumor growth delay. We have also investigated the kinetics of transgene expression and demonstrated precise control of its activation using the inducible system, allowing for fine-tuning therapeutic effects, and minimizing adverse events associated with sustained transgene expression.

Overall, our findings establish the feasibility and potential of the developed lentiviral vector for not only the production of engineered T-cells with enhanced expression of two inserted genes but also their performance that resulted from better transduction efficiency with respect to safety standards, lower GMP production costs, and faster delivery. The novel vector design represents a significant advancement in T-cell-based immunotherapies for cancer treatment, with implications for improving the safety and efficacy of cancer therapy. This study provides a solid foundation for further investigations and future clinical applications to advance personalized cancer therapy and achieve better patient outcomes.



A lentiviral vector for the production of T cells with an inducible transgene and a constitutively expressed tumour-targeting receptor

Received: 15 March 2022

Accepted: 20 February 2023

Published online: 17 April 2023

Check for updates

Patrick Reichenbach^{1,2}, Greta Maria Paola Giordano Attianese^{1,2}, Khaoula Ouchen¹, Elisabetta Cribioli¹, Melanie Triboulet¹, Sarah Ash¹, Margaux Saillard¹, Romain Vuillefroy de Silly¹, George Coukos¹✉ & Melita Irving¹✉

Vectors that facilitate the engineering of T cells that can better harness endogenous immunity and overcome suppressive barriers in the tumour microenvironment would help improve the safety and efficacy of T-cell therapies for more patients. Here we report the design, production and applicability of T-cell engineering of a lentiviral vector leveraging an antisense configuration and comprising a promoter driving the constitutive expression of a tumour-directed receptor and a second promoter enabling the efficient activation-inducible expression of a genetic payload. The vector allows for the delivery of a variety of genes to human T cells, as we show for interleukin-2 and a microRNA-based short hairpin RNA for the knockdown of the gene coding for haematopoietic progenitor kinase 1, a negative regulator of T-cell-receptor signalling. We also show that a gene encoded under an activation-inducible promoter is specifically expressed by tumour-redirection T cells on encountering a target antigen in the tumour microenvironment. The single two-gene-encoding vector can be produced at high titres under an optimized protocol adaptable to good manufacturing practices.

Important technological advances in recent years in the field of cellular engineering have enabled increasing clinical translation of gene-modified cells for the treatment of cancer and other diseases^{1–6}. Transient or stable alterations can be made to host cells, such as hematopoietic stem cells⁷, or immune cells including T cells⁸, B cells⁹, natural killer cells¹⁰ and macrophages¹¹, to modify their properties for a desired therapeutic outcome upon re-infusion into a patient. Disruption of cellular processes can be attained by silencing, correcting or

overexpressing targets within the genome, or by RNA interference of transcribed genes such as by short hairpin (sh)RNA or microRNA (miR; non-coding RNAs)¹². If only temporary changes in gene expression are desired, such as for evaluating the safety of a previously untested cellular product, messenger (m)RNA electroporation can be used¹³, and advances in non-viral episomal vector design show promise in enabling longer-term modifications to gene expression^{14,15}. For permanent modifications, a variety of tools have been developed for genome editing

¹Department of Oncology, Ludwig Institute for Cancer Research Lausanne, Lausanne University Hospital and University of Lausanne, Lausanne, Switzerland. ²These authors contributed equally: Patrick Reichenbach, Greta Maria Paola Giordano Attianese. ✉e-mail: George.Coukos@chuv.ch; Melita.Irving@unil.ch

including zinc finger nucleases¹⁶, transcription activator-like (TAL) effector nucleases¹⁷, clustered regularly interspaced short palindromic repeats (CRISPR)/Cas9^{18,19} and viral vectors such as adenovirus, adeno-associated virus (AAV)²⁰ and retroviruses^{21–23}.

Both lentivirus and gamma-retrovirus are subtypes of retrovirus comprising an RNA genome that is converted to DNA in infected host cells by the virally encoded enzyme reverse transcriptase⁷, and they allow efficient non-site-directed integration of genes of interest into the genome²¹. Lentiviral and gamma-retroviral vector-based gene-engineering strategies have been widely and safely used in the clinic for both chimeric antigen receptor (CAR)- and T cell receptor (TCR)-T-cell therapy of cancer²³. In particular, CAR-T cells targeting the B-cell lineage antigen CD19 have conferred unprecedented clinical responses against certain haematological malignancies, such as acute lymphoblastic leukaemia. In addition, TCR-engineered T cells targeting the HLA-A2-restricted cancer testis epitope NY-ESO-1_{157–165} (A2/NY) have shown promise for the treatment of melanoma, myeloma and synovial cell sarcoma^{24–27}. The continued importance of lentiviral vectors as a tool for T-cell engineering purposes for clinical application is underscored by recent advances in improving CAR-T-cell manufacturing protocols²⁸.

CARs are synthetic receptors that can be used in place of a TCR-CD3 complex to link tumour-antigen binding and cellular activation upon target engagement in a non-major histocompatibility complex (MHC)-restricted manner. While first generation (1G) CARs comprise the endodomain of CD3-zeta for signal 1 of T-cell activation, 2G and 3G CARs further include one or more co-stimulatory endodomains, respectively. As previously mentioned, CAR therapy has been a powerful strategy for fighting some advanced haematological malignancies, but a considerable proportion of patients either do not benefit or experience relapse. Moreover, epithelial-derived solid tumours remain poorly responsive⁸ to CAR therapy, and the efficacy of TCR-engineered T cells²⁵, as well as of tumour-infiltrating lymphocyte transfer, have proven beneficial against relatively few cancer types in a modest proportion of patients²⁹. It is widely held, however, that the development of personalized combinatorial or/and co-engineering strategies to overcome barriers in tumour microenvironment (TME) and harness endogenous immunity can further improve responses to these different T-cell-based therapies^{30–32}. Co-engineered CAR-T cells are referred to as 4G CARs, armoured CARs or next-generation CARs, and the term TRUCK ('T cells redirected for universal cytokine mediated killing')³³ has been coined to define T cells specifically engineered to enforce expression of cytokines/interleukins (ILs). Examples of cytokines evaluated in the context of CAR- and TCR-T cells, and in some instances tumour-infiltrating lymphocytes, include IL-12^{32,34}, IL-15^{23,35} and IL-18^{36,37}.

While in early studies the co-expression of genes in T cells was achieved by dual transduction^{38,39}, the high cost of good manufacturing practice (GMP)-grade virus production and elevated risk for insertional mutagenesis⁴⁰ have driven the development of 'all-in-one' multi-gene encoding vectors^{41,42}. If both the receptor (CAR or TCR) and the gene cargo are constitutively expressed, they can be separated on the transfer vector by an internal ribosome entry site (IRES)⁴³. Alternatively, for equimolar expression of both genes, a picornavirus 2A peptide sequence (P2A)^{44,45} can be used. For both approaches, RNA is generated from a single promoter and co-expression is reliant upon functioning of the interspersed element. Disadvantages of IRES are its relatively large size (about 500 bp), cell-type dependency⁴⁶ and reduced expression of the downstream gene⁴³. Drawbacks of P2A are the risk of incomplete cleavage and potential immunogenicity of the gene product⁴⁷.

To minimize the risk of systemic toxicity and enhance T-cell function, it may be preferable to limit expression of the gene cargo to the TME. One approach to achieve this is to place the gene cargo under a T-cell-activation-dependent promoter such as nuclear factor of activated T cells (NFAT) response elements fused to the IL-2 minimal

promoter (6xNFAT)^{48,49}. Here we demonstrate that previously described dual promoter sense and bidirectional vectors are limited by interference of gene expression¹³ and promoter leakiness, respectively, in transduced cells. We subsequently present a dual inverted promoter vector design, along with an optimized protocol for the production of high-titre lentiviral particles to overcome the aforementioned obstacles. Overall, our antisense gene-cassette design and methodology for lentivirus vector production have important implications for improving the performance and safety of engineered T cells for cancer immunotherapy. Moreover, our approach can be considered universal as it can be applied to other vector types and different gene therapies.

Results

Antisense vector design to accommodate independent promoters

Here we sought to optimize lentivirus vector-mediated independent co-expression of two genes in transduced human T cells, with one gene under a constitutive promoter and the other under an inducible promoter, to improve adoptive T-cell transfer (ACT) of cancer. We began by building a panel of transfer vectors comprising the promoters in dual sense and bidirectional orientations (Fig. 1a,b, left). For our study, we selected the constitutive human phosphoglycerate kinase (PGK) promoter for gene A, and 6xNFAT for gene B. For screening purposes, we placed *egfp* under PGK and *mCherry* under 6xNFAT (lentivirus vector component sequences are found in Supplementary Table 1).

The production of second-generation lentivirus vectors relies on the co-transfection of: (1) a transfer, (2) a packaging and (3) an envelope vector into a producer cell line such as human embryonic kidney (HEK)293T cells (that is, HEK293 cells expressing the oncogenic SV40 large T-antigen thought to promote plasmid-mediated gene expression)⁵⁰. Lentiviral vectors typically comprise three HIV-1 genes: (1) *gag* (which is processed to matrix and other retroviral core proteins) and (2) *pol* (reverse transcriptase, RNase H and integrase functions), both found on the packaging plasmid, as well as (3) *env* (envelope protein that resides in the lipid bilayer and determines viral tropism) on the envelope vector. We have used the vesicular stomatitis virus G-protein (VSV-G) pseudotype⁵¹, which broadens the type of cells that can be infected⁵² as compared with the HIV envelope⁵³. Notably, the transfer vector does not encode viral sequences, except for necessary *cis*-acting sequences such as the long terminal repeat (LTR), packaging signals and the Woodchuck hepatitis virus post-transcriptional regulatory element (WPRE) to enhance expression of the transgene⁵⁴. The LTRs, located at each end of the provirus, comprise U3, R and U5 regions and function as a eukaryotic transcription unit. Specifically, the U3 region contains the viral promoter and enhancer elements, the R region includes the mRNA initiation site, and the U5 region is involved with polyadenylation. Notably, the 3'LTR of the transfer vector has been truncated (U3 has been removed) to generate self-inactivating lentivirus vectors⁵⁵.

Here, to produce lentiviral particles, HEK293T cells were transfected with lentiviral packaging and envelope plasmids, along with differently designed transfer vectors, and crude supernatant was used directly to transduce Jurkat cells. For the sense transfer vector configuration, the 6xNFAT promoter and gene B (*mCherry*) were placed in the same orientation upstream of the PGK promoter and gene A (*egfp*) (Fig. 1a, top left). Indeed, the inducible promoter cannot be placed downstream of the constitutive one as there will be readthrough, and hence constitutive expression, of both genes by the upstream promoter. Moreover, it is not possible to place a polyadenylation (PA) site between the two genes to avoid interference because this will abrogate virus production in the HEK293T cells (depicted in Fig. 1a, bottom left).

We evaluated expression of dual sense orientation genes as described above in unstimulated and stimulated Jurkat cells. We observed expression of EGFP in unstimulated Jurkat cells, and co-expression of both EGFP and mCherry upon stimulation (Fig. 1a, right). For the latter, transcription of both genes must reach the same

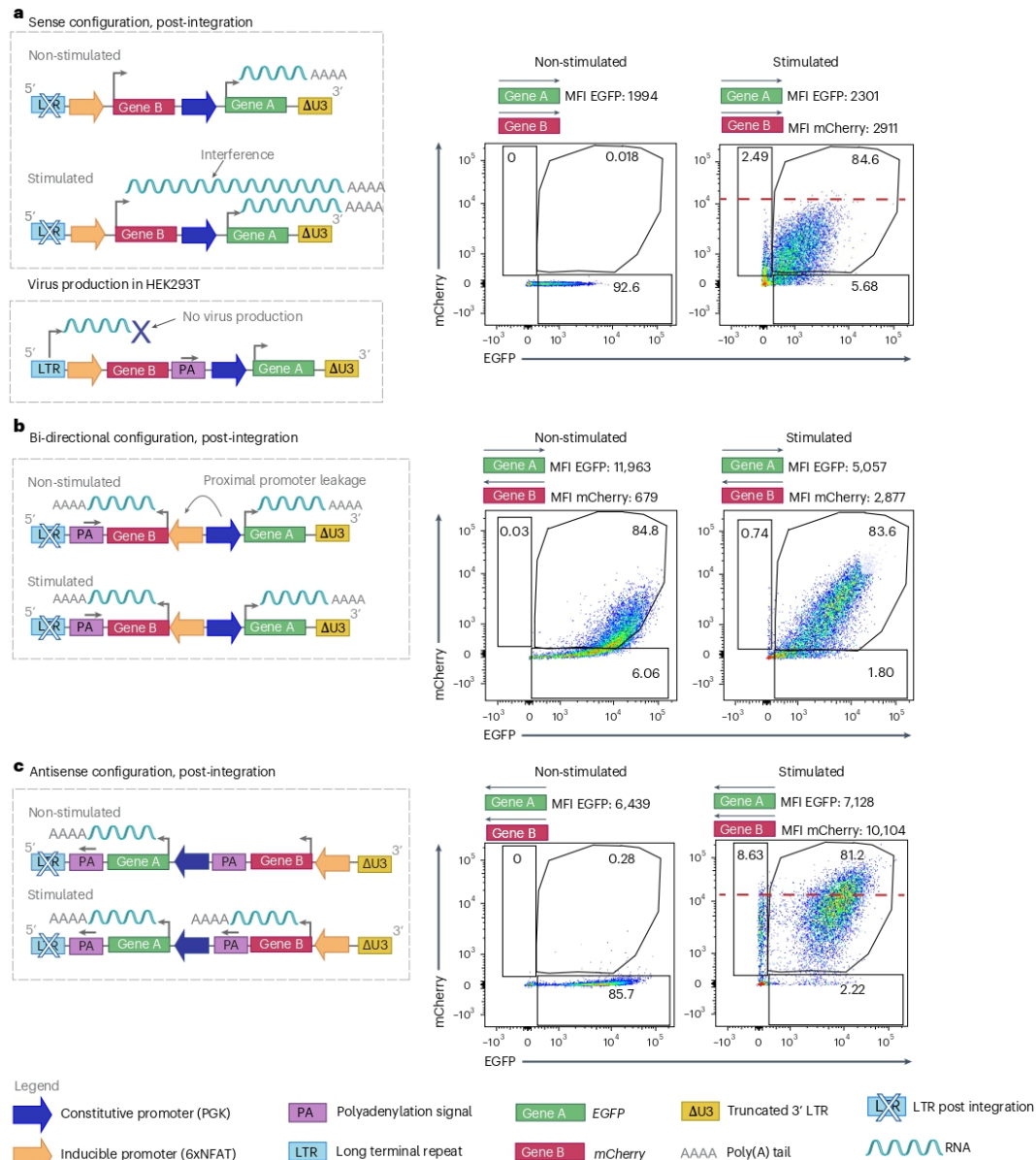


Fig. 1 | Dual antisense lentiviral transfer vector allows efficient constitutive expression of a transgene and controlled co-expression of an activation-inducible transgene. For all dual transfer constructs, EGFP (Gene A) expression is constitutively driven by the PGK promoter and mCherry (Gene B) by 6xNFAT. **a**, Left: schematic of dual sense orientation lentiviral transfer vector post-integration in non-stimulated (top) and stimulated (middle) transduced cells. Left, bottom: schematic illustrating that the inclusion of a PA site between the 2 genes will abrogate virus production in the packaging cells. Right: representative flow cytometric analysis of transfected Jurkat cells pre- and post-stimulation. **b**, Left:

schematic of bidirectional transfer vector post-integration in non-stimulated (top) and stimulated (bottom) transduced cells. Right: representative flow cytometric analysis of transduced Jurkat cells, pre- and post-stimulation. **c**, Left: schematic of antisense orientation lentiviral transfer vector post-integration in non-stimulated (top) and stimulated (bottom) transduced cells. Right: representative flow cytometric analysis of transduced Jurkat cells, pre- and post-stimulation. The dashed red line demarcates the increase in mCherry-EGFP MFI for dual antisense versus sense configuration vectors in stimulated Jurkat cells. The flow cytometry plots are representative of 5 independent experiments.

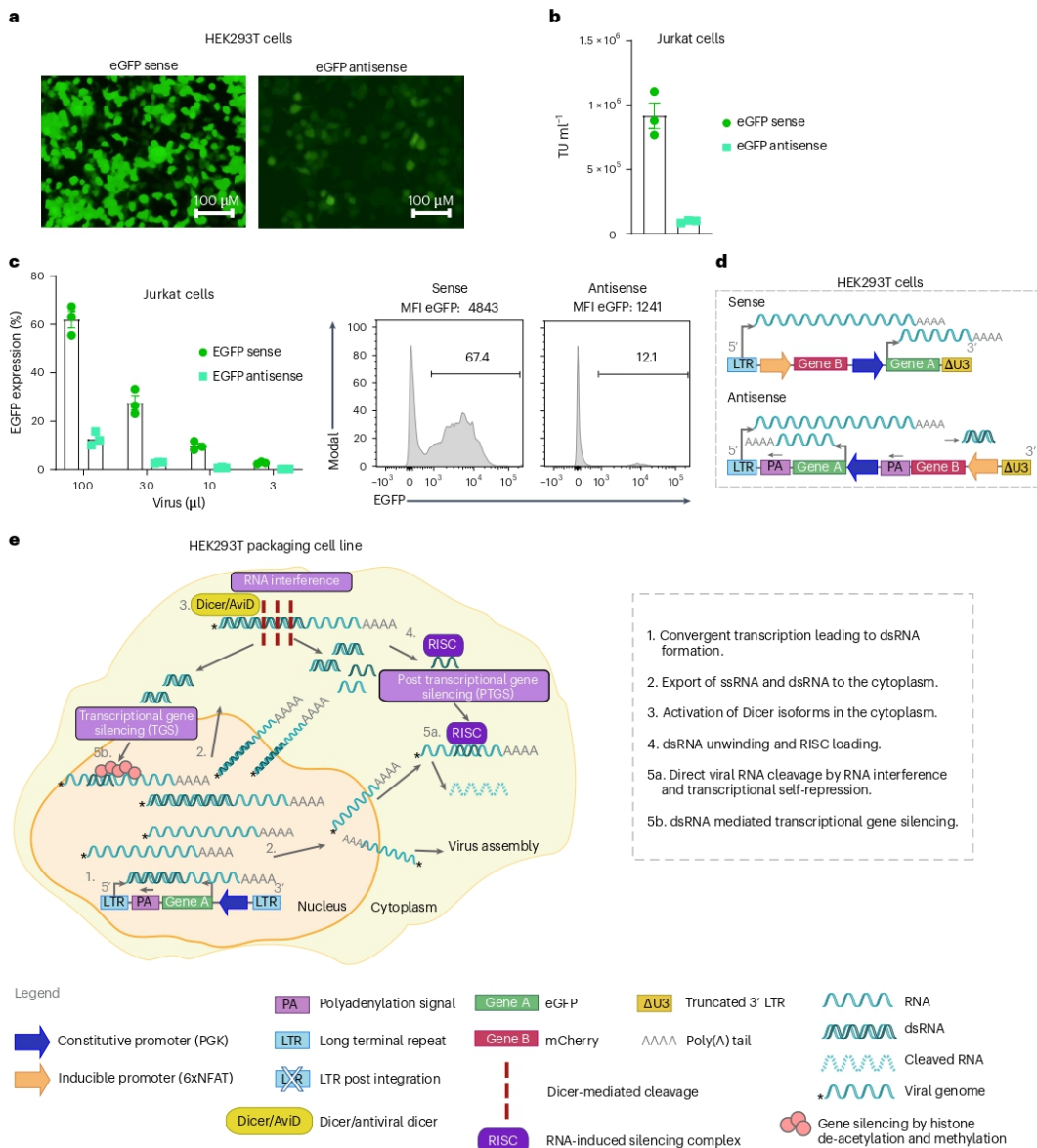


Fig. 2 | Antisense transfer vector yields lower lentivirus vector titre than sense vector. For all dual constructs, EGFP (Gene A) expression is constitutively driven by the PGK promoter and mCherry (Gene B) by 6xNFAT. **a**, Representative microscopy images (×10 magnification) of HEK293T cells transfected with dual sense (left) vs antisense lentiviral vectors (right) for lentivirus vector production. **b**, Viral titres (TU ml⁻¹). **c**, Transduction of Jurkat cells with decreasing volumes of lentivirus vector supernatant to evaluate %EGFP expression (on day 5) by flow

cytometry. Bar graphs represent the mean ± s.e.m. of technical duplicates for 3 independent experiments. Representative histograms of transduction with 100 μl virus supernatants are shown for dual sense (left) and antisense (right) approaches. **d**, Schematic of dual sense (top) vs antisense (bottom) orientation lentiviral transfer vectors encoding both EGFP and mCherry. **e**, Illustration of potential Dicer-associated mechanisms in response to dsRNA, which may be limiting to lentivirus vector production in HEK293T cells.

3' LTR for polyadenylation to occur and it has been previously reported that this configuration can cause transcriptional interference which limits transgene expression^{56,57}. Indeed, interference resulting from the dual sense configuration is evident upon comparison of the mean fluorescence intensity (MFI) for mCherry when encoded alone versus upstream of constitutively expressed EGFP (Extended Data Fig. 1a).

To avoid such interference, we next evaluated a bidirectional configuration (Fig. 1b, left) in which the orientation of Gene B and its promoter are inverted. Notably, for inverted Gene B, no longer restricted by polyadenylation at the LTR, we employed an inverted bovine growth hormone (BGH) PA site⁵⁸. Of note, an inverted PA site will not interfere with virus production. However, despite the separation of the two-gene cassettes, we observed leakage from the inducible promoter as evidenced by mCherry expression in non-activated Jurkat cells, presumably due to the proximity of strong enhancer elements of the constitutive promoter (Fig. 1b, right).

Finally, to prevent both interference and leakage issues as seen for the first two transfer vector designs, we built a dual antisense configuration vector (Fig. 1c, left) in which Gene A has its own PA signal derived from BGH, and Gene B is followed by a synthetic polyadenylation site (SPA) and a human transcription pausing site (to prevent transcriptional readthrough)⁵⁷. We observed the highest level of expression of both EGFP and mCherry in activated Jurkat cells among the 3 configurations evaluated, and there was no mCherry expressed in non-activated Jurkat cells. For example, in the representative experiment shown in Fig. 1, in stimulated Jurkat cells, an MFI for mCherry of 10,104 was observed for the antisense configuration (Fig. 1c, right) vs an MFI of 2,911 for the sense configuration vector (Fig. 1a, right). While absolute MFI values varied between independent assays, within a given experiment we consistently observed a higher MFI for both EGFP and mCherry in activated Jurkat cells transduced with the dual antisense in comparison with the dual sense lentiviral vector (Extended Data Figs. 1 and 2). This is probably due to the lack of transcriptional interference as well as the use of the BGH PA site, which is stronger than polyadenylation by the LTR⁵⁸. We thus continued our study with this dual inverted transfer vector configuration.

Overcoming low lentiviral titres by abrogating the anti-dsRNA response

Post-integration, the dual antisense vector configuration enabled the best co-expression of both a constitutive and an inducible gene in transduced activated Jurkat cells (that is, no competition to reach the PA site, no leakiness by the inducible promoter and highest MFI of both EGFP and mCherry post-activation) (Fig. 1 and Extended Data Figs. 1 and 2). However, during lentivirus vector production, we observed an obvious decrease in EGFP expression levels for vectors comprising the dual antisense vs sense orientation of the transgenes (Fig. 2a), which corresponded to much lower viral titres for the antisense lentiviral vectors (Fig. 2b). Indeed, transduction of Jurkat cells with 100 μ l lentiviral supernatant yielded about 60% transduction efficiency for the dual sense orientation vector vs about 10% (and lower MFI) for the dual inverted vector (Fig. 2c). Similarly, for single gene cassettes, lower viral titres were observed for antisense vs sense lentiviral vectors (Extended Data Fig. 3a).

Hence, we next sought to overcome barriers to the production of lentiviral particles comprising an antisense transfer vector. During lentivirus vector production in HEK293T cells, both the 5'LTR and the inverted PKG promoter of the antisense vector are active, thus resulting in the generation of double-stranded (ds)RNA by convergent transcription (as illustrated in Fig. 2d). Although intracellular innate immunity may be triggered in response to dsRNA upon detection by nuclear and cytosolic sensors such as during a natural viral infection, this has been shown not to limit lentivirus vector titre because HEK293T cells do not generate an interferon (IFN) response. Indeed, it has recently been revealed that HEK293T as well as various stem-cell-like lines employ an RNA interference (RNAi) response involving various Dicer isoforms upon detection of dsRNA^{59,60}. We thus postulated that the dsRNA resulting from convergent transcription⁶¹ may be subject to Dicer and/or Dicer isoform-mediated (for example, *avid*) cleavage within the nucleus or cytoplasm and that small interfering (si)RNA products created during this process are involved either in RNAi-mediated self-degradation or/and in transcriptional gene silencing of the viral RNA to be packaged⁶² (as illustrated in Fig. 2e).

We devised two approaches to overcome these potential barriers to lentivirus vector production arising from convergent transcription, the first being to inhibit the antiviral RNAi machinery to prevent disruption of the viral genome by taking advantage of a natural viral mechanism to evade immunity. Specifically, *Nodamura virus* expresses an RNA interference suppressor protein called B2 (hereafter referred to as NovB2)^{60,63} and it has been previously utilized to increase viral titres of bidirectional vectors by at least fivefold⁶⁴ via inhibition of Dicer isoforms^{60,64}. We hence took the strategy of co-expressing NovB2 from the envelope vector (Fig. 3a) and achieved an important increase in viral titre (Fig. 3b). Indeed, we observed a fivefold rise in the proportion of EGFP⁺ Jurkat cells upon transduction with dual antisense lentivirus vector (Fig. 3c). The use of NovB2 also increased titres for single gene cassette inverted lentiviral vectors (Extended Data Fig. 3b).

Overcoming low lentiviral titres favouring transcription of the viral genome

For our second approach to improve lentivirus vector titres, we sought to favour the transcription of the viral genome for packaging (that is, single stranded (ss)RNA transcription from the 5' LTR) by exploiting the human T-cell leukaemia virus 1 Tax protein. The Tax protein⁶⁵ is associated with the transcriptional promotion of viral proteins (including in the nucleus during infection), and the regulation of many signalling pathways including CREB/ATF, NF- κ B, AP-1 and RSF⁶⁶. To test whether Tax could be used to increase viral titres⁶⁵, we replaced the initial Rous sarcoma virus (RSV)-based promoter and enhancer region at the 5' LTR with the cytomegalovirus (CMV) promoter and enhancer which comprises 4 consensus NF- κ B binding motifs⁶⁷ (schematic in Fig. 3d). We then produced virus in the presence or absence of co-transfected Tax-expressing plasmid (Fig. 3d). We observed a similar gain in titre, transduction efficiency and transgene expression levels (MFI) as achieved in the context of NovB2 (Fig. 3e–g). It is likely that the Tax-mediated increase in lentivirus vector titre is due to a change in stoichiometry in favour of viral genome transcript, as well

Fig. 3 | Rescue of low dual antisense vector lentiviral titres in the presence of NovB2 and Tax proteins. For dual constructs, EGFP (Gene A) expression is constitutively driven by the PKG promoter and mCherry (Gene B) by 6xNFAT. **a**, Schematic of dual sense vs antisense orientation lentiviral transfer vectors encoding both EGFP and mCherry. Antisense transfer lentivirus vector was produced in the presence or absence of NovB2 (encoded on the envelope plasmid). **b**, Viral titres (TU ml⁻¹). **c**, Left: transduction of Jurkat cells with decreasing volumes of lentivirus vector supernatant to evaluate %EGFP expression (on day 5) by flow cytometry. Bar graphs represent the mean \pm s.e.m. of 3 independent experiments. Right: representative histograms for Jurkat cells transduced with 100 μ l of lentivirus vector supernatant produced in the absence

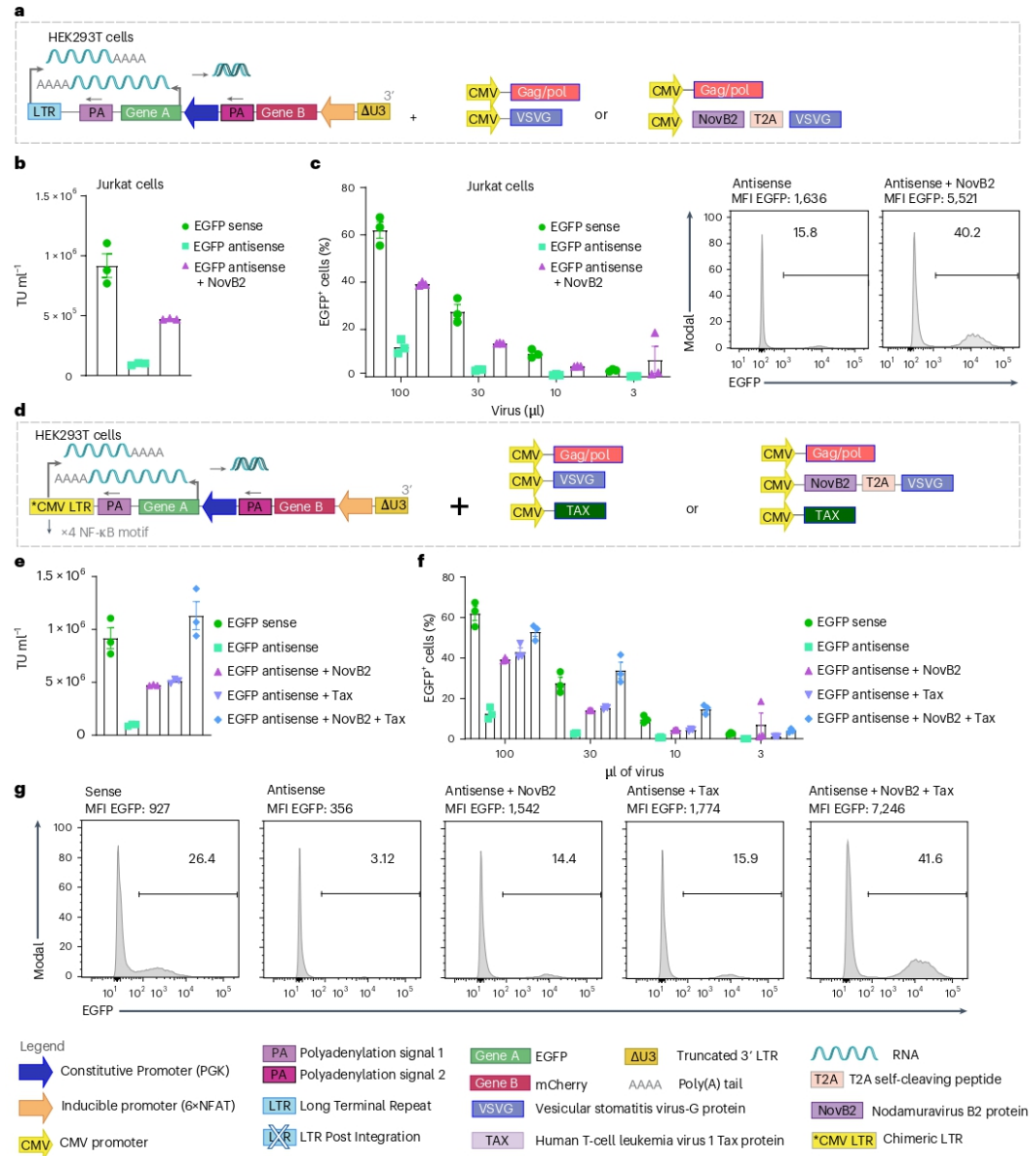
or presence of NovB2. **d**, Left: schematic of dual antisense vector encoding EGFP and comprising a chimeric LTR (Δ U3, R and U5) for which the RSV promoter and enhancer at the 5' LTR has been substituted by the complete CMV promoter and enhancer. Right: schematics representing antisense lentivirus vector production in the presence or absence of Tax protein (via vector co-transfection), or of NovB2 (encoded on the envelope plasmid), or of both Tax and NovB2. **e**, Transduction of Jurkat cells with decreasing volumes of lentivirus vector supernatant to evaluate %EGFP expression (on day 5) by flow cytometric analysis. Bar graph shows the mean \pm s.e.m. of 3 independent experiments. **f**, Viral titres (TU ml⁻¹). **g**, Representative histograms of Jurkat cells transduced with 30 μ l of lentiviral supernatant.

as higher transcription of the packaging and envelope vectors which also comprise CMV promoters. Finally, we observed that Tax and NovB2 were able to act jointly to restore antisense viral titres, transduction efficiency and levels of transgene expression (MFI) (Fig. 3e–g).

Inducible gene cargo encoded in antisense is efficiently expressed upon T-cell activation in vitro

We next sought to test our dual inverted vector design and optimized methodology for lentivirus vector production in the context of both

next-generation (4G) CAR- and TCR-T cells. For proof-of-principle, we began by constructing vectors comprising an anti-PSMA or anti-CD19 CAR (constitutively expressed under PGK)⁶⁵, along with luciferase as inducible gene cargo (under 6xNFAT) (Fig. 4a). We also generated an equivalent sense orientation transfer vector for the anti-PSMA CAR and luciferase. Lentivirus vector was produced in the presence of NovB2 and Tax and we observed that both human CD4⁺ and CD8⁺ T cells were efficiently transduced with the 4G constructs (Fig. 4b). To achieve an equivalent percentage of 4G CAR⁺ T cells for functional testing,



the transduced T cells were mixed with untransduced (UTD) T cells to reach 40% CAR⁺ (that is, the lowest transduction efficiency as achieved for CD8⁺ T cells with the 4G anti-CD19 CAR, Fig. 4b). The 4G CAR-T cells all efficiently and specifically killed target cells in co-culture assays (Fig. 4c, left and right). While there were no differences in specific target-cell killing by the 4G anti-PSMA CAR-T cells generated with sense vs antisense lentiviral vectors, significantly higher levels of luciferase mediated luminescence were observed for the antisense design (Fig. 4d).

We further compared sense and antisense lentiviral transfer vectors encoding the anti-PSMA CAR and mCherry as inducible gene cargo. Once again, we produced lentivirus vector in the presence of NovB2 and Tax and achieved efficient transduction of both human CD4⁺ and CD8⁺ T cells (Fig. 4e, left). We further observed a significantly higher MFI for CARs expressed from the dual antisense vs sense lentiviral vectors (Fig. 4e, right). In line with our findings above, we observed no differences in cytotoxicity of target PC3-PIP tumour cells by anti-PSMA CAR-T cells generated with the different orientation lentiviral vectors (Fig. 4f, left). It is possible that more stringent conditions, such as the use of a weaker CAR, the co-culture of fewer CAR-T cells to target cells or the use of tumour cells with lower levels of target antigen, may reveal lower relative activity levels of CAR-T cells generated with the sense lentiviral vector. Upon T-cell activation in co-culture assays, mCherry expression levels steadily increased over time for the antisense lentiviral vector-generated 4G CAR-T cells, but mCherry was not detectable for the sense lentiviral vector-engineered CAR-T cells, even at 16 h (Fig. 4f, right). To confirm that this lack of detection was a sensitivity issue for the InCyte instrument-based assay rather than a defect in the sense vector, we evaluated the 4G CAR-T cells following 24 h of co-culture without and with target cells by flow cytometric analysis. We observed higher background levels of mCherry expression for the antisense vector (both percentage and MFI) in non-activated 4G CAR-T cells (Fig. 4g). However, we achieved similar transduction efficiencies for both the sense and antisense vectors as evidenced by the percentage of T cells expressing mCherry upon T-cell activation (that is, the sense orientation lentiviral vector is functional; Fig. 4h, left), and the MFI for mCherry upon activation was significantly higher for the antisense lentiviral vector (Fig. 4h, right). Significantly higher levels of mCherry expression (MFI) were also observed upon phorbol myristate acetate (PMA)-ionomycin stimulation of the antisense lentiviral vector-generated 4G CAR-T cells (Fig. 4i).

Fig. 4 | In vitro testing reveals higher activation-induced expression levels of gene cargo by 4GCAR-T cells engineered with antisense vs sense lentiviral vectors. **a**, Schematic of lentiviral vectors encoding an anti-PSMA or anti-CD19 2G CAR (gene A) under the PKG promoter and luciferase or mCherry as gene cargo (gene B) under 6xNFAT, in both sense and antisense configurations. The 2G CARs comprise a tumour-targeted scFv, the linker region of CD8 α , the TM and ED of CD28, and the ED of CD3z. **b**, Transduction efficiency of primary human CD4⁺ and CD8⁺ T cells with the 2 different CARs and luciferase constructs as measured by cell-surface CAR staining on day 9. Shown are mean \pm s.e.m. for T cells from 3 independent healthy donors. **c**, PSMA⁺ PC3-PIP (right) or PC3-CD19⁺ engineered tumour cell lines (left) killing assay by the CAR-T cells and UTD-T cells as measured by the InCyte instrument (decrease in total green area per μm^2 corresponds to target-cell death) over time. Shown are mean \pm s.e.m. Symbols indicate individual donors ($n = 3$). (NS, not significant, $P = 0.9173$ sPSMA vs aPSMA; ** $P = 0.0049$ aPSMA vs UTD, $P = 0.0507$ sPSMA vs UTD, ** $P = 0.0025$ aCD19 vs UTD). Statistical significance was assessed using two-way ANOVA and post-hoc Tukey test vs UTD. **d**, Evaluation of luciferase expression levels (luminescence (counts)) by activated anti-PSMA- (left) and anti-CD19-CAR-T cells (right), measured by HIDEEX. Values for assay are the mean \pm s.e.m. for $n = 3$ human T-cell donors. (* $P = 0.0484$ aPSMA vs tumour control; *** $P < 0.001$ aCD19 vs tumour control). Statistical significance was assessed using one-way ANOVA vs tumour cells alone. **e**, Transduction efficiency of primary human CD4⁺ and CD8⁺ T cells. Left: percentage of CAR⁺ positive cells. Right: MFI of positive cells by direct

Subsequently, we developed lentiviral transfer vectors encoding a clinically relevant HLA-A2-restricted NY-ESO-1₁₅₇₋₁₆₅ specific TCR⁸⁹ along with either IL-2 or mCherry as inducible gene cargo (Extended Data Fig. 4a). Lentivirus vectors encoding the TCR and IL-2 were produced in the presence of NovB2 and Tax, and human CD4⁺ and CD8⁺ T cells were efficiently transduced (Extended Data Fig. 4b). As for the CAR-T cells, equivalent percentages of TCR⁺ T cells were generated by appropriate mixing with UTD-T cells for all comparative functional assays. We observed similar levels of target-cell killing (Extended Data Fig. 4c) as well as IFN γ production (Extended Data Fig. 4d) upon co-culture with A2⁺/NY⁺ Saos-2 target cells for the IL-2 co-engineered TCR-T cells generated either with sense or antisense vectors. However, significantly higher levels of IL-2 were produced by the next-generation TCR-T cells generated with the antisense vs sense vector upon co-culture with target cells (Extended Data Fig. 4e). Differences in IL-2 gene cargo expression levels were not observed upon PMA-ionomycin stimulation of the engineered T cells, a condition that drives the maximum production of endogenous IL-2 (Extended Data Fig. 4f). Finally, TCR-T cells with inducible mCherry as gene cargo generated from antisense vs sense vectors were tested. Upon T-cell activation in co-culture assays with target cells, an increase in mCherry was evident over time for the antisense but not for the sense lentiviral vector-generated TCR-T cells (Extended Data Fig. 4g). However, flow cytometric analysis of next-generation TCR-T cells following 24 h co-culture with A2⁺/NY⁺ Saos-2 target tumour cells confirmed that mCherry was in fact produced by T cells generated with both antisense and sense lentiviral vectors (Extended Data Fig. 4h, left) but that mCherry expression levels (MFI) were very low for the sense orientation (Extended Data Fig. 4h, right). Significantly higher levels of mCherry expression (MFI) were also observed upon PMA-ionomycin stimulation of the antisense vs sense lentiviral vector-generated TCR-T cells (Extended Data Fig. 4i).

Inducible gene cargo encoded in antisense is efficiently expressed upon T-cell activation in vivo

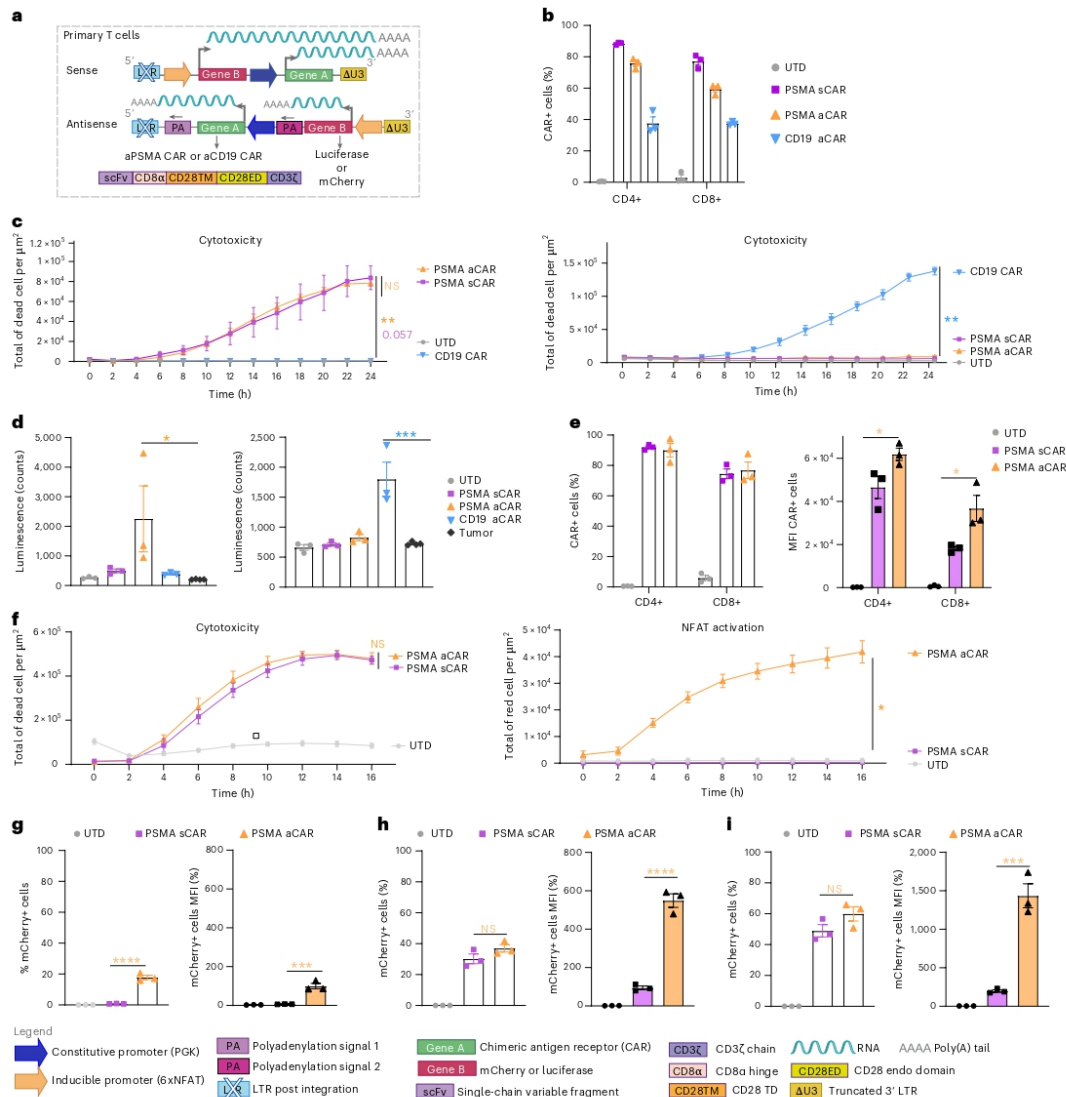
For in vivo proof-of-principle of our antisense lentiviral vector approach, we evaluated next-generation anti-PSMA and anti-CD19 CAR-T cells with luciferase (for imaging purposes) expressed under 6xNFAT as inducible gene cargo (Extended Data Fig. 5a). Efficient transduction of primary human T cells was achieved for both antisense lentiviral 4G CAR constructs (Extended Data Fig. 5b, left). We observed low levels of background mCherry expression in non-activated anti-CD19 CAR-T cells, presumably due to minor tonic signalling⁷⁹, but upon

surface cell staining on day 9 (* $P = 0.0447$ CD4⁺ sPSMA vs aPSMA; ** $P = 0.0229$ CD8⁺ sPSMA vs aPSMA). Values for assay are the mean \pm s.e.m. for $n = 3$ human T-cell donors. Statistical significance was assessed using one-way ANOVA. **f**, Left: PSMA⁺ PC3-PIP killing assay by CAR- and UTD-T cells as measured by the InCyte instrument (total green area per μm^2) over time. Shown are mean \pm s.e.m. Symbols indicate individual donors ($n = 3$). Statistical significance was assessed using two-way ANOVA and post-hoc Tukey test. (NS, $P = 0.961$ sPSMA vs aPSMA). Right: evaluation of mCherry expression (total red area per μm^2) by activated anti-PSMA tumour-cell reactive CAR-T cells. Values for the InCyte assay are the mean \pm s.e.m. for $n = 3$ human T-cell donors. Statistical significance was assessed by two-way ANOVA and post-hoc Tukey test. (* $P = 0.0182$ sPSMA vs aPSMA). **g**, Flow cytometric analysis to evaluate % mCherry (left) and mCherry MFI (right) background expression levels in non-activated CAR-T cells. **h**, Flow cytometric analysis to evaluate % mCherry (left) and mCherry MFI (right) expression by activated CAR-T cells upon 24 h co-culture with PSMA⁺ PC3-PIP tumour cells. **i**, Flow cytometric analysis to evaluate % mCherry (left) and mCherry MFI (right) by CAR-T cells after 24 h PMA-ionomycin stimulation. Bar graphs (**g-i**) show the mean \pm s.e.m. Symbols indicate individual healthy T-cell donors ($n = 3$). Statistical significance was assessed by one-way ANOVA (**g** left *** $P < 0.001$ sPSMA vs aPSMA; **g** right *** $P < 0.001$ sPSMA vs aPSMA; **h** left NS, $P = 0.1699$ sPSMA vs aPSMA; **h** right *** $P < 0.001$ sPSMA vs aPSMA; **i** left NS, $P = 0.1492$ sPSMA vs aPSMA; **i** right *** $P < 0.001$ sPSMA vs aPSMA). a, antisense; s, sense; mC, mCherry.

PMA-Iono activation we observed similar %mCherry expression for both CAR constructs (Extended Data Fig. 5b, right).

For the first in vivo study, NSG mice were inoculated with 5×10^6 PSMA⁺ PC3-PIP tumour cells and treated on day 5 by peritumoural transfer of 5×10^6 4G CAR- or UTD-T cells (Extended Data Fig. 5c). As expected, the 4G anti-PSMA CAR-T cells, but neither the 4G anti-CD19 CAR- nor the UTD-T cells, were able to control tumour growth (Extended Data Fig. 5d). In addition, luciferase activity upon luciferin injection in mice was only observed for the tumour-infiltrating 4G anti-PSMA CAR-T cells (Extended Data Fig. 5e, f). Subsequently, we repeated the in vivo study but further compared next-generation anti-PSMA CAR-T cells generated with antisense vs sense vectors (Fig. 5a, b). We observed no

significant differences in tumour control for antisense vs sense lentiviral vector-generated CAR-T cells (Fig. 5c), in line with our in vitro data for this very potent anti-PSMA CAR. In this study, we also sought to evaluate whether the use of Tax and NovB2 during lentivirus vector production (to increase titres) has any impact on CAR-T-cell function. We found that there was no significant difference in tumour control by anti-PSMA CAR-T cells generated with virus produced in the presence or absence of Tax and NovB2 (Fig. 5c). Importantly, however, we observed that luciferase activity levels of tumour-infiltrating CAR-T cells, as measured by luminescence imaging upon luciferin injection of the treated mice, were significantly higher for the antisense lentiviral vector-generated 4G CAR-T cells (Fig. 5d, e). This observation, which



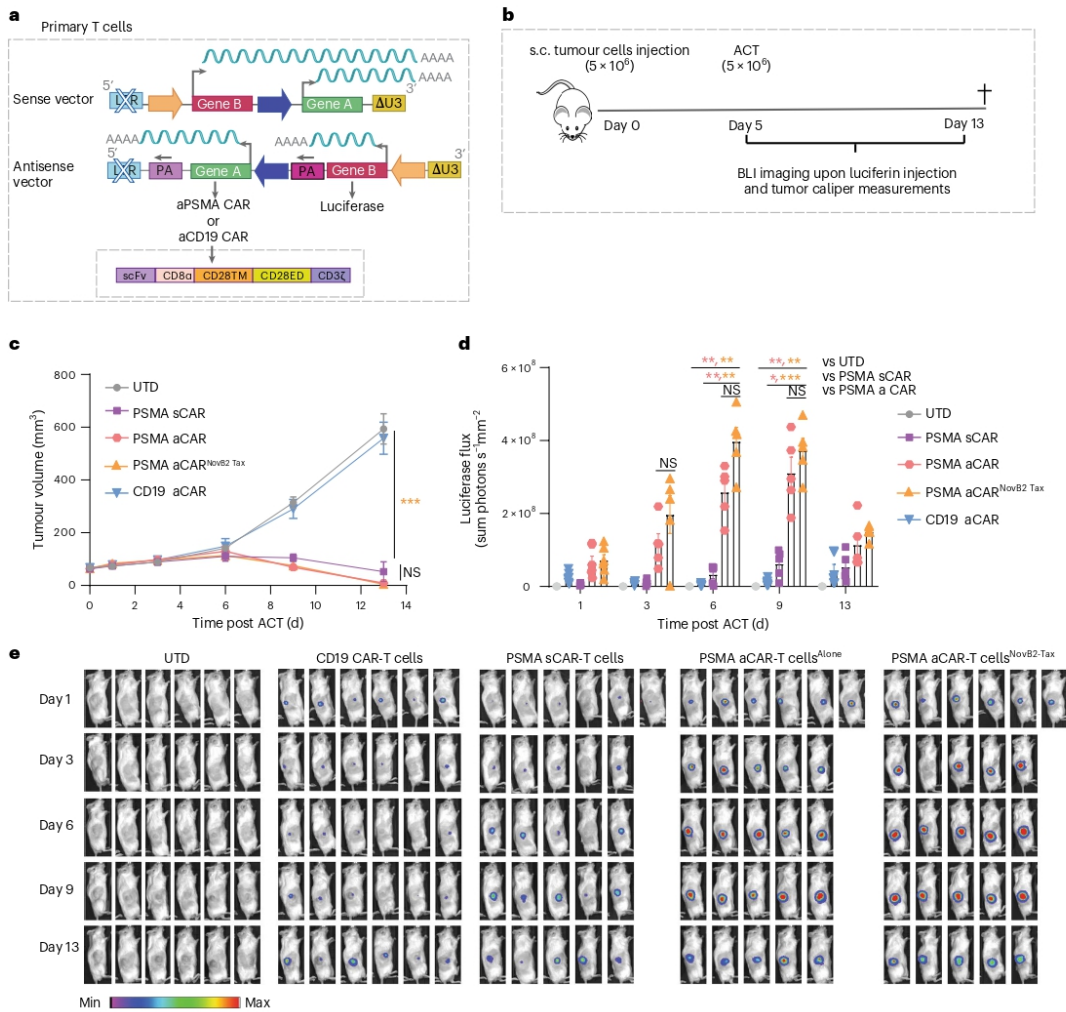


Fig. 5 | In vivo testing reveals higher activation-induced expression levels of gene cargo by 4G CAR-T cells engineered with antisense vs sense lentiviral vectors. **a**, Schematic of sense and antisense lentiviral vectors encoding anti-PSMA and anti-CD19 CARs under the PGK promoter and luciferase under 6xNFAT. **b**, Schematic of the in vivo study. **c**, Caliper tumour volume measurements over days. Values are the mean \pm s.e.m. for $n = 6$ mice per group. Statistical significance was determined by two-way ANOVA; *** $P < 0.001$ aPSMA vs UTD at endpoint; NS $P = 0.78$ aPSMA vs sPSMA. **d**, Luciferase flux as measured by bioluminescence imaging upon luciferin injection for all the experimental groups. Data are represented as mean \pm s.e.m. for $n = 6$ mice per group. Statistical

significance was assessed using two-way ANOVA and post-hoc Tukey test; **** $P < 0.0001$; Day 3: NS $P = 0.67$ aPSMA vs aPSMA Tax-NovB2; Day 6 NS $P = 0.13$ aPSMA vs aPSMA Tax-NovB2; ** $P = 0.006$ sPSMA vs aPSMA; ** $P = 0.002$ sPSMA vs aPSMA Tax-NovB2; ** $P = 0.006$ UTD vs aPSMA; ** $P = 0.002$ UTD vs aPSMA Tax-NovB2; Day 9 NS $P = 0.78$ aPSMA vs aPSMA Tax-NovB2; * $P = 0.01$ sPSMA vs aPSMA; *** $P < 0.001$ sPSMA vs aPSMA Tax-NovB2; ** $P = 0.009$ UTD vs aPSMA; ** $P = 0.002$ UTD vs aPSMA Tax-NovB2. **e**, Representative images of luciferase activity of the transferred tumour-infiltrating 4G CAR-T cells over days upon luciferin injection of mice.

correspond with our in vitro findings (Fig. 4), is presumably due to a lack of transcriptional interference in the engineered T cells as occurs upon the use of dual sense lentiviral vectors.

Finally, we evaluated the next-generation CAR-T cells in vivo against a CD19⁺ tumour model. Briefly, mice were inoculated with 10×10^6 Bjab tumour cells and on day 7 were treated by peritumoural

transfer of 5×10^6 antisense lentiviral vector-generated 4G CAR-T cells or UTD-T cells (Extended Data Fig. 5g). As expected, the anti-CD19 CAR⁻, but neither the anti-PSMA-CAR⁻ nor the UTD-T cells, were able to control tumour growth. We also observed no significant differences in tumour control (Extended Data Fig. 5h) or in NFAT-driven luciferase activity (Extended Data Fig. 5i,j) for 4G anti-CD19 CAR-T cells generated

with virus produced in the presence or absence of Tax and NovB2. We further showed that the use of NovB2 and Tax during lentivirus vector production (Extended Data Fig. 6a) had no impact on transduction efficiency (Extended Data Fig. 6b), the cytolytic capacity of CAR-T cells against target cells (Extended Data Fig. 6c), the levels of inducibly expressed gene cargo upon CAR-T cell co-culture with target cells (Extended Data Figs 6d,f) or tumour control by anti-CD19 CAR-T cells (Extended Data Fig. 6g,h).

Development of culture conditions suitable for clinical-grade lentivirus vector production

HTLV-Tax has been reported to act on several signalling pathways, among them NF- κ B⁷¹. Although no Tax protein is expected in the lentiviral particle preparation following ultracentrifugation, its tumourigenic potential⁶⁵ may raise regulatory concerns for clinical-grade production of lentivirus vector. We thus sought to identify a suitable alternative. As previously mentioned, the CMV promoter and enhancer comprises four NF- κ B consensus binding sites, and TNF α , IL-1 β , camptothecin and phorbol ester (PMA) have all been shown to efficiently activate NF- κ B in a dose-dependent manner⁷². To validate this effect in a simple manner, we transiently transfected HEK293T cells with a suboptimal concentration of pcDNA-EGFP which harbours a CMV promoter and treated the cells with the different compounds. At 48 h post-transfection, we observed an increase in both the percentage and MFI of cells expressing EGFP upon TNF α exposure (Extended Data Fig. 7a). Encouraged by this observation, we next tested the use of TNF α in the context of sense-orientation single gene cassette (Extended Data Fig. 7b) lentivirus vector production in HEK293T cells and observed an important increase in viral titre, percentage and MFI of EGFP⁺ cells (Extended Data Fig. 7c), presumably due to the effect of TNF α not only on the transfer vector but also on the envelope and packaging vectors which comprise CMV promoters. Of note, this NF- κ B-mediated strategy can in principle be applied to enhance the production and hence lower the costs of any viral vector comprising NF- κ B consensus binding sites in promoter/enhancer regions.

Evaluation of clinical-grade protocol in the context of 'difficult to produce' lentivirus vectors

Along with the development of tumour-redirection T cells that co-express additional molecules or receptors, gene-downregulation strategies³⁰ can also be employed to potentiate their function. However, transfer vectors encoding shRNA which comprise stem-loop structures are associated with low viral titres due to Dicer processing. Hence, to further validate the use of TNF α and NovB2 to augment viral titres, we developed different transfer vectors comprising a short miR-based shRNA hairpin^{73–75} (miR-based shRNA). Notably, NovB2 has been previously shown to increase the titre of such vectors due

to specific inhibition of the canonical activity of Dicer isoforms in processing microRNAs⁷⁶.

We began by expressing the miR-based shRNA under the constitutive U6 promoter with EGFP expressed downstream under the PGK promoter (Fig. 6a). Indeed, because the termination of transcription from polymerase III promoters comprises 5 thymidine residues, the vector was built in a dual sense orientation; there is no transcriptional interference to reach a PA site and hence no need to invert the gene cassette. Upon titration of viral supernatant produced in the presence of NovB2, TNF α or both, we observed an important gain in transduction efficiency as measured by percentage of EGFP⁺ cells (Fig. 6b), lentiviral titre (Fig. 6c) and relative expression level of EGFP per cell (MFI) (Fig. 6d).

Encouraged by these results, we subsequently built a sense vector comprising a miR-based shRNA under the U6 promoter targeting a therapeutically relevant target, Hematopoietic Progenitor Kinase 1 (Hpk1), a negative regulator of TCR signalling⁷⁷, also known as Mitogen-Activated Protein Kinase 1 (Map4k1). The miR-based shRNAs were followed by truncated human nerve growth factor receptor (tNGFR)⁷⁸ and the HLA-A2/NY-ESO-1₁₅₇₋₁₆₅ restricted TCR⁷⁹, both expressed under the PGK promoter and separated by a T2A element (Fig. 6e). Jurkat cells transduced with this construct showed an efficient knockdown of HPK1 (over 90% reduction by miR-based shRNA 'A') (Fig. 6f). We then transduced primary T cells and observed 85% and ~70% transduction efficiency of primary CD4⁺ and CD8⁺ T cells, respectively, as measured by HLA-A2/NY-ESO-1₁₅₇₋₁₆₅ tetramer staining (Fig. 6g). Efficient transduction was accompanied by strong HPK1 knockdown, similar to the levels observed in Jurkat cells (Fig. 6h). We subsequently evaluated the in vitro function of the TCR-T cells +/- HPK1 knockdown by miR-based shRNA upon co-culture with the A2⁺/NY⁺ target cell lines Me275 and A375, as well as the A2⁻/NY⁻ cell line Na8 as a negative control. Others have previously demonstrated that pharmacological inhibition or full gene knock-out of HPK1 in CD8⁺ T cells can improve their effector function and ability to control tumours^{77,79}. However, we did not observe significant differences in target-cell killing (Fig. 6i) or in IFN γ release (Fig. 6j) for the HPK1 knockdown TCR-T cells (HPK1 'A' and 'B') vs the control (CTRL) TCR-T cells comprising a scrambled miR-based shRNA, but we did observe higher proliferative capacity for the HPK1 'A' knockdown CD8⁺ T cells (Fig. 6k). Whether these differences are due to the use of miR-based shRNA to knockdown HPK1 or the in vitro conditions used in our experiments is unknown, but is beyond the scope of our study.

Evaluation of clinical-grade lentivirus vector production protocol for antisense transfer vectors

The use of TNF α in combination with NovB2 was next tested in the context of the antisense configuration transfer vector encoding mCherry under 6xNFAT and EGFP under PGK (Fig. 7a, left). Similar to when Tax

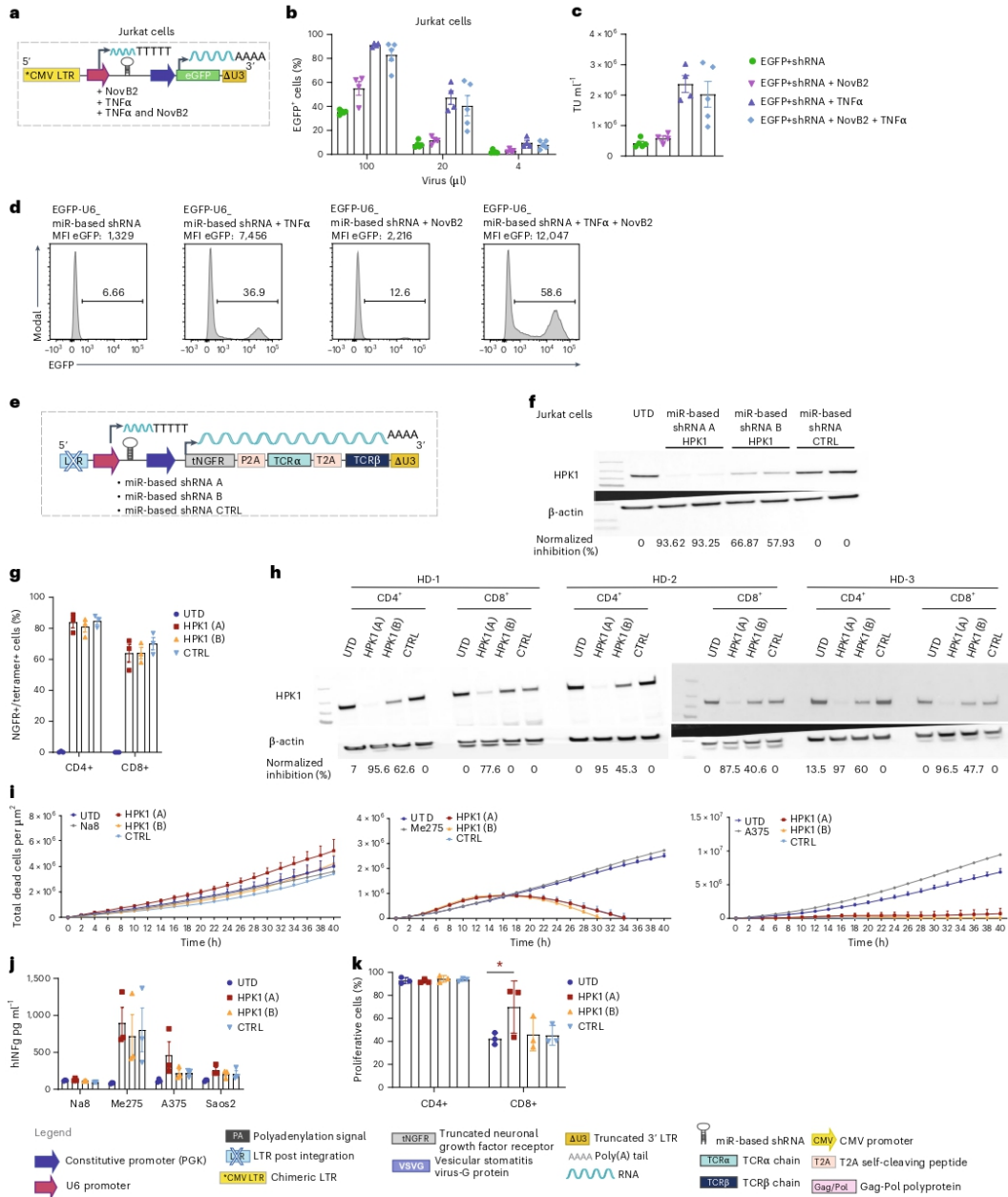
Fig. 6 | Optimized lentivirus vector production protocol yields high titres in the context of transfer vectors encoding miR-based shRNA. **a**, Schematic of sense lentiviral transfer vector encoding a chimeric CMV promoter and enhancer at the 5' LTR to allow enhanced replication in the presence of TNF α and EGFP. **b**, Transduction of Jurkat cells with decreasing volumes of lentivirus vector supernatant produced in the presence or absence of TNF α and NovB2, and flow cytometric evaluation (on day 5) of % EGFP expression. Bar graph represents the mean of 5 independent experiments. **c**, Viral titres (TU ml⁻¹). **d**, Representative histograms of EGFP expression by Jurkat cells transduced with 100 μ l of lentivirus vector supernatant. **e**, Schematic of sense lentiviral transfer vector encoding miR-based shRNA targeting HPK1 (shRNA A and shRNA B) or scramble control (shRNA CTRL) under the U6 promoter, as well as truncated nerve growth factor receptor (tNGFR) and a TCR, both under the PGK promoter and separated by T2A sequences. **f**, Western blot analysis to evaluate HPK1 downregulation in Jurkat cells (technical replicates shown), together with β -actin control. **g**, Transduction efficiency of primary human CD4⁺ and CD8⁺ T cells with lentivirus vector supernatant produced in the presence of TNF α and NovB2. At 5 d

post-transduction, the T cells were stained with HLA-A2/NY-ESO-1₁₅₇₋₁₆₅ tetramer and analysed by flow cytometry. Bar graph represents the mean \pm s.e.m. of $n = 3$ human T-cell donors. **h**, Western blot analysis to evaluate HPK1 downregulation, together with β -actin control blot for $n = 3$ human donors (HD) (Source Data for Fig. 6). **i**, Tumour-cell killing assay for Nuclei red A2⁺/NY⁺ targets Me275 and A375, and Nuclei red and A2⁻/NY⁻ cell line Na8, by TCR-T cells with miR-based shRNA knockdown of HPK1, TCR-T cells comprising a scrambled miR-based shRNA (CTRL) and UTD-T cells, as measured by the IncuCyte instrument as a loss in red area over time. Shown are mean \pm s.e.m. for $n = 3$ independent T-cell donors. **j**, IFN γ release as measured by ELISA upon 24 h co-culture of TCR-T cells with miR-based shRNA knockdown of HPK1 T cells, CTRL- or UTD-T cells with A2⁺/NY⁺ targets Me275, A375 and Saos-2, and A2⁻/NY⁻ cell line Na8. Bar graphs represent the mean \pm s.e.m. for $n = 3$ human T-cell donors. **k**, Percentage of CTV negative cells (cells that have undergone proliferation) upon tumour stimulation. Shown are mean \pm s.e.m. for $n = 3$ healthy T-cell donors. Statistical significance was assessed using two-way ANOVA, * $P = 0.0209$ HPK1 vs UTD CD8⁺.

was used, a gain in viral titre was observed in the presence of TNF α alone, but titres were even higher if NovB2 was combined with TNF α (Fig. 7a, middle and right).

It is well known that the use of vectors comprising U6-driven shRNAs can be toxic to transfected cells^{80–82}, and polymerase III promoters

do not allow for inducible expression of genes of interest. Hence, to overcome this obstacle we next built an antisense vector comprising an miR-based shRNA under 6xNFAT and EGFP under PGK (Fig. 7b, left), and produced lentivirus vectors using our optimized clinical-grade production protocol. We observed an important gain in viral titre in



the presence of NovB2 alone or combined with TNF α (Fig. 7b, middle and right).

We further evaluated an inverted configuration vector comprising the anti-PSMA CAR and miR-based shRNA 'A' targeting HPK1 under 6xNFAT in primary human T cells (Fig. 7c, left). Upon transduction with lentivirus vector produced in the presence of NovB2 and TNF α , we reached approximately 90% and about 60% CAR expression by CD4⁺ and CD8⁺ T cells, respectively (Fig. 7c, middle). Moreover, upon 6 h CAR-T-cell triggering with plate-coated anti-F(ab), we achieved over 90% HPK1 knockdown (Fig. 7c, right).

Finally, for the dual antisense vector, we cloned an miR-based shRNA targeting the TCR-alpha chain under an alternative constitutive Polymerase II promoter, SFFV (silencing prone spleen focus forming virus), and EGFP under PGK (Fig. 7d, left). This is a strategy that can be used to abrogate TCR chain mispairing upon engineering of T cells for ACT with an exogenous TCR²⁵. Transduced Jurkat cells demonstrated efficient knockdown of the TCR-alpha chain with our dual antisense vector as measured by cell-surface staining with a pan-anti-TCR antibody (Fig. 7d, bottom right).

Thus, in summary we have demonstrated that the use of TNF α during virus production when using antisense (or sense) transfer vectors in which the RSV-based promoter and enhancer at the 5' LTR is replaced with the complete CMV promoter and enhancer (which comprises 4 consensus NF- κ B binding motifs⁶⁷) can substantially increase titres. It is likely that the TNF α , in addition to favouring transcription of the transfer vector, also promotes replication of the packaging and envelope vectors. Moreover, the presence of TNF α in the culture media can synergize with NovB2, a protein that can abrogate Dicer-mediated dsRNA antiviral response generated during virus production in HEK293T cells. In addition, the protocol, which is feasible for the production of clinical-grade virus at reduced costs, can be used to generate high titres of 'difficult to produce' lentivirus vector, such as ones encoding miR-based shRNA. Indeed, NovB2 may further abrogate Dicer-mediated processing of such hairpin structures.

Discussion

In recent years, rational TCR- and CAR-T-cell co-engineering strategies have been under extensive investigation to improve responses against solid tumours, either by directly enhancing the intrinsic fitness and function of the T cells themselves or/and by TME reprogramming^{3,30}. In addition to barriers in the TME, the clinical success of T-cell therapy against solid tumours is constrained by adverse patient reactions such as on-target but off-tumour toxicity⁸³, as well as cytokine release syndrome by CAR-T cells⁸⁴ and unexpected cross-reactivity by TCR-T cells against vital organs⁸⁵. Hence, important research efforts are also being undertaken in the development of ON, OFF and STOP switches^{68,86–88} along with gene-modification strategies⁸⁹ and optimized vectors⁴⁴ to allow tighter control of the biological activities of engineered T cells post-infusion³⁰.

Although emerging gene-modification strategies such as Crispr/Cas9 hold tremendous potential for the development of next-generation TCR- and CAR-T cells¹⁹, in particular for gene knock-outs¹ but also gene knock-ins as approaches are developed to increase efficiencies^{90,91}, the (1) strong safety record of lentiviral vectors coupled with (2) enhanced manufacturing protocols³⁸ and (3) the high transduction efficiencies that can readily be achieved make lentivirus vectors an important clinical tool. Indeed, lentivirus vectors will probably be used for years to come in the clinic, likely also in combination with Crispr/Cas9¹⁹ and other gene-engineering techniques. Hence, further optimization of lentiviral vectors, virus production methods and transduction strategies are warranted²³.

Here we have developed an antisense transfer vector allowing efficient constitutive expression of a tumour-directed TCR or CAR and independent co-expression of gene cargo. While we have used the activation-inducible promoter 6xNFAT to express various gene cargoes including IL-2 and miR-based shRNAs to knockdown genes of interest, it is also feasible to employ promoters that respond to environmental cues including hypoxia⁹². Such an approach may be useful, for example, for co-expression of chemokines that can generate a gradient to attract additional lymphocytes into the tumour bed. The development of drug-inducible promoters⁹³, such as the tetracycline-controlled ON system (Tet-ON, of bacterial origin)⁹⁴, comprising non-immunogenic components suitable for the clinic and allowing sufficient expression levels of the target molecule(s) of interest for the therapeutic efficacy, would be of great benefit for tighter and safer control of next-generation TCR- and CAR-T cells and other cellular therapies.

In our study, side-by-side evaluation with comparative dual forward and bidirectional vectors revealed transcriptional interference for the former and leakiness of the inducible promoter for the latter configuration. However, we showed that primary human T cells could be efficiently engineered with lentivirus vector comprising a dual antisense transfer vector encoding a constitutively expressed CAR or TCR and inducible gene cargo without such problems. Moreover, next-generation TCR- and CAR-T cells engineered with the dual antisense lentiviral constructs were validated for functionality both in vitro and in vivo in the context of solid tumour-bearing mice.

While the antisense transfer vector design was limiting to virus production, evidently because of convergent transcription in HEK293T cells, we developed a robust protocol to restore titres. First, we showed that the presence of the RNA interference suppressor protein NovB2²¹, previously demonstrated to inhibit isoforms of Dicer⁶⁵, could augment lentiviral titres. We subsequently sought to address the issue that transcriptional interference is limiting to the levels of the ssRNA viral genome available for packaging. We began by using the Tax protein⁶⁶ which, in addition to a variety of oncogenic properties, can act as a potent transactivator of CMV promoters as they harbour 4 NF- κ B binding motifs⁶⁷. Indeed, we replaced the RSV-based promoter and enhancer at the 5' LTR of the transfer vector with the complete CMV promoter and

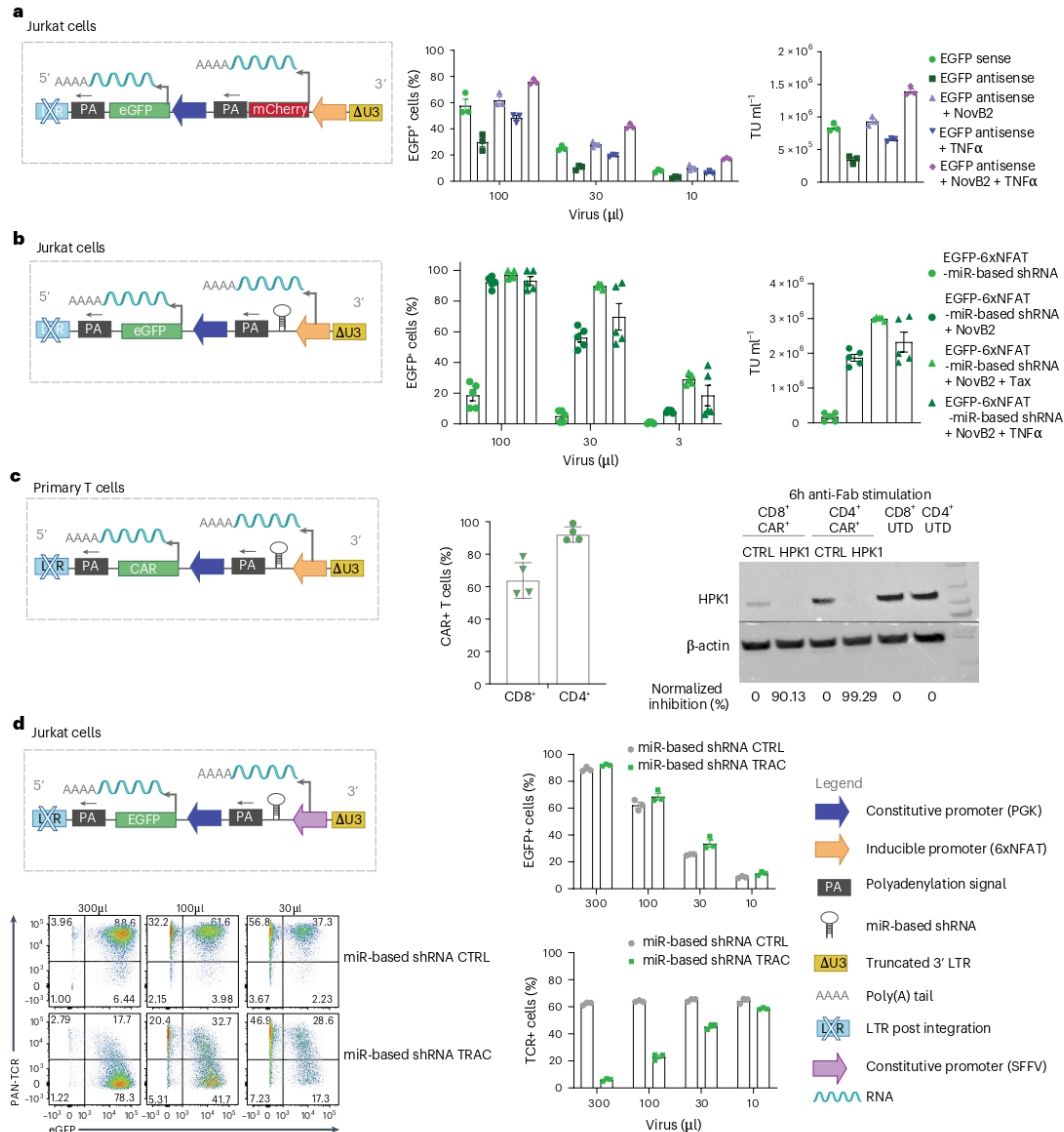
Fig. 7 | Optimized clinical-grade protocol for high-titre lentivirus vector production can be used in the context of antisense vectors encoding miR-based shRNA. **a**, Left: schematic of antisense lentiviral transfer vector encoding EGFP under PGK and mCherry under 6xNFAT. Middle: transduction of Jurkat cells with titrated lentivirus vector supernatant produced in the presence or absence of TNF α in combination with NovB2; flow cytometric evaluation of % EGFP expression on day 5. Bar graphs represent the mean \pm s.e.m. of 3 independent experiments. Right: viral titres (TU ml⁻¹). **b**, Left: schematic of dual antisense lentiviral transfer vector encoding EGFP under PGK and miR-based shRNA under 6xNFAT. Middle: transduction of Jurkat cells with titrated lentivirus vector supernatant produced in the presence or absence of TNF α or Tax in combination with NovB2; flow cytometric evaluation of % EGFP expression on day 5. Bar graphs represent the mean \pm s.e.m. of 5 independent experiments. Right: viral titres (TU ml⁻¹). **c**, Left: schematic of antisense lentiviral transfer vector encoding an anti-PSMA-CAR under PGK and miRNA under 6xNFAT.

Middle: transduction efficiency of primary human CD4⁺ and CD8⁺ T cells with lentivirus vector supernatant produced in the presence of TNF α and NovB2. T cells were stained with fluorescenciated anti-Fab Ab to evaluate cell-surface CAR expression on day 5 post-infection. Bar graphs represent the mean \pm s.e.m. of $n = 4$ human T-cell donors. Right: western blot analysis showing specific downregulation of HPK1 upon 6 h stimulation with plate-coated anti-F(ab)₂, together with β -actin control blot of $n = 2$ human T-cell donors (Source Data for Fig. 7). **d**, Top left: schematic of antisense lentiviral transfer vector encoding EGFP under PGK and miR-based shRNA targeting TRAC, or control miR-based shRNA, under the constitutive promoter SFFV. Bottom left: representative dot plot of flow cytometric evaluation of % EGFP expression on day 5 and PAN-anti-TCR antibody staining to evaluate TCR knockdown. Top right: transduction of Jurkat cells with different amounts of lentivirus vector supernatant. Bar graphs represent the mean \pm s.e.m. of EGFP⁺ cells. Bottom right: the percentage of TCR⁺ cells for 3 independent experiments.

enhancer, and showed that we could increase viral titres in the presence of Tax⁴⁵, and to a greater extent when combined with NovB2.

For potential clinical GMP-grade production of lentivirus vector, we sought a substitution for Tax. We demonstrated that the presence of TNF α (previously shown to efficiently act on NF- κ B binding motifs in a dose-dependent manner⁷³) in the culture supernatant also increased viral titres. Notably, the use of TNF α to increase viral titres may be applicable to other viruses produced from vectors comprising promoters with NF- κ B binding motifs. Moreover, TNF α may be useful for increasing plasmid production (that is, comprising NF- κ B binding motifs) in transfected cells.

Recently, an 'all in one' dual sense lentiviral vector system was described comprising inducible expression of a gene upstream of a constitutively expressed second gene. However, in line with previous work, our data suggest transcriptional interference for this design and consequently lower gene expression⁵⁶, presumably due to competition for the same PA site and the simultaneous occupancy of the DNA template. This lower expression may be limiting to the therapeutic efficacy of the cellular product, such as T cells gene-modified to secrete a decoy molecule targeting an immune checkpoint such as programmed death-protein 1 (PD-1)⁹⁵. The enhanced expression of genes from our dual inverted vector is probably due both to a lack of transcriptional



interference as well as the use of the potent BGH polyadenylation signal⁵⁸. A full head-to-head comparison of the vector designs cannot be undertaken as it is not possible to include independent PA sites in the sense vector as this will abrogate virus production. Notably, it is important to evaluate potential 'leakiness' from vectors comprising inducible promoters. For example, tonic CAR signalling⁷⁰ can lead to gene expression under 6xNFAT in a target antigen-independent manner.

We further tested a bidirectional transfer vector design but observed expression of the inducible gene in non-activated cells. While it may be possible to abrogate leakiness by further buffering the two promoters, this will be limiting to the size of the genes that can subsequently be accommodated; beyond a genomic load of 10,000 bp, lentiviral vectors become increasingly inefficient^{96,97}. We did not test a convergent design for the transfer vectors because we reasoned that there would be interference in gene expression in transduced T cells⁴². Moreover, a convergent design runs the risk of an unwanted IFN response in gene-modified T cells due to the generation of dsRNA.

Taken together, our work presents an improved dual antisense transfer vector and accompanying lentivirus vector production protocol enabling efficient transduction of primary human T cells with a constitutively expressed tumour-targeting receptor along with independent activation-inducible co-expression of gene cargo. We demonstrated functionality of the dual inverted vector encoding either a CAR or a TCR under PGK and various gene cargoes under 6xNFAT including IL-2 and miR-based shRNA targeting HPK1. We further demonstrated proof-of-principle for the use of our dual inverted vector for generating 4G CAR-T cells for ACT. We showed that the inducible gene cargo (luciferase) was expressed by T cells in tumours only if target antigen for the CARs was present. Notably, our overall approach is universal in that it can be applied to the engineering of other cell types, alternative polymerase II promoters and different engineering purposes in the context of other diseases. Importantly, our strategy can lower costs due to the use of a single vector and higher titres achieved, and it holds important promise towards effective and safety-enhanced next-generation cellular therapies reaching the clinic.

Methods

Cell lines and culture

The prostate carcinoma cell line PC3-PIP (PMSA⁺), PC3 engineered with human CD19+ cells, Bjab, Na8, Me275, A375, Saos-2, 293T human embryonic kidney (HEK293T) cells and Jurkat cells were cultured in RPMI-1640 medium supplemented with 10% heat-inactivated fetal bovine serum (FBS), 2 mmol l⁻¹ L-glutamine, 100 µg ml⁻¹ penicillin and 100 U ml⁻¹ streptomycin, at 37 °C in a 5% CO₂ atmosphere (Invitrogen, Life technologies). Na8, Me275, A375, Saos-2, 293T and Jurkat cell lines were purchased from the ATCC. The PC3-PIP and PC3 cell lines were kindly provided by Dr A. Rosato (University of Padua, Padova, Italy)⁹⁸. Bjab was kindly provided by Dr C. Arber (University of Lausanne, Switzerland). The PC3 and PC3-PIP cells lentivirally transduced to enforce expression of CD19 (PC3-CD19⁺ and PC3-PIP CD19⁺) were kindly provided by Dr Y. Muller (University of Lausanne, Switzerland). The HEK293T cell line was used for lentivirus vector production.

Vector construction

Second-generation CARs comprising the CD8α hinge, CD28 transmembrane (TM), CD28 endodomain (ED) and CD3-zeta ED were cloned into a 2G self-inactivating lentiviral expression vector pELNS under the PGK promoter. The HLA-A2/NY-ESO-1₁₅₇₋₁₆₅ restricted TCR was cloned in vector pRRL, with expression also driven by the PGK promoter. The anti-PSMA scFv derived from monoclonal antibody J591⁹⁹ and the anti-CD19 CAR scFv derived from monoclonal antibody FMC63¹⁰⁰ were used to confer tumour-antigen specificity. The HLA-A2/NY-ESO-1₁₅₇₋₁₆₅ restricted TCR has been previously described⁶⁹. The (NFAT)₆ response elements-IL-2 minimal promoter, abbreviated as 6xNFAT, was used to evaluate inducible expression of different gene cargoes. Replacement

of the RSV promoter with the CMV promoter in the 5' LTR was used to enable TNFα in the culture supernatant to favour transcription of the ssRNA viral genome.

Lentivirus vector production

For large-scale production: briefly, 24 h before transfection, 293T cells were seeded at 10 × 10⁶ cells in 30 ml medium in a T-150 tissue culture flask. All plasmid DNA was purified using the Endo-free Maxiprep kit (Invitrogen, Life Technologies). 293T cells were transfected with 7 µg pVSVG (VSV glycoprotein expression plasmid) or 7 µg pVSVG-T2A-NovB2, 18 µg of R874 (Rev and Gag/Pol expression plasmid) and 15 µg of pELNS or pCRRL transgene plasmid using a mix of Turbofect (Thermo Fisher) and OptiMem media (Invitrogen, Life Technologies, 180 µl of Turbofect for 3 ml of OptiMem). The cells were further transfected with a plasmid encoding the T-cell leukaemia virus 1, TAX protein, or the medium was further supplemented with TNFα at 10 ng ml⁻¹ working concentration. The viral supernatant was collected at 48 h post-transfection. Viral particles were concentrated by ultracentrifugation for 2 h at 24,000 g and resuspended in 400 µl complete RPMI-1640 media, followed by immediate snap freezing on dry ice.

For small-scale production: briefly, 4–5 h before transfection, 293T cells were seeded at 1.25 × 10⁶ cells in 2 ml medium per well in a 6-well plate. 293T cells were transfected with 2.5 µg total DNA (divided as 0.282 µg pVSVG or pVSVG-T2A-NovB2, 0.846 µg R874, and 1.125 µg pELNS or pCRRL transgene plasmid), using a mix of Lipofectamine 2000 (Invitrogen) and OptiMem media (Invitrogen, Life Technologies) according to the manufacturer's instructions. The cells were further transfected with a plasmid encoding the T-cell leukaemia virus 1, TAX protein, or the medium was further supplemented with TNFα at 10 ng ml⁻¹. The viral supernatant was collected at 48 h post-transfection and supernatant was used directly.

Jurkat cell transduction for viral titration

Jurkat cells were suspended at 1 × 10⁵ cells per ml and seeded into 24-well plates at 1 ml per well. Different volumes of viral supernatant were used for transduction, as indicated, ranging from 300 µl down to 3 µl. Cell media were refreshed after incubation for 24 h at 37 °C. Viral titres (transducing units per ml (TU ml⁻¹)) were calculated as follows: ((total number of cells/100) × percentage of transduced cells) × dilution of the virus supernatant).

Primary human T-cell purification, activation, transduction and expansion

Primary human T cells were isolated from the peripheral blood mononuclear cells (PBMCs) of healthy donors (HDs; prepared as buffy coats) collected with informed consent by the blood bank. Total PBMCs were obtained via Lymphoprep (Axonlab) separation solution by a standard protocol of centrifugation. CD4⁺ and CD8⁺ T cells were isolated by negative selection using magnetic beads following the manufacturer's protocol (easySEP, Stem Cell Technology). Purified CD4⁺ and CD8⁺ T cells were cultured separately in RPMI-1640 with GlutaMax, supplemented with 10% heat-inactivated FBS, 100 U ml⁻¹ penicillin, 100 µg ml⁻¹ streptomycin sulfate, and stimulated with anti-CD3 and anti-CD28 monoclonal antibody (mAb)-coated beads (Invitrogen, Life Technologies) at a 1:2 ratio of T cells to beads. T cells were transduced with lentivirus vector particles at 18–22 h post-activation. Human recombinant interleukin-2 (h-IL-2; Glaxo) was replenished every other day for a concentration of 50 IU ml⁻¹ until 5 d post-stimulation (day +5). At day +5, magnetic beads were removed, and h-IL-7 and h-IL-15 (Miltenyi Biotec) were added to the cultures at 10 ng ml⁻¹. A cell density of 0.5–1 × 10⁶ cells per ml was maintained for expansion. Rested engineered T cells were adjusted for equivalent transgene expression before all functional assays; the more efficiently transduced samples were diluted with appropriate numbers of UTD-T cells.

Cytotoxicity assays

Cytotoxicity assays were performed using the IncuCyte Instrument (Essen Bioscience). Briefly, 1.25×10^4 target cells were seeded in flat-bottom 96-well plates (Costar, Vitaris). Four hours later, rested T cells (no cytokine for 48 h) were washed and seeded at 2.5×10^4 cells per well, at a 2:1 effector:target (E:T) ratio in complete media. No exogenous cytokines were added during the co-culture period of the assay. CytotoxRed or Caspase-3/7green reagent (Essen Bioscience) was added at a final concentration of 125 nM in a total volume of 200 μ l. Internal experimental negative controls were included in all assays, including co-incubation of UTD-T cells and tumour cells, as well as tumour cells alone, to monitor tumour cell death over time. As a positive control, tumour cells alone were treated with 1% triton solution to evaluate maximal killing in the assay. In some assays (as indicated in the figure legends), freshly generated nuclei red and nuclei green engineered tumour cells were used. The nuclei red/green target cells were generated with IncuCyte Nuclight Lentivirus (Essen Bioscience) for nuclear-restricted expression of tagGFP2 (green fluorescent protein) and mKate2 (red fluorescent protein), according to the manufacturer's instructions. Activation of co-engineered TCR-T and CAR-T cells upon specific antigen stimulation was assessed by mCherry IncuCyte quantification over time. Images of total red area per well and green area per well were collected every 2 h of the co-culture. The total red area per well and green area per well were obtained using the analysis protocol provided by Essen Bioscience. Data were normalized by subtracting the background fluorescence observed at time 0 (that is, before any cell killing by CAR-T cells) from all further timepoints. Data are expressed as mean \pm s.e.m. of different HDs.

Cell staining and flow cytometric analysis

To evaluate CAR cell-surface expression, transduced cells were stained with fluorescinated anti-human F(ab')mAb (BD Biosciences). To evaluate TCR cell-surface expression, transduced cells were stained with fluorescinated HLA-A2/NY-ESO-1₁₅₇₋₁₆₅ tetramer produced in-house. Aqua live Dye BV510 and near-infrared fluorescent reactive dye (APC Cy-7) were used to assess viability (Invitrogen, Life Technologies). To evaluate mCherry induction upon stimulation, T cells were stained with near-infrared fluorescent reactive dye (APC Cy-7) (Invitrogen, Life Technologies). Acquisition and analysis were performed using a BD FACS LRSII flow cytometer and FACS DIVA software (BD Biosciences).

Immunoblotting

Cells were lysed in RIPA buffer supplemented with Halt phosphate/protease inhibitors (ThermoFisher) and boiled at 97 °C for 10 min with Bolt LDS sample buffer and reducing agent (ThermoFisher). Protein samples (10 μ g) were separated by SDS-PAGE and transferred to PVDF membranes using the iBlot2 system (ThermoFisher). Antibody staining of the molecules of interest was carried out according to the manufacturer's instructions. Rabbit monoclonal antibody (EP630Y) specific to MAP4K1/HPK1 antibody (ab33910) was purchased from Abcam and anti- β -actin (sc-47778) from Santa Cruz. Images were acquired with a western blot imager (Fusion, Vilber Lourmat), and protein levels were quantified using the ImageJ software by analysing pixel intensity of the bands. Total HPK1 level was calculated by dividing its signal to the β -actin signal.

Mouse strain and in vivo experimentation

NOD scid gamma (NSG) male mice were bred and housed in a specific and opportunistic pathogen-free (SOPF) animal facility at the University of Lausanne (Epalinges, Switzerland). All in vivo experiments were conducted in accordance with and approval from the Service of Consumer and Veterinary Affairs (SCAV) of the Canton of Vaud. All cages housed 5 mice in an enriched environment providing free access to food and water. Mice were monitored at least every other day for signs of distress during experimentation and euthanized at endpoint by carbon dioxide overdose.

Subcutaneous tumour model and adoptive T-cell transfer

NSG male mice aged 8–12 weeks were subcutaneously injected with 5×10^6 PC3-PIP (or PC3-CD19⁺) tumour cells or 10×10^6 Bjab. Once tumour was palpable (day 5 for PC3 and day 7 for Bjab), the mice were treated by peritumoural injection of 5×10^6 UTD or CAR-T cells. Tumour volume was assessed every other day by caliper measurement. Tumour volumes were calculated using the formula $V = 1/2(\text{length} \times \text{width}^2)$, where length is the greatest longitudinal diameter and width is the greatest transverse diameter determined via caliper measurement.

In vitro bioluminescence assay to evaluate inducible gene cargo expression levels for sense vs antisense lentiviral vectors

To evaluate gene-cargo expression levels for CAR- or TCR-T cells transduced with sense vs antisense lentiviral vectors containing luciferase as the inducible gene cargo under 6xNFAT, 2.5×10^4 UTD and transduced T cells were co-cultured with target tumour cells at 1:1 E:T ratio for 24 h in 96-well plates. The following day, the culture media were washed away and 10 μ l per well of optimally diluted Reporter Lysis 5X buffer (Promega) was added and the cells resuspended. Luciferin (50 μ l per well) (PerkinElmer) was then added and cell lysates were transferred into white 96-well white optiplates (PerkinElmer) for bioluminescence acquisition. Luciferase activity was measured by total counts acquired using the HIDEX sense 425-30li plate reader and software (Hidex).

Proliferation assay

To assess the proliferative capacity of A2/NY-specific TCR-T cells co-expressing an miR-based shRNA, both transduced and UTD-T cells ($n = 3$ donors) were stained with CTV (Invitrogen, Life Technologies) according to the manufacturer's instructions. Cells were then stimulated for 96 h with anti-CD3 and anti-CD28 monoclonal antibody (mAb)-coated-beads (Invitrogen, Life Technologies) at a 2:1 ratio of beads:T cells, or with A2'/NY' tumour cells lines (Me275, A375 and Saos-2) and an A2'/NY' cell line (Na8 cells) at an E:T ratio of 1:1.

In vivo bioluminescence imaging using luciferase

Luciferase expression was evaluated in vivo from day 1 to day 11 post T-cell transfer. Mice were injected intraperitoneally with 150 mg kg⁻¹ d-luciferin (PerkinElmer) in 100 μ l of PBS and transferred into an anaesthesia chamber induced by 3% mixture of isoflurane and 1.5% oxygen. Anaesthetized animals were imaged at 10–35 min post-luciferin injection using the In-Vivo Xtreme system (In-Vivo Xtrem, Bruker) reducing anaesthesia level to 1%. The photons emitted from the luciferase-expressing T cells were quantified using Molecular Imaging software (Bruker). A pseudocolour image representing the luminescence flux intensity was generated (violet and red colours refer to the least and the most intense flux, respectively) and then superimposed over the greyscale reference image. The luminescent region of interest was determined by drawing a gate and intensity of the signal was measured as total photon s⁻¹ mm⁻², which correlates proportionally with the expression of luciferase gene in transduced T cells. Mice were euthanized when the tumour volume reached 1,000 mm³ according to the following formula $V = 1/2(\text{length} \times \text{width}^2)$, or when they met euthanasia criteria (weight loss, signs of distress) in accordance with the Swiss Federal Veterinary Office and the Cantonal Veterinary Office guidelines.

Statistical analysis

GraphPad Prism 9.0 software was used to determine statistically significant differences using one-way analysis of variance (ANOVA) followed by Tukey post-hoc correction for multiple comparisons (column groups, one variable tested). A two-way repeated measurement ANOVA followed by Tukey post-hoc correction was used for statistical analysis of tumour growth curves, in vitro cytotoxicity and mCherry induction analysis (two-variables analysis for multiple groups). Differences were

considered significant when $*P < 0.05$, very significant when $**P < 0.01$ and highly significant when $***P < 0.001$.

Reporting summary

Further information on research design is available in the Nature Portfolio Reporting Summary linked to this article.

Data availability

The main data supporting the findings of this study are available within the article and its Supplementary Information. All raw data generated during the study are available from the corresponding authors on request. Source data for the figures are provided with this paper.

References

1. Stadtmayer, E. A. et al. CRISPR-engineered T cells in patients with refractory cancer. *Science* **367**, eaba7365 (2020).
2. Maude, S. L. et al. Chimeric antigen receptor T cells for sustained remissions in leukemia. *N. Engl. J. Med.* **371**, 1507–1517 (2014).
3. Aiuti, A. et al. Lentiviral hematopoietic stem cell gene therapy in patients with Wiskott-Aldrich syndrome. *Science* **341**, 1233151 (2013).
4. Biffi, A. et al. Lentiviral hematopoietic stem cell gene therapy benefits metachromatic leukodystrophy. *Science* **341**, 1233158 (2013).
5. Frangoul, H. et al. CRISPR-Cas9 gene editing for sickle cell disease and beta-thalassemia. *N. Engl. J. Med.* **384**, 252–260 (2021).
6. Cavazzana-Calvo, M. et al. Transfusion independence and HMGA2 activation after gene therapy of human beta-thalassaemia. *Nature* **467**, 318–322 (2010).
7. Milone, M. C. & O'Doherty, U. Clinical use of lentiviral vectors. *Leukemia* **32**, 1529–1541 (2018).
8. Irving, M., Vuillefroy de Silly, R., Scholten, K., Dilek, N. & Coukos, G. Engineering chimeric antigen receptor T-cells for racing in solid tumors: don't forget the fuel. *Front. Immunol.* **8**, 267 (2017).
9. Wennhold, K., Shimabukuro-Vornhagen, A. & von Bergwelt-Baildon, M. B cell-based cancer immunotherapy. *Transfus. Med. Hemother.* **46**, 36–46 (2019).
10. Rezvani, K., Rouce, R., Liu, E. & Shpall, E. Engineering natural killer cells for cancer immunotherapy. *Mol. Ther.* **25**, 1769–1781 (2017).
11. Klichinsky, M. et al. Human chimeric antigen receptor macrophages for cancer immunotherapy. *Nat. Biotechnol.* **38**, 947–953 (2020).
12. Hanna, J., Hossain, G. S. & Kocerha, J. The potential for microRNA therapeutics and clinical research. *Front. Genet.* **10**, 478 (2019).
13. Beatty, G. L. et al. Mesothelin-specific chimeric antigen receptor mRNA-engineered T cells induce anti-tumor activity in solid malignancies. *Cancer Immunol. Res.* **2**, 112–120 (2014).
14. Bozza, M. et al. A nonviral, nonintegrating DNA nanovector platform for the safe, rapid, and persistent manufacture of recombinant T cells. *Sci. Adv.* **7**, eabf1333 (2021).
15. Mulia, G. E., Picanco-Castro, V., Stavrou, E. F., Athanassiadou, A. & Figueiredo, M. L. Advances in the development and the applications of nonviral, episomal vectors for gene therapy. *Hum. Gene Ther.* **32**, 1076–1095 (2021).
16. Urnov, F. D., Rebar, E. J., Holmes, M. C., Zhang, H. S. & Gregory, P. D. Genome editing with engineered zinc finger nucleases. *Nat. Rev. Genet.* **11**, 636–646 (2010).
17. Jung, J. K. & Sander, J. D. TALENs: a widely applicable technology for targeted genome editing. *Nat. Rev. Mol. Cell Biol.* **14**, 49–55 (2013).
18. Doudna, J. A. & Charpentier, E. Genome editing. The new frontier of genome engineering with CRISPR-Cas9. *Science* **346**, 1258096 (2014).
19. Wellhausen, N., Agarwal, S., Rommel, P. C., Gill, S. I. & June, C. H. Better living through chemistry: CRISPR/Cas engineered T cells for cancer immunotherapy. *Curr. Opin. Immunol.* **74**, 76–84 (2021).
20. Hacker, U. T., Bentler, M., Kaniowska, D., Morgan, M. & Buning, H. Towards clinical implementation of adeno-associated virus (AAV) vectors for cancer gene therapy: current status and future perspectives. *Cancers* **12**, 1889 (2020).
21. Anson, D. S. The use of retroviral vectors for gene therapy—what are the risks? A review of retroviral pathogenesis and its relevance to retroviral vector-mediated gene delivery. *Genet. Vaccines Ther.* **2**, 9 (2004).
22. Thomas, C. E., Ehrhardt, A. & Kay, M. A. Progress and problems with the use of viral vectors for gene therapy. *Nat. Rev. Genet.* **4**, 346–358 (2003).
23. Irving, M., Lanitis, E., Migliorini, D., Ivics, Z. & Guedan, S. Choosing the right tool for genetic engineering: clinical lessons from chimeric antigen receptor-T cells. *Hum. Gene Ther.* **32**, 1044–1058 (2021).
24. D'Angelo, S. P. et al. Antitumor activity associated with prolonged persistence of adoptively transferred NY-ESO-1 (c259) T cells in synovial sarcoma. *Cancer Discov.* **8**, 944–957 (2018).
25. Manfredi, F. et al. TCR redirected T cells for cancer treatment: achievements, hurdles, and goals. *Front. Immunol.* **11**, 1689 (2020).
26. Ishihara, M. et al. NY-ESO-1-specific redirected T cells with endogenous TCR knockdown mediate tumor response and cytokine release syndrome. *J. Immunother. Cancer* **10**, e003811 (2022).
27. Thomas, R. et al. NY-ESO-1 based immunotherapy of cancer: current perspectives. *Front. Immunol.* **9**, 947 (2018).
28. Ghassemi, S. et al. Rapid manufacturing of non-activated potent CAR T cells. *Nat. Biomed. Eng.* **6**, 118–128 (2022).
29. Rosenberg, S. A. et al. Durable complete responses in heavily pretreated patients with metastatic melanoma using T-cell transfer immunotherapy. *Clin. Cancer Res.* **17**, 4550–4557 (2011).
30. Lanitis, E., Coukos, G. & Irving, M. All systems go: converging synthetic biology and combinatorial treatment for CAR-T cell therapy. *Curr. Opin. Biotechnol.* **65**, 75–87 (2020).
31. Lanitis, E., Dangaj, D., Irving, M. & Coukos, G. Mechanisms regulating T-cell infiltration and activity in solid tumors. *Ann. Oncol.* **28**, xii18–xii32 (2017).
32. Zhang, L. et al. Tumor-infiltrating lymphocytes genetically engineered with an inducible gene encoding interleukin-12 for the immunotherapy of metastatic melanoma. *Clin. Cancer Res.* **21**, 2278–2288 (2015).
33. Chmielewski, M. & Abken, H. CAR T cells transform to trucks: chimeric antigen receptor-redirectioned T cells engineered to deliver inducible IL-12 modulate the tumour stroma to combat cancer. *Cancer Immunol. Immunother.* **61**, 1269–1277 (2012).
34. Chinnasamy, D. et al. Local delivery of interleukin-12 using T cells targeting VEGF receptor-2 eradicates multiple vascularized tumors in mice. *Clin. Cancer Res.* **18**, 1672–1683 (2012).
35. Hoyos, V. et al. Engineering CD19-specific T lymphocytes with interleukin-15 and a suicide gene to enhance their anti-lymphoma/leukemia effects and safety. *Leukemia* **24**, 1160–1170 (2010).
36. Chmielewski, M. & Abken, H. CAR T cells releasing IL-18 convert to T-Bet(high) FoxO1(low) effectors that exhibit augmented activity against advanced solid tumors. *Cell Rep.* **21**, 3205–3219 (2017).
37. Drakes, D. J. et al. Optimization of T-cell receptor-modified T cells for cancer therapy. *Cancer Immunol. Res.* **8**, 743–755 (2020).
38. Chmielewski, M., Kopecky, C., Hombach, A. A. & Abken, H. IL-12 release by engineered T cells expressing chimeric antigen receptors can effectively Muster an antigen-independent macrophage response on tumor cells that have shut down tumor antigen expression. *Cancer Res.* **71**, 5697–5706 (2011).
39. Yeku, O. O. & Brentjens, R. J. Armored CAR T-cells: utilizing cytokines and pro-inflammatory ligands to enhance CAR T-cell anti-tumour efficacy. *Biochem. Soc. Trans.* **44**, 412–418 (2016).

40. David, R. M. & Doherty, A. T. Viral vectors: the road to reducing genotoxicity. *Toxicol. Sci.* **155**, 315–325 (2017).
41. Zimmermann, K. et al. Design and characterization of an “all-in-one” lentiviral vector system combining constitutive anti-GD2 CAR expression and inducible cytokines. *Cancers* **12**, 375 (2020).
42. Liu, Y. et al. Armored inducible expression of IL-12 enhances antitumor activity of glypican-3-targeted chimeric antigen receptor-engineered T cells in hepatocellular carcinoma. *J. Immunol.* **203**, 198–207 (2019).
43. Mizuguchi, H., Xu, Z., Ishii-Watabe, A., Uchida, E. & Hayakawa, T. IRES-dependent second gene expression is significantly lower than cap-dependent first gene expression in a bicistronic vector. *Mol. Ther.* **1**, 376–382 (2000).
44. Leisegang, M. et al. Enhanced functionality of T cell receptor-redirection T cells is defined by the transgene cassette. *J. Mol. Med.* **86**, 573–583 (2008).
45. de Felipe, P., Martin, V., Cortes, M. L., Ryan, M. & Izquierdo, M. Use of the 2A sequence from foot-and-mouth disease virus in the generation of retroviral vectors for gene therapy. *Gene Ther.* **6**, 198–208 (1999).
46. Borman, A. M., Le Mercier, P., Girard, M. & Kean, K. M. Comparison of picornaviral IRES-driven internal initiation of translation in cultured cells of different origins. *Nucleic Acids Res.* **25**, 925–932 (1997).
47. de Felipe, P. Polycistronic viral vectors. *Curr. Gene Ther.* **2**, 355–378 (2002).
48. Hooijberg, E., Bakker, A. Q., Ruizendaal, J. J. & Spits, H. NFAT-controlled expression of GFP permits visualization and isolation of antigen-stimulated primary human T cells. *Blood* **96**, 459–466 (2000).
49. Zhang, L. et al. Improving adoptive T cell therapy by targeting and controlling IL-12 expression to the tumor environment. *Mol. Ther.* **19**, 751–759 (2011).
50. Merten, O. W., Hebben, M. & Bovolenta, C. Production of lentiviral vectors. *Mol. Ther. Methods Clin. Dev.* **3**, 16017 (2016).
51. Amado, R. G. & Chen, I. S. Lentiviral vectors—the promise of gene therapy within reach? *Science* **285**, 674–676 (1999).
52. Escors, D. & Breckpot, K. Lentiviral vectors in gene therapy: their current status and future potential. *Arch. Immunol. Ther. Exp.* **58**, 107–119 (2010).
53. Kutner, R. H., Zhang, X. Y. & Reiser, J. Production, concentration and titration of pseudotyped HIV-1-based lentiviral vectors. *Nat. Protoc.* **4**, 495–505 (2009).
54. Zufferey, R., Donello, J. E., Trono, D. & Hope, T. J. Woodchuck hepatitis virus posttranscriptional regulatory element enhances expression of transgenes delivered by retroviral vectors. *J. Virol.* **73**, 2886–2892 (1999).
55. Zufferey, R. et al. Self-inactivating lentivirus vector for safe and efficient in vivo gene delivery. *J. Virol.* **72**, 9873–9880 (1998).
56. Curtin, J. A., Dane, A. P., Swanson, A., Alexander, I. E. & Ginn, S. L. Bidirectional promoter interference between two widely used internal heterologous promoters in a late-generation lentiviral construct. *Gene Ther.* **15**, 384–390 (2008).
57. Tian, J. & Andreadis, S. T. Independent and high-level dual-gene expression in adult stem-progenitor cells from a single lentiviral vector. *Gene Ther.* **16**, 874–884 (2009).
58. West, S. & Proudfoot, N. J. Transcriptional termination enhances protein expression in human cells. *Mol. Cell* **33**, 354–364 (2009).
59. Ferreira, C. B. et al. Lentiviral vector production titer is not limited in HEK293T by induced intracellular innate immunity. *Mol. Ther. Methods Clin. Dev.* **17**, 209–219 (2020).
60. Poirier, E. Z. et al. An isoform of Dicer protects mammalian stem cells against multiple RNA viruses. *Science* **373**, 231–236 (2021).
61. Maetzig, T. et al. Mechanisms controlling titer and expression of bidirectional lentiviral and gammaretroviral vectors. *Gene Ther.* **17**, 400–411 (2010).
62. Gullerova, M. & Proudfoot, N. J. Convergent transcription induces transcriptional gene silencing in fission yeast and mammalian cells. *Nat. Struct. Mol. Biol.* **19**, 1193–1201 (2012).
63. Sullivan, C. S. & Ganem, D. A virus-encoded inhibitor that blocks RNA interference in mammalian cells. *J. Virol.* **79**, 7371–7379 (2005).
64. Maillard, P. V. et al. Antiviral RNA interference in mammalian cells. *Science* **342**, 235–238 (2013).
65. Suzuki, N. et al. Robust enhancement of lentivirus production by promoter activation. *Sci. Rep.* **8**, 15036 (2018).
66. Jeang, K. T., Giam, C. Z., Majone, F. & Aboud, M. Life, death, and tax: role of HTLV-1 oncoprotein in genetic instability and cellular transformation. *J. Biol. Chem.* **279**, 31991–31994 (2004).
67. Moch, H., Lang, D. & Stamminger, T. Strong *trans* activation of the human cytomegalovirus major immediate-early enhancer by p40tax of human T-cell leukemia virus type I via two repetitive tax-responsive sequence elements. *J. Virol.* **66**, 7346–7354 (1992).
68. Giordano-Atianese, G. et al. A computationally designed chimeric antigen receptor provides a small-molecule safety switch for T-cell therapy. *Nat. Biotechnol.* <https://doi.org/10.1038/s41587-019-0403-9> (2020).
69. Irving, M. et al. Interplay between T cell receptor binding kinetics and the level of cognate peptide presented by major histocompatibility complexes governs CD8+ T cell responsiveness. *J. Biol. Chem.* **287**, 23068–23078 (2012).
70. Long, A. H. et al. 4-1BB costimulation ameliorates T cell exhaustion induced by tonic signaling of chimeric antigen receptors. *Nat. Med.* **21**, 581–590 (2015).
71. Sampey, G. C. et al. Complex role of microRNAs in HTLV-1 infections. *Front. Genet.* **3**, 295 (2012).
72. Hellweg, C. E., Arenz, A., Bogner, S., Schmitz, C. & Baumstark-Khan, C. Activation of nuclear factor kappa B by different agents: influence of culture conditions in a cell-based assay. *Ann. N. Y. Acad. Sci.* **1091**, 191–204 (2006).
73. Zeng, Y., Wagner, E. J. & Cullen, B. R. Both natural and designed micro RNAs can inhibit the expression of cognate mRNAs when expressed in human cells. *Mol. Cell* **9**, 1327–1333 (2002).
74. Chung, K. H. et al. Polycistronic RNA polymerase II expression vectors for RNA interference based on BIC/miR-155. *Nucleic Acids Res.* **34**, e53 (2006).
75. Zhu, X. et al. A versatile approach to multiple gene RNA interference using microRNA-based short hairpin RNAs. *BMC Mol. Biol.* **8**, 98 (2007).
76. Poluri, A. & Sutton, R. E. Titers of HIV-based vectors encoding shRNAs are reduced by a dicer-dependent mechanism. *Mol. Ther.* **16**, 378–386 (2008).
77. Si, J. et al. Hematopoietic progenitor kinase1 (HPK1) mediates T cell dysfunction and is a druggable target for T cell-based immunotherapies. *Cancer Cell* **38**, 551–566 (2020).
78. Rudolph, T. et al. High-efficiency retroviral vector mediated gene transfer into human peripheral blood CD4+ T lymphocytes. *Gene Ther.* **3**, 695–705 (1996).
79. Wang, Y. et al. Pharmacological inhibition of hematopoietic progenitor kinase 1 positively regulates T-cell function. *PLoS ONE* **15**, e0243145 (2020).
80. Grimm, D. et al. Fatality in mice due to oversaturation of cellular microRNA/short hairpin RNA pathways. *Nature* **441**, 537–541 (2006).
81. Castanotto, D. et al. Combinatorial delivery of small interfering RNAs reduces RNAi efficacy by selective incorporation into RISC. *Nucleic Acids Res.* **35**, 5154–5164 (2007).

82. Boudreau, R. L., Martins, I. & Davidson, B. L. Artificial microRNAs as siRNA shuttles: improved safety as compared to shRNAs in vitro and in vivo. *Mol. Ther.* **17**, 169–175 (2009).
83. Morgan, R. A. et al. Case report of a serious adverse event following the administration of T cells transduced with a chimeric antigen receptor recognizing ERBB2. *Mol. Ther.* **18**, 843–851 (2010).
84. Wolf, B. et al. Safety and tolerability of adoptive cell therapy in cancer. *Drug Saf.* **42**, 315–334 (2019).
85. Linette, G. P. et al. Cardiovascular toxicity and titin cross-reactivity of affinity-enhanced T cells in myeloma and melanoma. *Blood* **122**, 863–871 (2013).
86. Jan, M. et al. Reversible ON- and OFF-switch chimeric antigen receptors controlled by lenalidomide. *Sci. Transl. Med.* **13**, eabb6295 (2021).
87. Wu, C. Y., Roybal, K. T., Puchner, E. M., Onuffer, J. & Lim, W. A. Remote control of therapeutic T cells through a small molecule-gated chimeric receptor. *Science* **350**, aab4077 (2015).
88. Li, H. S. et al. High-performance multiplex drug-gated CAR circuits. *Cancer Cell* <https://doi.org/10.1016/j.ccell.2022.08.008> (2022).
89. Roybal, K. T. et al. Precision tumor recognition by T cells with combinatorial antigen-sensing circuits. *Cell* **164**, 770–779 (2016).
90. Shy, B. R. et al. High-yield genome engineering in primary cells using a hybrid ssDNA repair template and small-molecule cocktails. *Nat. Biotechnol.* <https://doi.org/10.1038/s41587-022-01418-8> (2022).
91. Oh, S. A. et al. High-efficiency nonviral CRISPR/Cas9-mediated gene editing of human T cells using plasmid donor DNA. *J. Exp. Med.* **219**, e20211530 (2022).
92. Liao, Q. et al. Engineering T cells with hypoxia-inducible chimeric antigen receptor (HiCAR) for selective tumor killing. *Biomark. Res.* **8**, 56 (2020).
93. Liu, X. et al. De novo design of programmable inducible promoters. *Nucleic Acids Res.* **47**, 10452–10463 (2019).
94. Das, A. T., Tenenbaum, L. & Berkhout, B. Tet-On systems for doxycycline-inducible gene expression. *Curr. Gene Ther.* **16**, 156–167 (2016).
95. Rafiq, S. et al. Targeted delivery of a PD-1-blocking scFv by CAR-T cells enhances anti-tumor efficacy in vivo. *Nat. Biotechnol.* **36**, 847–856 (2018).
96. Kumar, M., Keller, B., Makalou, N. & Sutton, R. E. Systematic determination of the packaging limit of lentiviral vectors. *Hum. Gene Ther.* **12**, 1893–1905 (2001).
97. Yacoub, N., Romanowska, M., Haritonova, N. & Foerster, J. Optimized production and concentration of lentiviral vectors containing large inserts. *J. Gene Med.* **9**, 579–584 (2007).
98. Ghosh, A., Wang, X., Klein, E. & Heston, W. D. Novel role of prostate-specific membrane antigen in suppressing prostate cancer invasiveness. *Cancer Res.* **65**, 727–731 (2005).
99. Gong, M. C., Chang, S. S., Sadelain, M., Bander, N. H. & Heston, W. D. Prostate-specific membrane antigen (PSMA)-specific monoclonal antibodies in the treatment of prostate and other cancers. *Cancer Metastasis Rev.* **18**, 483–490 (1999).
100. Kochenderfer, J. N. et al. Construction and preclinical evaluation of an anti-CD19 chimeric antigen receptor. *J. Immunother.* **32**, 689–702 (2009).

Acknowledgements

We thank members of the Flow Cytometry Platform and the Animal Care Facility of the Epalinges Campus of the University of Lausanne for their excellent support, and Dr J. A. Rath from the University of Lausanne for his advice on in vivo imaging acquisition and analysis. This work was generously supported by Ludwig Cancer Research, an Advanced European Research Council Grant to G.C. (1400206AdG-322875), the Prostate Cancer Foundation, the Biltema Foundation, Cancer and the Swiss National Science Foundation to M.I.

(SNSF# 310030_204326). We also thank the Swiss Confederation for generously supporting the PhD salary of K.O. via the Swiss Government Excellence Scholarships programme.

Author contributions

M.I. and G.C. directed the study. M.I. supervised the research. P.R. and G.M.P.G.A. conceived and planned experiments and performed them with M.T., K.O., E.C., M.S., S.A. and R.V.d.S. Data were analysed and interpreted by P.R., G.M.P.G.A., E.C., M.T., S.A., K.O. and M.I. The manuscript was written by G.M.P.G.A. and M.I., and finalized by M.I.

Funding

Open access funding provided by University of Lausanne.

Competing interests

In the past 3 years, G.C. has received grants and research support or has been co-investigator in clinical trials by Bristol-Myers Squibb, Tigen Pharma, Iovance, F. Hoffmann La Roche AG and Boehringer Ingelheim. The Lausanne University Hospital (CHUV) has received honoraria for advisory services that G.C. has provided to Genentech, AstraZeneca AG and EVIR. G.C. has previously received royalties from the University of Pennsylvania for CAR-T-cell therapy licensed to Novartis and Tmunity Therapeutics. A provisional patent regarding the dual inverted vector and associated methodologies for increasing virus titres as described in this manuscript has been filed (2022 U.S. Provisional Patent Application No. 63/290,528 ANTISENSE TRANSFER VECTORS AND METHODS OF USE THEREOF) with M.I., G.C., P.R. and G.M.P.G.A. as co-inventors. The other authors declare no competing interests.

Additional information

Extended data is available for this paper at <https://doi.org/10.1038/s41551-023-01013-5>.

Supplementary information The online version contains supplementary material available at <https://doi.org/10.1038/s41551-023-01013-5>.

Correspondence and requests for materials should be addressed to George Coukos or Melita Irving.

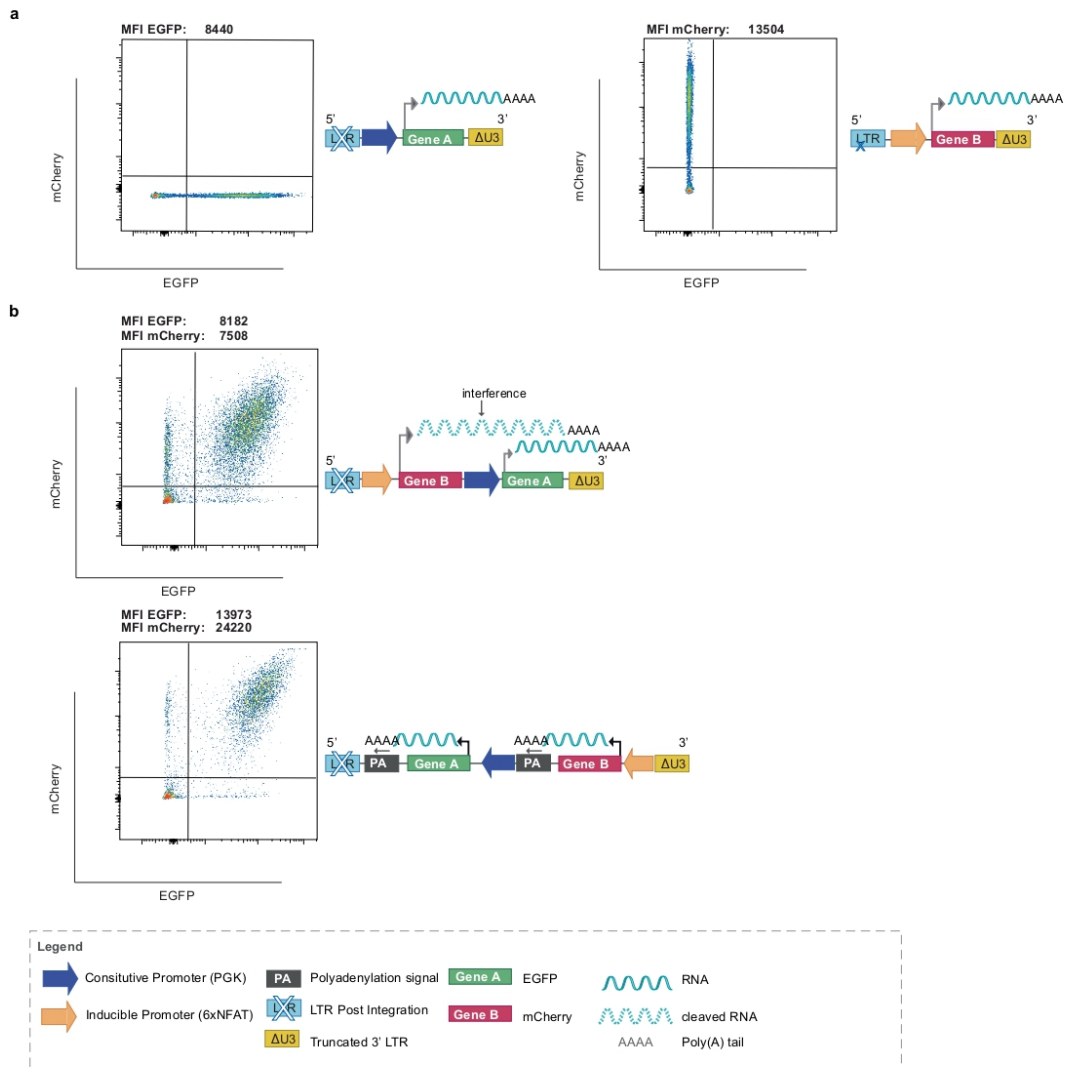
Peer review information *Nature Biomedical Engineering* thanks Reno Debets, Stephen Gottschalk and the other, anonymous, reviewer(s) for their contribution to the peer review of this work. Peer reviewer reports are available.

Reprints and permissions information is available at www.nature.com/reprints.

Publisher's note Springer Nature remains neutral with regard to jurisdictional claims in published maps and institutional affiliations.

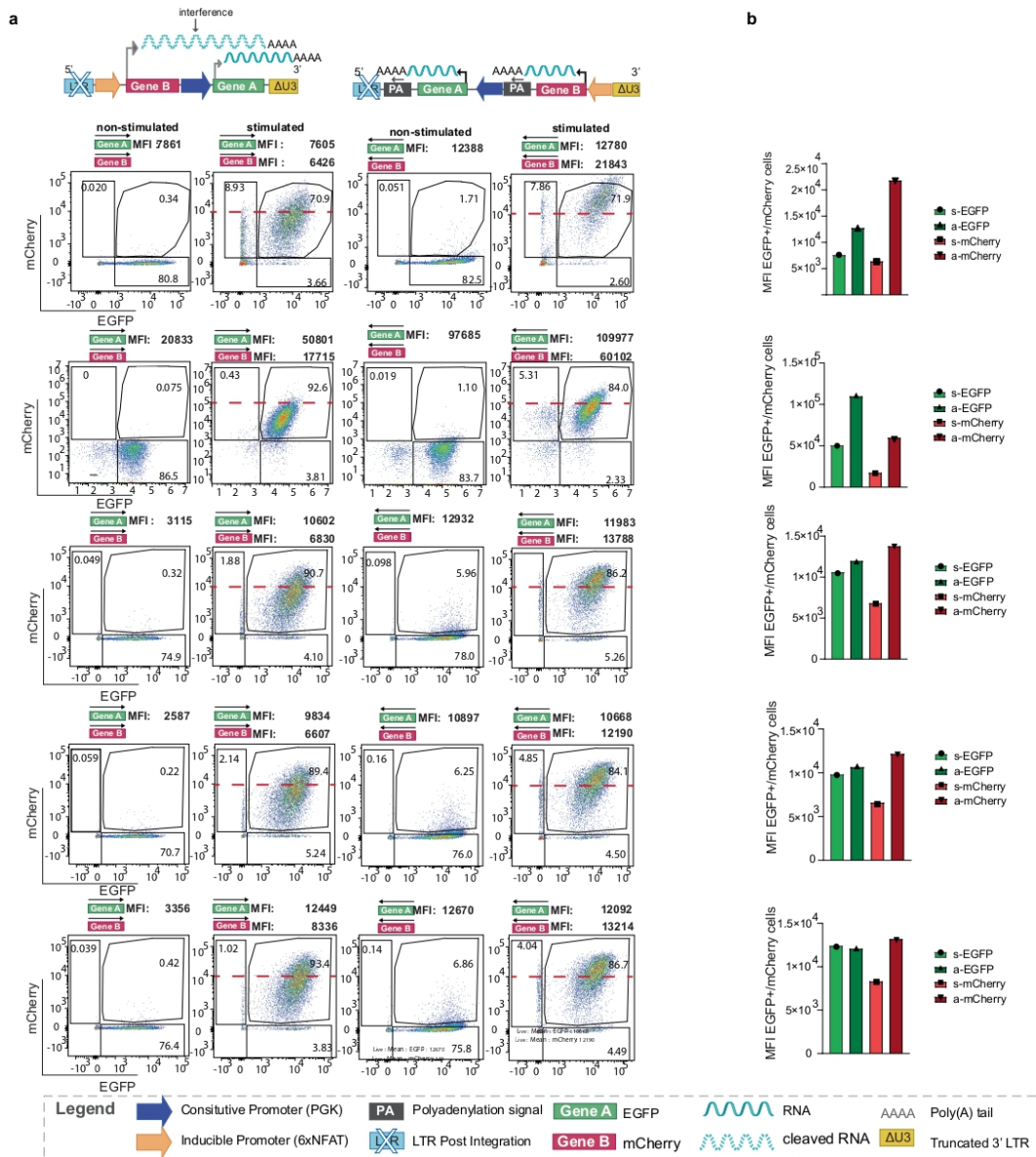
Open Access This article is licensed under a Creative Commons Attribution 4.0 International License, which permits use, sharing, adaptation, distribution and reproduction in any medium or format, as long as you give appropriate credit to the original author(s) and the source, provide a link to the Creative Commons license, and indicate if changes were made. The images or other third party material in this article are included in the article's Creative Commons license, unless indicated otherwise in a credit line to the material. If material is not included in the article's Creative Commons license and your intended use is not permitted by statutory regulation or exceeds the permitted use, you will need to obtain permission directly from the copyright holder. To view a copy of this license, visit <http://creativecommons.org/licenses/by/4.0/>.

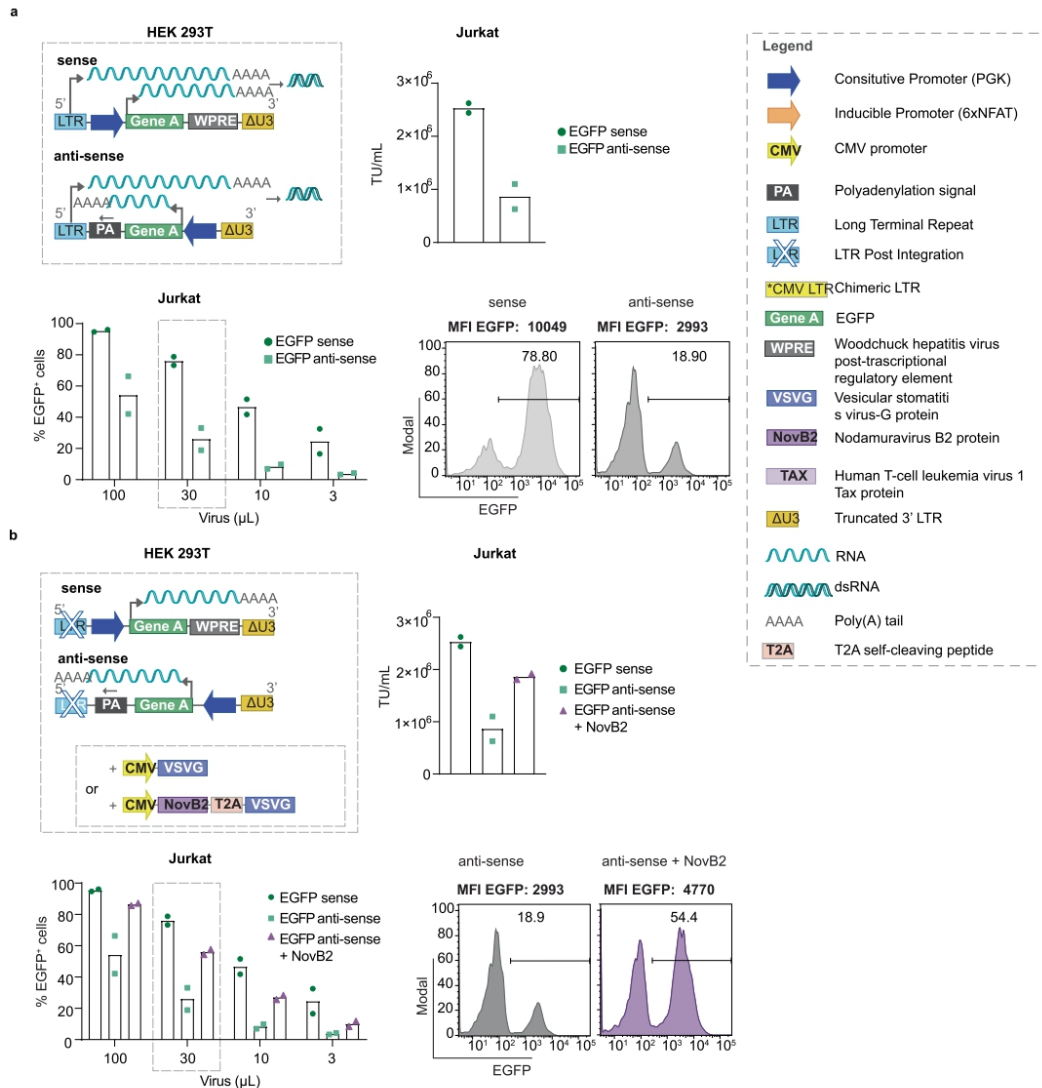
© The Author(s) 2023



Extended Data Fig. 1 | Antisense lentiviral vectors overcome the transcriptional interference that occurs for dual gene-cassette sense vectors. (a) Representative flow cytometric analysis to evaluate expression levels (MFI) of EGFP (gene A) and mCherry (gene B) in activated Jurkat cells

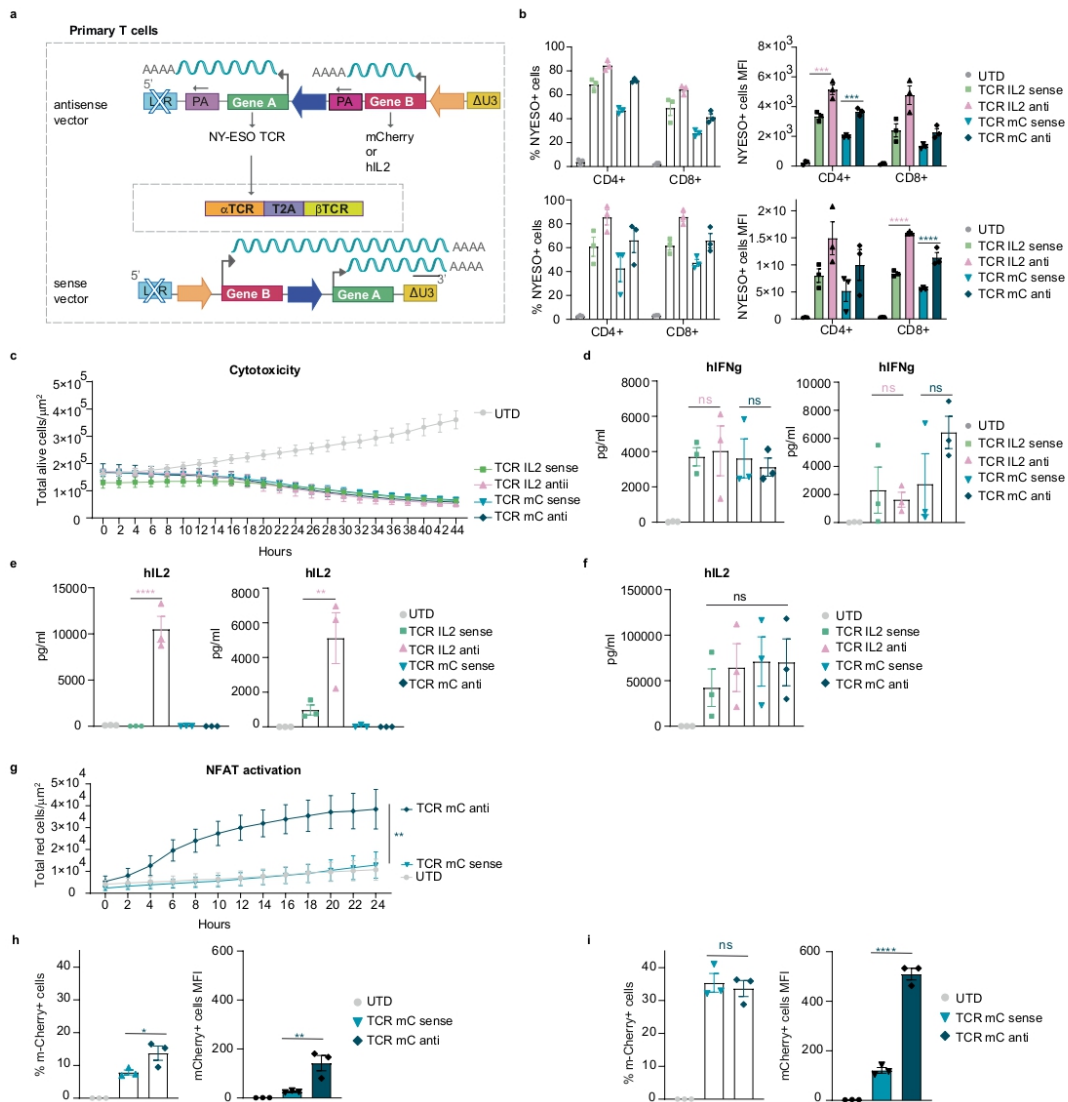
transduced with **(top)** single gene sense vectors in comparison to **(b)** sense **(top)** and antisense **(bottom)** dual gene cassette antisense vectors. Vector schematics are shown next to each plot. Plots are representative of three independent experiments each performed in replicate.





Extended Data Fig. 3 | Antisense lentiviral transfer vector yields lower lentiviral titer than sense transfer vector and this can partially be restored by NovB2. (a) Top left; schematic of sense and antisense constructs encoding EGFP only. **Top right;** titer measurement expressed as Transducing Units (TU) per ml, for two independent experiments. **Bottom left;** transduction of Jurkat cells with decreasing volumes of lentivirus vector supernatant to evaluate %EGFP expression by flow cytometric analysis on day 5. Bar graph represents the mean of two independent experiments. **Bottom right;** representative histograms of Jurkat cells transduced with 30 μ l sense and antisense lentivirus vector supernatant. **(b) Top left;** schematic of sense and antisense orientation lentiviral

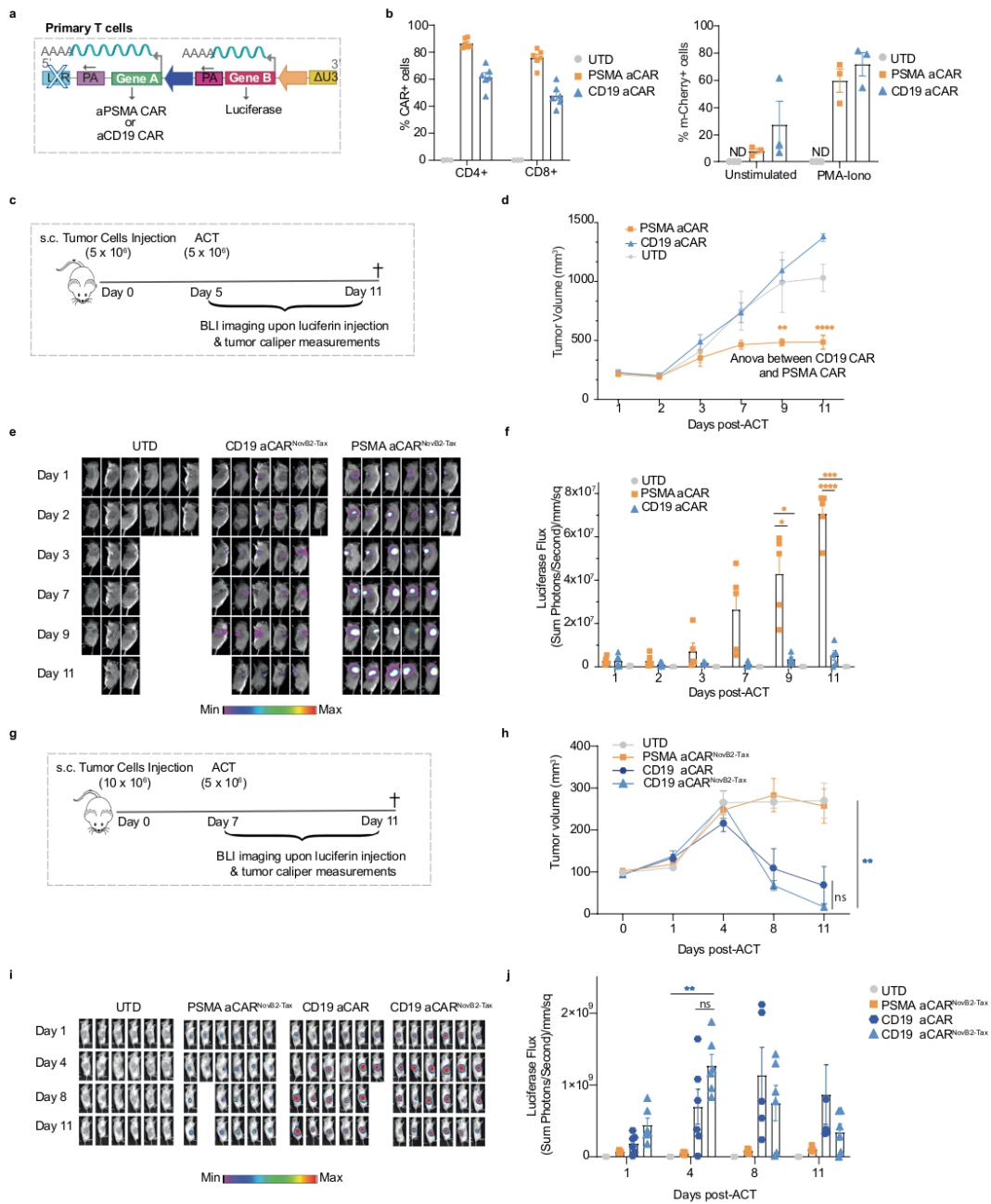
transfer vectors encoding EGFP post-integration in transduced cells. Antisense lentiviral vector was produced in the absence or presence of NovB2 (encoded on the envelope plasmid). **Top right;** titer measurement expressed as Transducing Units (TU) per ml for two independent experiments. **Bottom left;** transduction of Jurkat cells with decreasing volumes of lentivirus vector supernatant to evaluate %EGFP expression by flow cytometric analysis on day 5. Bar graph shows the mean of two independent experiments. **Bottom right;** representative histograms of Jurkat cells transduced with 30 μ l anti-sense lentiviral vector supernatant produced in the absence or presence of NovB2.



Extended Data Fig. 4 | See next page for caption.

Extended Data Fig. 4 | Higher levels of inducible gene-cargo are produced by TCR-T cells transduced with the dual antisense versus sense lentiviral vector. (a) Schematic of sense and antisense constructs encoding an HL A-2 restricted NY-ESO-1_{157,165} specific TCR (Gene A) under the control of the PGK promoter and mCherry or h-IL-2 (Gene B) under the 6xNFAT promoter. (b) **Top and bottom left;** percentage TCR expression as measured by tetramer staining of primary human CD4⁺ and CD8⁺ T cells transduced with sense and antisense lentivirus vector supernatant produced in the presence of TNF α and NovB2. **Top and bottom right;** TCR expression levels (MFI values) for primary human CD4⁺ and CD8⁺ T cells transduced with sense and antisense lentivirus vector supernatant produced in the presence of TNF α and NovB2. Bar graph shows the mean \pm S.E.M. for $n = 6$ human donors for two independent experiments ($n = 3$ per experiment); *** $P < 0,001$ upper panel TCR sense versus TCR IL2 antisense; **** $P < 0,001$ bottom panel TCR IL2 sense versus TCR IL2 antisense) (c) Killing assay for TCR-T cells and UTD T cells against A2/ NY⁺ Saos-2 tumour cells labelled with nuclei green at ratio of 2:1 as measured by the IncuCyte instrument over time. Loss of total green area/ μm^2 is proportional to killing activity. Shown are mean values \pm S.E.M. for T cells from $n = 3$ human donors. (d) IFN γ quantification by ELISA assay of TCR- and UTD-T cells co-cultured with A2/ NY⁺ Saos-2 tumour cells at ratio of 2:1. Shown are mean values \pm S.E.M. for T cells from $n = 6$ human donors for two independent experiments (left panel $ns = 0,9392$ TCR IL2 sense versus TCR IL2 antisense, $ns > 0,9999$ TCR mC sense versus TCR mC antisense; right panel $ns = 0,9959$ TCR IL2 sense versus TCR IL2 antisense, $ns = 0,3562$ TCR mC sense versus TCR mC antisense). (e) Human (h)

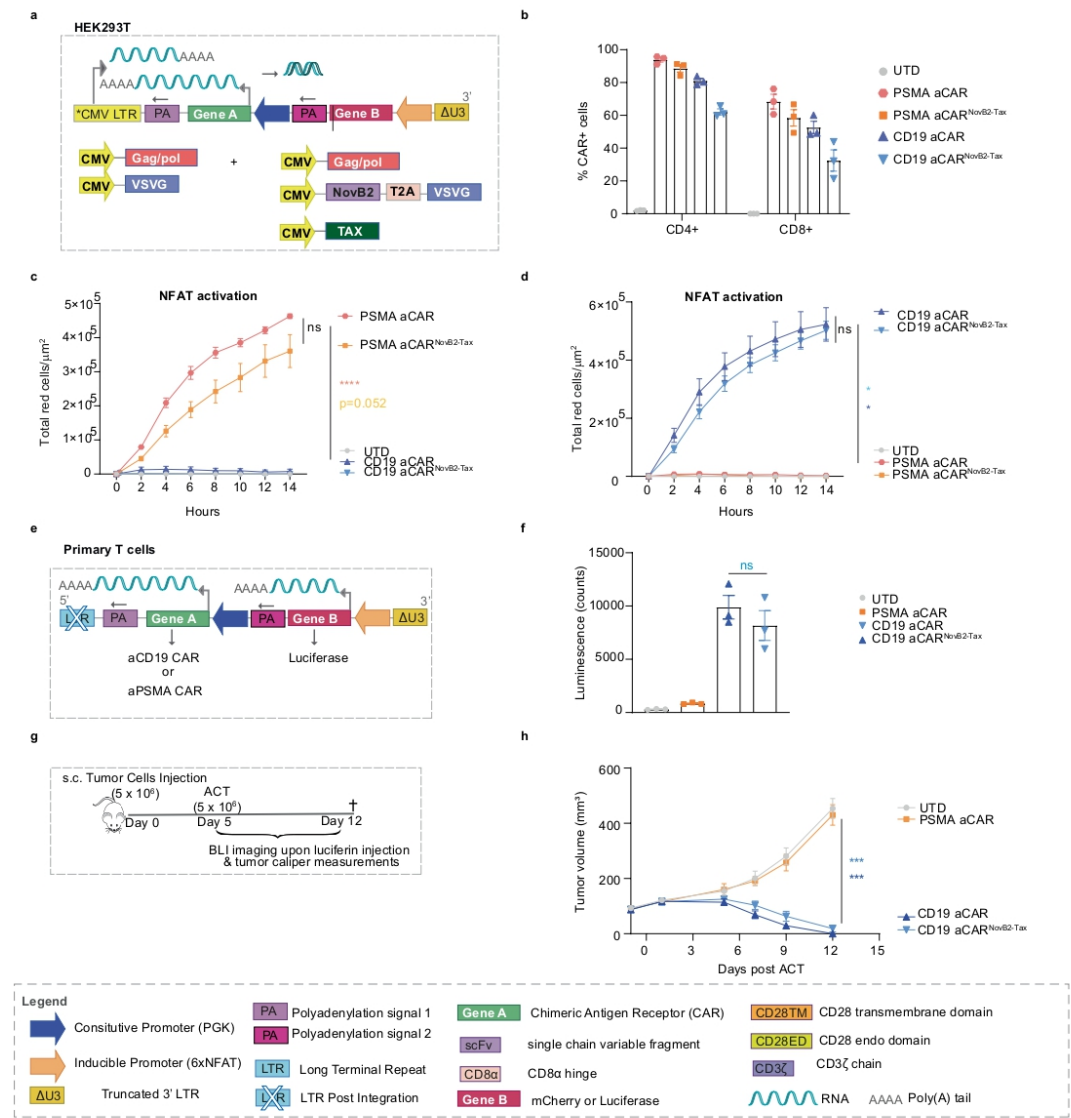
IL-2 quantification by ELISA assay of TCR- and UTD-T cells co-cultured with A2/ NY⁺ Saos-2 tumour cells at a ratio of 2:1. Shown are mean values \pm S.E.M. for T cells from $n = 6$ human donors for two independent experiments (panel left **** $P < 0,0001$ TCR IL2 sense versus TCR IL2 antisense; panel right ** $P < 0,0023$ TCR IL2 sense versus TCR IL2 antisense). (f) hIL-2 quantification by ELISA assay of TCR- and UTD-T cells cultured overnight in the presence of PMA-Ionomycin (left panel $ns = 0,953$ TCR IL2 sense versus TCR IL2 antisense, $ns > 0,9999$ TCR mC sense versus TCR mC antisense). (g) Induced mCherry expression by TCR- and UTD-T cells against A2/ NY⁺ Saos-2 tumour cells at a ratio of 2:1 as measured by the IncuCyte instrument (total red area/ μm^2) over time. Shown are mean values \pm S.E.M. for T cells from $n = 6$ human donors (** $P = 0,0031$ TCR mC sense versus TCR mC antisense at endpoint). (h) Flow cytometric analysis of mCherry expression for TCR- and UTD-T cells co-cultured with A2/ NY⁺ Saos-2 tumour cells at a ratio of 2:1. Shown are mean values \pm S.E.M. for T cells from $n = 3$ human donors. **Left;** percentage of mCherry⁺ cells (* $P = 0,0461$ TCR mC sense versus TCR mC antisense). **Right;** mCherry expression levels (MFI) (** $P = 0,0092$ TCR mC sense versus TCR mC antisense). (i) Flow cytometric analysis of mCherry expression for TCR- and UTD-T cells after overnight stimulation with PMA-Ionomycin. Shown are the mean values \pm S.E.M. for T cells from $n = 3$ human donors **Left;** percentage of mCherry⁺ cells ($ns = 0,8478$ TCR mC sense versus TCR mC antisense). **Right;** mCherry expression levels (relative MFI) (**** $P < 0,0001$ TCR mC sense versus TCR mC antisense). Two-way (panel c and g) and One-way Anova (panels b, d, e, f, h and i) tests were used to determine statistical significance.



Extended Data Fig. 5 | See next page for caption.

Extended Data Fig. 5 | T cells transduced with antisense lentiviral vector encoding a CAR and inducible gene-cargo demonstrate specific in vitro and in vivo function and are not impacted by the use of NovB2 and Tax during virus production. (a) Schematic of sense and antisense lentiviral vector encoding the anti-PSMA and anti-CD19 CARs under the PGK promoter and firefly luciferase under 6xNFAT. (b) **Left:** Transduction efficiency of CD4⁺ and CD8⁺ primary T cells as measured by cell-surface CAR expression. Bar graphs show the mean \pm S.E.M. of the percentage of CAR⁺ T cells. Data are for T cells from $n = 6$ healthy donors and symbols on the graphs represent individual donors. **Right:** mCherry expression at 12 h post PMA-Ionomycin stimulation by equivalently transduced T cells as measured by flow cytometric analysis. With the T cells normalized to approximately 40% cell-surface CAR-expression the graph indicates that all transduced T cells express mCherry upon activation by PMA-Ionomycin. Shown are mean values \pm S.E.M. Symbols indicate individual donors ($n = 3$) (c) Schematic of CAR-T cell transfer study in PSMA⁺ PC3-PIP tumour bearing mice. (d) Caliper tumour volume measurements over days. Values are the mean \pm S.E.M. for $n = 5$ mice per group. Statistical significance was determined by Two-way ANOVA. (Day9 ** $P = 0,034$ aPSMA versus aCD19;

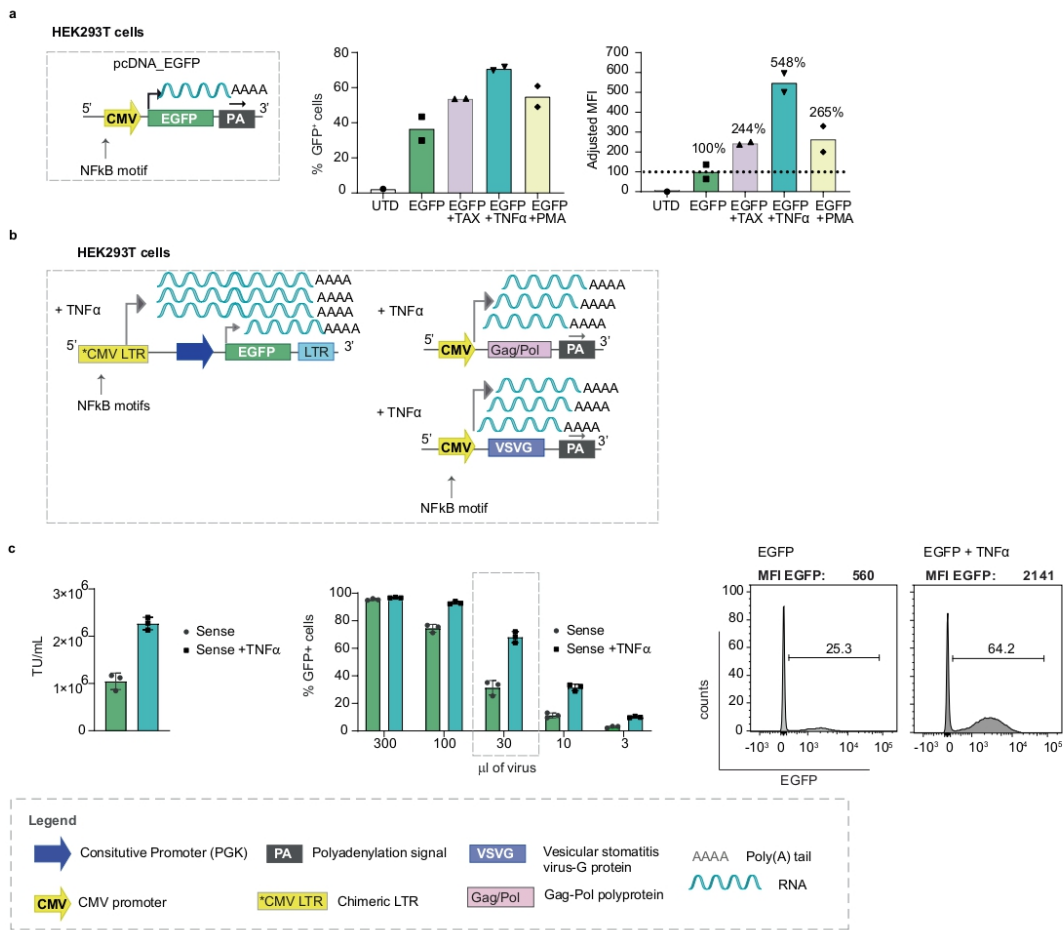
Day11 **** $P < 0,0001$ aPSMA versus aCD19) (e) Representative images of luciferase activity of the transferred T cells over days upon luciferin injection in mice. (f) Bar graph shows the mean value of luciferase flux for all experimental groups. Data are represented as the mean \pm S.E.M. and for $n = 5$ mice per group. Statistical significance was assessed using a Two-Way ANOVA and Post-hoc Tukey test. (Day9 * $P = 0,0201$ aPSMA versus aCD19, * $P = 0,0156$ aPSMA versus UTD; Day11 **** $P < 0,0001$ aPSMA versus aCD19, *** $P = 0,0003$ aPSMA versus UTD). (g) Schematic of CAR-T cell transfer study in CD19⁺ Bjab tumour bearing mice. (h) Caliper tumour volume measurements over days. Values are the mean \pm S.E.M. for $n = 6$ mice per group. Statistical significance was determined by Two-way ANOVA (Day11 ns= $0,726$ aCD19 versus aCD19 Tax-NovB2, ** $P = 0,0051$ aCD19 Tax-NovB2 versus UTD. (i) Representative images of luciferase activity of the transferred T cells over days upon luciferin injection in mice. (j) Bar graph shows the mean value of luciferase flux for all the experimental groups. Data are represented as the mean \pm S.E.M. and for $n = 6$ mice per group. Statistical significance was assessed using Two-Way ANOVA and Post-hoc Tukey test. (Day11 ns= $0,1589$ aCD19 versus aCD19 Tax-NovB2, ** $p = 0,0019$ aCD19 Tax-NovB2 versus UTD. (ns = non-significant, ** $P < 0,01$ and **** $P < 0,0001$).



Extended Data Fig. 6 | The production of antisense lentiviral vector in the presence of NovB2 and Tax does not impact the activity levels of transduced T cells.

(a) Schematic of antisense lentiviral vector encoding the anti-PSMA (Gene A) and anti-CD19 (Gene B) CARs under the PGK promoter along with mCherry under 6xNFAT. (b) Transduction efficiency of CD4⁺ and CD8⁺ primary T cells using lentiviral supernatant produced in absence or presence of both NovB2 and Tax. Bar graphs show the mean \pm S.E.M. of percentage of CAR⁺ T cells. Data shown are for T cells from $n = 3$ human donors and symbols represent individual donors. (c) Evaluation of mCherry expression (total red area/ μm^2) by activated anti-PSMA and (d) Evaluation of mCherry expression (total red area/ μm^2) by activated anti-CD19 CAR-T cells upon co-culture with PSMA + PC3-PIP tumour cells (panel c $ns = 0.4921$ aPSMA versus aPSMA Tax-NovB2, **** $P < 0.0001$ aPSMA versus UTD, $P = 0.0525$ aPSMA Tax-NovB2 versus UTD); (panel d $ns = 0.9671$ aCD19 versus aCD19 Tax-NovB2, * $P < 0.0361$ aCD19 versus UTD, ** $P = 0.0121$ aCD19 Tax-

NovB2 versus UTD). Values for the IncuCyte assay are the mean \pm S.E.M. for T cells from $n = 3$ human donors. Statistical significance was assessed using a Two-Way ANOVA and Post-hoc Tukey test. (e) Schematic of antisense lentiviral vectors encoding the anti-PSMA or anti-CD19 CARs (Gene A) and luciferase as gene cargo (Gene B). The CARs are expressed under the PGK promoter and luciferase under 6xNFAT. (f) Induction of luciferase in anti-CD19 CAR-T cells upon 24 h co-culture with PC3-CD19⁺ tumour cells. Bar graph represents mean \pm S.E.M. of luminescence (counts) measured by HIDEEX. Data are for T cells from $n = 3$ human donors. ($ns = 0.5563$ aCD19 versus aCD19 Tax-NovB2). (g) Schematic of CAR-T cell transfer study in PC3-CD19 tumour bearing mice. (h) Caliper tumour volume measurements over days. Values are the mean \pm S.E.M. for $n = 6$ mice per group. Statistical significance was determined by Two-way ANOVA (Day12 $ns = 0.46$ aCD19 versus aCD19 Tax-NovB2, *** $P < 0.001$ aCD19 versus UTD, *** $P < 0.001$ aCD19 Tax-NovB2 versus UTD).



Extended Data Fig. 7 | TNFα can be used instead of Tax to augment transcription from vectors comprising a CMV promoter. (a) **Left**; schematic of pcDNA plasmid encoding EGFP under a CMV promoter in the sense orientation. **Middle**; bar graph representing %EGFP expressing HEK293T cells 48 hours after transfection with suboptimal levels of plasmid in the presence or not of co-transfected plasmid encoding Tax, soluble TNFα, or PMA. **Right**; bar graph shows relative mean fluorescence intensity (MFI) of EGFP under the different experimental conditions (EGFP encoding plasmid alone is set to 100%). (b)

Schematic of sense lentiviral vector encoding EGFP and produced in absence or presence of TNFα (c) **Left**; titer measurement expressed as Transducing Units (TU) per ml for three independent experiments. **Middle**; transduction of Jurkat cells with decreasing volumes of lentivirus vector supernatant to evaluate percentage EGFP expression by flow cytometric analysis on day 5. Bar graph represents the mean of three independent experiments. **Right**; representative histograms of Jurkat cells transduced with 30 μl sense and antisense lentivirus vector supernatant.

2. Evaluation of the antitumor activity of CAR/TCR T-cell expressing miRNAs for HPK1 downregulation:

2.1. Summary:

To improve T-cell fitness in the context of solid tumors, one promising approach is to engineer TCR/CAR-T-cells to resist suppressive mechanisms. This can be achieved by downregulating master negative regulatory genes involved in attenuating T-cell activity following chronic TCR stimulation, such as HPK1, which was reported in several studies that is a crucial negative intracellular regulator of human and murine CD8⁺ T-cell effector function (discussed in the introduction section of “Intracellular negative regulators downstream TCR signaling pathways”).

Given the fact that targeting HPK1 holds promise for improving T-cell-mediated immune responses, we hypothesized that HPK1 KD in human primary T-cells would significantly increase the potency of T-cells to initiate a more robust response, better persist, and infiltrate the TME. Here, we have evaluated HPK1 KD in the context of Pz1-CAR and HLA/A2-NY-ESO-1₁₅₇₋₁₆₅ (referred to, here, as NYESO-1) restricted TCR-engineered T-cells for ACT. However, we also anticipated that our gene-engineering approach would not come without difficulties as we sought to downregulate HPK1 using a miRNA, which we considered the best fit for our therapeutical goal (i.e., stable downregulation and clinically translated approach for gene KD) due to its biology and cellular processing machinery that make it difficult to be delivered (please refer to the introduction section of “Gene inhibitory strategies”). Still, these facts did not compromise our objective, and we opted to use our optimized tools to tackle these issues.

2.2. Material and Methods:

Cell lines and culture

The prostate carcinoma cell line PC3-PIP (PMSA+), Na8, Me275, A375, Saos-2, 293T human embryonic kidney (HEK293T) cells, and Jurkat cells were cultured in Roswell Park Memorial Institute medium (RPMI) complete medium, consisting of Roswell Park Memorial Institute medium (RPMI) 1640 Glutamax medium (61870010, Invitrogen) supplemented with 10% heat-inactivated (HI) fetal bovine serum (FBS) (for 30 min at 56°C) (26140-079, Gibco) and 1% Penicillin/Streptomycin (P/S) (penicillin 10'000 IU ml⁻¹–streptomycin 10'000 µg ml⁻¹ (100X)) (BioConcept) at 37 °C in a 5% CO₂ atmosphere. Na8, Me275, A375, Saos-2, 293T, and Jurkat cell lines were purchased from the American Type Culture Collection (ATCC). The PC3-PIP and PC3 cell lines were kindly provided by Dr. A. Rosato (University of Padua, Italy).

Vector construction

- In the context of Pz1-CAR: Second-generation Pz1-CAR comprising the CD8α hinge, CD28 transmembrane (TM), CD28 endodomain (ED), and CD3ζ ED, along with the miRNA targeting HPK1 (miRNA B) and the control miRNA (miRNA CTRL) were cloned in an antisense configuration pCRRL vector available in the lab. The anti-PSMA scFv derived from monoclonal antibody J59199 was used to confer tumor-antigen specificity and was constitutively expressed under the phosphoglycerate kinase (PGK) promoter. The (NFAT)6 response elements-IL-2 minimal promoter, abbreviated as 6xNFAT, was used to promote the inducible expression of the miRNAs.
- In the context of NYESO-1 TCR: In a sense configuration pCRRL vector, the human truncated nerve growth factor receptor (tNGFR) and HLA-A2/NY-ESO-1₁₅₇₋₁₆₅ restricted TCR bearing the I53F mutation (I53F-NYESO-TCR) were constitutively expressed by the PGK promoter. In addition, miRNAs targeting HPK1 (miRNA A and B), and the miRNA control (miRNA CTRL) were expressed under the U6 promoter followed by a leader sequence (LS). The HLA-A2/NY-ESO-1₁₅₇₋₁₆₅ restricted TCR has been previously described⁵⁷⁰.

Replacement of the RSV promoter with the CMV promoter in the 5' long terminal repeat (LTR) was used to enable soluble TNFα in the culture supernatant to favor transcription of the single-strand RNA (ssRNA) viral genome.

Cloning strategies

The gene strings of the transgenes were ordered from Addgene, and the cloning was done in lentiviral (pCRRL) vectors. Vectors' amplification was performed in Stellar competent cells (*E. coli* HST08, 636763, Takara). All plasmids were purified using PureLink HiPure Plasmid Filter Maxiprep kit (Invitrogen, Life Technologies) or Miniprep kit (Qiagen) upon confirmative sequencing (from Microsynth AG, Switzerland)

Lentivirus supernatant production

- For large-scale virus production to transduce primary human T cells: 24 h before transfection, 293T-cells were seeded at 10×10^6 cells in 30 ml medium in a T-150 tissue culture flask. All plasmid DNA was purified using the Endo-free Maxiprep kit (Invitrogen, Life Technologies). 293T-cells were transfected with 7 µg pVSVG or 7 µg pVSVG-T2A-NovB2, 18 µg of R874 (Rev and Gag/Pol expression plasmid), and 15 µg of pCRRL transgene plasmid added to a mixture of 180µl Turbofect (Thermo Fisher) and 3 ml Optimem media (Invitrogen, Life Technologies). The medium was further supplemented with TNFα at 10 ng ml⁻¹ working concentration. The viral supernatant was collected at 48 h post-transfection. Viral particles were concentrated by ultracentrifugation for 2 h at 24,000 g and resuspended in 400µl complete RPMI-1640 media, followed by immediate snap freezing on dry ice.
- For small-scale virus production to transduce Jurkat cells: Viral supernatant was produced by seeding 293T cells in a 12-well plate at 0.65×10^6 cells in 2 ml medium per well 5-6 h prior to transfection. 293T cells were transfected with 2 µg total DNA mixture consisting of 1 µg pVSVG/R874 and 1 µg of pCRRL

transgene plasmid. The DNA mixture was added to a mix of Turbofect (Thermo Fisher) and Optimem media (Invitrogen, Life Technologies) according to the manufacturer's instructions, then incubated for 10–20 min at room temperature (RT). After 24h, the medium was refreshed, and at 48h post-transfection, the viral supernatant was collected and then used directly to transduce Jurkat cells.

Jurkat cell transduction for viral titration

Jurkat cells were suspended at 1×10^5 cells per ml and seeded into 24-well plates at 1 ml per well. Different volumes of viral supernatant were used for transduction, as indicated, ranging from 300 μ l down to 3 μ l. Cell media were refreshed after incubation for 24 h at 37 °C. Viral titers (transducing units per ml (TU ml⁻¹) were calculated as follows: ((total number of cells/100) \times percentage of transduced cells) \times dilution of the virus supernatant).

Primary human T-cell purification, activation, transduction, and expansion

Primary human T-cells were isolated from the PBMCs of healthy donors (HDs; prepared as buffycoats) collected with informed consent by the blood bank. Total PBMCs were obtained via Lymphoprep (Axonlab) separation solution by a standard centrifugation protocol. CD4⁺ and CD8⁺ T-cells were isolated by negative selection using magnetic beads following the manufacturer's protocol (easySEP, Stem Cell Technology). Purified CD4⁺ and CD8⁺ T-cells were cultured separately in complete RPMI-1640 and stimulated with anti-CD3 and anti-CD28 monoclonal antibody (mAb)-coated-beads (Invitrogen, Life Technologies) at a 1:2 ratio of T-cells to beads. T-cells were transduced with lentivirus vector particles at 18–22 h post-activation. Human recombinant interleukin-2 (h-IL-2; Glaxo) was replenished every other day for a concentration of 50 IU ml⁻¹ until 5 d post-stimulation (day +5). At day +5, magnetic beads were removed, and h-IL-7 and h-IL-15 (Miltenyi Biotec) were added to the cultures at 10 ng ml⁻¹. A cell density of 0.5–1 $\times 10^6$ cells per ml was maintained for expansion. Rested engineered T-cells were adjusted for equivalent transgene expression before all functional assays; the more efficiently transduced samples were diluted with appropriate numbers of UTD-T-cells.

Cell staining and flow cytometric analysis

To evaluate CAR cell-surface expression, transduced cells were stained with fluorescent anti-human F(ab') mAb (BD Biosciences). For evaluating I53F-NYESO-TCR cell-surface expression, transduced cells were stained with fluorescent HLA-A2/NY-ESO-1₁₅₇₋₁₆₅ tetramer produced in-house. Aqua live Dye brilliant violet (BV510) and near-infrared fluorescent reactive dye (APC Cy-7) were used to assess viability (Invitrogen, Life Technologies). For assessing memory phenotype, cells were subjected to surface staining using CCR7 BV421 (clone G043H7, BioLegend) and CD45RA ECD (clone 2H4LDH11LDB9 (2H4), B49193, Beckman Coulter).

Proliferation assay

To assess the proliferative capacity of HLA-A2/NY-ESO-1₁₅₇₋₁₆₅ (A2/NYESO-1)-specific TCR-T-cells co-expressing a miRNA-based shRNA, both transduced and UTD-T-cells (n = 3 donors) were stained with cell trace violet (CTV) (Invitrogen, Life Technologies) according to the manufacturer's instructions. Cells were then stimulated for 96 h with anti-CD3 and anti-CD28 monoclonal antibody (mAb)-coated beads CTV (Invitrogen, Life Technologies) at a 2:1 ratio of beads:T-cells.

Immunoblotting

Cells were lysed in RIPA buffer supplemented with Halt phosphate/protease inhibitors (Thermo Fisher) and boiled at 97 °C for 10 min with Bolt LDS sample buffer and reducing agent (Thermo Fisher). Protein samples (10 μ g) were separated by SDS-PAGE and transferred to PVDF membranes using the iBlot2 system (Thermo Fisher). Antibody staining of the molecules of interest was carried out according to the manufacturer's instructions. Rabbit monoclonal antibody (EP630Y) specific to MAP4K1/HPK1 antibody (ab33910) was purchased from Abcam, and anti- β -actin (sc-47778) from Santa Cruz. Images were acquired with a western

blot imager (Fusion, Vilber Lourmat), and protein levels were quantified using the ImageJ software by analyzing the pixel intensity of the bands. Total HPK1 level was calculated by dividing its signal by the β -actin signal.

Enzyme-Linked Immunosorbent Assay (ELISA) for IFN γ detection

To assess human IFN γ (hIFN γ) secretion by engineered T-cells, 5×10^4 primary untransduced (UTD) and transduced T-cells were cocultured with 5×10^4 target cells per well, at a ratio of effector: target (E:T) of 1:1, as duplicates in 96-well round bottom plates in a final volume of 200 μ L complete RPMI media. After 24-hrs, supernatants of the coculture were harvested and tested for the presence of IFN- γ using the Human IFN γ ELISA MAX Deluxe kit (Cat n°430104, BioLegend) upon appropriate dilution (1/25-100) according to the manufacturer protocol.

Cytotoxicity with IncuCyte System

Cytotoxicity assays were performed using the IncuCyte System (Essen Bioscience). Briefly, 1.5×10^4 engineered nuclei red target cells per well were seeded in flat bottom 96well plates (Costar, Vitaris) 4h before to the coculture. Rested T-cells (80% CD8+ and 20% CD4+ T-cells) not receiving cytokines for 48h were washed and seeded at 3×10^4 cells per well, at a ratio of the E:T = 0,25:1, 0,5:1, 1:1 or 2:1 in complete media of 200 μ l total volume with or without the presence of inhibitory factors 2-chloroadenosine CADO (Sigma-Aldrich), Forskolin (FSK) (Sigma-Aldrich) and PGE2 (Sigma-Aldrich) in an increasing dose manner. No exogenous cytokine was added to the assay medium during the coculture period. Internal experimental negative controls were included in all assays, including coculture with UTD-T-cells, tumor cells, and tumor cells alone, to monitor tumor cell death over time. As a positive control, tumor cells alone were treated with 1% triton solution (T8787, Sigma-Aldrich) to evaluate maximal killing in the assay. The nuclei red target cells were generated with IncuCyte NuLight Lentivirus (Essen Bioscience) for nuclear-restricted expression of mKate2 (red fluorescent protein), according to the manufacturer's instructions. Images of the total red area per well were collected every 2 h of the coculture for up to three days. The total red area per well was obtained using the analysis protocol on the software provided by Essen Bioscience manufacturer. Data were normalized by subtracting the background fluorescence observed at time 0h (before any cell killing by Pz1-CAR- or NYESO-1-TCR-T-cells) from all further time points. Data are expressed as mean \pm s.e.m. of different donors.

Mouse strain and *in vivo* experimentation

Mouse Strains and Housing

NSG (NOD scid gamma) and NSG -IL15 mice (The Jackson Laboratory) were bred and housed in a specific and opportunistic pathogen-free animal facility (SOPF) providing a temperature-controlled environment and a light-dark (12 h/12 h) cycle in the Oncology Department of the University of Lausanne (Epalinges, Switzerland). All *in vivo* experiments were conducted according to the Swiss Federal Veterinary Office guidelines and were approved by the Cantonal Veterinary Office. Experiments used mice at least six weeks old, and all cages housed five animals in an enriched environment providing free access to food and water. During experimentation, all animals were monitored for signs of distress at least every other day. Mice were euthanized at the endpoint by carbon dioxide overdose.

***In vivo* experiments with xenogeneic tumor models**

NSG-IL15 male mice aged 8–12 weeks were blindly selected, then subcutaneously (s.c.) injected in the flank with 5×10^6 Me275 melanoma tumor cells in 100 μ l of PBS. Once tumors were palpable (day 5), the mice were randomized and grouped for similar mean tumor volume and standard deviation (SD) prior to T-cell treatment. The T-cell transfer was performed by intravenous (i.v.) injection of 5×10^6 UTD or NYESO1-T-cells in 100 μ l of PBS. NYESO1-T-cells were distinguished into three groups: (1) CTRL, (2) HPK1 (A), and (3) HPK1 (B). In each group of T-cell treatment, 80% of CD8+T-cells and 20% of CD4+T-cells were mixed. Tumor volume

was monitored via caliper measurement every two days. It was calculated using the formula $V (\text{mm}^3) = 1/2 (\text{length} \times \text{width}^2)$, where length is the greatest longitudinal diameter and width is the greatest transverse diameter.

Statistical analysis

Statistical analyses were performed using GraphPad Prism 9.0 (GraphPad Software, La Jolla, CA). For single variable testing, one-way analysis of variance (ANOVA) followed by Tukey post-hoc correction was utilized for multiple comparisons across column groups. In the case of two/multiple-variable analysis involving multiple groups, a two-way repeated measure ANOVA, coupled with either a Tukey post-hoc correction or a Šidák post-hoc analysis, was employed. Differences were considered significant when $*P < 0.05$, very significant when $**P < 0.01$, and highly significant when $***P < 0.001$.

2.3. Results:

2.3.1. In the context of Pz1-CAR T-cells:

To address our study objectives, we started initially by evaluating the KD potency of three microRNAs (miRs) - A, B, and C (from Transomic Technologies Inc.) targeting HPK1 in comparison to a control miRNA (CTRL), that has no target in primary cells, using a commercial retroviral vector (**Figure 11a**).

By performing a western blot in Jurkat cells transduced with the aforementioned vector, we could demonstrate that miRs A and C demonstrated substantial KD potency resulting in approximately 85-86% downregulation of HPK1. Notably, miR B achieved the highest level of KD with over 92% downregulation of HPK1 expression compared to the miR CTRL, exhibiting its efficacy in targeting HPK1 (**Figure 11b**).

To take our approach a step further and investigate the HPK1 KD's potential in primary human T-cells, we took advantage of the novel lentiviral vector design we have developed in our lab (discussed previously in the section "1.3 article" of the previous chapter) and cloned the miR B and miR CTRL in a pCRRL lentiviral vector construct harboring an antisense configuration, wherein miR B was inducibly expressed under the NFAT promoter (to induce the downregulation only when T-cell engage with tumor antigen as a way to avoid any potential toxicities due to T-cell overactivation). In contrast, second-generation Pz1-CAR recognizing the PSMA antigen of prostate cancer cells and comprising 28z endodomain was constitutively expressed under the PGK promoter (**Figure 11c**).

Isolated human primary CD4⁺ and CD8⁺ T-cells were then transduced with lentivirus-bearing Pz-1-CAR-miR B/miR CTRL and stained cells with anti-fab Ab recognizing the single chain fragment variable (scFv) of the CAR to determine the TE by flow cytometry on day 7 post-transduction (**Figure 1d**). Data were displayed as percentages and mean fluorescence intensity (MFI) of CAR expression. The results revealed TE rates exceeding 90% and 60% of CD4⁺ cells and CD8⁺ T-cells, respectively, for both miR B targeting HPK1 and CTRL miR. No statistical difference (ns) is to be reported between CD4⁺Ctrl and KD or CD8⁺Ctrl and KD.

Moreover, to determine the level of HPK1 KD, sorted Pz-1-CAR⁺ T-cells were stimulated with either anti-fab, anti-CD3 Ab, or anti-CD3/CD28 dynabeads for 6h, 24h, and 48h. Western blot analysis of one representative donor indicated that miR B effectively downregulated HPK1 expression, with over 99% KD level observed in CD4⁺ and 90% efficiency in CD8⁺ T-cells following activation of the NFAT promoter through anti-fab stimulation for 6 hours (**Figure 11e**) (**Figure 7c, right of the attached published article**).

Lastly, we investigated whether HPK1 KD affected the fraction of live CD4⁺ and CD8⁺ T-cells stained by the near-infrared fluorescent reactive dye (**Figure 1f**) and could demonstrate that the percentage of live cells remained unaltered upon HPK1 downregulation compared to the CTRL condition highlighting the potential of miR B in efficiently reducing HPK1 expression without compromising the viability of CD4⁺ and CD8⁺T-cells. Taken together, these results emphasize the effectiveness of miR B in downregulating HPK1 expression in human primary Pz1-CAR T-cells and the successful cell transduction using both miR B and the CTRL miR, resulting in a significant milestone achievement in this study.

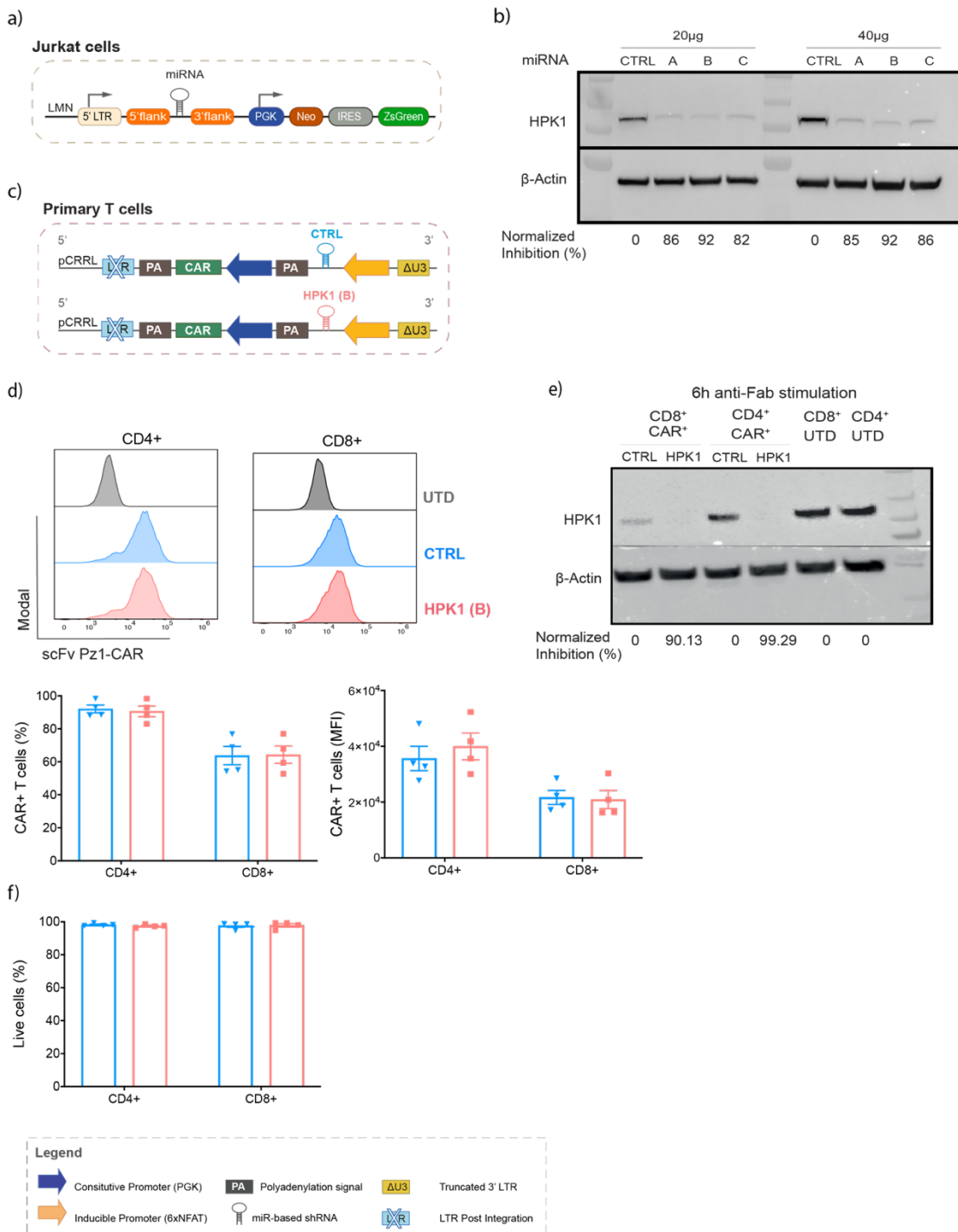


Figure 11: Characterization of HPK1 Knockdown in transduced Jurkat cells and anti-PSMA-CAR primary CD4+ and CD8+ T-cells.

(a) Schematic of the commercial vector used for Jurkat cell transduction. (b) Western blot analysis showing HPK1 KD levels using miR A, B, and C compared to miR CTRL together with β-actin control blot for 20µg and 40µg Jurkat cell protein extract. (c) Schematic of antisense lentiviral transfer vector encoding an anti-PSMA-CAR under PGK and miRNA either targeting HPK1 (HPK1 (B)) or miR CTRL (CTRL) under 6xNFAT. (d) Evaluation of transduction efficiency 7 days post-transduction; top: representative flow cytometry histogram of Pz-1-CAR CD4+ and CD8+ T-cells downregulating HPK1 (HPK1 (B)), CTRL T-cell, and UTD T-cells used as a baseline for the gating strategy to exclude the fluorescence background; bottom: bar graphs presenting the mean ± s.e.m of the percentage (%) (bottom left) and as MFI (Bottom right) of the Pz1 derived CAR expression in primary CD4+ and CD8+ T-cells (n=4 donors) determined by flow cytometric analysis using anti-fab targeting Pz-1-CAR scFv. (e). Western blot analysis showing specific downregulation of HPK1 using miR B compared to miR CTRL together with β-actin control blot of a representative human T-cell donor (out of n=2 donors) upon 6h stimulation with plate-coated anti-F(ab)². (f) Bar graph depicting the mean ± s.e.m of the percentage of cell viability of transduced CD4+ and CD8+ T-cells stained with near-infrared fluorescent reactive dye (n=4 donors) 7 days post-transduction.

Next, we wanted to investigate the impact of HPK1 downregulation on various aspects of Pz1-CAR T-cell functionality when stimulated and even challenged in immunosuppressive conditions. We designed experimental settings to provide insights into the impact of HPK1 downregulation without or with immunosuppressive inhibitors, mimicking the immunosuppressive conditions in the TME using PGE2, CADO (stable adenosine analog), and Fsk (specific activator of adenylate cyclase), on T-cell proliferation, cytokine secretion, and tumor-killing potential. To examine the proliferation capacity of HPK1 KD T-cells, we performed a CTV-based proliferation assay where CD4⁺ and CD8⁺ Pz-1-CAR T-cells downregulating or not HPK1 were stimulated in technical duplicates with aCD3/aCD28 dynabeads at a ratio of E:T=2:1. The results highlighted the positive impact of miR B-mediated HPK1 downregulation on CD8⁺ T-cell proliferation, as a significant difference was found between HPK1 KD and CTRL T-cells, whereas no difference was observed in CD4⁺ T-cells (**Figure 12a**).

Next, we exposed HPK1 KD and CTRL CD4⁺T-cells to CADO and PGE2 in cell culture at increasing concentrations. We stained them intracellularly for flow cytometric analysis to measure IL2, IFN γ , and TNF α expression by the T-cells. Notably, significantly higher IFN γ secretion was observed in HPK1 KD CD4⁺ T-cells compared to the CTRL for intermediate to high concentrations of CADO and PGE2 (**Figure 12b**). However, *in vitro* cytotoxicity analysis using the IncuCyte system did not reveal a significant difference in tumor killing when coculturing HPK1 KD and CTRL T-cells (80% CD8⁺ and 20% CD4⁺ T-cells) with PC3 PIP cells at E:T ratios of 2:1 and 1:1 over a 48 hour period, as shown by the line graphs depicting the percentage of tumor survival, suggesting comparable efficacy in tumor cell elimination (**Figure 12c**). Similarly, no discernible difference was observed in tumor killing between T-cells bearing or not HPK1 downregulation when cocultured at an E:T ratio of 2:1 with PC3 PIP cells under different conditions, including the immunosuppressive inhibitors CADO, PGE2, and FSK at increasing concentrations (**Figure 12d**).

These findings offer valuable perspectives into the role of HPK1 in modulating T-cell responses and tumor immunity of both CD4⁺ and CD8⁺ T-cells.

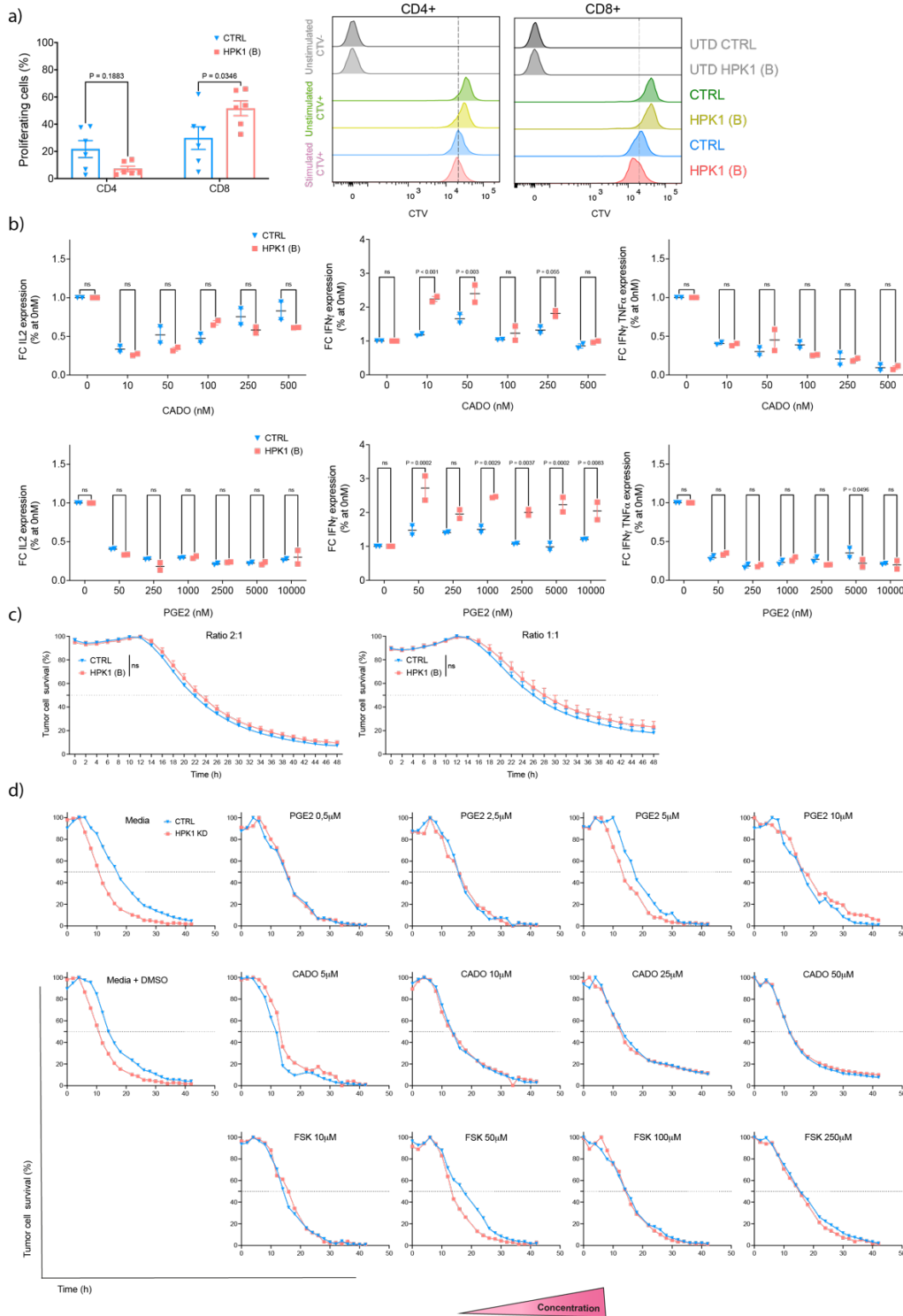


Figure 12: Functional effect of HPK1 downregulation on human primary Pz1-CAR T-cells.

(a) CTV-based proliferation assay; left: Bar graph presenting the mean \pm s.e.m of the percentage of proliferating HPK1 KD (HPK1 B) and CTRL CD4+ and CD8+ T-cells (n=3 donors). Statistical significance determined using Two-Way ANOVA and post-hoc Šidák analysis; right: Flow cytometry histograms displaying non-stimulated CTV-unstained cells and stimulated CTV-stained cells as the baseline for analysis in addition to miR B targeting HPK1 (HPK1 B) and CTRL T-cells. (b) Bar graphs showing the mean \pm s.e.m. of the fold change (FC) of cytokine expression in the presence of inhibitor reagents CADO and PGE2 at increasing concentrations normalized to the percentage of expression upon cell culture at 0nM of inhibitors, Two-Way ANOVA and post-hoc Šidák analysis were performed of n=2. (c) Line graph representing the mean \pm s.e.m. of tumor survival upon HPK1 (B) and CTRL T-cell (n=3 donors) coculture with PC3 PIP Nucred cells at a ratio of E:T of 2:1 and 1:1 over 48h. Statistical analysis was done using mixed-effect analysis over time and post-hoc Tukey's multiple comparisons analysis test. (d) Line graph representing the mean of technical duplicates of tumor survival upon HPK1 (B) and CTRL T-cell coculture with PC3 PIP Nucred cells at a ratio of E:T of 2:1 and 1:1 over 48h (n=1 donors) in the presence of PGE2, FSK, and CADO at increasing concentrations and in media alone and media with DMSO as control, *t* test analysis was used to compare the mean of n=2 between CTRL and HPK1 KD.

2.3.2. In the context of NYESO-1 TCR T-cells:

Encouraged by the foreseen potential of HPK1 KD to enhance CD8+Pz-1-CAR T-cell proliferation and CD4+Pz-1-CAR T-cell cytokine expression in the presence of immunosuppressive inhibitors, we sought to evaluate the effect of HPK1 KD in the context of HLA/A2-NY-ESO-1₁₅₇₋₁₆₅ (NYSESO-1) restricted TCR bearing the I53F mutation (I53F-NYESO-TCR). For this, we used a pCRRL lentiviral vector which included a constitutively expressed NYESO-1 TCR under the PGK promoter, U6 promoter-based constitutive expression of miRs (A and B) targeting HPK1 or a miR CTRL (targeting no molecule), the NGFR reporter gene, and the NYESO-1 TCR, all arranged in the sense configuration vector. A leader sequence was inserted after the U6 promoter to facilitate miR processing, as it was reported (also tested in our lab; data not shown) that it was necessary for an effective gene downregulation (**Figure 13a**).

A proportional increase in TE of Jurkat cells was observed for HPK1 KD (using miR A and B) as well as CTRL-T-cells upon infecting with different volumes (3, 10, 30, 100, and 300 μ l) of viral supernatants, as indicated by the percentage of double positive (DP) cells for the NGFR and the tetramer, which specifically recognizing for NYESO-1 TCR. TE ranged from less than 5% for the lowest volume (3 μ l) to over 70-80% for the highest volume (300 μ l) (**Figure 13b**) (**Figure 6f of the attached published article**).

Moreover, Western blot analysis of extracted proteins from transduced Jurkat cells demonstrated a KD level of over 93% with miR A and an average of 60% with miR B compared to the CTRL (**Figure 13c**). In primary human T-cells, and by using these lentiviral vectors, we could induce high levels of TE that exceeded 80% in CD4+ T-cells and over 60% in CD8+T-cells for all miRs (**Figure 13d**). Furthermore, through western blot data analysis, we determined the efficiency of HPK1 KD using miR A and miR B compared to miR CTRL and UTD cells in CD4+ and CD8+T-cells. The results indicated an HPK1 KD level exceeding 95% in CD4+T-cells and between 70% to 97% in CD8+T-cells with miR A, as compared to the CTRL miR (**Figure 13e**) (**Figure 6h of the attached published article**).

These results provide valuable insights into the KD efficiency of HPK1 using specific miRNAs in primary human T-cells and the impact of TE on transduced Jurkat cells, CD4+ T-cells, and CD8+ T-cells.

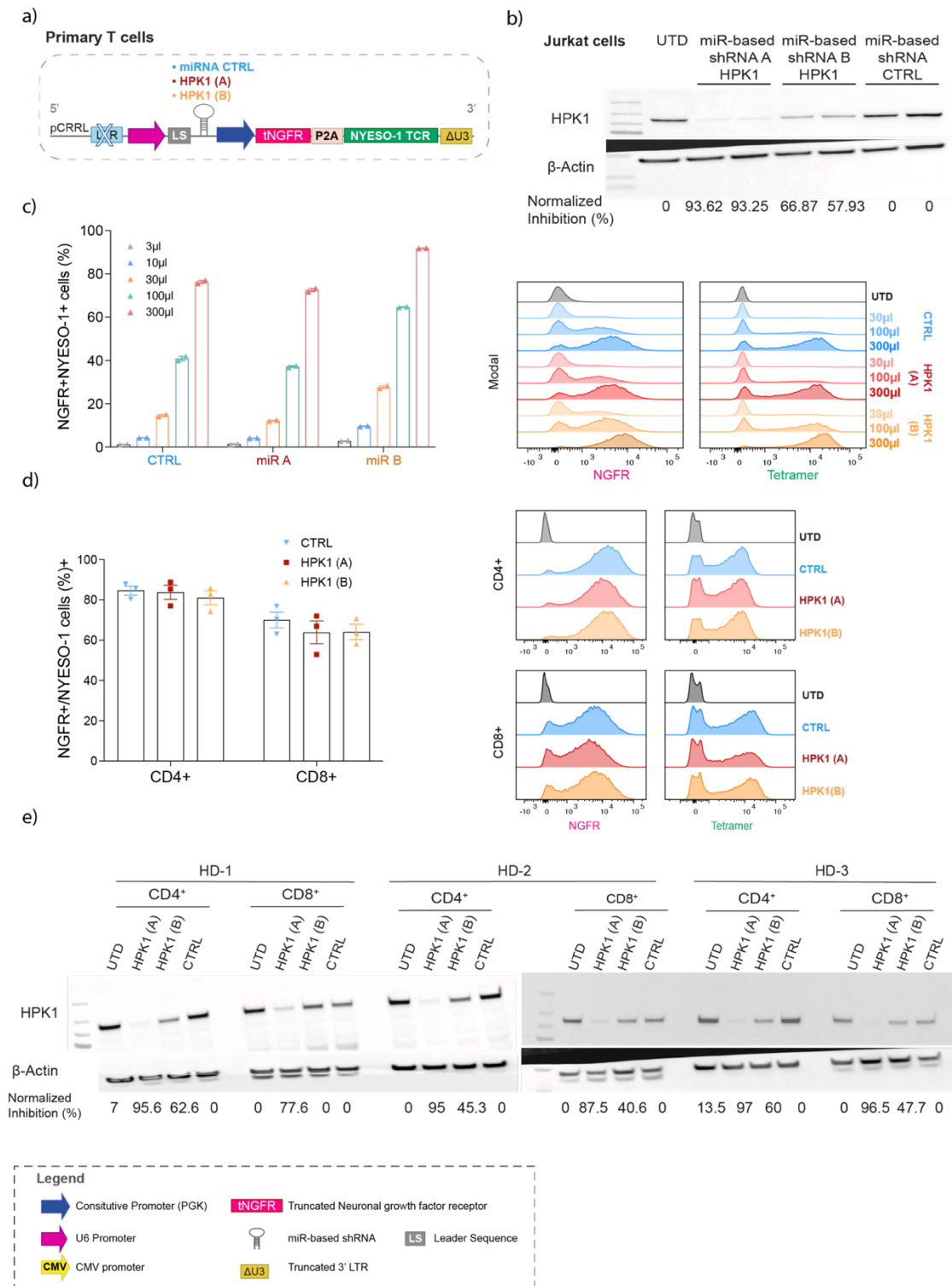


Figure 13: Evaluation of knockdown levels using miRs targeting HPK1 in transduced NYESO-1-TCR CD4+ and CD8+ T-cells. (a) Schematic of sense lentiviral transfer vector encoding miRNAs targeting HPK1 (A and B) or scramble control (miRNA CTRL) under the U6 promoter, as well as tNGFR and the I53F-NYESO-TCR, both under the PGK promoter and separated by P2A sequence. (b) Evaluating the TE in Jurkat cells; left: Bar graph as mean \pm s.e.m of the percentage of Jurkat cell DP for NGFR and NYESO-1 TCR in technical duplicates; right: Representative flow cytometry histograms showing Jurkat cells' TE with miR CTRL, miR A, and miR B for HPK1 KD as UTD as a baseline for gating. (c) Western blot analysis of HPK1 KD levels in Jurkat cells using miR A, miR B, and miR CTRL together with β -actin control blot of technical duplicates for each condition in addition to UTD cells. (d) Evaluating the TE in primary T-cells; left: Bar graph as mean \pm s.e.m of primary human CD4+ and CD8+ T-cell percentage DP for NGFR and tetramer (n=3 donors); right: representative flow cytometry histograms showing CD4+ and CD8+ T-cell TE with miR A, and miR B targeting HPK1, miR CTRL and with UTD being a baseline for gating. (e) Western blot data comparing HPK1 KD efficiency of miR A and miR B with miR CTRL in CD4+ and CD8+ T-cells together with β -actin control blot (n=3 donors).

After successfully transducing primary human T-cells with NYESO-1 HPK1 KD, we sought to assess their functionality *in vitro*. However, we wanted first to investigate whether downregulation of HPK1 can compromise their ability to expand in moderate-to-long *in vitro* cell expansion or perhaps modulate their phenotype, based on the hypothesis that HPK1 could push more toward an effector state rather than memory phenotype before performing an ACT. This could substantially lead to the generation of terminally differentiated effector cells after a long-term *in vitro* cell culture prior to *in vivo* injection.

Interestingly, when examining the rate of expanding UTD and engineered T-cells CD4⁺ and CD8⁺ T-cells, no significant difference was observed between T-cells with or without HPK1 downregulation, indicating that HPK1 KD did not alter the *in vitro* expansion capacity of the T-cells (**Figure 14a**). Similarly, no significant difference was to be reported in the phenotype of HPK1 KD T-cells compared to the control (CTRL) T-cells as measured by the ratio of memory cells over effector cells (**Figure 14b**), suggesting that HPK1 downregulation does not affect the cell phenotype of the engineered T-cells *in vitro*.

Next, to elucidate the proliferation capacity of HPK1 KD T-cells upon TCR stimulation with anti-CD3/CD28 dynabeads (E:T=2:1), a CTV-based proliferation assay was performed on CD4⁺ and CD8⁺ T-cells and results demonstrated a significant increase in the proliferation capacity of CD8⁺ T-cells with HPK1 KD using miR A compared to the control (CTRL) T-cells. A representative histogram of CD8⁺ T-cells clearly shows the enhanced proliferation of HPK1 KD T-cells. However, no significant difference was observed in the proliferation of CD4⁺ T-cells. These findings indicate that HPK1 downregulation using miR A specifically enhances the proliferative response of CD8⁺ T-cells *in vitro* (**Figure 14c**) (**Figure 6k of the attached published article**).

We further evaluated the secretion of IFN γ by HPK1 KD and CTRL T-cells measured by ELISA upon coculture with HLA2⁺/NYESO-1⁺ (A2⁺/NY⁺) tumor cells (Me275, A375, and Saos2) in addition to coculture with the (A2⁻/NY⁻) cells Na8 for 24h at a ratio of E:T=1:1. While no significant differences were detected among the different conditions, the data suggested that HPK1 KD T-cells using miR A tended to secrete more IFN γ than the CTRL T-cells when cocultured with Me275 melanoma cells (**Figure 14d**) (**Figure 6j of the attached published article**). Although not statistically significant, this finding suggests a potential role for HPK1 in regulating IFN γ secretion, particularly in the context of Me275 melanoma cells.

These findings suggest that HPK1 KD may not significantly impact T-cell expansion or phenotype *in vitro*. However, it may play a role in regulating the proliferative response of CD8⁺ T-cells and potentially IFN γ secretion in specific tumor cell contexts.

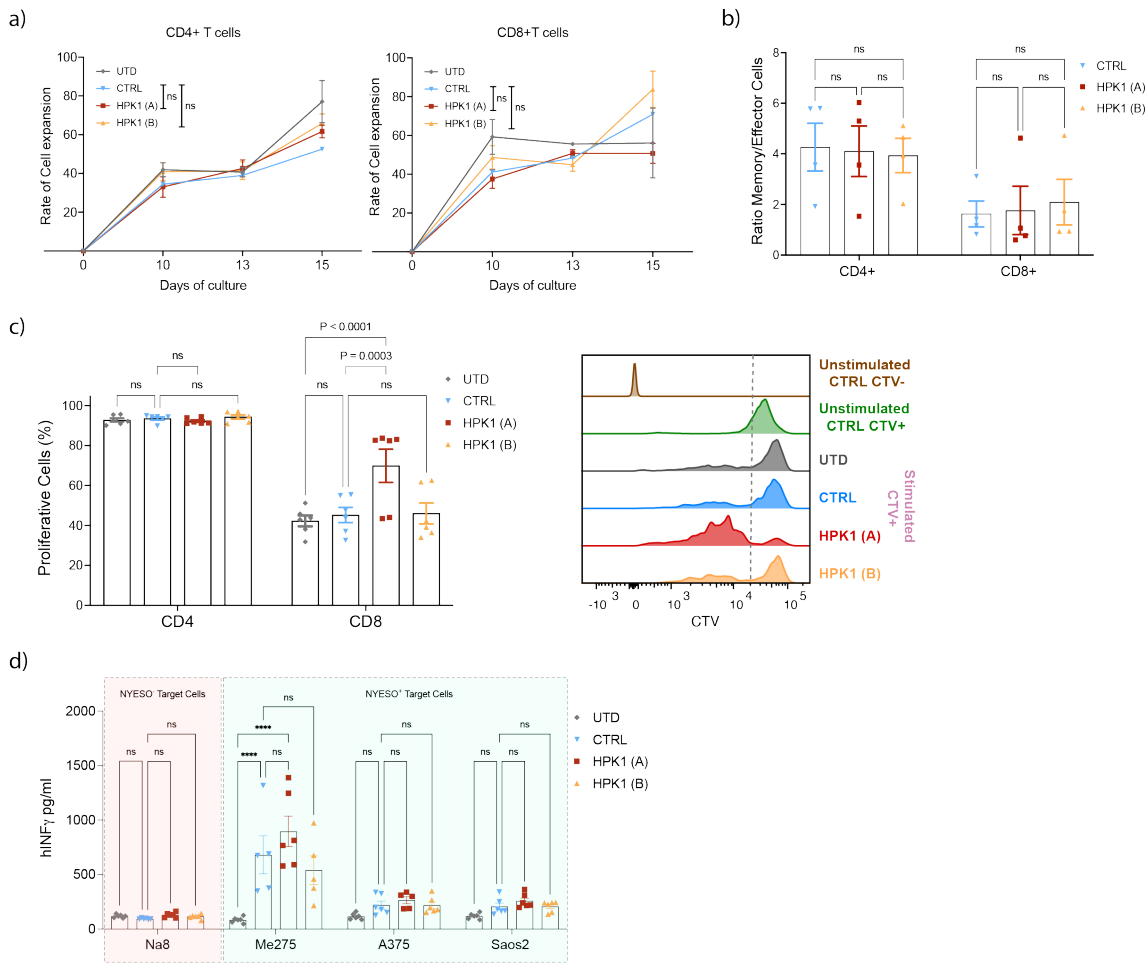


Figure 14: *In vitro* characterization of NYESO-1⁺ T-cells downregulating HPK1 using miR A and B compared to CTRL NYESO-1⁺ T-cells.

(a) Cell expansion rate of UTD and NYESO-1⁺ T-cells with miR A and B for HPK1 KD and miR CTRL over time of CD4⁺ and CD8⁺ T-cell *in vitro* cell culture measured by dividing the total number of cells in each condition by the number of cells at the beginning of the *in vitro* cell culture day 0, data presented as mean \pm s.e.m (n=3 donors), statistical significance was assessed using Two-way ANOVA and post-hoc Tukey analysis. (b) The ratio of memory over effector cells in engineered T-cells (HPK1 KD vs. CTRL), and the phenotypic state of T-cells was determined by flow cytometric analysis of CCR7- and CD45RO-stained T-cells, data presented as mean \pm s.e.m (n=4 donors) and Two-way ANOVA and post-hoc Tukey's multiple comparison was used for statistical analysis. (c) CTV-based proliferation assay; left: bar graph presenting the mean \pm s.e.m of the percentage of proliferating HPK1 KD (HPK1 B) and CTRL CD4⁺ and CD8⁺ T-cells (n=3 donors), statistical significance was determined by Two-way ANOVA and post-hoc Tukey analysis; right: flow cytometry histograms displaying non-stimulated CTV-unstained cells and stimulated CTV-stained cells as the baseline for analysis in addition to UTD, HPK1 (A), HPK1 (B) and CTRL T-cells. (d) IFN γ secretion measured by ELISA upon overnight coculture of HPK1 KD and CTRL T-cells with A2⁺/NY⁺ and A2⁻/NY⁻ tumor cells at ratio E:T of 1:1, data are shown as mean \pm s.e.m (n=3 donors) and analyzed for statistical significance using Two-Way ANOVA and post-hoc Tukey's multiple comparisons where ****P<0,0001.

When investigating the antitumor activity *in vivo* of NYESO-1+-T-cells downregulating HPK1, NSG-IL15 mice (n= 5 mice/ group) were subcutaneously injected with 5M Me275 melanoma cancer cells. When tumors became palpable 10 days after inoculation, an ACT was conducted using 10×10^6 UTD and engineered T-cells. We then monitored tumor growth over time and evaluated survival. **(Figure 15a)**. The engineered T-cells were downregulating HPK1 using miR A and B, and their performance was compared to control (CTRL) T-cells, UTD T-cells, and tumors alone (saline). T-cells exhibiting the highest KD level of HPK1 through the use of miR A (HPK1 (A)) demonstrated significantly improved tumor control compared to the CTRL T-cells ($p=0,0002$ comparing CTRL and HPK1 (A) transduced T-cells using student *t* test) **(Figure 15b, left)**, as also indicated by the lowest tumor volume at day 24 **(Figure 15b, right)**. Furthermore, HPK1 KD using miR A significantly enhanced mice's probability of survival compared to CTRL T-cells ($P=0,01$ using Kaplan Meier analysis) **(Figure 15c)**.

Here, we provide evidence that downregulating HPK1, particularly through miR A with the highest KD level, can significantly enhance tumor control and improve survival *in vivo*.

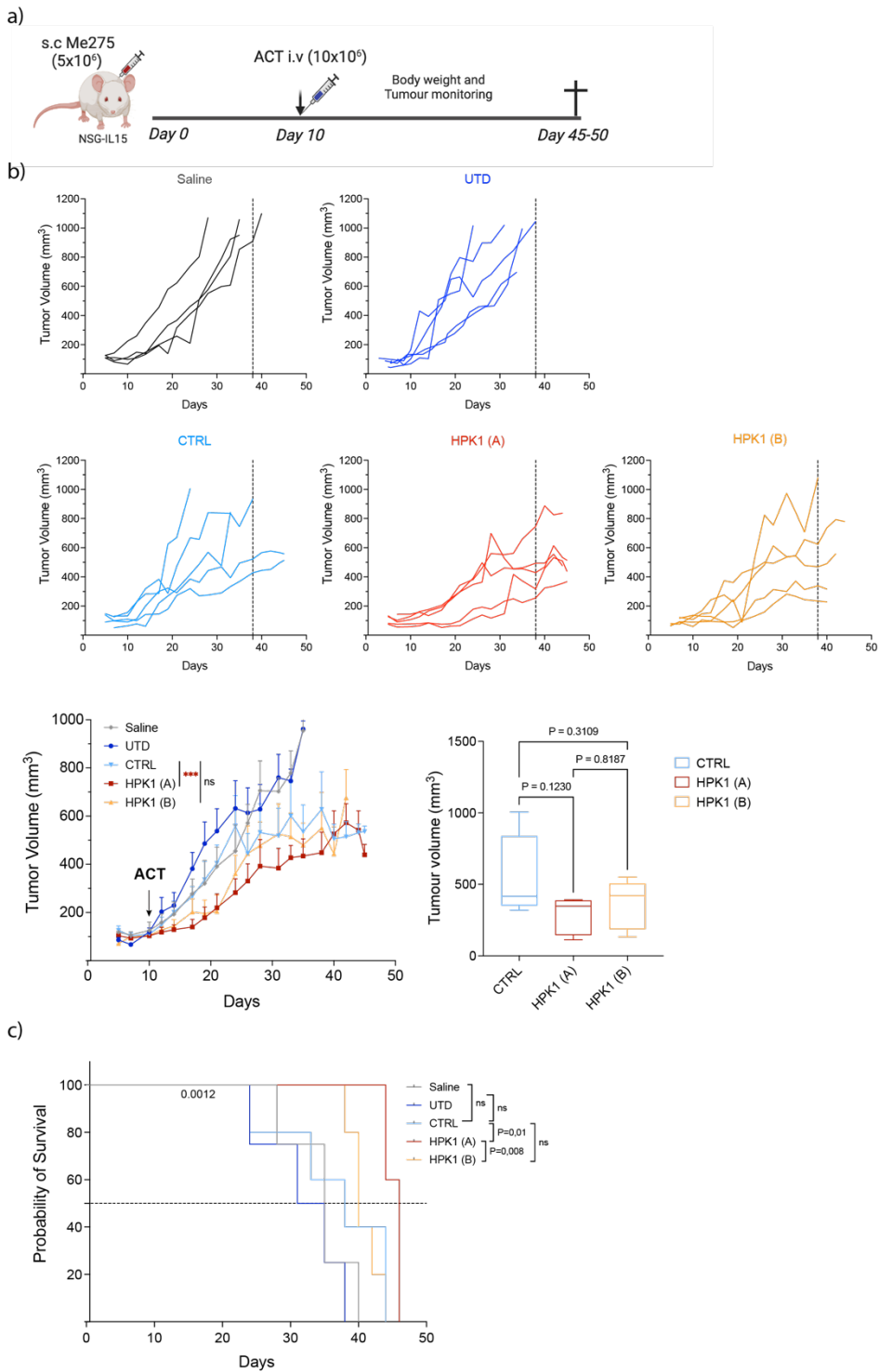


Figure 15: *In vivo* evaluation of HPK1 KD impact on NYESO-1⁺ T-cells' antitumor activity.

(a) *In vivo* experimental design for ACT of engineered T-cells targeting HPK1 in NSG-IL15 mice using the Me275 melanoma cancer tumor model. (b) Tumor volume in mm² measured by caliper over time; top: individual tumor growth curves of different groups; bottom left: Tumor growth curves of different groups over time presented as mean ± s.e.m. for n = 4 (saline) to 5 mice/group. Statistical significance was determined by student *t* test between CTRL vs. HPK1 (A) or vs. HPK1 (B) T-cells, ***P = 0,0002 and ns = 0,163; bottom right: bar graph representing total tumor volumes at day 24 of CTRL, HPK1 (A) and HPK1 (B) as mean ± s.e.m. for n = 4 (saline) to 5 mice/group until the endpoint. Statistical significance was determined using One-Way ANOVA and post-hoc Tukey's analysis. (c) Probability of survival of different conditions presented using Kaplan Meier analysis of mice's survival up to the endpoint after tumor injection of n = 5 mice /group.

We subsequently evaluated the *in vitro* cytotoxicity of the NYESO-1 T-cells with or without HPK1 KD against A2+/NY+ target cell lines Me275, A375, and Saos2, as well as the A2-/NY- cell line Na8 as a negative control. Tumor killing capacity was quantified over 44h using the IncuCyte system, where UTD and +/- HPK1 KD T-cells were cocultured at different E:T ratios of 2:1, 1:1, and 0.5:1 with target cells engineered to express the nucleic dye. Thus, the number of dead tumor cells is proportional to the loss of NucRed signal by tumors quantified in each well. Although no significant difference *in vitro* cytotoxicity was observed overall between T-cells with or without HPK1 KD compared to the control (CTRL) at different E:T ratios tested using different target cells, the most striking results emerged from the coculture with Me275 tumors at an E:T ratio of 2:1, where HPK1 loss using miR B significantly enhanced T-cell killing capacity *in vitro* compared to CTRL T-cells (P= 0,012 using two-way ANOVA analysis and post-hoc Tukey test for multiple comparisons at last time point of n=3 donors in technical duplicates) (**Figure 16a**).

To elucidate the underlying mechanisms of these findings, we analyzed by flow cytometry the expression of surface inhibitory markers on HPK1 (A), HPK1 (B), and CTRL T-cells at the end of the IncuCyte assay from each coculture condition tested. The cells were then stained with Ab against CTLA4, PD-1, TIGIT, and TIM-3. Data shown in **Figure 16b** revealed that T-cells downregulating HPK1 and specifically using miR A exhibited significantly higher levels of TIGIT, TIM-3, and CTLA4 expression in all tested A2+/NY+ tumor models. Additionally, HPK1 (A) T-cells displayed a greater upregulation of PD-1 when cocultured with Me275 cells at an E:T ratio of 0.5:1. These results suggest HPK1 KD in T-cells may contribute to an enhanced immune checkpoint inhibitor profile *in vitro* and could also explain why we couldn't replicate the same findings as *in vivo*.

However, this could highlight a potential for enhanced immunoregulatory functions and open a path for exploring the benefit of a combinatorial approach involving HPK1 KD with ICB to boost HPK1 KD NYESO-1 T-cell cytotoxicity.

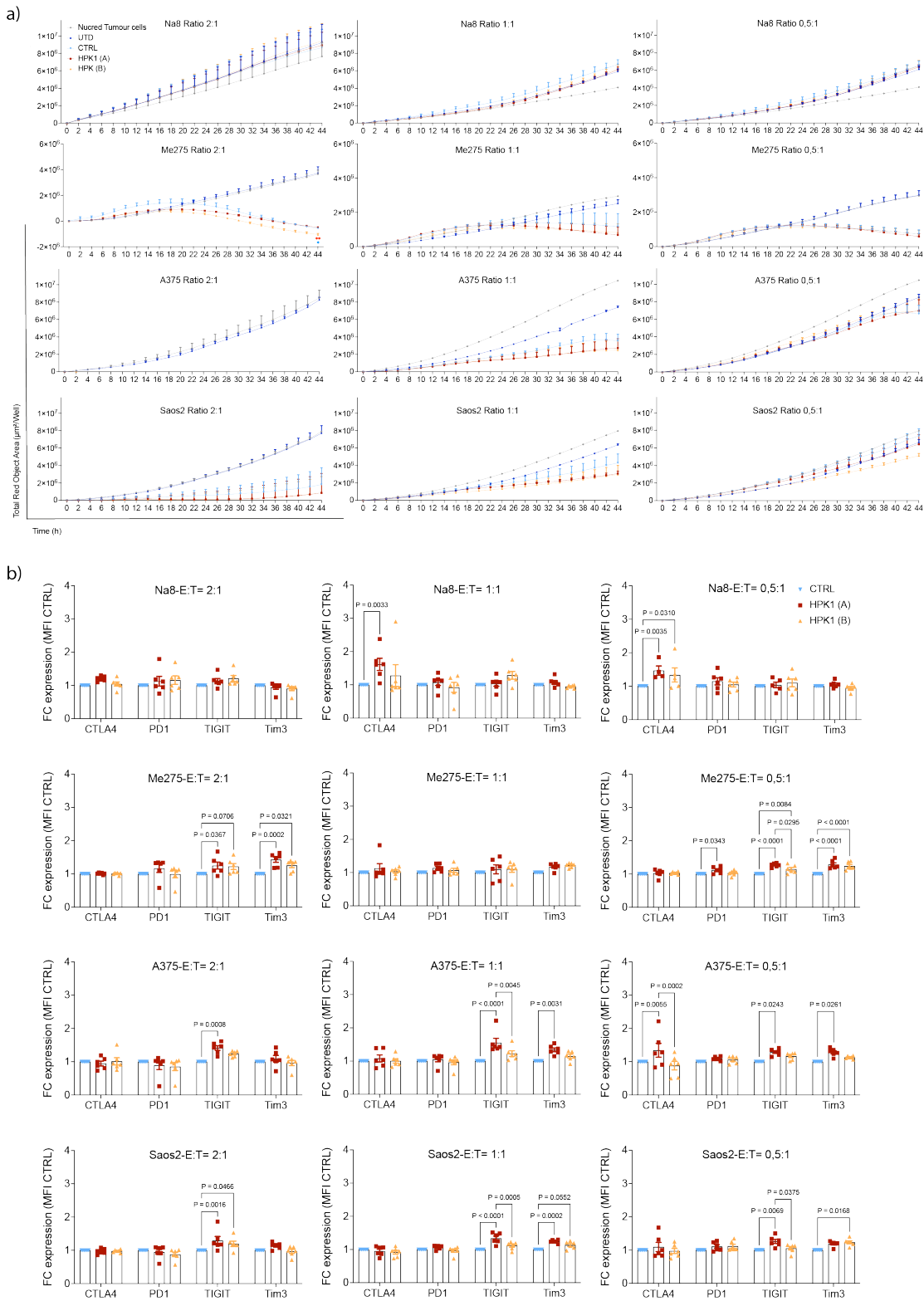


Figure 16: Assessment of cytotoxicity and inhibitory checkpoints expression upon HPK1 knockdown in NYESO-1 T-cells.

(a) NYESO-1 +/- killing assay by +/- HPK1 KD-NYESO-1+T-cells measured by IncuCyte system as total red area per μm^2 overtime at 3 different E:T ratios using A2+/NY+ Me275, A375, and Saos2 target cells along with A2-/NY- Na8 target cells as a negative control. Data presented as mean \pm s.e.m. (n = 3 donors in technical duplicates). Statistical significance was assessed using Two-way ANOVA and post-hoc Tukey test, where indicated, **P=0,0046 and *P= 0,012. (b) Fold change expression of surface checkpoint inhibitors of CTRL, HPK1 (A), and HPK1 (B) NYESO-1+ T-cells measured by flow cytometric analysis at the end of IncuCyte assay at 3 ratios E:T and using A2+/NY+ Me275, A375 and Saos2 target cells along with A2-/NY- Na8 target cells. Data are shown as mean \pm s.e.m. (n = 3 donors in technical duplicates). Statistical significance was assessed using Two-way ANOVA and post-hoc Tukey test.

3. A combinatorial gene-engineering approach targeting multiple TCR intracellular negative regulators for enhanced T-cell persistence and functionality.

3.1. Summary

Given the wide range of suppressive barriers in the TME, chronic antigen exposure and inflammatory signals can render T-cells exhausted. To counteract this effect, we further proposed to evaluate HPK1 KD in combination with additional downregulation of other suppressor molecules downstream of TCR. One possible combinatorial approach to improve T-cell function is to downregulate the inhibitory lipid kinases, such as DGKs, responsible for “switching off” the MAPK pathway in T-cells⁵⁵⁹ or kinases belonging to the E3 ligases family responsible for attenuating TCR signaling through the ubiquitylation machinery. These E3 ligases include Cbl-b, Itch, GRAIL, and NEDD4-1 linked anergy and exhaustion.^{479,480} Indeed, several studies have shown that many intracellular suppressor regulators can dampen TCR signaling and attenuate T-cell response and their killing capacity in the context of tumors; thus, downregulating each of these target genes could significantly enhance T-cell function. Overall, our strategy aims to engineer CAR/TCR T-cells with two combined KDs to strengthen the TCR signaling and protect it from degradation and suppression. We believe combinatorial gene KD T-cell therapy will be a potent approach against solid tumors.

Furthermore, to determine the optimal combinatorial gene KD strategy to complement HPK1 KD in our investigation, we transitioned from employing a Xenograft model to using a syngeneic mouse model. This transition allowed for a comprehensive examination of the TME. It facilitated a thorough assessment of the impact of potential combinatorial downregulation of suppressor genes on overcoming immunosuppressive barriers within tumors. Additionally, we selected the B16 OVA tumor model, known for its characteristics as a cold solid tumor with limited T-cell infiltration, attributed to its low immunogenicity.

3.2. Material and Methods:

Molecular Biology:

Vector construction and insert cloning:

DNA fragment inserts were designed using SnapGene software version 5.2 (San Diego, USA), purchased from Microsynth (Microsynth AG, Switzerland) or from Transomic for shRNA-based miRNAs, then cloned in frame in retroviral (pMSGV) or in pSUPER (kindly provided by Ping-Chi-Ho lab) vectors available in the lab. The vectors amplification was performed in Stellar competent cells (*E. coli* HST08, 636763, Takara) and purified with PureLink HiPure plasmid Filter mini/maxi-prep kit (K210016, ThermoFisher Scientific) upon confirmative sequencing (Microsynth AG, Switzerland).

mRNA extraction and quantitative PCR

The mRNA was extracted using the Rneasy Mini extraction kit (74104, Qiagen) following the manufacturer's instructions. Post purification, less than 1 µg of RNA was reversely transcribed to cDNA with the PrimeScript 1st strand cDNA Synthesis Kit (Takara 6110). The quantitative polymerase chain reaction (qPCR) primers HPK1 (MAP4K1, Mm01152700_m1, Taqman), Cbl-b (Mm01343092_m1, Taqman), NEDD4 (Mm00456829_m1, Taqman), IFNγ (mM-01168134_m1, Taqman), TNFα (Mm00443258_m1, Taqman), GzmB (Mm00442837_m1, Taqman), PD-1 (Mm01285676_m1, Taqman), CD69 (Mm01183378_m1, Taqman), GAPDH (Mm99999915_g1, Taqman) were used to perform quantitative PCR (qPCR) with TaqMan Fast Universal PCR Master Mix kit (4352042, Lifetechnologies) using manufacturer's suggested plates (4346906, Lifetechnologies) with appropriate optical cover plates (4360954, Lifetechnologies). The qPCR using housekeeping gene GAPDH was performed as a control to allow the normalization of samples. Each sample was run in duplicate or triplicate, and each experiment included two non-template control wells. The relative mRNA levels (fold change) of each transgene among the different samples were quantified using the comparative $2^{-\Delta\Delta C_t}$ method.

Retroviral supernatant production

Phoenix-Eco cells (ATCC CRL-3214) were seeded at 2.5×10^6 per T-150 tissue culture (Corning, 430825) in 35ml RPMI complete medium 3 days before transfection. On the day of transfection, the medium was then removed from each T-150 flask bearing Phoenix Eco cells of 80–90% confluency and was reconstituted with a transfection mixture that comprised plasmid DNA mix added to 180µl of Turbofect (ThermoFisher Scientific) or Polyethyleneimine (PEI) (Chemie Brunschwig) and 3 ml of Optimem (Invitrogen, Life Technologies) added on top of the cells then incubated for 30 min at RT followed by the addition of 30 ml fresh medium. Plasmid DNA mix included 14,4µg pCLEco retrovirus packaging vector and 21,4 µg transfer plasmid using Turbofect. The viral supernatant was harvested at 48 h and 72h post-transfection. Viral particles per each T-150 flask were concentrated by ultracentrifugation at 24,000 g for 2h at 4°C in 38,5 ml tubes (244058, Beckman Coulter) with a Beckman JS-24 rotor (Beckman Coulter) and resuspended in 400µl of T-cell medium consisting of complete RPMI medium further supplemented with 1% sodium pyruvate (11360070, ThermoFisher Scientific), 1% nonessential amino acids (MEM nonessential amino acids solution 100X) (11140035, ThermoFisher Scientific) and 0.1% 2-mercaptoethanol (31350010, ThermoFisher Scientific). The retrovirus was used immediately or aliquoted for snap-freeze and storage at –80°C until the day of cell transduction.

Cell line Culture:

The B16 cell line was purchased from ATCC (ATCC CRL-6475) and genetically manipulated to express the OVA peptide presented on major histocompatibility complex (MHC) class I molecules. Wild type (WT) B16, B16-OVA, C1498, and Phoenix-Eco (ATCC CRL-3214) cell lines were kept in complete RPMI medium at

37 °C in a 5% CO² atmosphere. Cell media was refreshed three times per week to maintain the cells in culture at a maximum of 80% confluency.

Primary murine T-cells isolation, stimulation, transduction, and culture

OTI/OT3.CD45.1⁺ or OT1/OT3 CD45.1⁺ Cas9 GFP murine T-cells were isolated from single-cell suspensions of dissociated spleens from CD45.1/2⁺ congenic C57BL/6 or C57BL/6 whole body cas9 mice bred in-house at the animal facility of the University of Lausanne (UNIL; Epalinges, Switzerland) using the EasySep Mouse T-cell Isolation Kit (StemCell Technologies). Briefly, upon mice euthanasia with high doses of CO² atmosphere, the spleen was harvested, smashed on a 40 µm size strainer (352340, Corning) using a 2 ml syringe plunger (01227, Becton Dickinson) and RPMI-1640 Glutamax medium. Collected splenocytes were lysed using red blood lysis buffer (420301, BioLegend), then T-cells were negatively selected using antibody complexes and magnetic beads of the EasySep Mouse T-cells Isolation Kit (Stem Cell) according to the manufacturer's protocol (19851, Stem Cell Technology). Purified murine T-cells were resuspended in mouse T-cells complete medium, activated on the same day using αCD3/αCD28 monoclonal antibody (mAb) magnetic beads (Gibco, Thermo Fisher Scientific) at a bead-to-cell ratio of 2:1, in addition to 50 IU/ml of hIL-2 (Glaxo) then seeded at 1×10^6 cells per ml in a cell culture treated 48-well plate in a total volume of 1 ml per well of T-cell media (CLS3548, Corning). Non-treated 48 or 24-well plate cell culture plates (Corning) were precoated with 0,25 ml or 0,5 ml, respectively, of Human recombinant RetroNectin (T100A, Takara Bio) at a final concentration of 20 µg/ml, overnight (O/N) at 4°C prior murine T-cell transduction. 24h post-T-cell activation, the RetroNectin-precoated plates were washed twice with PBS and then blocked with T-cell media for 30 min at RT. Subsequently, a volume of T-cell media equal to virus volume to be used is removed and replaced by the retrovirus for a final volume of 500µl per well and with a multiplicity of infection (MOI) of 2,5 or 5. In some experiments, the transduction procedure was performed at 48h or both at 24h and 48h after activation. Later, the plates were spun at 2'000 g for 2h at 32°C. Finally, the supernatants were aspirated, and the 24h-activated cells were transferred to each coated well for a final volume of 500µl. The plates were centrifuged at 300g for 10 min before incubation at 37 °C in a 5% CO² atmosphere. Starting from the third day of culture, the cells were maintained at a cell density of 0.5×10^6 /ml and replenished with fresh T-cell medium supplemented with human IL2 at 20UI/ml, IL15 at 25ng/ml (130-093-955, Miltenyi Biotech) and human IL7 at 2,5ng/ml (130-093-937, Miltenyi Biotech) every other day. To maintain the cell density at 0.5×10^6 /ml, cells were manually counted over time with a Neubauer chamber (140527, Milian) with trypan blue (15250061, Invitrogen) dilution to distinguish live and dead cells. Alternatively, cells were counted with NucleoCounter®200 (Chemometec) counting machine to automatically assess cell number, viability, and size (in µM). At day 6 post-activation, magnetic beads were removed, and T-cells were stained for flow cytometric analysis before performing an *in vivo* ACT or *in vitro* assays.

***In vitro* assays with primary murine T-cells**

T-cells stimulation

OTI and OT3 cells were stimulated in duplicate or triplicate by coculturing $0,5 \times 10^6$ primary murine T-cells with WT B16 or B16 OVA target cell lines at a ratio of E:T = 2:1 or 1:1 in 200µl T-cell media. Where indicated, we stimulated OTI or OT3 cells with the daily addition of OVA SIINFEKL peptide (EMC microcollections GmbH) in the culture at 0,01µg/ml. 24h, 48h, 72h, and 96h post-coculture or peptide stimulation, 100µl of cell culture supernatant were collected and frozen at -80°C for reverse transcription qPCR (RT-qPCR) analysis or cytokines release analysis.

Proliferation assessment with CFSE trace assay

For evaluating the proliferative capacity of murine primary T-cells, OTI or OT3 cells were stained with Carboxyfluorescein succinimidyl ester (CFSE) (C34554, Invitrogen) according to the manufacturer's

instructions and seeded at a cell density of 10^4 in 200 μ l of T-cell medium per well in duplicate or triplicate prior coculture with WT B16 or B16-OVA cells at a ratio of E:T = 1:1. Upon 72h of coculture, cell division was evaluated by dilution of the CFSE dye in live CD8⁺ T-cells by flow cytometric analysis.

Intracellular and extracellular staining for Flow Cytometry

For analyzing molecular-cell surface expression, cells were collected in a 96-well round or V-shaped bottom plate (Corning), washed with FACS buffer containing PBS (CHUV) with 1% bovine serum albumin (BSA) (268131000, Chemie Brunschwig) and 0,1% NaN₃ sodium azide (S2002-100G, Sigma-Aldrich) then incubated with the antibody mixture on ice for 30min at 4°C.

For cell surface staining, the following anti-murine antibodies were used: aCD8⁺ BV510 (clone 145-2C111) or BV711 (clone 53-6.7), aCD90.1 (Thy1.1) BV650 (clone OX-7) or BV605 (clone OX-7), aCD45 PE Cy5.5 (clone 104), aPD-1 APC Cy7 (clone 29F.1A12), aCD69 BV605 (clone H1.2F3) and aCD25 BV605 (clone PC61). Abs were purchased from eBioscience or BioLegend. For distinguishing the live versus dead cells, the Live/dead Fixable Aqua dead (BV510) staining kit was used (L34957, ThermoFisher Scientific).

For intracellular staining, the cells were collected in a 96-well round or V-shaped bottom plate (Corning) and washed with FACS buffer before adding Fc Block (BD Biosciences-clone 2.4G2). After washing, cells were cell surface stained, fixed, and permeabilized for 30 min at RT with the Fix/Perm buffer set kit according to the manufacturer's instructions (88-8824-00, eBioscience) before adding the intracellular antibodies mixture resuspended in permeabilization buffer on the ice at 4°C for 30 min as following: aIFN γ Peridinin chlorophyll protein (PerCp) (clone XMG12), aTNF α Pacific Blue (PB) (clone MP6-XT22), aTOX PE (clone REA473), aTCF1 (C63D9), aHPK1 Alexa Fluor 647 (clone G-9), aCbl-b Fluorescein isothiocyanate (FITC) (clone G-1), aNEDD4 (PA5-17463), aDGK α (PA5-87278, Invitrogen), AKAP5 (NBP2-92620), Cabin1 (PA5-68119), PTPN3 (NBP2-93945), PTPN12 (AG10), PTPN22 (D6D1H), 14-3-3 ζ/δ (D7H5), XBP1 (NBP-77681), and secondary anti-rabbit IgG Fab² Alexa Fluor 488 (4412S, Cell Signaling) or PE (8885S, Cell Signaling). Abs for intracellular staining were purchased from eBioscience, BioLegend, Invitrogen, Miltenyi, Cell signaling, Santa Cruz Biotechnology, or Novus Bio. The stained samples were kept on ice and acquired with the LSRII machines at the UNIL Flow Cytometry Facility.

Cytotoxicity with IncuCyte System

The IncuCyte System (Essen Bioscience) was used for assessing the cytotoxicity of murine primary OTI. 1×10^4 target cells were seeded 4h before the coculture was set up in flat bottom 96well plates. Rested T-cells (no cytokine addition for 48h) were counted and seeded at 1×10^4 cells/well, at a ratio E:T = 1:1 in T-cell media. Cytotox Red reagent (Essen Bioscience) was added at a final concentration of 125nM in a total volume of 200 μ l. No exogenous cytokine was added to the assay medium during the coculture period. Internal experimental negative controls were included in all assays, involving untransduced cells and co-incubation with WT B16 cells, as well as T-cells and tumor cells alone in the presence of Cytotoxic Red reagent to monitor spontaneous cell death over time. As a positive control, tumor cells alone were treated with 1% Triton (T8787, Sigma-Aldrich) solution to represent maximal killing in the assay. Images of the total red area/well were collected every two hours of the coculture for up to three days. The total red area per well was obtained using the analysis protocol on the software provided by Essen Bioscience manufacturer. Data were normalized by subtracting the background fluorescence observed at time 0, which consists of any cell killing by primary murine transduced or untransduced OTI cells from all further time points. Data are expressed as mean \pm s.e.m. of different donors.

***In vivo* adoptive cell transfer experiments with syngeneic tumor models**

C57Bl/6 CD45.1/2 female mice (purchased from Harlan Laboratories) and OTI/OT3-CD45.1 whole-body Cas9 GFP were housed in a dedicated and opportunistic pathogen-free animal facility (SOPF) in the Oncology Department of the University of Lausanne. B16 OVA tumor cells were harvested with Accutase (Sigma-Aldrich), washed, and resuspended in PBS at 1×10^5 cells per 100 μ l, then subcutaneously injected in the flank of 8-12 weeks old mice. Once the tumor volume reached 50-100 mm³ after 8 days, mice were irradiated with 5Gy prior to ACT which was performed twice on day 9 and 11 post-tumor injections by administering intravenously $2.5-5 \times 10^6$ OTI/OT3 CD45.1⁺ cells or OTI/OT3 CD45.1⁺ Cas9 GFP cells. Tumor growth was monitored via caliper measurement every two days. It was calculated using the formula $V (\text{mm}^3) = 1/2 (\text{length} \times \text{width}^2)$, where length is the greatest longitudinal diameter and width is the greatest transverse diameter. During experimentation, all animals were monitored for signs of distress at least every other day. Mice were sacrificed at the endpoint by carbon dioxide overdose, and where indicated, tumors, spleens, and lymph nodes were collected.

***Ex vivo* analysis of syngeneic tumor models**

At the terminal point, solid tumor mass was excised from the mice, cut into small pieces with a scalpel, passed through 40mm pore cell strainers (Grenier Bio-One), processed in GentleMACS dissociator system using tumor dissociation kit (130-096-730, Miltenyi) according to the manufacturer's guidelines, then centrifuged for 5 min at 1500 rpm to pellet the cells. Upon washes, the obtained cells were stained with anti-CD45.1 (clone A20) Ab to assess the presence of TILs post ACT by flow cytometry.

Statistical Analysis

All the statistical analyses were performed using GraphPad Prism 9.0 (GraphPad Software, La Jolla, CA). Student t-test or Mann-Whitney u test were used to evaluate differences among two groups, one-way analysis of variance (ANOVA) followed by post-hoc Tukey correction for multiple comparisons was used for evaluating significant differences among column groups when one variable was tested. Two-way ANOVA followed by post-hoc Tukey correction was used for statistical analysis of multiple groups with more than one variable. Differences were considered significant when * $P < 0.05$, very significant when ** $P < 0.01$, and highly significant when *** $P < 0.001$.

CRISPR screen data visualization

For identifying essential and suppressor genes downstream of the TCR signaling in the OTI model in the context of *in vivo* persistence, the MAGeCKFlute pipeline was adopted. It combines the MAGeCK and MAGeCK-VISPR algorithms⁵⁷¹. The volcano plot and the ranking plot based of the fold change of the output (TILs) vs. the input (OTI+Cas9+GFP+ cells) were created using the R program, version 4.1.2.

Graphical and schematic illustrations

The graphical figures depicted in the introduction, as well as the schematic visualization elucidating the design of vector constructs and *in vivo* experimental designs, were created using Biorender.com.

3.3. Results

3.3.1. Identification of relevant intracellular negative regulators for miRNA targeting downstream the TCR signaling pathway.

Following a comprehensive literature review, as detailed in the introduction section of "Intracellular negative regulators downstream TCR signaling pathways," twelve initial genes were identified as potential targets for gene inhibitory strategies. The selection process considered several factors: the role each intracellular checkpoint plays in CD4⁺ and CD8⁺ T-cell activity, the risk of autoimmunity, and the availability of clinical or preclinical data pertaining to ACT combined with the inhibition of these molecules (**Table 2**). The chosen targets include HPK1, Cbl-b, NEDD4, DGK α , CISH, PTPN3, PTPN12, PTPN22, AKAP5, Cabin1, 14-3-3z, and XBP1 (**Figure 17a**).

3.3.2. Evaluation of gene expression of the selected negative regulators in high-affinity CD8⁺ cells:

Prior to implementing our strategy for downregulating the activity of selected downstream TCR suppressor genes, it was imperative to evaluate their expression levels following antigen stimulation. This approach aimed to mimic the conditions observed within the TME and allowed us to ascertain that these negative regulators were indeed upregulated when T-cells experienced chronic stimulation. This preliminary assessment was crucial to ensure that a KD strategy targeting these regulators would yield meaningful outcomes and could effectively release the TCR brakes and enhance the antitumor functionality of T-cells upon TCR stimulation.

To achieve this, we employed an *in vitro* protocol adapted from the Katsikis laboratory's publication in 2020⁵⁶¹, which focused on generating an exhausted-like state in T-cells through chronic antigen stimulation. Using OTI mouse T-cells as a model of high-affinity TCR, T-cells were isolated and then chronically stimulated at day 6 post *in vitro* culture with SIINFEKL OVA peptide repeatedly for three consecutive days (repeated peptide condition, RP). The single peptide condition (SP), where OTI cells encountered the peptide only once on day 6, in addition to OTI cells that did not receive any peptide stimulation (NP), were included as a control (**Figure 17b**).

Post-stimulation, the influence of peptide-TCR engagement was assessed through flow cytometric analysis. Two primary effects were observed: First, an indication of OTI-cell exhaustion, evidenced by the upregulated expression of PD-1 and TOX, alongside the downregulation of TCF1 in the RP condition compared to the NP condition (**Figure 17c**). Second, the expression of the chosen target negative regulator was observed (**Figure 17d**).

Notably, HPK1, together with other selected molecules, Cbl-b, NEDD4, DGK α , CISH, PTPN22, and XBP1, exhibited upregulation upon stimulation, with the highest levels observed when OTI cells were chronically stimulated (RP) compared to when the TCR engaged only once (SP). At the same time, the difference was much greater when OTI cells that were not stimulated by the peptide (NP) or when they are freshly isolated as naïve T-cells. On the other hand, the expression of AKAP5, Cabin1, 14-3-3z, PTPN3, and PTPN12 was similar in both RP and NP conditions (**Supplementary Figure 1a**).

These data suggest that chronic antigen stimulation induces the upregulation of selected negative regulators associated with high-affinity TCR T-cell exhaustion, supporting the potential effectiveness of a KD approach targeting these regulators to enhance the antitumor function of T-cells by relieving TCR brakes.

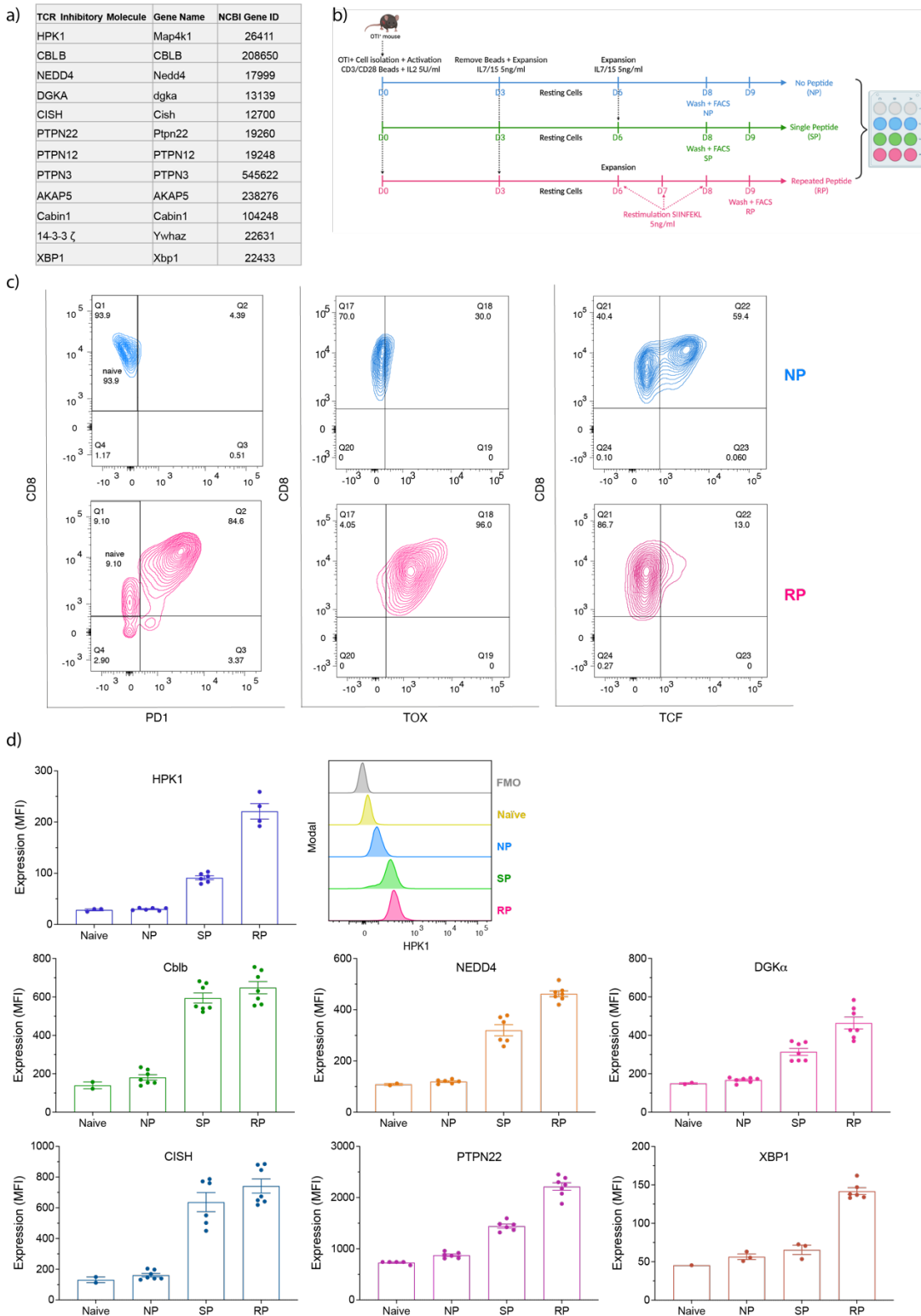


Figure 17: Evaluation of selected negative regulators' expression levels in the context of *in vitro* exhaustion assay using high-affinity TCR OTI cells.

(a) List of selected negative regulators targeted for downregulation. (b) Schematic of the *in vitro* exhaustion assay with different peptide stimulation conditions: repeated peptide (RP), single peptide (SP), and no peptide (NP). (c) Representative flow cytometry contour plots illustrating the expression of PD-1, TOX, and TCF1 in CD8+ OTI cells in RP compared to NP condition. (d) right: Representative histogram depicting HPK1 expression in NP, SP, and RP compared to Naïve OTI cells and FMO (Fluorescence Minus One); left and bottom: Bar graphs demonstrating the expression as mean fluorescence intensity (MFI) of TCR downstream checkpoints i.e., HPK1, Cbl-b, NEDD4, DGK α , CISH, PTPN22, and XBP1, in NP, SP, and RP conditions compared to naïve cells, data shown as mean \pm s.e.m. of two independent experiments (n=6).

3.3.3. miRNA screening for achieving a high knockdown level of the selected targets using the single-miRNA vector in high-affinity CD8+ cells.

After the confirmation of TCR suppressor molecule candidates, we proceeded with cloning the Transomic miRNA targeting mRNA corresponding to each TCR negative regulator candidate in an MSGV retroviral vector developed in-house. This vector was employed to introduce miRNAs targeting each selected negative regulator (**listed in Figure 7a**) to assess their KD efficiency. Three distinct miRs were tested for downregulating each negative regulator alongside a control miRNA (CTRL) (devoid of any targeted sequence in primary murine OTI cells).

The miRNAs were constitutively induced by the U6 promoter, followed by a leader sequence for facilitating miR processing, and the Thy1.1 reporter gene was also expressed constitutively under the PGK promoter, enabling the measurement of transduced T-cells, all arranged in a sense configuration (**Figure 18a**). Thereafter, we determined the efficacy of retroviral vector transduction (MOI=5) by assessing the percentage of Thy1.1 expression in live CD8+T-cells relative to UTD CD8+T-cells, which was found to be high, reaching above 90%, indicating successful transduction of the T-cells with the retroviral constructs (**Figure 18b**).

Next, the KD potency was evaluated within the *in vitro* exhaustion assay context and by performing intracellular staining for flow cytometric analysis to detect each molecule expression within each condition. Representative histograms showcase the reduction in expression of selected molecules, notably HPK1, in different experimental conditions: NP, SP, and RP compared to Naïve OTI cells and FMO (**Figure 18c**). Each of the selected molecules underwent downregulation using three distinct miRNAs (A, B, and C) in OTI cells compared to the control miRNA (miR CTRL) under the *in vitro* exhaustion assay. Subsequently, flow cytometric analysis was conducted to determine the percentage (%) and mean fluorescence intensity (MFI) of expression for each targeted molecule, as we anticipated that the KD could impact either the percentage of the positive population expressing the molecule or reduce the expression level within individual cells. Additionally, we established a fixed minimum threshold for the KD level set at 30% to evaluate the effectiveness of the downregulation. Data was presented based on the condition where the KD demonstrated the most KD efficacy.

A strong KD level was observed for HPK1 of approximately 70%, for Cbl-b of above 40%, and for NEDD4 with more than 50% of KD (**Figure 18d**). Other miRNAs targeting the remaining molecules were also evaluated for their downregulation potency, with some achieving KD levels above 30% and others below 30% (**Supplementary Figure 1b**). An alternative approach was pursued to downregulate molecules whose KD levels were below 30%. Three newly designed miRNAs targeting each of those molecules were developed using a specific algorithm (SplashRNA) published by Pelossof, Fairchild, et al. in 2017⁵⁷². However, the introduction of these new "splash" miRNAs (sp-miRs) did not significantly improve the KD potency of the targeted genes (**Supplementary Figure 1c**). As a result, the focus was narrowed down to HPK1, Cbl-b, and NEDD4, encompassing two E3 ligases of the TCR ubiquitination pathway along with the main target, HPK1, for combinatorial gene downregulation.

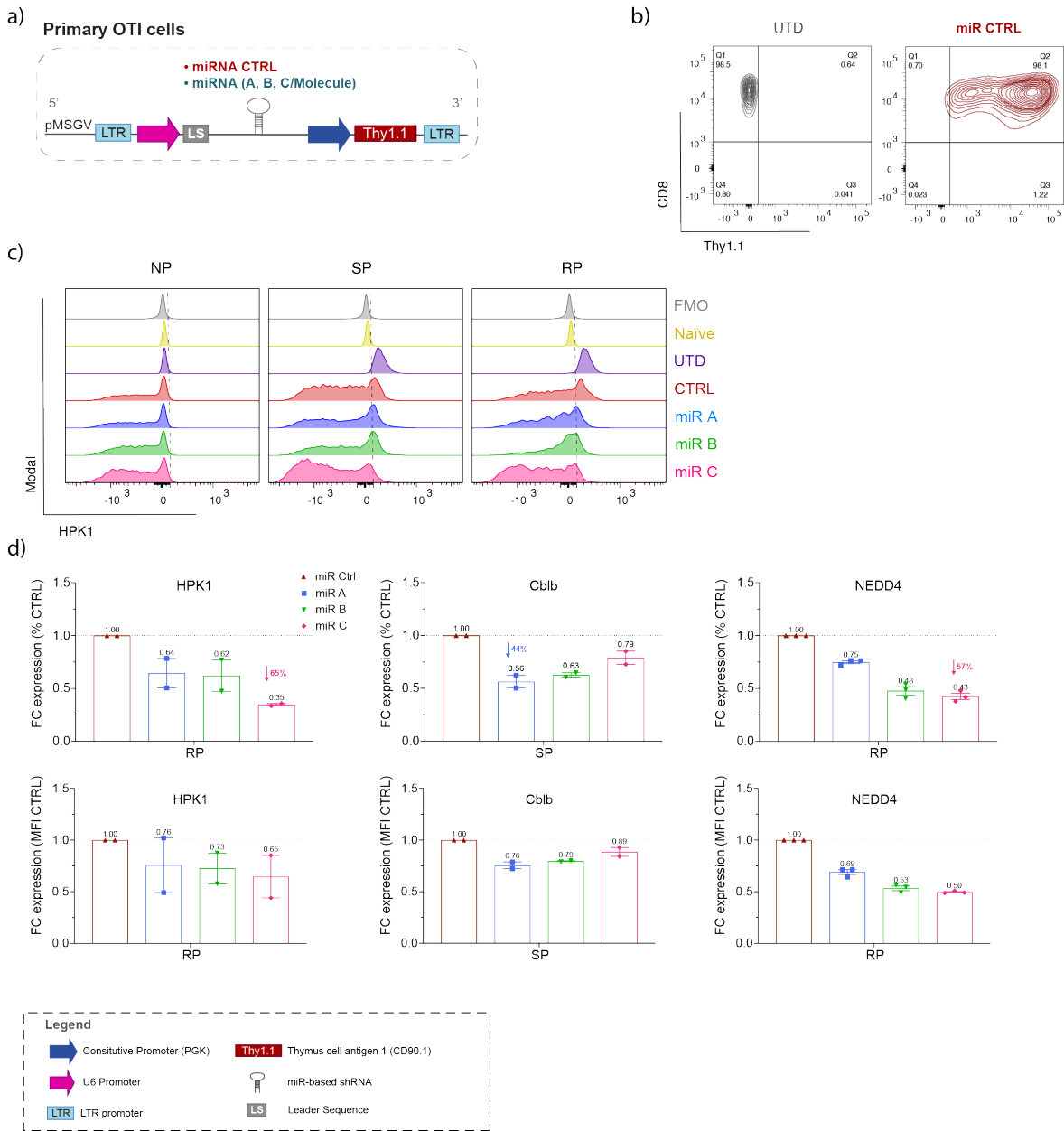


Figure 18: Downregulation of selected TCR negative regulators in transduced OTI cells with single miRNA retroviral vector
 (a) Schematic of the MSGV retroviral constructs containing a single miRNA, either miR CTRL or a miRNA targeting TCR intracellular checkpoint molecule, expressed under the U6 promoter, a leader sequence for miRNA processing, and a constitutively expressed Thy1.1 reporter gene under the PGK promoter. (b) Representative flow cytometry contour plots showing high TE measured by the percentage of Thy1.1 expression in live transduced miR CTRL-CD8⁺T-cells (right plot) compared to untransduced CD8⁺T-cells (left plot). (c) Representative histograms illustrating the downregulation of HPK1 in different experimental conditions (NP, SP, RP) along with the OTI naïve cells and FMO as a baseline for gating strategy. (d) Bar graphs demonstrating the fold change of percentage (%) and mean fluorescence intensity (MFI) of expression of targeted intracellular checkpoint inhibitors upon downregulation using miR A, B, and C compared to miR CTRL (CTRL) for each targeted molecule. Data are presented as mean ± s.e.m. (n=2 or 3 technical replicates).

3.3.4. Vector design for dual and multiple targeting of the selected TCR intracellular inhibitory checkpoints:

To accomplish concomitant downregulation of two or three selected HPK1, Cbl-b, and NEDD4 negative regulators, retroviral vectors were generated comprising dual miR vectors for targeting two genes and a multiple miR vector for targeting all three molecules simultaneously. The positioning of each miRNA sequence within the vector presented numerous possibilities, including placing the miR directly after the U6 promoter and leader sequence, at the last miRNA position, or in the middle in the case of the multiple miR vector. In our approach, HPK1 was consistently positioned as the first miR after the U6 promoter, while the last position was filled by the miRNA that exhibited the highest KD level. This selection was based on the hypothesis that the miR processing machinery would be more potent closer to the promoter, resulting in stronger KD. In contrast, reduced efficacy might be observed as the distance from the promoter increases (this hypothesis was tested and confirmed by colleagues and me; the data is not shown in this report).

Furthermore, we have also considered expressing all miRs under individual U6 promoters for each miR to enhance the KD efficacy. Thus, we designed retroviral vectors using consecutive U6 promoters to induce individual miR-mediated KD. However, we encountered challenges during the cloning steps, including bacterial recombination (data not shown). Therefore, we present here only the vectors utilized in the forthcoming studies.

The retroviral vectors were generated using the NEB Golden Gate assembly method (NEB Labs), which involves a streamlined and efficient DNA assembly technique based on the use of type IIS restriction enzymes. The dual and multiple miR vectors utilized in this section shared identical compositions with the single miR vectors, differing solely in the number of miRs incorporated. These are the miRs selected based on their demonstrated highest KD levels, as presented in **Figure 18d**. Consequently, two distinct types of dual miR vectors were generated: the first contained two miRs targeting HPK1 and Cbl-b, while the second incorporated two miRs targeting HPK1 and NEDD4. In addition, a multiple miR vector was also developed, encompassing three miRs targeting HPK1, Cbl-b, and NEDD4 simultaneously. Spacers comprising specific and distinct restriction enzymes were employed to ensure proper separation and proper processing of the miRs within the dual and multiple miR vectors (**Figure 19a**).

To comprehensively evaluate the effectiveness of our combinatorial gene KD approach, we sought to examine its performance in the context of both high-affinity and low-affinity TCR systems. Therefore, our developed vectors' transduction efficiency and KD levels were assessed in two distinct contexts: OTI cells, representing the high-affinity TCR, and OT3 cells representing the low-affinity TCR. This investigation allowed us to gauge the functionality and versatility of our vectors across varying TCR affinity scenarios. Subsequently, flow cytometric analysis of Thy1.1 expression indicated high TE levels ranging from >60% to 90% when employing single, dual, and triple miRNA vectors in OT3, while in OTI cells, TE was beyond 50% to 90%, which is considered a success considering the utilization of constructs comprising complex secondary structure miRNAs (**Figure 19b**). The KD levels in Thy1.1⁺sorted OTI cells were measured by RT-qPCR as a more sensitive detection of molecules' downregulation. They are shown as relative mRNA expression normalized to the CTRL murine T-cells (miR CTRL). The results demonstrated high KD levels achieved using single and multiple miRNA vectors, ranging from 30% to 70% with the multiple miR vector and 40% to 90% with the dual miRNA vectors (**Figure 19c**).

Another comparative strategy was employed to double or triple transduce OTI cells with single miR vectors using an equal MOI for the selected combinations; however, this approach failed to reach the same KD levels as the one achieved by our developed vector constructs for downregulating HPK1 and NEDD4 while a

nonsignificant increase of Cbl-b KD was observed using the double or triple transduction (DT or TT) of single miR targeting HPK1 and single miR targeting Cbl-b (**Supplementary Figure 2a**).

Furthermore, we have assessed the kinetics of the KD levels for the dual KD combination, specifically HPK1-Cbl-b KD, upon antigen stimulation and over a 72-hour period compared to the control miR (CTRL). For this, engineered OTI cells were cocultured with B16 OVA cells at an E:T ratio of 1:1, along with B16 cells as a negative control. The obtained data demonstrated that upon antigen stimulation (with B16 OVA cells), the KD level of HPK1, as well as Cbl-b expressions, remained suppressed over time with a significant decrease at 24h ($P=0,0141$) for HPK1 expression and at 48h ($P=0,0479$) for Cbl-b expression. As anticipated, the expression of both HPK1 and Cbl-b was reduced to negligible levels in the B16 control for both conditions due to the absence of stimulation (**Supplementary Figure 2b**). Moreover, the KD levels observed in Thy1.1⁺sorted OT3 cells were remarkably high for both the dual and multiple miR vectors and the single miR targeting HPK1, ranging from 80% to 90% for downregulating HPK1, 40% to 70% for Cbl-b KD, and 50% to 70% for NEDD4 KD (**Figure 19d**).

Here we demonstrate the successful generation of dual and multiple miRNA retroviral vectors for transducing murine T-cells and inducing multiple perturbations of selected TCR downstream suppressor molecules. Indeed, the vectors exhibit high transduction efficiency and achieve significant KD levels, highlighting their potential utility for studying and manipulating TCR signaling pathways.

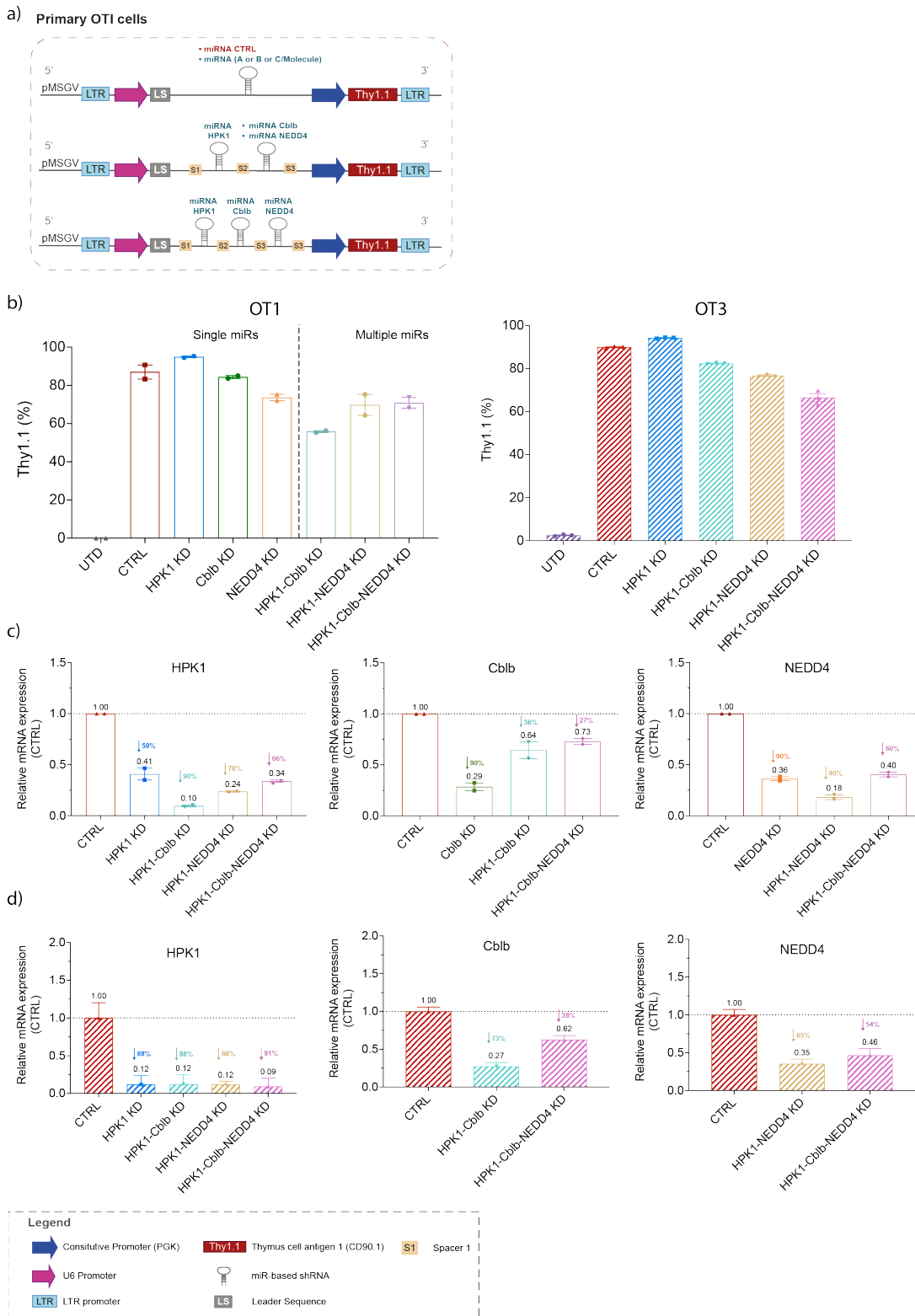


Figure 19: Generation and evaluation of dual and multiple miR retroviral vectors for knocking down HPK1, Cbl-b, and NEDD4 in OTI and OT3 cells.

(a) Schematic representing different MSGV retroviral constructs, similar to single miRNA vectors (as shown in Figure 8a), additional dual and multiple miRNA vectors were generated. (b) TE measured by flow cytometric analysis of Thy1.1 expression in primary murine OTI and OT3 cells for single, dual, and multiple miR vectors, data presented as mean \pm s.e.m (n=2 and n=3 for OTI and OT3, respectively). (c) KD levels in Thy1.1⁺-sorted OTI cells were measured by relative mRNA expression of selected genes using single, dual, and multiple miR vectors compared to the miR control (CTRL), data shown as mean \pm s.e.m (n=2). (d) KD levels in Thy1.1⁺-sorted OT3 cells were measured by relative mRNA expression of selected genes using single, dual, and multiple miR vectors compared to the miR control (CTRL), data presented as mean \pm SD (n=2).

3.3.5. Evaluation of *in vitro* and *in vivo* T-cell antitumor activity upon multiple perturbations targeting the TCR negative regulators in high and low-affinity CD8+ cells:

Subsequent to the successful induction of KD for the targeted molecules, namely HPK1, Cbl-b, and NEDD4, our investigation progressed toward the *in vivo* assessment of the antitumor impact upon their downregulation in T-cells.

This evaluation encompassed single perturbations, dual and multiple KD combinations, with a focus on survival and tumor control. To initiate this investigation, we first examined the antitumor effect within the context of high-affinity TCR using OTI cells for ACT in the B16 OVA tumor model. C57BL/6 female mice (n=5 mice/group) were subcutaneously injected with 0.1M tumor cells. On day 11 post-inoculation, when tumors became around 100mm³, mice were subject to lymphodepletion with 5Gy total body irradiation (TBI) prior to performing an ACT using 5x10⁶ of engineered OTI cells (TE and KD levels shown in Figure 19) administered in two sequential injections on day 12 and day 14, then we monitored tumor growth over time and evaluated survival. (**Figure 20a**).

The *in vivo* evaluation was performed on multiple occasions, with a minimum of two repetitions. The results revealed that individual downregulation involving the KD of HPK1, Cbl-b, and NEDD4 did not substantially improve in OTI cell-mediated tumor control compared to the control group (ns; One-way ANOVA analysis). In contrast, dual KD targeting HPK1 and Cbl-b significantly enhanced tumor control compared to the CTRL (P=0,019; One-Way ANOVA analysis), while unexpectedly, concomitant downregulation of HPK1, Cbl-b, and NEDD4 did not (**Figure 20b**). Despite the observed distinct effects on tumor growth, the survival outcomes were comparable across the tested conditions, as no significant difference in survival was detected between single and multiple gene perturbations compared to the CTRL (**Figure 20c**).

In summary, these results indicate that individual downregulation of HPK1, Cbl-b, and NEDD4 could not significantly delay tumor growth. However, the combined effects of dual HPK1 and Cbl-b KD resulted in a substantial significant enhancement of tumor growth delay, although it did not improve overall survival compared to the control group.

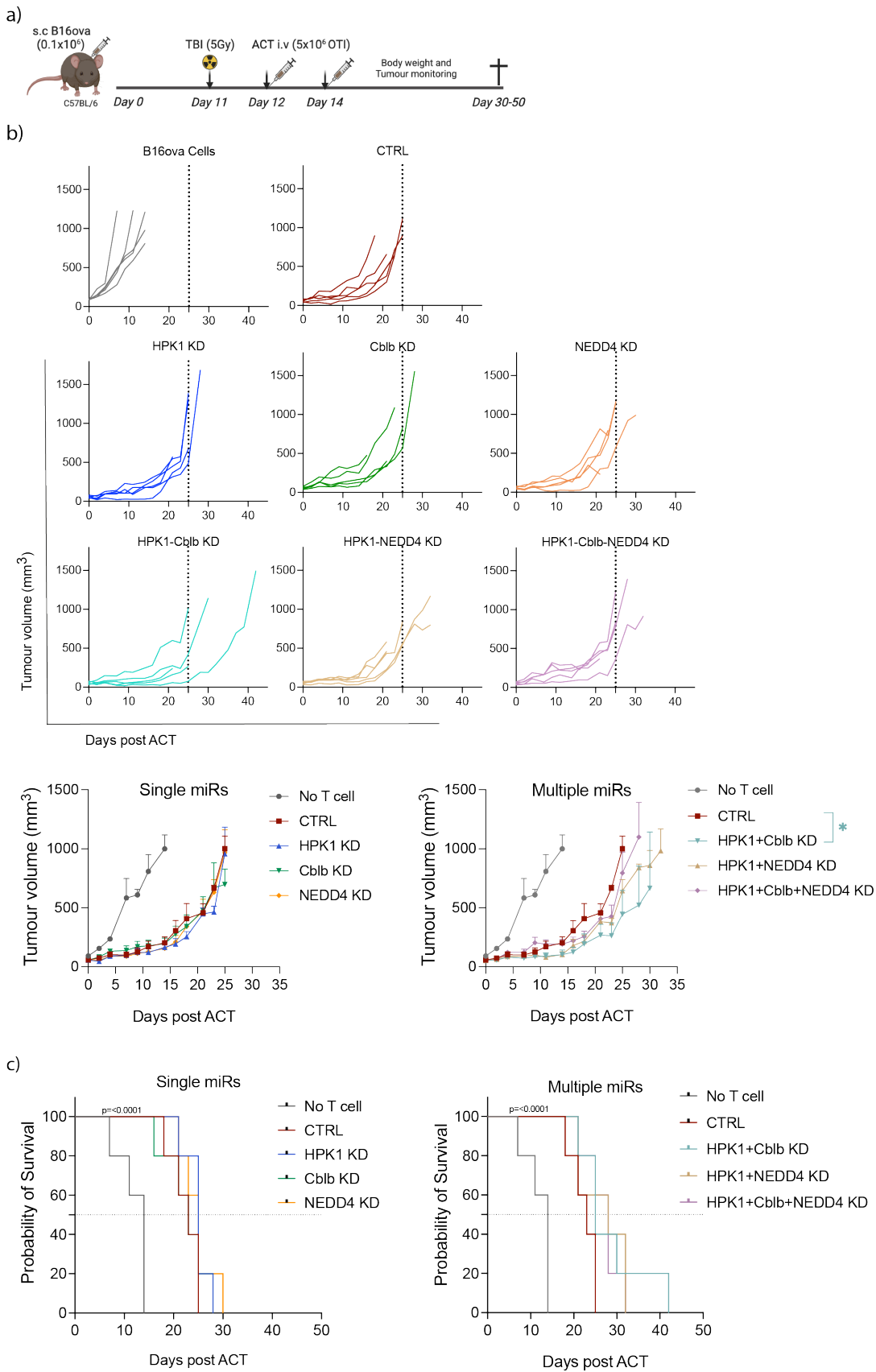


Figure 20: *In vivo* study in the B16 OVA tumor model to evaluate the antitumor activity of OTI cells downregulating HPK1, Cbl-b, and NEDD4 as single and combinatorial perturbations.

(a) Schematic *in vivo* study design using the B16 OVA tumor model and OTI cells for ACT. (b) Tumor volume in mm² measured by caliper over time; top: Individual tumor growth curves of different groups; bottom left: Tumor growth curves of single HPK1, Cbl-b,

and NEDD4 KD over time compared to CTRL OTI cells and no T-cells as control, data presented as mean \pm s.e.m. for n = 5 mice/group. Statistical significance was determined by mixed-effect analysis post-hoc Tukey's multiple comparisons where no statistical significance was detected among groups; bottom right: Tumor growth curves of combined HPK1-Cbl-b KD, HPK1-NEDD4 KD, and HPK1-Cbl-b-NEDD4 KD over time compared to CTRL OTI cells and no T-cells as control, data presented as mean \pm s.e.m. for n = 5 mice/group. Statistical significance was determined by mixed-effect analysis post-hoc Tukey's multiple comparisons where *P=0,019; (c) left: Probability of survival of single HPK1, Cbl-b, and NEDD4 KD compared to CTRL OTI cells and no T-cells as control, presented using Kaplan Meier analysis of mice survival up to the endpoint, post ACT of n=5 mice /group; right: Probability of survival of combined HPK1-Cbl-b KD, HPK1-NEDD4 KD and HPK1-Cbl-b-NEDD4 KD compared to CTRL OTI cells and no T-cells as control, presented using Kaplan Meier analysis of mice survival up to the endpoint, post ACT of n=5 mice /group, no statistical significance was detected between groups using single or multiple gene KD approach.

Next, we proceeded *in vitro* to assess the impact of HPK1-Cbl-b KD on OTI, then in OT3, cell activity. Using B16 OVA tumor cells, we assessed their cytokine expression, proliferation capacity, and cytotoxicity against target cells. As a negative control, B16 cancer cells were included in the experiment, maintaining a ratio of E:T at 1:1. In the initial dataset, cytokine expression and cellular proliferation, measured via Kiel University's experiment number 67 (ki67) expression in HPK1 KD and HPK1-Cbl-b KD OTI cells were compared to a CTRL OTI cell. The relative mRNA expression levels of IFN γ , TNF α , ki67, and GzmB over time were quantified using RT-qPCR.

Interestingly, albeit not reaching standard statistical significance, both HPK1-Cbl-b KD and HPK1 KD displayed higher IFN γ cytokine expression in addition to greater proliferative ability demonstrated by higher levels of ki67 expression than the CTRL OTI cells. However, regarding Gzmb and TNF α expression, all conditions demonstrated similar levels to the CTRL OTI cells (**Figure 21a**).

To address the second segment of our study, the *in vitro* cytotoxicity of OTI cells engineered with either single (only for HPK1), dual, or multiple miR vectors was evaluated by quantifying the incorporation of a nucleic acid dye that correlates with the number of dead tumor cells using IncuCyte assay. This evaluation was conducted at least twice to ensure reliability. OTI cells were either stimulated or not with B16 OVA cells at an E:T ratio of 1:1. The results indicated that the single, dual, and multiple combinatorial KD approaches did not improve the *in vitro* tumor killing compared to the control condition (CTRL) (**Figure 21b**).

Taken together, downregulating HPK1 and HPK1 along with Cbl-b leads to increased IFN γ expression in OTI cells, while the combination of HPK1 KD with Cbl-b and NEDD4 KD as dual or multiple TCR downstream perturbations did not significantly enhance TNF α or GzmB expression compared to the CTRL cells. Moreover, none of the single, dual, or multiple KD strategies resulted in improved *in vitro* cytotoxicity against tumor cells.

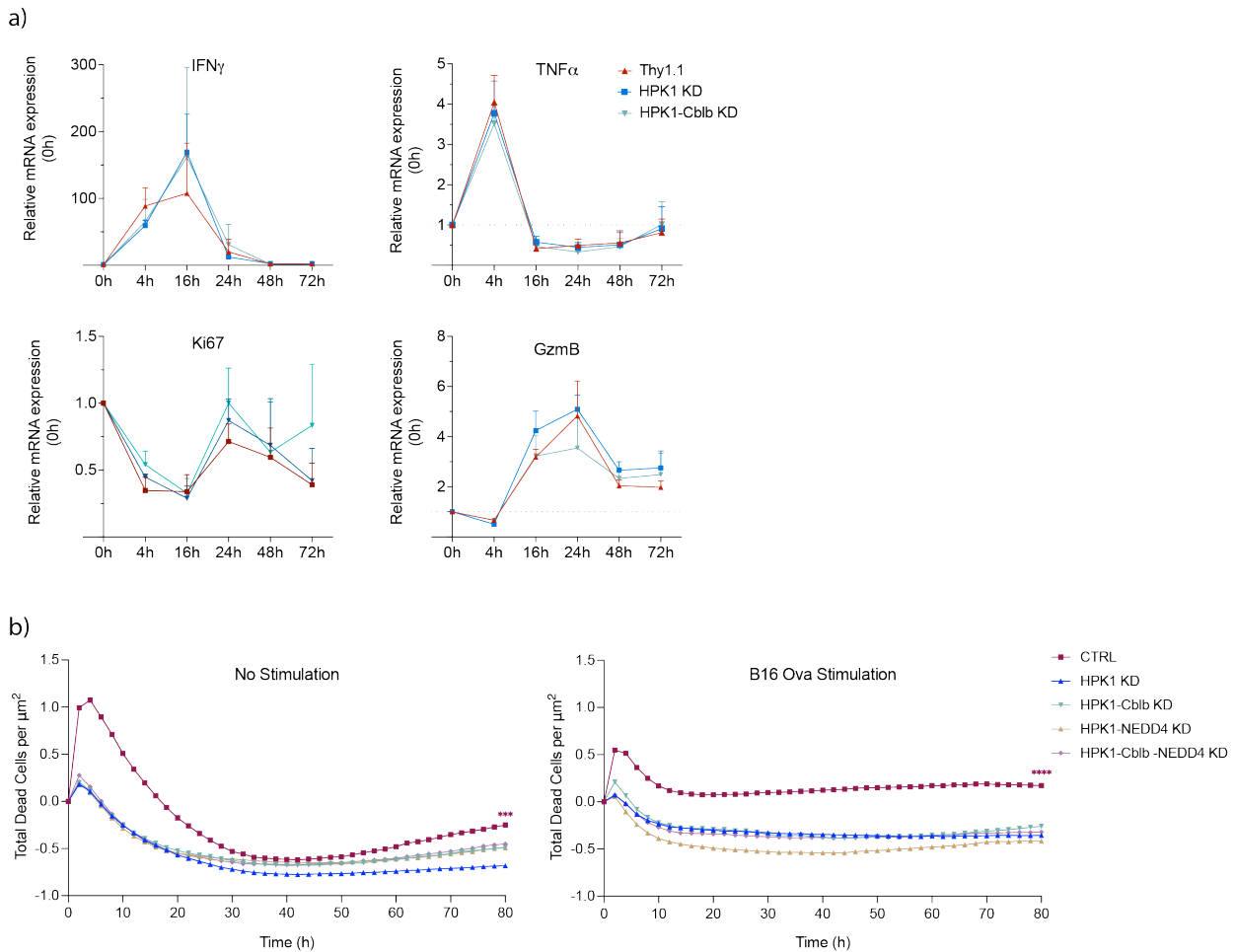


Figure 21: *In vitro* evaluation of cellular cytokine expression and cytotoxicity upon downregulating HPK1 as single or in combination with Cbl-b KD and/or NEDD4 KD in OT1 cells.

(a) Relative mRNA expression of IFN γ , TNF α , ki67, and GzmB measured over time by RT-qPCR; data presented as mean \pm s.e.m for $n=3$. Statistical analysis was done using Two-Way ANOVA and post-hoc Tukey's analysis (no statistical difference was detected); (b) *In vitro* cytotoxicity assessed by nucleic acid dye incorporation in OT1 bearing single HPK1 KD and in combinations with Cbl-b and/or NEDD4 data presented as mean for $n=2$. Statistical analysis using One-Way ANOVA and post-hoc Tukey's analysis where *** $P=0,0008$ and **** $P<0,0001$.

Next, we turned our attention toward investigating the *in vivo* outcomes of downregulating HPK1, along with Cbl-b and/or NEDD4 in low-affinity CD8 $^+$ T cells using the OT3 model. This investigation was endorsed by the hypothesis that our induced TCR downstream perturbations might yield more significant benefits for low-affinity TCR T-cells to enhance their tumor infiltration into the tumor bed and antitumor activity by relieving the inhibitory effects imposed by these suppressor genes. Following the identical *in vivo* study design employed in the OT1 model, engineered OT3 *in vivo* antitumor activity was assessed. For this, 5 female C57BL/6 mice were subcutaneously injected with 0.1×10^6 tumor cells. Once the tumors became palpable on day 11 post-inoculation, the mice underwent lymphodepletion with 5Gy TBI before initiating an ACT using 5×10^6 engineered OT3 cells administered on day 12 and then on day 14 in a raw. Subsequently, tumor growth was monitored over time, and survival was evaluated post-ACT (**Figure 22a**).

Notably, the downregulation of HPK1 as single gene perturbations or combined with combination with Cbl-b KD and/or NEDD4 did not significantly improve OT3-mediated tumor control relative to CTRL cells (**Figure 22b**). Furthermore, this downregulation strategy did not lead to enhanced survival rates when compared to the control OT3 cells since the survival outcomes were comparable across the different conditions (**Figure 22c**).

Furthermore, the *in vitro* cytotoxicity of OT3 cells engineered with single HPK1, dual, or multiple miR vectors was assessed to determine their ability to induce tumor cell death. This evaluation was conducted by quantifying the incorporation of a nucleic acid dye, which is proportional to the number of dead tumor cells using the InCuCyte assay. For this purpose, OT3 cells were either stimulated or not stimulated with B16OVA cells, maintaining an effector-to-target (E:T) ratio of 1:1. In line with the outcomes observed in the *in vivo* experiments, the findings demonstrated that the single, dual, and multiple combinatorial KD approaches did not yield an improvement in the *in vitro* tumor killing as compared to the control condition (CTRL) (Data not shown).

These results indicate that the downregulation strategies employed, whether individually or in combination, did not enhance the cytotoxicity of OT3 cells against tumor cells in both the *in vitro* and *in vivo* settings.

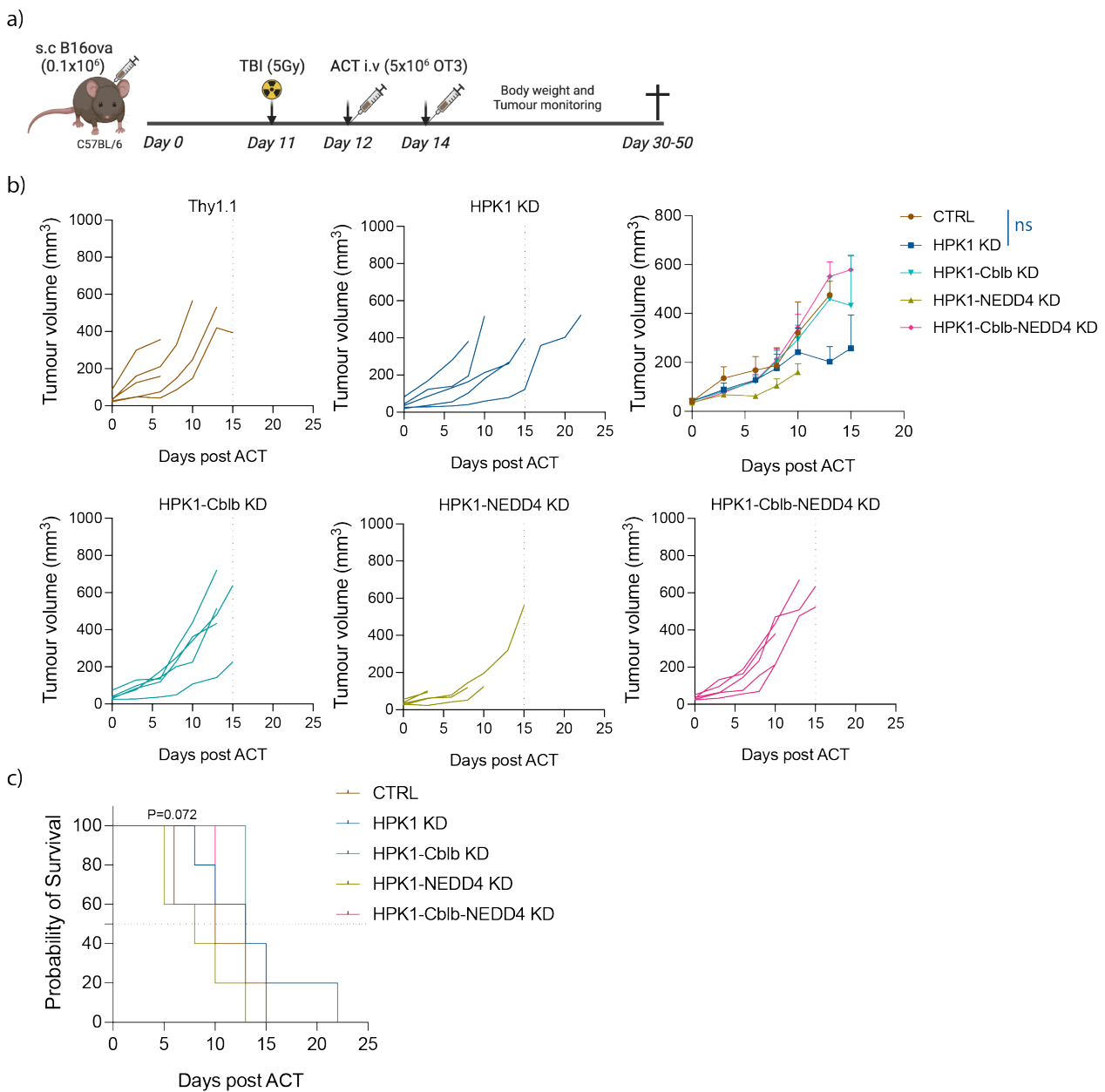


Figure 22: *In vivo* evaluation of OT3 cell antitumor activity bearing single and combined HPK1, Cbl-b, and NEDD4 downregulation.

(a) Schematic *in vivo* study design using the B16 OVA tumor model and OT3 cells for ACT. (b) Tumor volume in mm² measured by caliper over time; top left and bottom: individual tumor growth curves of different groups; top right: Tumor growth curves of single

HPK1 and combined HPK1-Cbl-b KD, HPK1-NEDD4 KD, and HPK1-Cbl-b-NEDD4 KD over time compared to CTRL OT3 cells as control, data presented as mean \pm s.e.m. for n= 5 mice/group. One-way ANOVA and post-hoc Tukey analysis revealed no statistical significance between groups (ns); (c) Probability of survival of single HPK1 and combined HPK1-Cbl-b KD, HPK1-NEDD4 KD, and HPK1-Cbl-b-NEDD4 KD compared to CTRL OTI cells, data presented using Kaplan Meier analysis of mice survival up to the endpoint, post ACT of n=5 mice /group. No statistical significance was detected among the groups.

In order to gain a comprehensive understanding of the dissimilar antitumor responses observed in OTI and OT3 cells, as well as the underlying mechanisms contributing to the limited enhancement of *in vivo* and *in vitro* antitumor capacity in OT3 cells when employing HPK1-Cbl-b KD or other combinatorial KD approaches, we conducted a thorough investigation. Our investigation aimed to assess the baseline functionality and explore potential disparities in the antitumor responses between high-affinity and low-affinity TCR in CD8⁺ cells. Additionally, we examined the kinetics of upregulation for each targeted molecule. To achieve this, we performed measurements of cytokine and activation markers' expression in these cells during coculture with target cells, precisely when TCR engagement occurred. Furthermore, we compared the expression patterns of these markers over time upon antigen engagement and TCR stimulation in the context of both high-affinity CD8⁺ cells (OTI cells) and low-affinity CD8⁺ cells (OT3 cells).

Upon TCR stimulation with B16 OVA cells at a ratio of E:T=1:1 or via chronic stimulation by SIINFEKL OVA peptide at 10ng/ml for 3 days *in vivo*. In basal levels, we observed that OTI cells exhibited significantly enhanced proliferation compared to OT3 cells (**Figure 24a**). Furthermore, OTI cells demonstrated markedly improved cytotoxicity compared to OT3 cells, as determined by the IncuCyte assay, where engineered miR CTRL T-cells (CTRL) were cocultured with B16 OVA tumor cells alongside non-stimulated cells as the control at a ratio of E:T=2:1 in which dead cells were quantified by the total red area of added nucleic dye incorporation over time (**Figure 24b**).

Additionally, these findings align with the observed high *in vivo* antitumor capacity of OTI cells compared to OT3 cells engineered to express the miR CTRL in the B16 tumor model. Notably, significant tumor control was demonstrated by OTI CTRL cells (P=0.049 at day 13 post ACT) compared to OT3 CTRL cells, which was accompanied by improved survival, although the difference did not reach statistical significance (**Figure 24c**).

Subsequent to the previous findings, OTI and OT3 cells were subjected to coculture with B16 OVA cells or B16 cells as a control, with an E:T ratio of 1:1 and was maintained over a period of time, including time points at 0h, 4h, 16h, 24h, 48h, and 72 h. The expression levels of target genes, namely HPK1, Cbl-b, and NEDD4, along with the expression levels of cytokines IFN γ , TNF α , and activation markers PD-1 and CD69, were measured by RT-qPCR. For analysis purposes, the baseline expression at 0h was used, and relative mRNA expression values were calculated (n=2). The experiment was repeated on multiple occasions to ensure its reliability.

Remarkable upregulation of HPK1, Cbl-b, and NEDD4 TCR suppressor genes was observed over time in the OTI cells upon TCR engagement with the antigen OVA presented on B16 OVA tumor cells. This upregulation correlated with an increase in CD69 and PD-1 activation markers and GzmB expression; additionally, gene expression levels of IFN γ and TNF α were also more prominent in OTI cells. Interestingly, these patterns were not observed in OT3 cells as they showed decreased expression below thresholds at all time points (**Figure 24d**), suggesting that differences in HPK1, Cbl-b, and NEDD4 gene expression levels in high vs. low-affinity TCRs may contribute to the inability to downregulate these molecules in low-affinity TCR (OT3) cells. Thus, the incapacity to enhance the antitumor function of OT3 cells.

Likewise, upon evaluating HPK1, Cbl-b and NEDD4 expression levels by flow cytometric analysis upon SIINFEKL OVA peptide stimulation at 10ug/ml along with increasing concentrations of aCD3/aCD28

dynabeads in each of the following conditions: NP, SP and RP of *in vitro* exhaustion assay (described in Figure 7b) (at least in two independent experiments), the results affirmed that those suppressor molecules were highly upregulated in high-affinity TCR (OTI) cells compared to low-affinity TCR (OT3) cells (**Supplementary Figure 3a**). To ensure the reliability of the results, these assessments were repeated on a minimum of two occasions.

These data collectively support the notion that low-affinity TCR (OT3) cells possess lower expression levels of HPK1, Cbl-b, and NEDD4 upon antigen engagement, along with reduced proliferative capacity and lower tumor-killing ability compared to OTI cells, explaining their reduced *in vivo* antitumor functionality, albeit they were engineered to suppress negative TCR regulators.

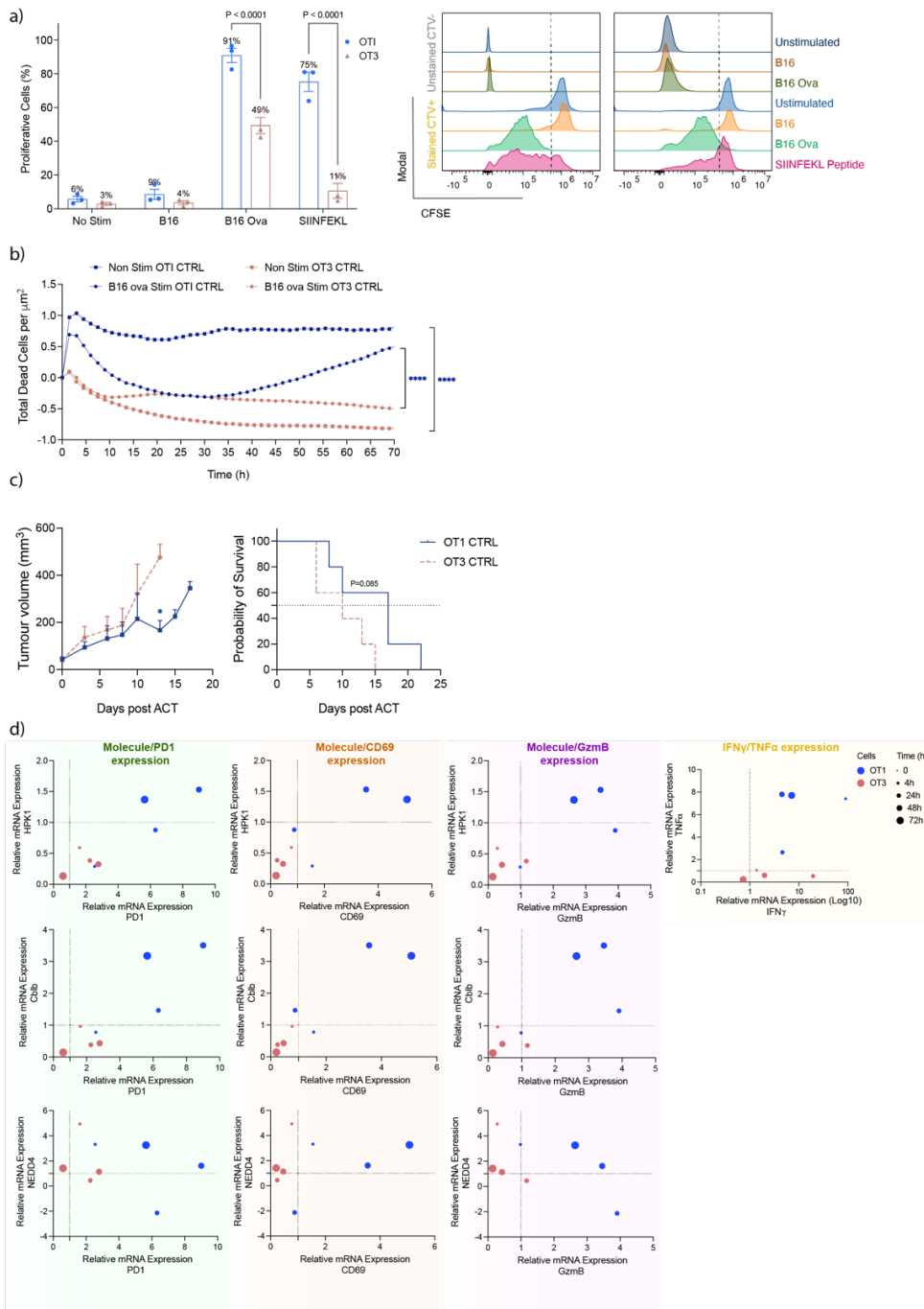


Figure 23: Functional characterization and evaluation of TCR signaling suppressive molecules in OT1 and OT3 cells in the context of the B16 OVA tumor model.

(a) CFSE-based proliferation assessment; left: bar graph of CTV stained unstimulated and B16-, B16 OVA and SIINFEKL peptide (10ng/ml for 3 days)-stimulated cells, data shown as mean \pm s.e.m. for $n=3$. Statistical significance was determined by Two-Way ANOVA analysis and post-hoc Tukey analysis; right: representative histogram of CFSE-stained OT1 and OT3 cells stimulated with SIINFEKL OVA peptide (10 ng/ μl for 3 days) and with B16 OVA coculture at ratio E:T=1:1 along with +/-CFSE unstimulated OTI and OT3 cells as control and baseline for gating. (b) Line graph indicating CTRL-OTI and -OT3 *in vitro* cytotoxicity against B16 OVA target cells upon coculture at E:T=2:1 along with non-stimulated CTRL-OTI and -OT3 cells as control presented as dead cells per μm^2 and as mean $n=2$. Statistical significance was determined by One-Way ANOVA analysis and post-hoc Tukey analysis, where $****P<0,0001$. (c) left: Tumor growth curve of OTI CTRL cells over time compared to OT3 CTRL cells, data presented as mean \pm s.e.m. for $n=5$ mice/group. Student *t* test analysis revealed statistical significance between the two groups at day 13 post ACT where $*P=0,049$; right: Probability of survival of OTI CTRL cells over time compared to OT3 CTRL cells, data presented using Kaplan Meier analysis of mice survival up to the endpoint, post ACT of $n=5$ mice /group. No statistical significance was detected among the groups, $P=0,085$. (d) Combined multiple variables graphs depicting relative mRNA expression of HPK1, Cbl-b, NEDD4, CD69, PD-1, TNF α and IFN γ in OT1 and OT3 cells over time upon coculture with B16 OVA cells at a ratio of E:T=1:1 (data shown are the mean of $n=2$ /plotted value).

3.3.6. Development of an unbiased high throughput screening approach for identifying inhibitory genes in the context of high versus low-affinity CD8⁺ cells.

Despite the promising results observed in high-affinity TCR (OTI) cells engineered to downregulate HPK1 and Cbl-b, which resulted in a tumor growth delay *in vivo*, the impact on survival enhancement remains modest. In an effort to further refine our approach, we sought to introduce an additional TCR downstream perturbation by targeting another TCR negative regulator. Our objective was not to be limited to the previously selected molecules but also to explore a broader range of potential targets. Thus, we turned to an unbiased and well-validated high-throughput method, namely the CRISPR screening, to identify potential targets for downregulation in combination with the HPK1-Cbl-b KD strategy. This involved the utilization of a small TCR library, generated in-house, comprising three to five sgRNAs per gene, aiming to evaluate the effect of each gene deletion on one aspect of T-cell function, notably T-cell persistence, within the context of this chapter.

The TCR small CRISPR library included TCR downstream molecules along with positive control genes that have been published and widely used in similar approaches as crucial genes for cell survival (essential genes) or genes well-known to inhibit T-cell function (suppressor genes) in which their deletion will make T-cells persist more in TME. Additionally, a negative control was included, consisting of non-targeting sgRNAs.

Initially, the TCR CRISPR library was generated by designing three sgRNAs targeting each listed gene using the CrisPick algorithm⁵⁷³ and cloning them in bulk into the pSUPER retroviral vector kindly provided by Prof. Ping Chi Ho (**Supplementary Figure 4a**). However, upon performing a quality control test involving DNA isolation from all bacterial clones and next-generation sequencing (NGS), it was observed that the sgRNAs were not equally distributed among the clones, as evidenced by the non-gaussian distribution of sgRNA in the pool library (**Supplementary Figure 4b**). As an alternative approach, we opted for manually and individually cloning three to five each sgRNA targeting each listed molecule (**Figure 25a**), including 27 TCR downstream molecules, 26 positive control genes, and 20 non-targeting sgRNAs as a total of 222 sgRNAs (the positive and negative control sgRNAs were cloned by Dr. Catherine Ronet and Aodrenn Spill).

Consequently, using individual sgRNA cloning into the retroviral vector, we could achieve a homogeneous distribution of sgRNAs (**Supplementary Figure 4c**). To establish the conditions for transducing the TCR small CRISPR library into OTI and OT3 cells, we first had to determine the proper MOI that would result in 15-30% TE to allow the integration of one sgRNA per one cell, measured by double positivity for Thy1.1-GFP (GFP is a reporter gene for Cas9 in OTI/OT3 CD4Cre Cas9 eGFP cells). Different MOIs were tested, and an MOI of 1 or 1.2 was chosen, resulting in TE of 15-20% (**Supplementary Figure 4d**). The TCR CRISPR library was initially tested *in vitro* using the *in vitro* exhaustion assay using the OTI model, with the NP condition being the input and the RP condition as the output (data not shown). The results were plotted as a volcano plot, highlighting the top five suppressor genes (with positive scores) for which OTI cells were enriched upon those gene KOs, as well as the top five essential genes with the lowest scores in which their deletion-induced cell death (**Supplementary Figure 4f**).

For selecting TCR negative regulator candidates in the *in vivo* context, we implemented the experimental setting presented in **Figure 25b**, in which C57BL/6 cas9⁺ eGFP mice (n= at least 5-7 mice/group with at least 2 groups) were initially injected subcutaneously with 0.1M B16 OVA tumor cells, followed by TBI at a dose of 5Gy on day 11. On day 12, an ACT was performed using either 5M OTI or OT3 Cas9⁺GFP⁺ cells that had been transduced with our small TCR CRISPR library (DP for Thy1.1 +Cas9⁺ GFP expression). At this point, a fraction of these cells was reserved for sorting based on the double positivity for Thy1.1 and GFP (Cas9), which would serve as our input sample. Subsequently, at 7 days post-ACT, we sorted the TILs that had integrated the library (DP for Thy1.1 and GFP (Cas9)), lymph nodes, and spleens as they will constitute our

output sample. Genomic DNA was then isolated from both the input and output samples and therefore sent for NSG sequencing. The generated sequencing data were analyzed using the MAGeCKFlute CRISPR screening Analysis⁵⁷¹. The results were then presented as a volcano plot, where the enriched fraction represents the cells that persisted within tumors, and for which deleted genes functioned as suppressive inhibitors within the TCR network. Conversely, the negative fraction of the volcano plot comprised genes deemed essential for T-cell function. *In vivo* experiments were conducted at least in two independent experiments with (n>=5/group/experiment) for OTI and OT3 cell models (data not shown for OT3 cells).

Besides positive controls, the volcano plot retrieved from the analyzed NGS data of OTI TILs revealed an absence of hits that can be potentially targeted via gene silencing to enhance TIL persistence (**Figure 25c**). This suggests that individually inhibiting TCR negative regulators does not improve the persistence of high-affinity CD8⁺ cells *in vivo*. However, there were some genes, namely Peli1, CISH, and Ubash3a, whose sgRNA were clearly enriched, although not significant, relative to the input. These genes hold potential for targeted inhibition strategies (**Figure 25d**) and present promising candidates for the combinatorial gene KD approach, supplementing the dual downregulation of HPK1 and Cbl-b.

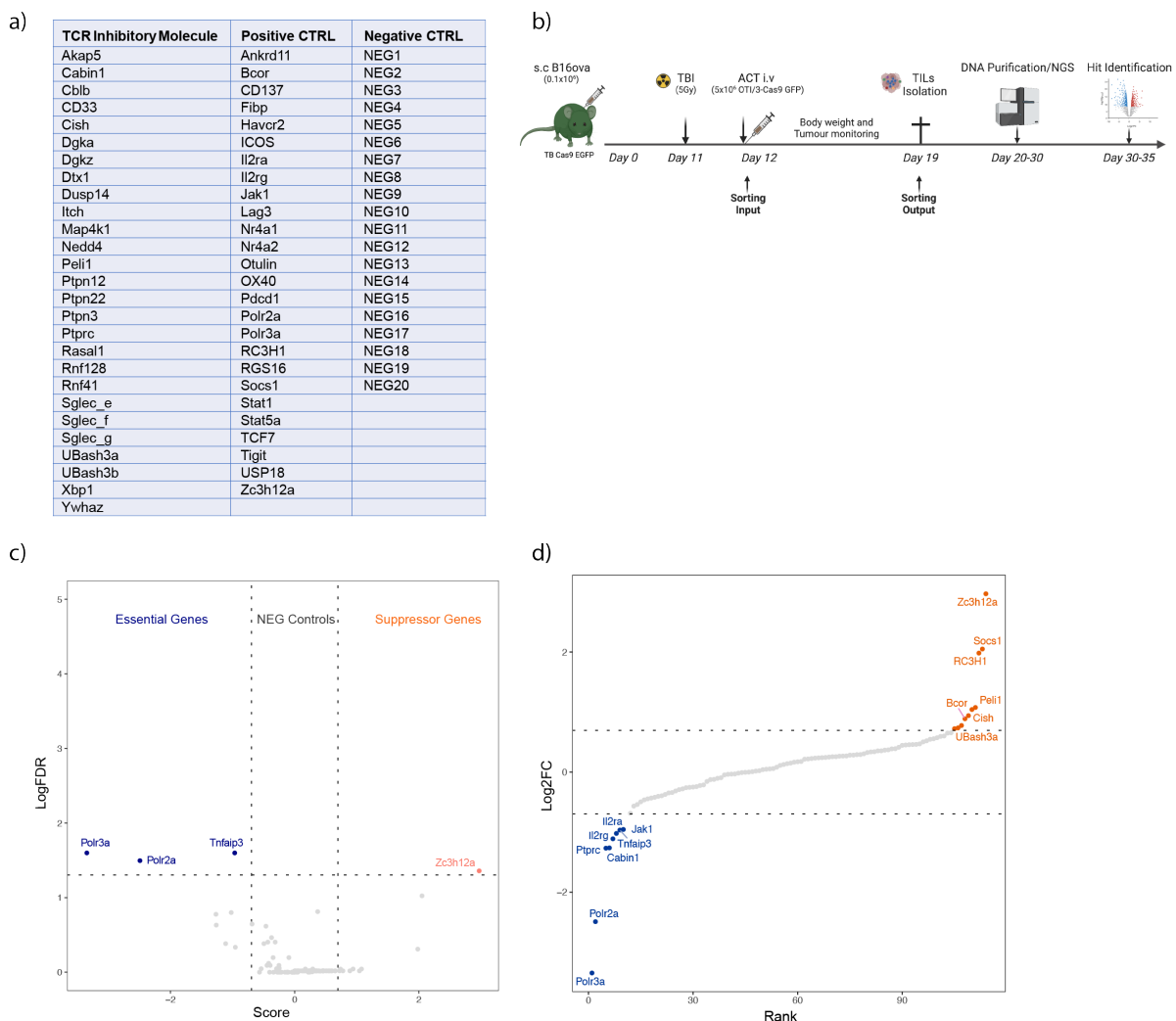
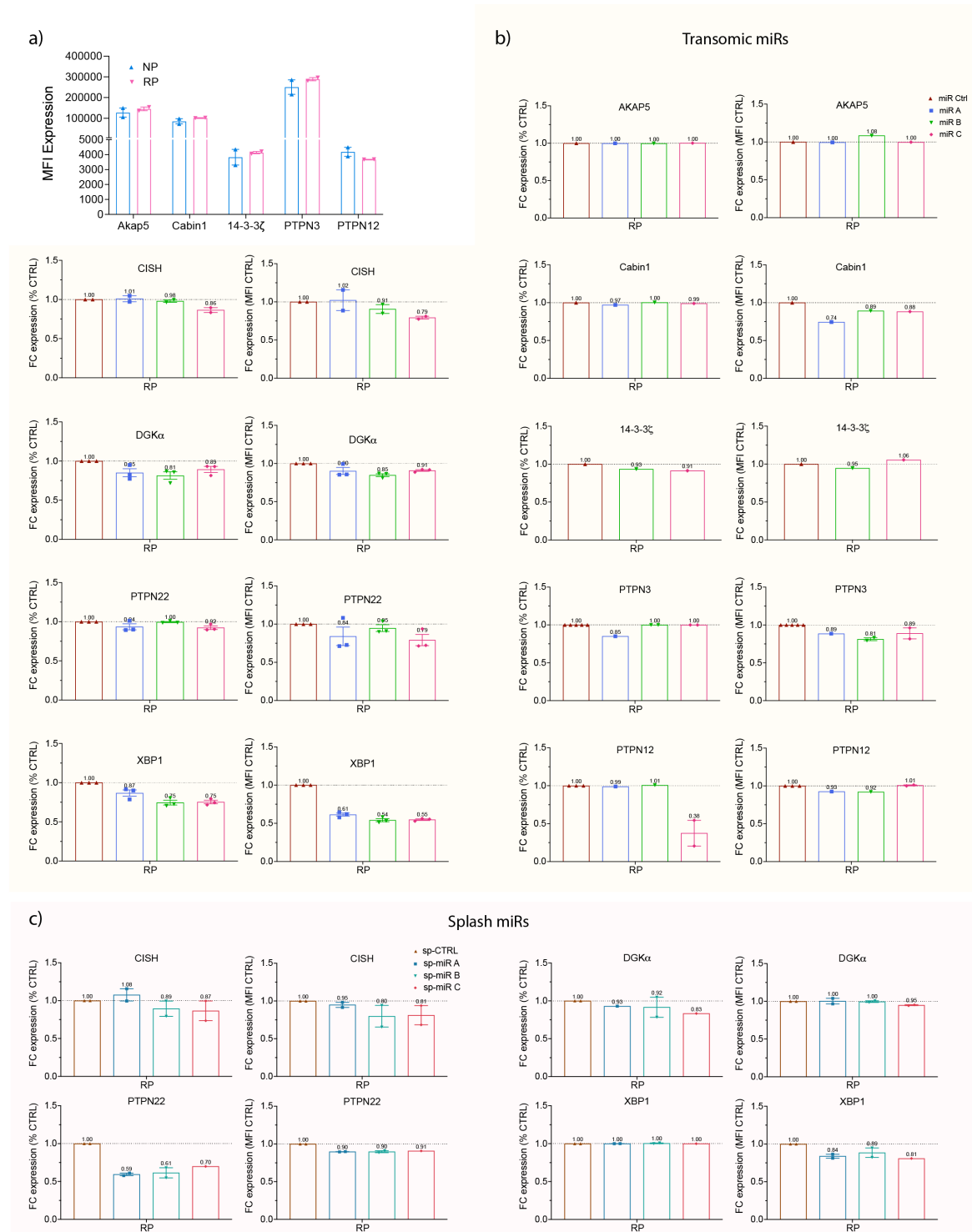


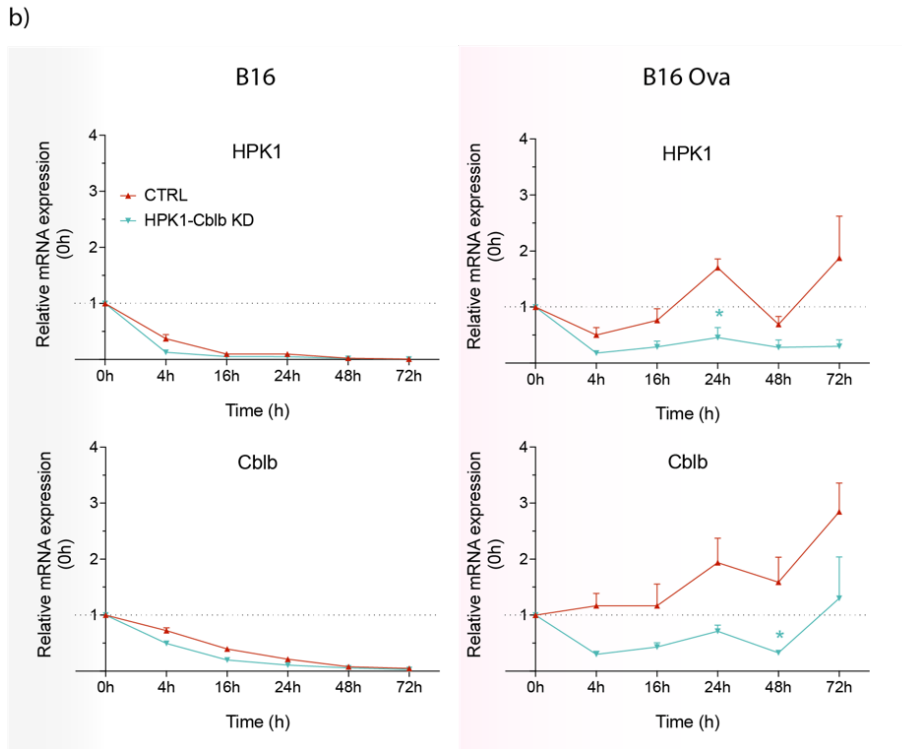
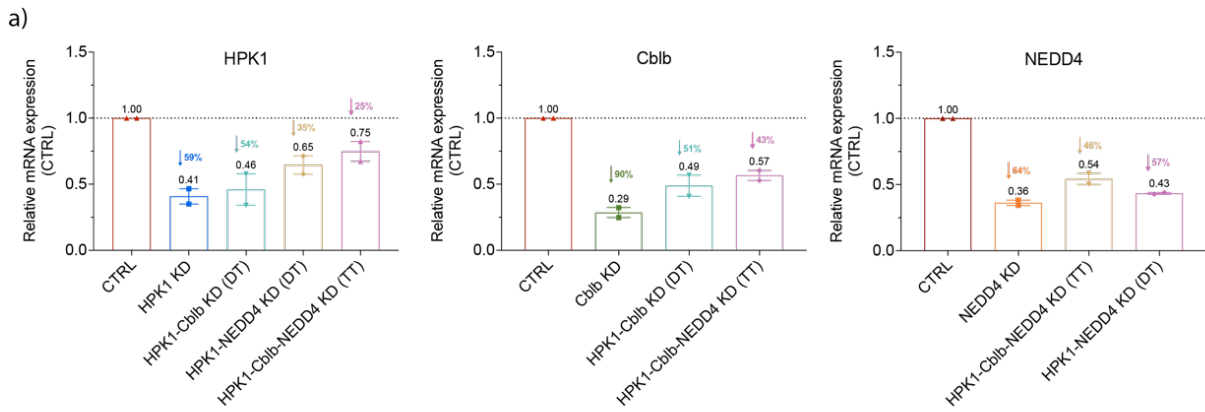
Figure 24: Identification of TCR suppressor and essential genes for *in vivo* T-cell persistence using small TCR CRISPR Library. (a) List of genes integrated into the TCR CRISPR library, including positive control and negative control molecules. (b) Schematic representation of the *in vivo* experimental design. (c) Volcano plot highlighting the top ten suppressors and essential genes identified in the OTI cell model according to the statistical significance threshold. Data was presented based on two independent *in vivo* experiments. (d) Rank plot based on the fold change of the output (TILs) vs. the input (injected OTI+Cas9+GFP+ cells) identified in the OTI cell model according to the statistical significance threshold. Data is presented based on two independent *in vivo* experiments.

3.4. Extended data:



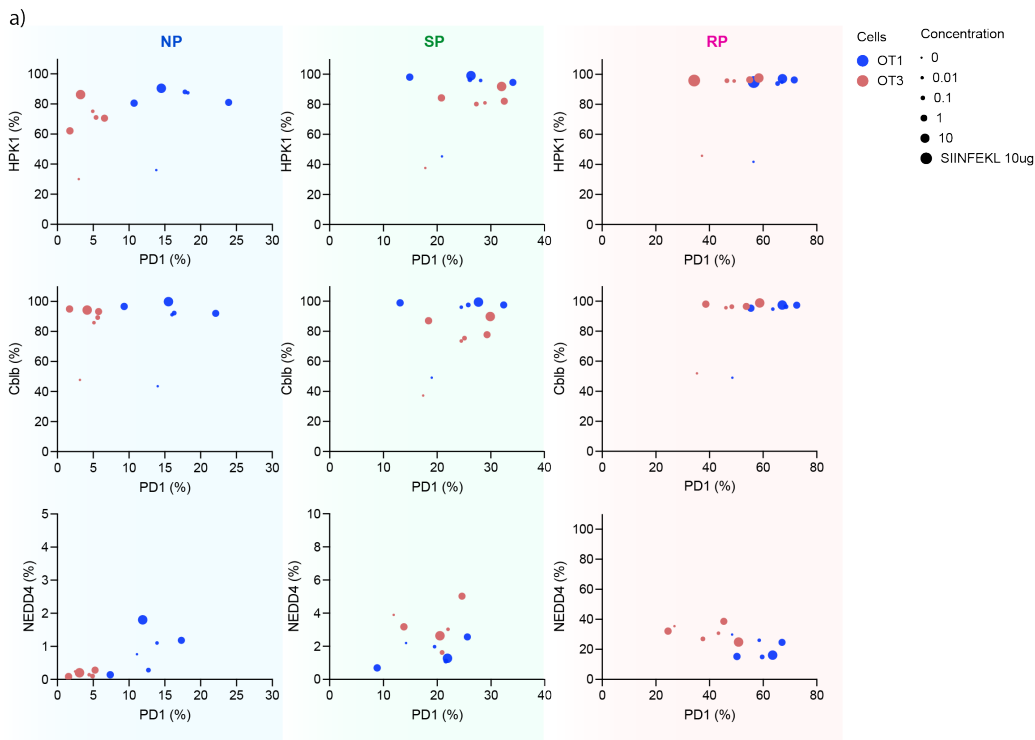
Supplementary Figure 1: Evaluation of selected TCR checkpoint inhibitors' expression levels and their downregulation by miRs.

(a) Bar graphs demonstrating the expression as mean fluorescence intensity (MFI) of AKAP5, Cabin1, 14-3-3z, PTPN3, and PTPN12 in RP compared to NP condition, data shown as mean \pm s.e.m. of $n=2$. (b) Bar graphs demonstrating the fold change of percentage (%) and mean fluorescence intensity (MFI) of expression of targeted intracellular checkpoint inhibitors upon downregulation using Transomic miRNAs: miR A, B, and C compared to miR CTRL (CTRL) for each targeted molecule. Data are presented as mean \pm s.e.m. ($n=2$ or 3 technical replicates). (c) Bar graphs demonstrating the fold change of percentage (%) and mean fluorescence intensity (MFI) of expression of targeted intracellular checkpoint inhibitors upon downregulation using splash miR (sp-miR) A, B, and C compared to sp-miR CTRL (CTRL) for each targeted molecule. Data are presented as mean \pm s.e.m. (n =single or technical replicates).



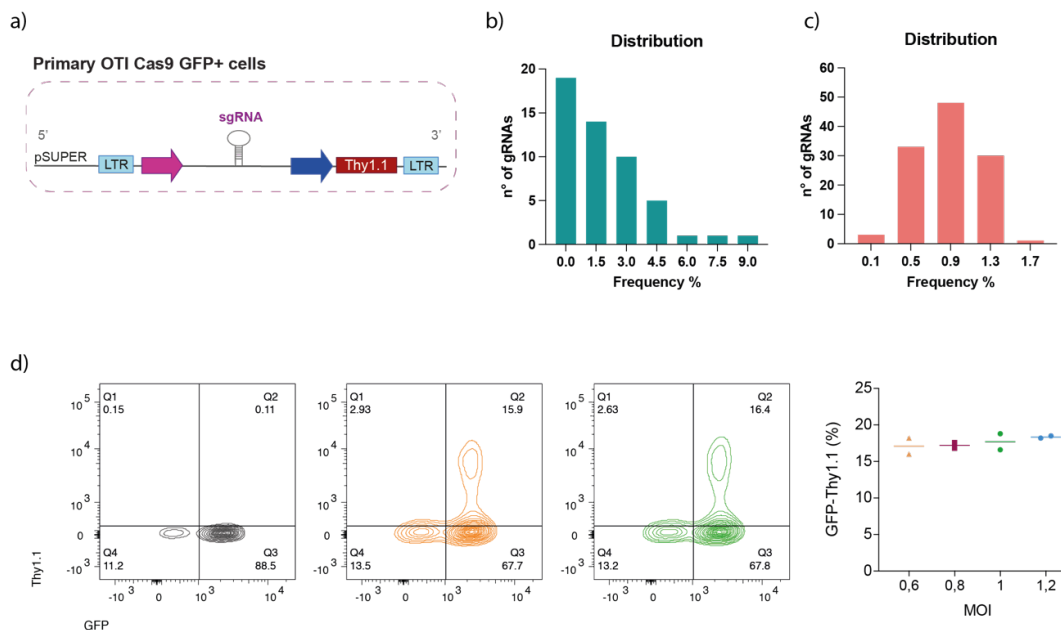
Supplementary Figure 2: Assessment of HPK1, Cbl-b, and NEDD4 knockdown levels in OTI cells

(a) KD levels of HPK1, Cbl-b, and NEDD4 measured by relative mRNA expression of selected genes compared to CTRL using single miR vectors for transducing OTI cells either as single, double, or triple cell transduction (DT or TT). Total MOI=5 was deployed across all conditions, data shown as mean \pm s.e.m (n=2). (b) Kinetics of the HPK1 and Cbl-b KD level over time using dual miR targeting HPK1-Cbl-b upon B16 OVA stimulation along with B16 as a negative control at ratio E:T=1:1. Data are shown as mean \pm s.e.m (n=3) and statistical analysis was assessed Two-Way ANOVA and post-hoc Tukey's multiple comparisons.



Supplementary Figure 3: Flow cytometric analysis of HPK1, Cbl-b, and NEDD4 expression in OT1 cells stimulated with aCD8/aCD28 dynabeads and SIINFEKL peptide.

(a) Combined multiple variables graphs presenting the percentage of expression of HPK1, Cbl-b, and NEDD4 measured by flow cytometry in OT1 and OT3 cells upon culture with increasing concentrations of aCD3/aCD28 along with SIINFEKL peptide stimulation at 10 μ g/ml.



Supplementary Figure 4: Design, implementation, and *in vitro* evaluation of generated small TCR CRISPR Library using OT1 cells.

(a) Vector design of the pSUPER retroviral vector. (b) sgRNA Frequency distribution measured by counts gathered from NSG sequencing of isolated DNA from transformed bacteria clones as a pool. (c) sgRNA frequency distribution measured by counts gathered from NGS sequencing of transformed bacterial cloned individually so that each clone of bacteria contains one sgRNA before being pooled. (d) TE using different MOIs for OT1+Cas9 (GFP) cell transduction by TCR small library determined by DP population for Thy1.1 and GFP expression.

IV. General discussion and perspectives:

Gene therapy has emerged as a foundational tool in cancer immunotherapy, with particular emphasis on the genetic modification of T-cells to express either CARs or TCRs. These strategies have demonstrated considerable potential for the treatment of solid tumors. Nevertheless, there is still ample room for improvement in several key areas. Efforts are underway to enhance the ability of engineered T-cells to selectively recognize tumor cells while simultaneously bolstering their TCR activation, metabolic profile, overall fitness, and cytokine secretion capabilities to reprogram the TME. Moreover, various engineering approaches are being pursued to mitigate potential side effects associated with T-cell adoptive therapy, such as TCR T-cell cross-reactivities, cytokine release syndrome, and on-target/off-tumor toxicities. These approaches involve refining gene-engineering strategies, such as optimizing vector design and ensuring precise control over gene cargo expression. These advancements are crucial in meeting the growing demand for effective gene therapy strategies in clinical settings.

The primary objective of this dissertation study is to elucidate the regulatory mechanisms of TCR signaling and develop effective genetic modification techniques that can be applied in potential clinical settings for improved T-cell-based immunotherapy against tumors. To accomplish this objective, this research investigation focuses on identifying negative regulators of TCRs and implementing T-cell engineering techniques to downregulate their activity, thereby enhancing the antitumor function of T-cells. In parallel, the underlying mechanisms responsible for the improved T-cell function are also explored.

In this regard, careful selection of the appropriate method was undertaken to attenuate the activity of suppressor TCR genes, notably to choose between a complete KO or a KD of TCR suppressor genes. In our specific context, we opted for gene downregulation by utilizing a synthetic miRNA. This method was preferred due to its stability, endogenous processing within cells, and ability to promote constitutive and inducible expression using a Pol II or Pol III.

1. Optimizing lentiviral vector design for dual gene insertion and inducible gene knockdown in engineered T-cells for enhanced antitumor activity.

The primary aim was to exploit the potential of gene downregulation in the context of an inducible expression for precise gene regulation, specifically when desiring that the outcome of gene downregulation occurs solely upon T-cell engagement with the antigen or subsequent stimulation within the TME. This approach was favored to prevent potential cytotoxicity associated with constitutive or overexpression of miRNA expression, which could disrupt other genes' regulatory processes or lead to cytotoxic effects due to a constant lack of gene-negative regulators. Moreover, we harbored uncertainty regarding the hyper- or continuous activation of T-cells resulting from suppressing the TCR negative feedback. Such activation might lead to early exhaustion states and potentially compromise their functionality.

Subsequently, we endeavored to enhance the antitumor activity of primary human CAR/TCR T-cells by incorporating an inducible gene KD strategy. However, the successful implementation of this strategy necessitated addressing certain challenges associated with designing a vector construct encompassing both a constitutively expressed CAR or TCR for targeted tumor eradication, and an inducible expression of the miRNA. In our pursuit to address these issues, we encountered the need to meticulously design a construct utilizing lentiviral vectors. Lentiviral vectors have gained prominence in gene therapy due to their safety profile, clinical translatability, and ability to efficiently deliver genes, thereby enhancing T-cell function. Several vector designs have been developed to enhance co-engineering strategies, taking into consideration the challenges associated with standard dual co-gene delivery employing independent promoters.

Notably, when using forward-oriented promoters, with the first constitutive and the second inducible, weak gene expression for the second gene can occur due to transcriptional interference. An alternative approach involves a bidirectional configuration, allowing inducible gene expression without compromising its responsiveness to stimulation. However, this approach is undermined by the potential leakiness of the constitutive promoter into the inducible one.

Nevertheless, these challenges necessitated the development of a novel dual antisense transfer vector and an optimized protocol for T-cell lentiviral transduction. Remarkably, the utilization of the dual antisense configuration resulted in the formation of dsRNA during virus production in the packaging cells (293 T-cells) due to the simultaneous transcription occurring from both the LTR promoter and the NFAT promoter in the transfected cells. dsRNA triggers the intracellular anti-dsRNA response involving DICER and RISK complex, which may lead to low titer virus production. To mitigate this issue, we employed the RNAi suppressor protein NovB2, previously demonstrated to inhibit Dicer isoforms, thereby preventing the undesirable effects of dsRNA formation.

Furthermore, we introduced modifications to the transfer vector by replacing the RSV-based promoter and enhancer at the 5' LTR with the complete CMV promoter and enhancer. This strategy was undertaken to facilitate the transcription of the entire gene insert by utilizing TNF α , which promotes the expression of the CMV promoter containing four NF- κ B binding motifs. Consequently, the effect of TNF α in increasing viral titers was significant and was further improved when combined with the NovB2 approach.

In summary, a lentiviral vector design has been developed to facilitate the insertion of two specific genes. One of these genes encodes an inducible or constitutive miRNA that promotes gene KD, while the other gene induces the expression of a constitutive CAR or TCR in primary human CD4⁺ and CD8⁺ T cells, allowing targeted tumor antigen recognition. Moreover, an optimized protocol for high-titer viral particle production suitable for clinical application has been established to enable efficient genetic modification of these cells.

2. Enhancing primary human T-cell function and antitumor response through HPK1 downregulation

In continuation of our previous findings, we sought to validate the feasibility of our approach by investigating the functionality of CAR/TCR T-cells downregulating a TCR negative regulator using the vector we developed. This provided a valuable opportunity to assess the vector's capability in effectively accommodating what is commonly referred to as "hard to express gene cargo," exemplified by the miRNA construct used in our study. HPK1 was the initial target we have identified for gene silencing. It is noteworthy that extensive studies have underscored the role of HPK1 in T-cells by examining HPK1-deficient mice³⁶⁰ and HPK1 kinase-dead mice^{359,365}. These investigations have revealed enhanced proliferation in response to TCR stimulation compared to wild-type mice, suggesting the potential of HPK1 inhibition in cancer treatment. Various classes of pharmacological small-molecule inhibitors targeting HPK1 have been identified.

Moreover, in a separate study, CRISPR Cas9 technology was employed to KO HPK1, improving CAR-T-cell-based immunotherapies' efficacy in diverse preclinical mouse models of hematological and solid tumors³⁵⁴. Therefore, we successfully implemented our developed dual antisense lentiviral vector design to clone the Pz1 CAR, which recognizes the PSMA prostate cancer antigen. This CAR construct was placed under the constitutive expression of the PGK promoter, while the inverted miRNA targeting HPK1 was positioned under the inducible NFAT promoter.

Among the three miRNAs (initially inserted in a commercial plasmid) targeting HPK1, we selected the miRNA with the highest KD efficiency (miRNA B) in Jurkat cells to be cloned into our lentiviral vector. Notably, the lentiviral vector bearing miRNA B exhibited high transduction efficiency and achieved a downregulation

exceeding 90% in CD4⁺ and CD8⁺ T-cells. Importantly, HPK1 KD did not compromise cell viability, revealing no detrimental impact on the internal cellular system of T cells. Consequently, we could proceed with characterizing the impact of HPK1 KD on T-cell function. Notably, our findings showed that HPK1 KD specifically enhanced the proliferation of CD8⁺ T-cells and augmented the expression of IFN γ under the influence of intermediate concentrations of immunosuppressive inhibitors typically present in the TME, such as PGE2 and the adenosine agonist CADO. However, T-cell cytotoxicity remained unaffected by HPK1 KD with or without the use of inhibitors.

In our subsequent examinations, we shifted our focus to a different tumor-specific targeting model by employing the NYESO-1 TCR. We used a sense configuration lentiviral vector to clone the NYESO-1 TCR and NGFR reporter gene, expressed under the constitutive PGK promoter. To achieve different levels of KD strength, we introduced two miRNAs (miRNA A and B) targeting HPK1, comparing their outcomes to the control miRNA (miRNA CTRL) expressed under the constitutive U6 promoter. This exploration allowed us to fully understand the impact of HPK1 downregulation in T-cells.

To ensure optimal vector design, the 3' flank of the miRNA included a polyadenylation site to effectively terminate miRNA transcription to avoid transcriptional interference. However, to overcome the potential viral titer decrease associated with using the double-stranded hairpin secondary structure of the miRNA, we incorporated TNF α to boost the transcription of our gene insert. This modification aimed to enhance viral titer and ensure efficient gene transfer.

Using this vector design, we could achieve high transduction efficiency in both transduced Jurkat cells and primary human NYESO-1 CD4⁺/CD8⁺ T-cells. However, for an efficient HPK1 KD, the inclusion of a leader sequence was imperative to ensure proper miRNA (miR) biogenesis and processing (data not shown). Indeed, placing the leader sequence immediately after the U6 promoter enabled us to achieve substantial HPK1 KD levels, ranging from 80% to over 90%, using miR A in CD4⁺ and CD8⁺ T-cells. On the other hand, the downregulation was moderate when utilizing miR B, with KD levels ranging between 45% and 60%. This discovery was unexpected, considering that miR B showed the highest KD level in Jurkat cells using the commercially available vector, compared to the miR CTRL and other tested miRs. Interestingly, in the case of primary Pz1-CAR CD4⁺ and CD8⁺ T-cells, miR B exhibited higher KD levels compared to miR CTRL. This suggests that the downregulation mechanism may be influenced by the vector or the cell type, indicating that the cellular context plays a significant role in determining the level of KD.

Encouragingly, downregulating HPK1 did not impact the memory and effector phenotypes of CD4⁺ and CD8⁺ T-cells. This is noteworthy because, while a memory-like phenotype is desirable for ACT due to its advantages, we expected the loss of TCR inhibition to result in an effector-like phenotype or terminally differentiated T-cells after long-term *in vitro* expansion prior to ACT. Functionally, CD8⁺ T-cells with HPK1 KD exhibited increased proliferation capacity compared to control cells, similar to what was observed in the context of Pz1-CAR T-cells. In contrast, within our experimental setup, we did not observe significant differences in IFN γ secretion levels upon stimulation with A2+/NY+ target cells (Me275, A375, and Saos2). Nevertheless, in *in vivo* experiments, the highest level of HPK1 KD achieved using miR A significantly improved tumor control, leading to significant tumor growth delay and improved survival outcomes.

3. Combinatorial strategies targeting TCR negative regulators for enhanced functionality in high-affinity TCR T-cells

Following the validation of our vector design and the promising results obtained through HPK1 KD in both Pz1-CAR and NYESO-1 TCR T-cells, we aimed to further enhance T-cell functionality and gain a deeper understanding of the complex interplay between T-cells and the TME. However, we encountered limitations

in conducting comprehensive characterization using a xenograft mouse model. Consequently, we transitioned to a syngeneic mouse model, which not only facilitated the investigation of T-cell interaction with TME but also allowed us to explore the impact of downregulating negative regulators in a more physiologically relevant setting. Initially, we identified twelve relevant molecular targets based on existing literature that demonstrated improved T-cell function upon their complete deletion or downregulation. Subsequently, we assessed the expression levels of these target molecules upon antigen stimulation, aiming to mimic the conditions that occur *in vivo* within the TME. All evaluated TCR-negative regulators exhibited elevated expression levels upon chronic antigen stimulation and during cellular exhaustion. However, upon repeated antigen stimulation, certain targets, namely AKAP5, cabin1, 14-3-3 ζ , PTPN3, and PTPN12, did not show increased expression. Instead, their expression remained similar to the basal level observed in unstimulated cells.

Next, we carefully selected the miRNAs that resulted in the highest KD levels (based on the percentage and the MFI of expression) compared to the miRNA CTRL for each of the chosen targets, namely those targeting HPK1, Cbl-b, and NEDD4. These miRNAs were cloned in a retroviral vector available in the lab. It is noteworthy that both Cbl-b and NEDD4 are part of the E3 ligases family. They play crucial roles within the ubiquitination pathway responsible for the degradation of key components downstream of the TCR signaling network.

As we observed only moderate antitumor effects when using single perturbations downstream of the TCR, we decided to combine them as dual and triple combinatorial KD. The chosen miRNAs were then cloned in dual and multiple miRNA vectors we have developed, with HPK1 as the primary target, alongside Cbl-b and/or NEDD4. The design of these vectors took into consideration several aspects linked to the concomitant miRNA delivery, such as the spacing between the miRNA, the positioning, and the length of the miRNA sequences. Significant transduction efficiency and high KD levels were observed in high (OTI) and low-affinity (OT3) TCR cells using dual and multiple miRNA vectors. Interestingly, the KD levels achieved in OTI cells using the dual and multiple miRNA vectors surpassed those achieved through double or triple transduction by single miRNA vectors. This highlights the efficacy of the miRNA vectors generated in our study for inducing efficient multiple gene silencing.

Consequently, the dual KD of HPK1 and Cbl-b in OTI cells demonstrated a significant improvement in tumor control; however, it did not result in enhanced survival outcomes. Conversely, in the low-affinity TCR model represented by OT3 cells, neither the individual nor the combinatorial KD of TCR suppressive molecules led to improved tumor control or survival. Upon investigating the reasons behind these observations in OT3 cells, we found that HPK1, Cbl-b, and NEDD4 were highly upregulated in OTI cells but not in OT3 cells upon antigen encounter and TCR stimulation with B16 OVA target cells over time, and with the SIINFEKL OVA peptide. Furthermore, our investigations confirmed previous findings that OT3 cells exhibit lower proliferation rates and reduced cytotoxic capacities *in vitro* and *in vivo* compared to high-affinity TCR (OTI) cells. These observations underscore the intrinsic limitations of low-affinity TCR cells in terms of their basal antitumor activity.

Collectively, these findings support the notion that downregulating TCR suppressor genes is particularly relevant in the context of high-affinity TCR cells, which aligns with previous studies demonstrating various advantages of using high-affinity TCR over low-affinity TCR T-cells. This is mainly due to their increased tumor infiltration, capacity to effectively eradicate tumors, and ability to sense lower peptide epitope densities, in addition to their lower expression of inhibitory molecules, including PD-1, LAG-3, and NKG2A^{574,575}. Moreover, high TCR affinities enhance CD8⁺ T-cell effector function and have the potential to redirect CD4⁺ T-cells to the tumor^{576,577}. In contrast, TCRs with nanomolar range affinities may impair T-cell function, leading to activation-induced cell death, early exhaustion, or undesired cross-reactivity with self-antigens

^{261,578}. On the other hand, controversial studies have demonstrated that high-affinity TCR T-cells may be more susceptible to exhaustion and negative regulatory mechanisms upon chronic stimulation that limit their long-term functionality ⁵⁷⁹ and have also indicated that *in vivo* selection processes naturally maintain low TCR affinities to avoid diminished function and self-peptide cross-reactivity ^{574,580,581}.

Given the limited outcomes observed thus far regarding the positive effect of the concomitant deletion of HPK1 and Cbl-b on the *in vitro* function in high-affinity TCR T-cells, further research is warranted to characterize the impact of these deletions in OTI cells *in vitro*. Additionally, investigations into the behavior of these engineered T-cells within the TME are essential to elucidate the reasons underlying the significant tumor control achieved by this specific combination. It is crucial to understand how these engineered T-cells interact with immunosuppressive components and inhibitors in the TME, such as PGE2, adenosine, and various suppressive immune cells, such as Tregs and myeloid cells. Moreover, comprehensive *ex vivo* characterization studies are necessary to assess the outcomes of these deletions on other critical pathways, including apoptosis and metabolic features. A thorough understanding of these mechanisms will provide valuable insights into the functionality and behavior of engineered T-cells in complex immunosuppressive environments, ultimately informing the development of more effective therapeutic strategies.

Finally, in order to expand the scope of our approach, we employed a small TCR CRISPR library as a high-throughput and unbiased method to systematically screen more than 27 TCR suppressor molecules. Through this analysis, we were able to confirm that individual deletions of these molecules alone cannot enhance high-affinity TCR T-cell persistence. Consequently, it became evident that implementing combinatorial strategies is necessary to achieve the desired improvements in T-cell function. Of note, when employing the same TCR library for CRISPR screening using low-affinity TCR cells in at least two separate experiments, we encountered technical challenges due to the limited number of OT3 TILs retrieved from B16 tumors, which could have compromised the quality of the analysis. However, the data indicates that OT3 cells are not retained in the tumor bed, rendering efforts to enhance low-affinity TCR signaling futile if the cells fail to infiltrate the TME and get stimulated by the antigen. This hypothesis could be potentially verified by co-transferring OTI and OT3 cells in an ACT with a specific ratio, allowing the evaluation of their respective *in vivo* persistence and the significance of suppressing TCR intracellular checkpoints.

Several studies have investigated similar questions by targeting different TCR suppressor genes. For instance, individual loss of Cbl-b has been shown to enhance T-cell function and increase *in vivo* antitumoral activity upon T-cell stimulation ^{480,481}. In contrast, a study led by Ventura, PMO. et al., (2022) demonstrated *in vivo* that sustained or acute deletion of PTPN6 along with PTPN11 deletion does not improve T-cell-mediated tumor control. Furthermore, sustained loss of PTPN6/11 impairs the therapeutic effects of anti-PD1 treatment⁵⁸². In this study, *in vitro* findings revealed that Ptpn6/11-deleted CD8+ T-cells exhibit impaired expansion due to a survival defect, and proteomics analyses also highlighted significant alterations, including changes in apoptosis-related pathways⁵⁸². These observations emphasize the need for caution when choosing negative regulators for gene inhibition strategies, specifically when considering clinical applications.

Intriguingly, the question of combinatorial deletion or loss of TCR negative regulators remains relatively unexplored. This may be attributed to the challenges faced when combining multiple miRNAs or shRNAs for knocking down multiple genes or concerns regarding off-target effects when using the CRISPR/Cas9 system for gene deletion. However, there is apprehension regarding the risk of inducing T-cell exhaustion due to overactivation or the potential for cytotoxicity or autoimmune responses resulting from the loss of negative regulatory loops in TCR signaling, particularly in high-affinity TCR cells. This recalls the need for introducing suicide genes into the vector construct, such as the epidermal growth factor receptor (EGFR), for inducing modified T-cell death to encounter cellular cytotoxicity if it occurs.

As a perspective of our study, we plan to explore the combination of HPK1-Cbl-b KD with the deletion or complete loss of other TCR suppressive molecules, such as Peli1, CISH, and Ubash3a using the syngeneic mouse model. We also aim to incorporate cytokines or molecules known to enhance T-cell persistence *in vivo*, such as IL2v or CD40L, or 41BBL which have been developed and utilized in our laboratory. Furthermore, we plan to extend the scope of our study beyond the TCR intracellular pathway and include target molecules from various regulatory pathways, such as anergy, cAMP, apoptosis, and others. This comprehensive approach addresses the regulatory mechanisms governing T-cell function, fitness, and *in vivo* persistence.

In the xenograft mouse model, we aim to evaluate the efficacy of the HPK1-Cbl-b KD setting using CAR/TCR T-cells. We plan to further enhance our combinatorial KD approach by deploying inhibitory checkpoint blockade, considering the upregulation inhibitory checkpoints, such as PD-1, TIM-3, and TIGIT, upon TCR engagement with melanoma (Me275 and A375) and sarcoma (Saos2) target cells.

Looking ahead to our future research directions, we propose developing the CRISPR screening approach to explore individual TCR perturbations based on other aspects of T-cell function, such as proliferation, cytokine expression, and metabolic fitness. Specifically, we anticipate that focusing on proliferation outcomes in our CRISPR screening approach will yield interesting data and reveal potential targets. This prediction is based on evidence from our investigations with HPK1 KD on primary human and murine T cells, which showed an increase in their proliferative capacity. Notably, HPK1 KD significantly improves primary human CD8⁺ proliferation *in vitro* in both the Pz1-CAR and NYESO-1 TCR models.

In summary, we have successfully demonstrated the efficacy of our novel antisense configuration lentiviral vector and high titer lentiviral production protocol in overcoming the limitations observed with previous vector designs and enhancing cell transduction efficiency even when using complex miRNA structures. This vector contains two gene cargos; an inducible miRNA targeting HPK1 and the Pz1 CAR or NYESO-1 TCR constitutively expressed, allowing for specific T-cell redirection to target cancer cells. This was shown to boost CD8⁺ T cell proliferation, *in vivo* antitumor control, and survival in the context of human tumor models. Additionally, we also explored the effectiveness of a combinatorial gene KD strategy in the syngeneic mouse model by inhibiting other TCR negative regulators using a multi-miRNA retroviral vector we developed. This retroviral vector enabled constitutive expression of multiple miRNAs targeting different intracellular checkpoints downstream of high and low-affinity TCR signaling networks, further enhancing the therapeutic potential of engineered T-cells. In particular, simultaneous downregulation of HPK1 and Cbl-b led to a significant delay in tumor growth of high-affinity TCR T cells. We also suggest various future strategies to improve T cell antitumor activity. Lastly, we highlighted the relevance of using our combinatorial KD strategy in the context of high-affinity TCR over the low-affinity TCR T-cells. Furthermore, we used a CRISPR screening with a small TCR library to establish that individual deletions of TCR intracellular checkpoints do not sufficiently improve T cell persistence, hence, necessitating the combinatorial gene KD approach.

Overall, this dissertation contributes significantly to cancer immunotherapy by providing new approaches for suppressing intracellular T-cell checkpoints for adoptive cell therapy and paving the way for future research exploration and development.

V. References:

1. Murphy K, Weaver C. *Janeway's immunobiology*. Garland science; 2016.
2. Janeway C. *Immunobiology 5 : the immune system in health and disease*. 5th ed. Garland Pub.; 2001:xviii, 732 p.
3. Alberts B. *Molecular biology of the cell*. 4th ed. Garland Science; 2002:xxxiv, 1463, 86 p.
4. Kolter J, Henneke P, Groß O, et al. Paradoxical immunodeficiencies—When failures of innate immunity cause immunopathology. *European Journal of Immunology*. 2022;52(9):1419-1430.
5. Shi F-D, Ljunggren H-G, Sarvetnick N. Innate immunity and autoimmunity: from self-protection to self-destruction. *Trends in immunology*. 2001;22(2):97-101.
6. Pickup JC. Inflammation and Activated Innate Immunity in the Pathogenesis of Type 2 Diabetes. *Diabetes Care*. 2004;27(3):813-823. doi:10.2337/diacare.27.3.813
7. Jana M, Palencia CA, Pahan K. Fibrillar amyloid-beta peptides activate microglia via TLR2: implications for Alzheimer's disease. *J Immunol*. Nov 15 2008;181(10):7254-62. doi:10.4049/jimmunol.181.10.7254
8. Shaw AC, Goldstein DR, Montgomery RR. Age-dependent dysregulation of innate immunity. *Nature Reviews Immunology*. 2013/12/01 2013;13(12):875-887. doi:10.1038/nri3547
9. Marshall JS, Warrington R, Watson W, Kim HL. An introduction to immunology and immunopathology. *Allergy, Asthma & Clinical Immunology*. 2018/09/12 2018;14(2):49. doi:10.1186/s13223-018-0278-1
10. Fu YL, Harrison RE. Microbial Phagocytic Receptors and Their Potential Involvement in Cytokine Induction in Macrophages. *Front Immunol*. 2021;12:662063. doi:10.3389/fimmu.2021.662063
11. Kawai T, Akira S. The role of pattern-recognition receptors in innate immunity: update on Toll-like receptors. *Nat Immunol*. May 2010;11(5):373-84. doi:10.1038/ni.1863
12. Decout A, Katz JD, Venkatraman S, Ablasser A. The cGAS–STING pathway as a therapeutic target in inflammatory diseases. *Nature Reviews Immunology*. 2021/09/01 2021;21(9):548-569. doi:10.1038/s41577-021-00524-z
13. Chen Q, Sun L, Chen ZJ. Regulation and function of the cGAS–STING pathway of cytosolic DNA sensing. *Nature Immunology*. 2016/10/01 2016;17(10):1142-1149. doi:10.1038/ni.3558
14. Harding CV, Geuze HJ. Class II MHC molecules are present in macrophage lysosomes and phagolysosomes that function in the phagocytic processing of *Listeria monocytogenes* for presentation to T cells. *Journal of Cell Biology*. 1992;119(3):531-542. doi:10.1083/jcb.119.3.531
15. Wynn TA, Chawla A, Pollard JW. Macrophage biology in development, homeostasis and disease. *Nature*. 2013/04/01 2013;496(7446):445-455. doi:10.1038/nature12034
16. Dress RJ, Dutertre C-A, Giladi A, et al. Plasmacytoid dendritic cells develop from Ly6D+ lymphoid progenitors distinct from the myeloid lineage. *Nature Immunology*. 2019/07/01 2019;20(7):852-864. doi:10.1038/s41590-019-0420-3
17. Worbs T, Hammerschmidt SI, Förster R. Dendritic cell migration in health and disease. *Nature Reviews Immunology*. 2017/01/01 2017;17(1):30-48. doi:10.1038/nri.2016.116
18. Hoebeke I, De Smedt M, Stolz F, et al. T-, B- and NK-lymphoid, but not myeloid cells arise from human CD34+CD38–CD7+ common lymphoid progenitors expressing lymphoid-specific genes. *Leukemia*. 2007/02/01 2007;21(2):311-319. doi:10.1038/sj.leu.2404488
19. Lanier LL, Le AM, Civin CI, Loken MR, Phillips JH. The relationship of CD16 (Leu-11) and Leu-19 (NKH-1) antigen expression on human peripheral blood NK cells and cytotoxic T lymphocytes. *J Immunol*. Jun 15 1986;136(12):4480-6.
20. Campbell JJ, Qin S, Unutmaz D, et al. Unique subpopulations of CD56+ NK and NK-T peripheral blood lymphocytes identified by chemokine receptor expression repertoire. *The Journal of Immunology*. 2001;166(11):6477-6482.
21. Cooper MA, Fehniger TA, Turner SC, et al. Human natural killer cells: a unique innate immunoregulatory role for the CD56bright subset. *Blood, The Journal of the American Society of Hematology*. 2001;97(10):3146-3151.
22. De Maria A, Bozzano F, Cantoni C, Moretta L. Revisiting human natural killer cell subset function revealed cytolytic CD56dimCD16+ NK cells as rapid producers of abundant IFN- γ on activation. *Proceedings of the National Academy of Sciences*. 2011;108(2):728-732.

23. Talmadge JE, Meyers KM, Prieur DJ, Starkey JR. Role of natural killer cells in tumor growth and metastasis: C57BL/6 normal and beige mice. *Journal of the National Cancer Institute*. 1980;65(5):929-935.
24. Schantz SP, Shillitoe EJ, Brown B, Campbell B. Natural killer cell activity and head and neck cancer: a clinical assessment. *Journal of the National Cancer Institute*. 1986;77(4):869-875.
25. Pross HF, Lotzova E. Role of natural killer cells in cancer. *Natural immunity*. 1993;12(4-5):279-292.
26. Morvan MG, Lanier LL. NK cells and cancer: you can teach innate cells new tricks. *Nature Reviews Cancer*. 2016/01/01 2016;16(1):7-19. doi:10.1038/nrc.2015.5
27. Vahlne G, Lindholm K, Meier A, et al. In vivo tumor cell rejection induced by NK cell inhibitory receptor blockade: Maintained tolerance to normal cells even in the presence of IL-2. *European journal of immunology*. 2010;40(3):813-823.
28. Chiossone L, Vienne M, Kerdiles YM, Vivier E. Natural killer cell immunotherapies against cancer: checkpoint inhibitors and more. *Seminars in Immunology*. 2017/06/01/ 2017;31:55-63. doi:<https://doi.org/10.1016/j.smim.2017.08.003>
29. Honda K, Littman DR. The microbiome in infectious disease and inflammation. *Annu Rev Immunol*. 2012;30:759-95. doi:10.1146/annurev-immunol-020711-074937
30. Peterson DA, McNulty NP, Guruge JL, Gordon JI. IgA response to symbiotic bacteria as a mediator of gut homeostasis. *Cell host & microbe*. 2007;2(5):328-339.
31. Colonna M. Interleukin-22-producing natural killer cells and lymphoid tissue inducer-like cells in mucosal immunity. *Immunity*. 2009;31(1):15-23.
32. Wang M, Wu H, Lu L, Jiang L, Yu Q. Lactobacillus reuteri Promotes Intestinal Development and Regulates Mucosal Immune Function in Newborn Piglets. *Front Vet Sci*. 2020;7:42. doi:10.3389/fvets.2020.00042
33. Flajnik MF, Du Pasquier L. Evolution of innate and adaptive immunity: can we draw a line? *Trends in Immunology*. 2004/12/01/ 2004;25(12):640-644. doi:<https://doi.org/10.1016/j.it.2004.10.001>
34. Katsnelson A. Kicking off adaptive immunity: the discovery of dendritic cells. *J Exp Med*. Jul 10 2006;203(7):1622. doi:10.1084/jem.2037fta
35. Flajnik MF, Kasahara M. Origin and evolution of the adaptive immune system: genetic events and selective pressures. *Nature Reviews Genetics*. 2010/01/01 2010;11(1):47-59. doi:10.1038/nrg2703
36. Ehrlich PR, Himmelweit F, Dale H. *The Collected Papers of Paul Ehrlich*. vol 3. Pergamon; 1960.
37. Silverstein AM. Autoimmunity versus horror autotoxicus: the struggle for recognition. *Nature immunology*. 2001;2(4):279-281.
38. Silverstein AM. *A history of immunology*. Academic Press; 2009.
39. Margo CE, Harman LE. Autoimmune disease: Conceptual history and contributions of ocular immunology. *Survey of Ophthalmology*. 2016/09/01/ 2016;61(5):680-688. doi:<https://doi.org/10.1016/j.survophthal.2016.04.006>
40. Farhud DD, Zarif Yeganeh M. A brief history of human blood groups. *Iran J Public Health*. 2013;42(1):1-6.
41. Mudd S. A hypothetical mechanism of antibody formation. *The Journal of Immunology*. 1932;23(6):423-427.
42. Owen RD. IMMUNOGENETIC CONSEQUENCES OF VASCULAR ANASTOMOSES BETWEEN BOVINE TWINS. *Science*. Oct 19 1945;102(2651):400-1. doi:10.1126/science.102.2651.400
43. Billingham RE, Brent L, Medawar PB. 'Actively acquired tolerance' of foreign cells. *Nature*. 1953;172:603-606.
44. Billingham RE, Brent L, Medawar PB. Quantitative studies on tissue transplantation immunity. III. Actively acquired tolerance. *Philosophical Transactions of the Royal Society of London Series B, Biological Sciences*. 1956:357-414.
45. Camara NOS, Lepique AP, Basso AS. Lymphocyte differentiation and effector functions. *Journal of Immunology Research*. 2012;2012
46. Morgan D, Tergaonkar V. Unraveling B cell trajectories at single cell resolution. *Trends in Immunology*. 2022/03/01/ 2022;43(3):210-229. doi:<https://doi.org/10.1016/j.it.2022.01.003>
47. Oettinger MA, Schatz DG, Gorka C, Baltimore D. RAG-1 and RAG-2, adjacent genes that synergistically activate V (D) J recombination. *Science*. 1990;248(4962):1517-1523.
48. Teillaud J-L. Antibody-dependent cellular cytotoxicity (ADCC). *eLS*. 2012;
49. Zent CS, Pinney JJ, Chu CC, Elliott MR. Complement Activation in the Treatment of B-Cell Malignancies. *Antibodies*. 2020;9(4):68.

50. Janjic BM, Kulkarni A, Ferris RL, Vujanovic L, Vujanovic NL. Human B Cells Mediate Innate Anti-Cancer Cytotoxicity Through Concurrent Engagement of Multiple TNF Superfamily Ligands. *Front Immunol.* 2022;13:837842. doi:10.3389/fimmu.2022.837842
51. Klein L, Kyewski B, Allen PM, Hogquist KA. Positive and negative selection of the T cell repertoire: what thymocytes see (and don't see). *Nature Reviews Immunology.* 2014/06/01 2014;14(6):377-391. doi:10.1038/nri3667
52. Armstrong Kathryn M, Piepenbrink Kurt H, Baker Brian M. Conformational changes and flexibility in T-cell receptor recognition of peptide–MHC complexes. *Biochemical Journal.* 2008;415(2):183-196. doi:10.1042/bj20080850
53. Gutiérrez-Vázquez C, Villarroya-Beltri C, Mittelbrunn M, Sánchez-Madrid F. Transfer of extracellular vesicles during immune cell-cell interactions. *Immunol Rev.* Jan 2013;251(1):125-42. doi:10.1111/imr.12013
54. Lopez JA, Susanto O, Jenkins MR, et al. Perforin forms transient pores on the target cell plasma membrane to facilitate rapid access of granzymes during killer cell attack. *Blood.* 2013;121(14):2659-2668. doi:10.1182/blood-2012-07-446146
55. Dong C. Cytokine Regulation and Function in T Cells. *Annu Rev Immunol.* Apr 26 2021;39:51-76. doi:10.1146/annurev-immunol-061020-053702
56. Ni L, Lu J. Interferon gamma in cancer immunotherapy. *Cancer medicine.* 2018;7(9):4509-4516.
57. Kursunel MA, Esendagli G. The untold story of IFN- γ in cancer biology. *Cytokine & Growth Factor Reviews.* 2016/10/01/ 2016;31:73-81. doi:<https://doi.org/10.1016/j.cytogfr.2016.07.005>
58. Clark R, Kupper T. Old Meets New: The Interaction Between Innate and Adaptive Immunity. *Journal of Investigative Dermatology.* 2005/10/01/ 2005;125(4):629-637. doi:<https://doi.org/10.1111/j.0022-202X.2005.23856.x>
59. World Health Organization. Cancer. WHO. Accessed 22 February 2023, <https://www.who.int/news-room/fact-sheets/detail/cancer>
60. Internatioal WCRF. Differences in cancer incidence and mortality across the globe. WCRF. Accessed 22 February 2023, <https://www.wcrf.org/differences-in-cancer-incidence-and-mortality-across-the-globe/>
61. Wishart DS. Is Cancer a Genetic Disease or a Metabolic Disease? *EBioMedicine.* 2015/06/01/ 2015;2(6):478-479. doi:<https://doi.org/10.1016/j.ebiom.2015.05.022>
62. Hanahan D, Weinberg RA. The Hallmarks of Cancer. *Cell.* 2000/01/07/ 2000;100(1):57-70. doi:[https://doi.org/10.1016/S0092-8674\(00\)81683-9](https://doi.org/10.1016/S0092-8674(00)81683-9)
63. Leong SP, Naxerova K, Keller L, Pantel K, Witte M. Molecular mechanisms of cancer metastasis via the lymphatic versus the blood vessels. *Clin Exp Metastasis.* Feb 2022;39(1):159-179. doi:10.1007/s10585-021-10120-z
64. Burrell RA, Swanton C. Tumour heterogeneity and the evolution of polyclonal drug resistance. *Molecular Oncology.* 2014/09/12/ 2014;8(6):1095-1111. doi:<https://doi.org/10.1016/j.molonc.2014.06.005>
65. Hanselmann RG, Welter C. Origin of Cancer: Cell work is the Key to Understanding Cancer Initiation and Progression. *Front Cell Dev Biol.* 2022;10:787995. doi:10.3389/fcell.2022.787995
66. Compton C, Compton C. *Cancer initiation, promotion, and progression and the acquisition of key behavioral traits.* Springer; 2020.
67. Feinberg AP, Ohlsson R, Henikoff S. The epigenetic progenitor origin of human cancer. *Nature Reviews Genetics.* 2006/01/01 2006;7(1):21-33. doi:10.1038/nrg1748
68. Feinberg AP, Tycko B. The history of cancer epigenetics. *Nature Reviews Cancer.* 2004;4(2):143-153.
69. de Visser KE, Joyce JA. The evolving tumor microenvironment: From cancer initiation to metastatic outgrowth. *Cancer Cell.* 2023/03/13/ 2023;41(3):374-403. doi:<https://doi.org/10.1016/j.ccell.2023.02.016>
70. Belli C, Trapani D, Viale G, et al. Targeting the microenvironment in solid tumors. *Cancer Treatment Reviews.* 2018/04/01/ 2018;65:22-32. doi:<https://doi.org/10.1016/j.ctrv.2018.02.004>
71. Khawar IA, Kim JH, Kuh H-J. Improving drug delivery to solid tumors: Priming the tumor microenvironment. *Journal of Controlled Release.* 2015/03/10/ 2015;201:78-89. doi:<https://doi.org/10.1016/j.jconrel.2014.12.018>
72. Ratti M, Lampis A, Ghidini M, et al. MicroRNAs (miRNAs) and Long Non-Coding RNAs (lncRNAs) as New Tools for Cancer Therapy: First Steps from Bench to Bedside. *Target Oncol.* Jun 2020;15(3):261-278. doi:10.1007/s11523-020-00717-x
73. Xue M, Zhuo Y, Shan B. MicroRNAs, Long Noncoding RNAs, and Their Functions in Human Disease. *Methods Mol Biol.* 2017;1617:1-25. doi:10.1007/978-1-4939-7046-9_1

74. Guo T, Li J, Zhang L, et al. Multidimensional communication of microRNAs and long non-coding RNAs in lung cancer. *J Cancer Res Clin Oncol*. Jan 2019;145(1):31-48. doi:10.1007/s00432-018-2767-5
75. Gopalakrishnan V, Helmink BA, Spencer CN, Reuben A, Wargo JA. The Influence of the Gut Microbiome on Cancer, Immunity, and Cancer Immunotherapy. *Cancer Cell*. Apr 9 2018;33(4):570-580. doi:10.1016/j.ccell.2018.03.015
76. Fessler J, Matson V, Gajewski TF. Exploring the emerging role of the microbiome in cancer immunotherapy. *J Immunother Cancer*. Apr 17 2019;7(1):108. doi:10.1186/s40425-019-0574-4
77. Baruch EN, Youngster I, Ben-Betzalel G, et al. Fecal microbiota transplant promotes response in immunotherapy-refractory melanoma patients. *Science*. Feb 5 2021;371(6529):602-609. doi:10.1126/science.abb5920
78. Hanahan D. Hallmarks of Cancer: New Dimensions. *Cancer Discovery*. 2022;12(1):31-46. doi:10.1158/2159-8290.Cd-21-1059
79. Brown JM, Giaccia AJ. The Unique Physiology of Solid Tumors: Opportunities (and Problems) for Cancer Therapy. *Cancer Research*. 1998;58(7):1408-1416.
80. Chizuka A, Suda M, Shibata T, et al. Difference between hematological malignancy and Solid tumor research articles published in four major medical journals. *Leukemia*. 2006/10/01 2006;20(10):1655-1657. doi:10.1038/sj.leu.2404369
81. Montironi C, Muñoz-Pinedo C, Eldering E. Hematopoietic versus Solid Cancers and T Cell Dysfunction: Looking for Similarities and Distinctions. *Cancers (Basel)*. Jan 14 2021;13(2)doi:10.3390/cancers13020284
82. Siegel RL, Miller KD, Wagle NS, Jemal A. Cancer statistics, 2023. *CA Cancer J Clin*. Jan 2023;73(1):17-48. doi:10.3322/caac.21763
83. Institute NC. Common Cancer Types. NCI. Accessed 15 March 2023, <https://www.cancer.gov/types/common-cancers>
84. Lugović-Mihić L, Česić D, Vuković P, Novak Bilić G, Šitum M, Špoljar S. Melanoma Development: Current Knowledge on Melanoma Pathogenesis. *Acta Dermatovenerol Croat*. Sep 2019;27(3):163-168.
85. Shain AH, Joseph NM, Yu R, et al. Genomic and Transcriptomic Analysis Reveals Incremental Disruption of Key Signaling Pathways during Melanoma Evolution. *Cancer Cell*. 2018/07/09/ 2018;34(1):45-55.e4. doi:<https://doi.org/10.1016/j.ccell.2018.06.005>
86. Teixido C, Castillo P, Martinez-Vila C, Arance A, Alos L. Molecular Markers and Targets in Melanoma. *Cells*. Sep 5 2021;10(9)doi:10.3390/cells10092320
87. Eddy K, Shah R, Chen S. Decoding melanoma development and progression: Identification of therapeutic vulnerabilities. *Frontiers in oncology*. 2021;10:626129.
88. Savoia P, Fava P, Casoni F, Cremona O. Targeting the ERK Signaling Pathway in Melanoma. *International Journal of Molecular Sciences*. 2019;20(6):1483.
89. Eddy K, Chen S. Overcoming Immune Evasion in Melanoma. *International Journal of Molecular Sciences*. 2020;21(23):8984.
90. Pires da Silva I, Ahmed T, McQuade JL, et al. Clinical Models to Define Response and Survival With Anti-PD-1 Antibodies Alone or Combined With Ipilimumab in Metastatic Melanoma. *J Clin Oncol*. Apr 1 2022;40(10):1068-1080. doi:10.1200/jco.21.01701
91. Mason R, Dearden HC, Nguyen B, et al. Combined ipilimumab and nivolumab first-line and after BRAF-targeted therapy in advanced melanoma. *Pigment Cell Melanoma Res*. Mar 2020;33(2):358-365. doi:10.1111/pcmr.12831
92. Indini A, Grossi F, Mandalà M, Taverna D, Audrito V. Metabolic Interplay between the Immune System and Melanoma Cells: Therapeutic Implications. *Biomedicines*. 2021;9(6):607.
93. Roesch A, Vultur A, Bogeski I, et al. Overcoming intrinsic multidrug resistance in melanoma by blocking the mitochondrial respiratory chain of slow-cycling JARID1B(high) cells. *Cancer Cell*. Jun 10 2013;23(6):811-25. doi:10.1016/j.ccr.2013.05.003
94. Polette M, Nawrocki-Raby B, Gilles C, Clavel C, Birembaut P. Tumour invasion and matrix metalloproteinases. *Crit Rev Oncol Hematol*. Mar 2004;49(3):179-86. doi:10.1016/j.critrevonc.2003.10.008
95. Marzagalli M, Ebelt ND, Manuel ER. Unraveling the crosstalk between melanoma and immune cells in the tumor microenvironment. *Seminars in Cancer Biology*. 2019/12/01/ 2019;59:236-250. doi:<https://doi.org/10.1016/j.semcancer.2019.08.002>
96. Mrázek J, Mekadim C, Kučerová P, et al. Melanoma-related changes in skin microbiome. *Folia Microbiologica*. 2019/05/01 2019;64(3):435-442. doi:10.1007/s12223-018-00670-3

97. Pal S, Perrien DS, Yumoto T, et al. The microbiome restrains melanoma bone growth by promoting intestinal NK and Th1 cell homing to bone. *The Journal of Clinical Investigation*. 2022;132(12)
98. Makaranka S, Scutt F, Frixou M, Wensley KE, Sharma R, Greenhowe J. The gut microbiome and melanoma: A review. *Experimental Dermatology*. 2022;31(9):1292-1301.
99. Mekadim C, Skalnikova HK, Cizkova J, et al. Dysbiosis of skin microbiome and gut microbiome in melanoma progression. *BMC Microbiology*. 2022/02/25 2022;22(1):63. doi:10.1186/s12866-022-02458-5
100. Guo W, Wang H, Li C. Signal pathways of melanoma and targeted therapy. *Signal Transduction and Targeted Therapy*. 2021/12/20 2021;6(1):424. doi:10.1038/s41392-021-00827-6
101. Rauwerdink DJW, van Doorn R, van der Hage J, et al. Systemic Therapy in Advanced Nodular Melanoma versus Superficial Spreading Melanoma: A Nation-Wide Study of the Dutch Melanoma Treatment Registry. *Cancers*. 2022;14(22):5694.
102. Wang Y, Wang Y, Ci X, et al. Molecular events in neuroendocrine prostate cancer development. *Nature Reviews Urology*. 2021;18(10):581-596.
103. Huang G, Zhang H, Shi H, et al. Clinicopathological and immunological profiles of prostate adenocarcinoma and neuroendocrine prostate cancer. *World Journal of Surgical Oncology*. 2022;20(1):1-9.
104. Bader DA, McGuire SE. Tumour metabolism and its unique properties in prostate adenocarcinoma. *Nature Reviews Urology*. 2020;17(4):214-231.
105. Zhao X, Lei Y, Li G, et al. Integrative analysis of cancer driver genes in prostate adenocarcinoma. *Molecular medicine reports*. 2019;19(4):2707-2715.
106. Klee EW, Bondar OP, Goodmanson MK, et al. Candidate Serum Biomarkers for Prostate Adenocarcinoma Identified by mRNA Differences in Prostate Tissue and Verified with Protein Measurements in Tissue and Blood. *Clinical Chemistry*. 2012;58(3):599-609. doi:10.1373/clinchem.2011.171637
107. Saleem M, Adhami VM, Zhong W, et al. A novel biomarker for staging human prostate adenocarcinoma: overexpression of matriptase with concomitant loss of its inhibitor, hepatocyte growth factor activator inhibitor-1. *Cancer Epidemiology Biomarkers & Prevention*. 2006;15(2):217-227.
108. Park JY. Promoter hypermethylation as a biomarker in prostate adenocarcinoma. *Cancer Epigenetics: risk Assessment, Diagnosis, Treatment, and Prognosis*. 2015:607-625.
109. Zhang T, Wang Y, Dong Y, et al. Identification of novel diagnostic biomarkers in prostate adenocarcinoma based on the stromal-immune score and analysis of the WGCNA and ceRNA network. *Disease Markers*. 2022;2022
110. O'Reilly D, Johnson P, Buchanan PJ. Hypoxia induced cancer stem cell enrichment promotes resistance to androgen deprivation therapy in prostate cancer. *Steroids*. 2019;152:108497.
111. Konoshenko MY, Bryzgunova OE, Laktionov PP. miRNAs and androgen deprivation therapy for prostate cancer. *Biochimica et Biophysica Acta (BBA)-Reviews on Cancer*. 2021;1876(2):188625.
112. Li H, Zhang Y, Li D, et al. Androgen receptor splice variant 7 predicts shorter response in patients with metastatic hormone-sensitive prostate cancer receiving androgen deprivation therapy. *European urology*. 2021;79(6):879-886.
113. Liu T, Wang Y, Zhou R, Li H, Cheng H, Zhang J. The update of prostatic ductal adenocarcinoma. *Chin J Cancer Res*. Feb 2016;28(1):50-7. doi:10.3978/j.issn.1000-9604.2016.02.02
114. Marcq G, Foerster B, Abufaraj M, et al. Novel Classification for Upper Tract Urothelial Carcinoma to Better Risk-stratify Patients Eligible for Kidney-sparing Strategies: An International Collaborative Study. *European Urology Focus*. 2022/03/01/ 2022;8(2):491-497. doi:<https://doi.org/10.1016/j.euf.2021.03.018>
115. Hanahan D, Weinberg Robert A. Hallmarks of Cancer: The Next Generation. *Cell*. 2011/03/04/ 2011;144(5):646-674. doi:<https://doi.org/10.1016/j.cell.2011.02.013>
116. Anderson NM, Simon MC. The tumor microenvironment. *Current Biology*. 2020/08/17/ 2020;30(16):R921-R925. doi:<https://doi.org/10.1016/j.cub.2020.06.081>
117. Bejarano L, Jordão MJC, Joyce JA. Therapeutic Targeting of the Tumor Microenvironment. *Cancer Discovery*. 2021;11(4):933-959. doi:10.1158/2159-8290.Cd-20-1808
118. Kao K-C, Vilbois S, Tsai C-H, Ho P-C. Metabolic communication in the tumour-immune microenvironment. *Nature Cell Biology*. 2022;24(11):1574-1583.
119. Wang C, Sun W, Ye Y, Hu Q, Bomba HN, Gu Z. In situ activation of platelets with checkpoint inhibitors for post-surgical cancer immunotherapy. *Nature Biomedical Engineering*. 2017;1(2):0011.
120. Vonderheide RH. The immune revolution: a case for priming, not checkpoint. *Cancer cell*. 2018;33(4):563-569.

121. Dall'Olio FG, Gelsomino F, Conci N, et al. PD-L1 Expression in Circulating Tumor Cells as a Promising Prognostic Biomarker in Advanced Non-small-cell Lung Cancer Treated with Immune Checkpoint Inhibitors. *Clinical Lung Cancer*. 2021/09/01/ 2021;22(5):423-431. doi:<https://doi.org/10.1016/j.clcc.2021.03.005>
122. Dash S, Sahu AK, Srivastava A, Chowdhury R, Mukherjee S. Exploring the extensive crosstalk between the antagonistic cytokines- TGF- β and TNF- α in regulating cancer pathogenesis. *Cytokine*. 2021/02/01/ 2021;138:155348. doi:<https://doi.org/10.1016/j.cyto.2020.155348>
123. Bhat AA, Nisar S, Maacha S, et al. Cytokine-chemokine network driven metastasis in esophageal cancer; promising avenue for targeted therapy. *Molecular Cancer*. 2021/01/04 2021;20(1):2. doi:10.1186/s12943-020-01294-3
124. Mao C, Ding Y, Xu N. A Double-Edged Sword Role of Cytokines in Prostate Cancer Immunotherapy. Review. *Frontiers in Oncology*. 2021-November-16 2021;11doi:10.3389/fonc.2021.688489
125. Voron T, Marcheteau E, Pernot S, et al. Control of the immune response by pro-angiogenic factors. *Frontiers in oncology*. 2014;4:70.
126. Schoenleber SJ, Kurtz DM, Talwalkar JA, Roberts LR, Gores GJ. Prognostic role of vascular endothelial growth factor in hepatocellular carcinoma: systematic review and meta-analysis. *British Journal of Cancer*. 2009/05/01 2009;100(9):1385-1392. doi:10.1038/sj.bjc.6605017
127. Bian X, Xiao Y-T, Wu T, et al. Microvesicles and chemokines in tumor microenvironment: mediators of intercellular communications in tumor progression. *Molecular Cancer*. 2019/03/30 2019;18(1):50. doi:10.1186/s12943-019-0973-7
128. Ozga AJ, Chow MT, Luster AD. Chemokines and the immune response to cancer. *Immunity*. 2021/05/11/ 2021;54(5):859-874. doi:<https://doi.org/10.1016/j.immuni.2021.01.012>
129. Kohli K, Pillarisetty VG, Kim TS. Key chemokines direct migration of immune cells in solid tumors. *Cancer Gene Therapy*. 2022/01/01 2022;29(1):10-21. doi:10.1038/s41417-021-00303-x
130. van der Veeken J, Gonzalez AJ, Cho H, et al. Memory of Inflammation in Regulatory T Cells. *Cell*. 2016/08/11/ 2016;166(4):977-990. doi:<https://doi.org/10.1016/j.cell.2016.07.006>
131. Newton R, Priyadharshini B, Turka LA. Immunometabolism of regulatory T cells. *Nature Immunology*. 2016/06/01 2016;17(6):618-625. doi:10.1038/ni.3466
132. Li C, Jiang P, Wei S, Xu X, Wang J. Regulatory T cells in tumor microenvironment: new mechanisms, potential therapeutic strategies and future prospects. *Molecular Cancer*. 2020/07/17 2020;19(1):116. doi:10.1186/s12943-020-01234-1
133. Starska-Kowarska K. The Role of Different Immunocompetent Cell Populations in the Pathogenesis of Head and Neck Cancer—Regulatory Mechanisms of Pro- and Anti-Cancer Activity and Their Impact on Immunotherapy. *Cancers*. 2023;15(6):1642.
134. Cuadrado E, van den Biggelaar M, de Kivit S, et al. Proteomic Analyses of Human Regulatory T Cells Reveal Adaptations in Signaling Pathways that Protect Cellular Identity. *Immunity*. 2018/05/15/ 2018;48(5):1046-1059.e6. doi:<https://doi.org/10.1016/j.immuni.2018.04.008>
135. Toker A, Ohashi PS. Chapter Five - Expression of costimulatory and inhibitory receptors in FoxP3+ regulatory T cells within the tumor microenvironment: Implications for combination immunotherapy approaches. In: Tew KD, Fisher PB, eds. *Advances in Cancer Research*. Academic Press; 2019:193-261.
136. Ohue Y, Nishikawa H. Regulatory T (Treg) cells in cancer: Can Treg cells be a new therapeutic target? *Cancer science*. 2019;110(7):2080-2089.
137. González-Navajas JM, Fan DD, Yang S, et al. The impact of Tregs on the anticancer immunity and the efficacy of immune checkpoint inhibitor therapies. *Frontiers in Immunology*. 2021;12:625783.
138. Shimizu J, Yamazaki S, Sakaguchi S. Induction of tumor immunity by removing CD25+CD4+ T cells: a common basis between tumor immunity and autoimmunity. *J Immunol*. Nov 15 1999;163(10):5211-8.
139. Tanaka A, Sakaguchi S. Targeting Treg cells in cancer immunotherapy. *European Journal of Immunology*. 2019;49(8):1140-1146. doi:<https://doi.org/10.1002/eji.201847659>
140. Dyck L, Mills KHG. Immune checkpoints and their inhibition in cancer and infectious diseases. *European Journal of Immunology*. 2017;47(5):765-779. doi:<https://doi.org/10.1002/eji.201646875>
141. Tanaka H, Tanaka J, Kjaergaard J, Shu S. Depletion of CD4+ CD25+ regulatory cells augments the generation of specific immune T cells in tumor-draining lymph nodes. *J Immunother*. May-Jun 2002;25(3):207-17. doi:10.1097/00002371-200205000-00003
142. Vetsika E-K, Koukos A, Kotsakis A. Myeloid-Derived Suppressor Cells: Major Figures that Shape the Immunosuppressive and Angiogenic Network in Cancer. *Cells*. 2019;8(12):1647.

143. Mao Y, Eissler N, Blanc KL, Johnsen JI, Kogner P, Kiessling R. Targeting Suppressive Myeloid Cells Potentiates Checkpoint Inhibitors to Control Spontaneous NeuroblastomaBlock CSF-1R to Improve Checkpoint Blockade in Neuroblastoma. *Clinical Cancer Research*. 2016;22(15):3849-3859.
144. Wang W, Zuo R, Long H, et al. Advances in the Masquelet technique: Myeloid-derived suppressor cells promote angiogenesis in PMMA-induced membranes. *Acta Biomaterialia*. 2020/05/01/ 2020;108:223-236. doi:<https://doi.org/10.1016/j.actbio.2020.03.010>
145. Lee WS, Yang H, Chon HJ, Kim C. Combination of anti-angiogenic therapy and immune checkpoint blockade normalizes vascular-immune crosstalk to potentiate cancer immunity. *Experimental & Molecular Medicine*. 2020/09/01 2020;52(9):1475-1485. doi:10.1038/s12276-020-00500-y
146. Demoulin S, Herfs M, Delvenne P, Hubert P. Tumor microenvironment converts plasmacytoid dendritic cells into immunosuppressive/tolerogenic cells: insight into the molecular mechanisms. *Journal of Leukocyte Biology*. 2013;93(3):343-352. doi:<https://doi.org/10.1189/jlb.08.12397>
147. Hernández SS, Jakobsen MR, Bak RO. Plasmacytoid Dendritic Cells as a Novel Cell-Based Cancer Immunotherapy. *International Journal of Molecular Sciences*. 2022;23(19):11397.
148. Reizis B. Plasmacytoid Dendritic Cells: Development, Regulation, and Function. *Immunity*. 2019/01/15/ 2019;50(1):37-50. doi:<https://doi.org/10.1016/j.immuni.2018.12.027>
149. Han N, Li X, Wang Y, et al. Increased tumor-infiltrating plasmacytoid dendritic cells promote cancer cell proliferation and invasion via TNF- α /NF- κ B/CXCR-4 pathway in oral squamous cell carcinoma. *J Cancer*. 2021;12(10):3045-3056. doi:10.7150/jca.55580
150. Pang L, Ng KT-P, Liu J, et al. Plasmacytoid dendritic cells recruited by HIF-1 α /eADO/ADORA1 signaling induce immunosuppression in hepatocellular carcinoma. *Cancer Letters*. 2021/12/01/ 2021;522:80-92. doi:<https://doi.org/10.1016/j.canlet.2021.09.022>
151. Moseman EA, Liang X, Dawson AJ, et al. Human plasmacytoid dendritic cells activated by CpG oligodeoxynucleotides induce the generation of CD4⁺ CD25⁺ regulatory T cells. *The Journal of Immunology*. 2004;173(7):4433-4442.
152. Conrad C, Gregorio J, Wang Y-H, et al. Plasmacytoid Dendritic Cells Promote Immunosuppression in Ovarian Cancer via ICOS Costimulation of Foxp3⁺ T-Regulatory Cells. *Cancer Research*. 2012;72(20):5240-5249. doi:10.1158/0008-5472.Can-12-2271
153. Munn DH, Sharma MD, Hou D, et al. Expression of indoleamine 2, 3-dioxygenase by plasmacytoid dendritic cells in tumor-draining lymph nodes. *The Journal of clinical investigation*. 2004;114(2):280-290.
154. Chauhan D, Singh AV, Brahmandam M, et al. Functional Interaction of Plasmacytoid Dendritic Cells with Multiple Myeloma Cells: A Therapeutic Target. *Cancer Cell*. 2009/10/06/ 2009;16(4):309-323. doi:<https://doi.org/10.1016/j.ccr.2009.08.019>
155. Kalluri R. The biology and function of fibroblasts in cancer. *Nature Reviews Cancer*. 2016;16(9):582-598.
156. Su S, Chen J, Yao H, et al. CD10⁺ GPR77⁺ cancer-associated fibroblasts promote cancer formation and chemoresistance by sustaining cancer stemness. *Cell*. 2018;172(4):841-856. e16.
157. Mariathasan S, Turley SJ, Nickles D, et al. TGF β attenuates tumour response to PD-L1 blockade by contributing to exclusion of T cells. *Nature*. 2018;554(7693):544-548.
158. Feig C, Jones JO, Kraman M, et al. Targeting CXCL12 from FAP-expressing carcinoma-associated fibroblasts synergizes with anti-PD-L1 immunotherapy in pancreatic cancer. *Proceedings of the National Academy of Sciences*. 2013;110(50):20212-20217.
159. Wu SZ, Roden DL, Wang C, et al. Stromal cell diversity associated with immune evasion in human triple-negative breast cancer. *The EMBO journal*. 2020;39(19):e104063.
160. Cohen N, Shani O, Raz Y, et al. Fibroblasts drive an immunosuppressive and growth-promoting microenvironment in breast cancer via secretion of Chitinase 3-like 1. *Oncogene*. 2017;36(31):4457-4468.
161. Costa A, Kieffer Y, Scholer-Dahirel A, et al. Fibroblast heterogeneity and immunosuppressive environment in human breast cancer. *Cancer cell*. 2018;33(3):463-479. e10.
162. Mace TA, Ameen Z, Collins A, et al. Pancreatic cancer-associated stellate cells promote differentiation of myeloid-derived suppressor cells in a STAT3-dependent manner. *Cancer research*. 2013;73(10):3007-3018.
163. Kumar V, Donthireddy L, Marvel D, et al. Cancer-associated fibroblasts neutralize the anti-tumor effect of CSF1 receptor blockade by inducing PMN-MDSC infiltration of tumors. *Cancer cell*. 2017;32(5):654-668. e5.

164. Ershaid N, Sharon Y, Doron H, et al. NLRP3 inflammasome in fibroblasts links tissue damage with inflammation in breast cancer progression and metastasis. *Nature communications*. 2019;10(1):4375.
165. Fidler IJ, Wilmanns C, Staroselsky A, Radinsky R, Dong Z, Fan D. Modulation of tumor cell response to chemotherapy by the organ environment. *Cancer and Metastasis Reviews*. 1994;13:209-222.
166. Li B, Xu H, Han H, et al. Exosome-mediated transfer of lncRUNX2-AS1 from multiple myeloma cells to MSCs contributes to osteogenesis. *Oncogene*. 2018;37(41):5508-5519.
167. Lu P, Weaver VM, Werb Z. The extracellular matrix: A dynamic niche in cancer progression. *Journal of Cell Biology*. 2012;196(4):395-406. doi:10.1083/jcb.201102147
168. Binder MJ, McCoombe S, Williams ED, McCulloch DR, Ward AC. The extracellular matrix in cancer progression: Role of hyalectan proteoglycans and ADAMTS enzymes. *Cancer Letters*. 2017/01/28/2017;385:55-64. doi:<https://doi.org/10.1016/j.canlet.2016.11.001>
169. Walker C, Mojares E, Del Río Hernández A. Role of Extracellular Matrix in Development and Cancer Progression. *International Journal of Molecular Sciences*. 2018;19(10):3028.
170. Venning FA, Wullkopf L, Erler JT. Targeting ECM Disrupts Cancer Progression. Review. *Frontiers in Oncology*. 2015-October-20 2015;5doi:10.3389/fonc.2015.00224
171. Deng L, Jin K, Zhou X, et al. Blockade of integrin signaling reduces chemotherapy-induced premature senescence in collagen cultured bladder cancer cells. *Precision Clinical Medicine*. 2022;5(2)doi:10.1093/pcmedi/pbac007
172. Lampi MC, Reinhart-King CA. Targeting extracellular matrix stiffness to attenuate disease: From molecular mechanisms to clinical trials. *Science Translational Medicine*. 2018;10(422):eaa0475. doi:doi:10.1126/scitranslmed.aao0475
173. Chakravarthy A, Khan L, Bensler NP, Bose P, De Carvalho DD. TGF- β -associated extracellular matrix genes link cancer-associated fibroblasts to immune evasion and immunotherapy failure. *Nature Communications*. 2018/11/08 2018;9(1):4692. doi:10.1038/s41467-018-06654-8
174. Kim J, Hong J, Lee J, Fakhraei Lahiji S, Kim Y-H. Recent advances in tumor microenvironment-targeted nanomedicine delivery approaches to overcome limitations of immune checkpoint blockade-based immunotherapy. *Journal of Controlled Release*. 2021/04/10/ 2021;332:109-126. doi:<https://doi.org/10.1016/j.jconrel.2021.02.002>
175. Li M, Xing S, Zhang H, et al. A matrix metalloproteinase inhibitor enhances anti-cytotoxic T lymphocyte antigen-4 antibody immunotherapy in breast cancer by reprogramming the tumor microenvironment. *Oncology Reports*. 2016;35(3):1329-1339.
176. Wherry EJ, Ha SJ, Kaech SM, et al. Molecular signature of CD8⁺ T cell exhaustion during chronic viral infection. *Immunity*. Oct 2007;27(4):670-84. doi:10.1016/j.immuni.2007.09.006
177. Schietinger A, Greenberg PD. Tolerance and exhaustion: defining mechanisms of T cell dysfunction. *Trends Immunol*. Feb 2014;35(2):51-60. doi:10.1016/j.it.2013.10.001
178. Wherry EJ. T cell exhaustion. *Nat Immunol*. Jun 2011;12(6):492-9. doi:10.1038/ni.2035
179. Man K, Gabriel SS, Liao Y, et al. Transcription Factor IRF4 Promotes CD8(+) T Cell Exhaustion and Limits the Development of Memory-like T Cells during Chronic Infection. *Immunity*. Dec 19 2017;47(6):1129-1141 e5. doi:10.1016/j.immuni.2017.11.021
180. Jin X, Bauer DE, Tuttleton SE, et al. Dramatic rise in plasma viremia after CD8(+) T cell depletion in simian immunodeficiency virus-infected macaques. *J Exp Med*. Mar 15 1999;189(6):991-8. doi:10.1084/jem.189.6.991
181. Dolina JS, Van Braeckel-Budimir N, Thomas GD, Salek-Ardakani S. CD8(+) T Cell Exhaustion in Cancer. *Front Immunol*. 2021;12:715234. doi:10.3389/fimmu.2021.715234
182. Jameson SC, Masopust D. Diversity in T cell memory: an embarrassment of riches. *Immunity*. Dec 18 2009;31(6):859-71. doi:10.1016/j.immuni.2009.11.007
183. Yao C, Sun HW, Lacey NE, et al. Single-cell RNA-seq reveals TOX as a key regulator of CD8(+) T cell persistence in chronic infection. *Nat Immunol*. Jul 2019;20(7):890-901. doi:10.1038/s41590-019-0403-4
184. Khan O, Giles JR, McDonald S, et al. TOX transcriptionally and epigenetically programs CD8(+) T cell exhaustion. *Nature*. Jul 2019;571(7764):211-218. doi:10.1038/s41586-019-1325-x
185. Alfei F, Kanev K, Hofmann M, et al. TOX reinforces the phenotype and longevity of exhausted T cells in chronic viral infection. *Nature*. Jul 2019;571(7764):265-269. doi:10.1038/s41586-019-1326-9
186. Seo H, Chen J, Gonzalez-Avalos E, et al. TOX and TOX2 transcription factors cooperate with NR4A transcription factors to impose CD8(+) T cell exhaustion. *Proc Natl Acad Sci U S A*. Jun 18 2019;116(25):12410-12415. doi:10.1073/pnas.1905675116

187. Scott AC, Dündar F, Zumbo P, et al. TOX is a critical regulator of tumour-specific T cell differentiation. *Nature*. Jul 2019;571(7764):270-274. doi:10.1038/s41586-019-1324-y
188. Chen J, López-Moyado IF, Seo H, et al. NR4A transcription factors limit CAR T cell function in solid tumours. *Nature*. Mar 2019;567(7749):530-534. doi:10.1038/s41586-019-0985-x
189. Man K, Gabriel SS, Liao Y, et al. Transcription Factor IRF4 Promotes CD8(+) T Cell Exhaustion and Limits the Development of Memory-like T Cells during Chronic Infection. *Immunity*. Dec 19 2017;47(6):1129-1141.e5. doi:10.1016/j.immuni.2017.11.021
190. Liu X, Wang Y, Lu H, et al. Genome-wide analysis identifies NR4A1 as a key mediator of T cell dysfunction. *Nature*. Mar 2019;567(7749):525-529. doi:10.1038/s41586-019-0979-8
191. Zebley CC, Youngblood B. Mechanisms of T cell exhaustion guiding next-generation immunotherapy. *Trends Cancer*. Sep 2022;8(9):726-734. doi:10.1016/j.trecan.2022.04.004
192. Beltra JC, Manne S, Abdel-Hakeem MS, et al. Developmental Relationships of Four Exhausted CD8(+) T Cell Subsets Reveals Underlying Transcriptional and Epigenetic Landscape Control Mechanisms. *Immunity*. May 19 2020;52(5):825-841.e8. doi:10.1016/j.immuni.2020.04.014
193. Mellman I, Coukos G, Dranoff G. Cancer immunotherapy comes of age. *Nature*. 2011/12/01 2011;480(7378):480-489. doi:10.1038/nature10673
194. Schuster M, Nechansky A, Kircheis R. Cancer immunotherapy. *Biotechnology Journal*. 2006;1(2):138-147. doi:<https://doi.org/10.1002/biot.200500044>
195. Couzin-Frankel J. Cancer Immunotherapy. *Science*. 2013;342(6165):1432-1433. doi:10.1126/science.342.6165.1432
196. Zhang Y, Zhang Z. The history and advances in cancer immunotherapy: understanding the characteristics of tumor-infiltrating immune cells and their therapeutic implications. *Cellular & molecular immunology*. 2020;17(8):807-821.
197. Starnes CO. Coley's toxins. *Nature*. 1992;360:23-23.
198. Starnes CO. Coley's toxins in perspective. *Nature*. 1992;357:11-12.
199. Dobosz P, Dzieciatkowski T. The intriguing history of cancer immunotherapy. *Frontiers in immunology*. 2019:2965.
200. Pardoll DM. The blockade of immune checkpoints in cancer immunotherapy. *Nature Reviews Cancer*. 2012/04/01 2012;12(4):252-264. doi:10.1038/nrc3239
201. Decker WK, da Silva RF, Sanabria MH, et al. Cancer Immunotherapy: Historical Perspective of a Clinical Revolution and Emerging Preclinical Animal Models. Review. *Frontiers in Immunology*. 2017-August-02 2017;8doi:10.3389/fimmu.2017.00829
202. Abbott M, Ustoyev Y. Cancer and the Immune System: The History and Background of Immunotherapy. *Seminars in Oncology Nursing*. 2019/10/01/ 2019;35(5):150923. doi:<https://doi.org/10.1016/j.soncn.2019.08.002>
203. Berry LJ, Moeller M, Darcy PK. Adoptive immunotherapy for cancer: the next generation of gene-engineered immune cells. *Tissue Antigens*. 2009;74(4):277-289. doi:<https://doi.org/10.1111/j.1399-0039.2009.01336.x>
204. Lanitis E, Rota G, Kosti P, et al. Optimized gene engineering of murine CAR-T cells reveals the beneficial effects of IL-15 coexpression. *Journal of Experimental Medicine*. 2020;218(2)doi:10.1084/jem.20192203
205. Goebeler M-E, Bargou RC. T cell-engaging therapies — BiTEs and beyond. *Nature Reviews Clinical Oncology*. 2020/07/01 2020;17(7):418-434. doi:10.1038/s41571-020-0347-5
206. Paul Symonds R, Foweraker K. Principles of chemotherapy and radiotherapy. *Current Obstetrics & Gynaecology*. 2006/04/01/ 2006;16(2):100-106. doi:<https://doi.org/10.1016/j.curobgyn.2006.01.006>
207. Rosenberg SA, Spiess P, Lafreniere R. A New Approach to the Adoptive Immunotherapy of Cancer with Tumor-Infiltrating Lymphocytes. *Science*. 1986;233(4770):1318-1321. doi:10.1126/science.3489291
208. Rosenberg SA, Packard BS, Aebersold PM, et al. Use of tumor-infiltrating lymphocytes and interleukin-2 in the immunotherapy of patients with metastatic melanoma. *New England Journal of Medicine*. 1988;319(25):1676-1680.
209. Rosenberg SA, Yannelli JR, Yang JC, et al. Treatment of patients with metastatic melanoma with autologous tumor-infiltrating lymphocytes and interleukin 2. *JNCI: Journal of the National Cancer Institute*. 1994;86(15):1159-1166.
210. Majzner RG, Mackall CL. Clinical lessons learned from the first leg of the CAR T cell journey. *Nature Medicine*. 2019/09/01 2019;25(9):1341-1355. doi:10.1038/s41591-019-0564-6

211. Braendstrup P, Levine BL, Ruella M. The long road to the first FDA-approved gene therapy: chimeric antigen receptor T cells targeting CD19. *Cytotherapy*. 2020/02/01/ 2020;22(2):57-69. doi:<https://doi.org/10.1016/j.jcyt.2019.12.004>
212. Mullard A. FDA approves first CAR T therapy. *Nature reviews Drug discovery*. 2017;16(10):669-670.
213. Prasad V. Tisagenlecleucel — the first approved CAR-T-cell therapy: implications for payers and policy makers. *Nature Reviews Clinical Oncology*. 2018/01/01 2018;15(1):11-12. doi:10.1038/nrclinonc.2017.156
214. June CH, O'Connor RS, Kawalekar OU, Ghassemi S, Milone MC. CAR T cell immunotherapy for human cancer. *Science*. 2018;359(6382):1361-1365. doi:doi:10.1126/science.aar6711
215. Rosenberg SA, Restifo NP. Adoptive cell transfer as personalized immunotherapy for human cancer. *Science*. 2015;348(6230):62-68. doi:doi:10.1126/science.aaa4967
216. Poorebrahim M, Abazari MF, Sadeghi S, et al. Genetically modified immune cells targeting tumor antigens. *Pharmacology & Therapeutics*. 2020/10/01/ 2020;214:107603. doi:<https://doi.org/10.1016/j.pharmthera.2020.107603>
217. Arnaud M, Coukos G, Harari A. Toward next-generation TIL therapy: TILs enriched in neoepitope-specific T cells. *Clin Transl Med*. Jan 2023;13(1):e1174. doi:10.1002/ctm2.1174
218. Stevanović S, Pasetto A, Helman SR, et al. Landscape of immunogenic tumor antigens in successful immunotherapy of virally induced epithelial cancer. *Science*. 2017;356(6334):200-205.
219. Parkhurst M, Gros A, Pasetto A, et al. Isolation of T-Cell Receptors Specifically Reactive with Mutated Tumor-Associated Antigens from Tumor-Infiltrating Lymphocytes Based on CD137 Expression Isolation of Tumor-Associated Mutation-Reactive TCRs. *Clinical cancer research*. 2017;23(10):2491-2505.
220. Zhao Y, Deng J, Rao S, et al. Tumor Infiltrating Lymphocyte (TIL) Therapy for Solid Tumor Treatment: Progressions and Challenges. *Cancers*. 2022;14(17):4160.
221. Friedmann T. A brief history of gene therapy. *Nature genetics*. 1992;2(2):93-98.
222. Crowther MD, Svane IM, Met Ö. T-Cell Gene Therapy in Cancer Immunotherapy: Why It Is No Longer Just CARs on The Road. *Cells*. 2020;9(7):1588.
223. Ilyas S, Yang JC. Landscape of tumor antigens in T cell immunotherapy. *The Journal of Immunology*. 2015;195(11):5117-5122.
224. Aldrich JF, Lowe DB, Shearer MH, Winn RE, Jumper CA, Kennedy RC. Vaccines and Immunotherapeutics for the Treatment of Malignant Disease. *Clinical and Developmental Immunology*. 2010/09/26 2010;2010:697158. doi:10.1155/2010/697158
225. Durgeau A, Virk Y, Corgnac S, Mami-Chouaib F. Recent Advances in Targeting CD8 T-Cell Immunity for More Effective Cancer Immunotherapy. Review. *Frontiers in Immunology*. 2018-January-22 2018;9doi:10.3389/fimmu.2018.00014
226. Lanitis E, Dangaj D, Irving M, Coukos G. Mechanisms regulating T-cell infiltration and activity in solid tumors. *Annals of Oncology*. 2017/12/01/ 2017;28:xii18-xii32. doi:<https://doi.org/10.1093/annonc/mdx238>
227. Gumber D, Wang LD. Improving CAR-T immunotherapy: Overcoming the challenges of T cell exhaustion. *eBioMedicine*. 2022/03/01/ 2022;77:103941. doi:<https://doi.org/10.1016/j.ebiom.2022.103941>
228. Mardiana S, Solomon BJ, Darcy PK, Beavis PA. Supercharging adoptive T cell therapy to overcome solid tumor-induced immunosuppression. *Science Translational Medicine*. 2019;11(495):eaaw2293. doi:doi:10.1126/scitranslmed.aaw2293
229. Kloss CC, Lee J, Zhang A, et al. Dominant-Negative TGF- β Receptor Enhances PSMA-Targeted Human CAR T Cell Proliferation And Augments Prostate Cancer Eradication. *Molecular Therapy*. 2018/07/05/ 2018;26(7):1855-1866. doi:<https://doi.org/10.1016/j.ymthe.2018.05.003>
230. Wong NM, Wong WW. Engineering a dual small molecule gated ZAP70 switch in T cells. *ACS Synthetic Biology*. 2018;7(4):969-977.
231. Peng W, Ye Y, Rabinovich BA, et al. Transduction of Tumor-Specific T Cells with CXCR2 Chemokine Receptor Improves Migration to Tumor and Antitumor Immune Responses Enhanced Migratory Ability in CXCR2-Expressing T Cells. *Clinical Cancer Research*. 2010;16(22):5458-5468.
232. Liu G, Rui W, Zheng H, et al. CXCR2-modified CAR-T cells have enhanced trafficking ability that improves treatment of hepatocellular carcinoma. *European Journal of Immunology*. 2020;50(5):712-724.

233. Hurton LV, Singh H, Najjar AM, et al. Tethered IL-15 augments antitumor activity and promotes a stem-cell memory subset in tumor-specific T cells. *Proceedings of the National Academy of Sciences*. 2016;113(48):E7788-E7797.
234. Ho P-C, Bihuniak Jessica D, Macintyre Andrew N, et al. Phosphoenolpyruvate Is a Metabolic Checkpoint of Anti-tumor T Cell Responses. *Cell*. 2015/09/10/ 2015;162(6):1217-1228. doi:<https://doi.org/10.1016/j.cell.2015.08.012>
235. Dumauthioz N, Tschumi B, Wenes M, et al. Enforced PGC-1 α expression promotes CD8 T cell fitness, memory formation and antitumor immunity. *Cellular & Molecular Immunology*. 2021/07/01 2021;18(7):1761-1771. doi:10.1038/s41423-020-0365-3
236. Zhang Y, Kurupati R, Liu L, et al. Enhancing CD8+ T Cell Fatty Acid Catabolism within a Metabolically Challenging Tumor Microenvironment Increases the Efficacy of Melanoma Immunotherapy. *Cancer Cell*. 2017/09/11/ 2017;32(3):377-391.e9. doi:<https://doi.org/10.1016/j.ccell.2017.08.004>
237. Klampatsa A, Leibowitz MS, Sun J, Liouisia M, Arguiri E, Albelda SM. Analysis and Augmentation of the Immunologic Bystander Effects of CAR T Cell Therapy in a Syngeneic Mouse Cancer Model. *Mol Ther Oncolytics*. Sep 25 2020;18:360-371. doi:10.1016/j.omto.2020.07.005
238. Eshhar Z, Waks T, Gross G, Schindler DG. Specific activation and targeting of cytotoxic lymphocytes through chimeric single chains consisting of antibody-binding domains and the gamma or zeta subunits of the immunoglobulin and T-cell receptors. *Proc Natl Acad Sci U S A*. Jan 15 1993;90(2):720-4. doi:10.1073/pnas.90.2.720
239. Sadelain M, Rivière I, Riddell S. Therapeutic T cell engineering. *Nature*. 2017;545(7655):423-431.
240. Guedan S, Posey AD, Jr., Shaw C, et al. Enhancing CAR T cell persistence through ICOS and 4-1BB costimulation. *JCI Insight*. Jan 11 2018;3(1)doi:10.1172/jci.insight.96976
241. Tokarew N, Ogonek J, Endres S, von Bergwelt-Baildon M, Kobold S. Teaching an old dog new tricks: next-generation CAR T cells. *British Journal of Cancer*. 2019/01/01 2019;120(1):26-37. doi:10.1038/s41416-018-0325-1
242. Young RM, Engel NW, Uslu U, Wellhausen N, June CH. Next-Generation CAR T-cell Therapies. *Cancer Discovery*. 2022;12(7):1625-1633. doi:10.1158/2159-8290.Cd-21-1683
243. Roselli E, Frieling JS, Thorner K, Ramello MC, Lynch CC, Abate-Daga D. CAR-T Engineering: Optimizing Signal Transduction and Effector Mechanisms. *BioDrugs*. 2019/12/01 2019;33(6):647-659. doi:10.1007/s40259-019-00384-z
244. Reddy OL, Stroncek DF, Panch SR. Improving CAR T cell therapy by optimizing critical quality attributes. *Seminars in Hematology*. 2020/04/01/ 2020;57(2):33-38. doi:<https://doi.org/10.1053/j.seminhematol.2020.07.005>
245. Sun S, Hao H, Yang G, Zhang Y, Fu Y. Immunotherapy with CAR-Modified T Cells: Toxicities and Overcoming Strategies. *J Immunol Res*. 2018;2018:2386187. doi:10.1155/2018/2386187
246. Lanitis E, Coukos G, Irving M. All systems go: converging synthetic biology and combinatorial treatment for CAR-T cell therapy. *Current Opinion in Biotechnology*. 2020/10/01/ 2020;65:75-87. doi:<https://doi.org/10.1016/j.copbio.2020.01.009>
247. Giordano-Attianese G, Gainza P, Gray-Gaillard E, et al. A computationally designed chimeric antigen receptor provides a small-molecule safety switch for T-cell therapy. *Nature biotechnology*. 2020;38(4):426-432.
248. Grosser R, Cherkassky L, Chintala N, Adusumilli PS. Combination Immunotherapy with CAR T Cells and Checkpoint Blockade for the Treatment of Solid Tumors. *Cancer Cell*. Nov 11 2019;36(5):471-482. doi:10.1016/j.ccell.2019.09.006
249. Robbins PF, Kassim SH, Tran TL, et al. A Pilot Trial Using Lymphocytes Genetically Engineered with an NY-ESO-1-Reactive T-cell Receptor: Long-term Follow-up and Correlates with Response Adoptive Immunotherapy Targeting the NY-ESO-1 Tumor Antigen. *Clinical Cancer Research*. 2015;21(5):1019-1027.
250. Rapoport AP, Stadtmauer EA, Binder-Scholl GK, et al. NY-ESO-1-specific TCR-engineered T cells mediate sustained antigen-specific antitumor effects in myeloma. *Nat Med*. Aug 2015;21(8):914-921. doi:10.1038/nm.3910
251. Johnson LA, June CH. Driving gene-engineered T cell immunotherapy of cancer. *Cell Research*. 2017/01/01 2017;27(1):38-58. doi:10.1038/cr.2016.154
252. Nakae Y, Oka Y, Fujiki F, et al. Two distinct effector memory cell populations of WT1 (Wilms' tumor gene 1)-specific cytotoxic T lymphocytes in acute myeloid leukemia patients. *Cancer Immunol Immunother*. Jul 2015;64(7):791-804. doi:10.1007/s00262-015-1683-7

253. Liddy N, Bossi G, Adams KJ, et al. Monoclonal TCR-redirection tumor cell killing. *Nat Med*. Jun 2012;18(6):980-7. doi:10.1038/nm.2764
254. van Amerongen RA, Hagedoorn RS, Remst DF, et al. WT1-specific TCRs directed against newly identified peptides install antitumor reactivity against acute myeloid leukemia and ovarian carcinoma. *Journal for Immunotherapy of Cancer*. 2022;10(6)
255. Tran E, Robbins PF, Rosenberg SA. 'Final common pathway' of human cancer immunotherapy: targeting random somatic mutations. *Nature Immunology*. 2017/03/01 2017;18(3):255-262. doi:10.1038/ni.3682
256. Schumacher TN, Scheper W, Kvistborg P. Cancer Neoantigens. *Annual Review of Immunology*. 2019;37(1):173-200. doi:10.1146/annurev-immunol-042617-053402
257. Xie N, Shen G, Gao W, Huang Z, Huang C, Fu L. Neoantigens: promising targets for cancer therapy. *Signal Transduction and Targeted Therapy*. 2023/01/06 2023;8(1):9. doi:10.1038/s41392-022-01270-x
258. Valmori D, Fonteneau JF, Lizana CM, et al. Enhanced generation of specific tumor-reactive CTL in vitro by selected Melan-A/MART-1 immunodominant peptide analogues. *J Immunol*. Feb 15 1998;160(4):1750-8.
259. Taylor BC, Balko JM. Mechanisms of MHC-I downregulation and role in immunotherapy response. *Frontiers in immunology*. 2022;13:844866.
260. Zhou G, Levitsky H. Toward curative cancer immunotherapy: overcoming posttherapy tumor escape. *Clin Dev Immunol*. 2012;2012:124187. doi:10.1155/2012/124187
261. Stone JD, Chervin AS, Kranz DM. T-cell receptor binding affinities and kinetics: impact on T-cell activity and specificity. *Immunology*. Feb 2009;126(2):165-76. doi:10.1111/j.1365-2567.2008.03015.x
262. Johnson LA, Heemskerk B, Powell DJ, et al. Gene transfer of tumor-reactive TCR confers both high avidity and tumor reactivity to nonreactive peripheral blood mononuclear cells and tumor-infiltrating lymphocytes. *The Journal of Immunology*. 2006;177(9):6548-6559.
263. Bownds S, Tong-On P, Rosenberg SA, Parkhurst M. Induction of tumor-reactive cytotoxic T-lymphocytes using a peptide from NY-ESO-1 modified at the carboxy-terminus to enhance HLA-A2. 1 binding affinity and stability in solution. *Journal of Immunotherapy*. 2001;24(1):1-9.
264. Wooldridge L, van den Berg HA, Glick M, et al. Interaction between the CD8 coreceptor and major histocompatibility complex class I stabilizes T cell receptor-antigen complexes at the cell surface. *Journal of Biological Chemistry*. 2005;280(30):27491-27501.
265. Govers C, Sebestyén Z, Coccoris M, Willemsen RA, Debets R. T cell receptor gene therapy: strategies for optimizing transgenic TCR pairing. *Trends in Molecular Medicine*. 2010/02/01/ 2010;16(2):77-87. doi:<https://doi.org/10.1016/j.molmed.2009.12.004>
266. Arcaro A, Grégoire C, Bakker TR, et al. CD8 β endows CD8 with efficient coreceptor function by coupling T cell receptor/CD3 to raft-associated CD8/p56lck complexes. *The Journal of experimental medicine*. 2001;194(10):1485-1495.
267. Holler PD, Kranz DM. Quantitative Analysis of the Contribution of TCR/pepMHC Affinity and CD8 to T Cell Activation. *Immunity*. 2003/02/01/ 2003;18(2):255-264. doi:[https://doi.org/10.1016/S1074-7613\(03\)00019-0](https://doi.org/10.1016/S1074-7613(03)00019-0)
268. Rath JA, Bajwa G, Carreres B, et al. Single-cell transcriptomics identifies multiple pathways underlying antitumor function of TCR-and CD8 $\alpha\beta$ -engineered human CD4⁺ T cells. *Science advances*. 2020;6(27):eaaz7809.
269. Morris EC, Tsallios A, Bendle GM, Xue S-a, Stauss HJ. A critical role of T cell antigen receptor-transduced MHC class I-restricted helper T cells in tumor protection. *Proceedings of the National Academy of Sciences*. 2005;102(22):7934-7939.
270. Huang X, Wilber AC, Bao L, et al. Stable gene transfer and expression in human primary T cells by the Sleeping Beauty transposon system. *Blood*. 2006;107(2):483-491. doi:10.1182/blood-2005-05-2133
271. Hudecek M, Ivics Z. Non-viral therapeutic cell engineering with the Sleeping Beauty transposon system. *Current Opinion in Genetics & Development*. 2018/10/01/ 2018;52:100-108. doi:<https://doi.org/10.1016/j.gde.2018.06.003>
272. Rostovskaya M, Fu J, Obst M, et al. Transposon-mediated BAC transgenesis in human ES cells. *Nucleic Acids Research*. 2012;40(19):e150-e150. doi:10.1093/nar/gks643
273. Maiti SN, Huls H, Singh H, et al. Sleeping beauty system to redirect T-cell specificity for human applications. *J Immunother*. Feb 2013;36(2):112-23. doi:10.1097/CJI.0b013e3182811ce9

274. Gao Q, Dong X, Xu Q, et al. Therapeutic potential of CRISPR/Cas9 gene editing in engineered T-cell therapy. *Cancer Medicine*. 2019;8(9):4254-4264. doi:<https://doi.org/10.1002/cam4.2257>
275. Kebriaci P, Huls H, Jena B, et al. Infusing CD19-directed T cells to augment disease control in patients undergoing autologous hematopoietic stem-cell transplantation for advanced B-lymphoid malignancies. *Hum Gene Ther*. May 2012;23(5):444-50. doi:10.1089/hum.2011.167
276. Kebriaci P, Singh H, Huls MH, et al. Phase I trials using Sleeping Beauty to generate CD19-specific CAR T cells. *J Clin Invest*. Sep 1 2016;126(9):3363-76. doi:10.1172/jci86721
277. Xue X, Huang X, Nodland SE, et al. Stable gene transfer and expression in cord blood-derived CD34+ hematopoietic stem and progenitor cells by a hyperactive Sleeping Beauty transposon system. *Blood*. 2009;114(7):1319-1330. doi:10.1182/blood-2009-03-210005
278. Gaj T, Gersbach CA, Barbas CF. ZFN, TALEN, and CRISPR/Cas-based methods for genome engineering. *Trends in Biotechnology*. 2013/07/01/ 2013;31(7):397-405. doi:<https://doi.org/10.1016/j.tibtech.2013.04.004>
279. Singh N, Shi J, June CH, Ruella M. Genome-Editing Technologies in Adoptive T Cell Immunotherapy for Cancer. *Current Hematologic Malignancy Reports*. 2017/12/01 2017;12(6):522-529. doi:10.1007/s11899-017-0417-7
280. Atsavapranee ES, Billingsley MM, Mitchell MJ. Delivery technologies for T cell gene editing: Applications in cancer immunotherapy. *EBioMedicine*. 2021/05/01/ 2021;67:103354. doi:<https://doi.org/10.1016/j.ebiom.2021.103354>
281. Urnov FD, Miller JC, Lee Y-L, et al. Highly efficient endogenous human gene correction using designed zinc-finger nucleases. *Nature*. 2005/06/01 2005;435(7042):646-651. doi:10.1038/nature03556
282. Paschon DE, Lussier S, Wangzor T, et al. Diversifying the structure of zinc finger nucleases for high-precision genome editing. *Nature Communications*. 2019/03/08 2019;10(1):1133. doi:10.1038/s41467-019-08867-x
283. Ramalingam S, London V, Kandavelou K, et al. Generation and genetic engineering of human induced pluripotent stem cells using designed zinc finger nucleases. *Stem cells and development*. 2013;22(4):595-610.
284. Li H, Yang Y, Hong W, Huang M, Wu M, Zhao X. Applications of genome editing technology in the targeted therapy of human diseases: mechanisms, advances and prospects. *Signal Transduction and Targeted Therapy*. 2020/01/03 2020;5(1):1. doi:10.1038/s41392-019-0089-y
285. Hirakawa MP, Krishnakumar R, Timlin JA, Carney JP, Butler KS. Gene editing and CRISPR in the clinic: current and future perspectives. *Bioscience reports*. 2020;40(4)
286. Irving M, Lanitis E, Migliorini D, Ivics Z, Guedan S. Choosing the right tool for genetic engineering: clinical lessons from chimeric antigen receptor-T cells. *Human gene therapy*. 2021;32(19-20):1044-1058.
287. Ren J, Zhang X, Liu X, et al. A versatile system for rapid multiplex genome-edited CAR T cell generation. *Oncotarget*. Mar 7 2017;8(10):17002-17011. doi:10.18632/oncotarget.15218
288. Georgiadis C, Preece R, Nickolay L, et al. Long Terminal Repeat CRISPR-CAR-Coupled “Universal” T Cells Mediate Potent Anti-leukemic Effects. *Molecular Therapy*. 2018/05/02/ 2018;26(5):1215-1227. doi:<https://doi.org/10.1016/j.ymthe.2018.02.025>
289. Stadtmauer EA, Fraietta JA, Davis MM, et al. CRISPR-engineered T cells in patients with refractory cancer. *Science*. 2020;367(6481):eaba7365. doi:doi:10.1126/science.aba7365
290. Al-Dosari MS, Gao X. Nonviral gene delivery: principle, limitations, and recent progress. *The AAPS journal*. 2009;11:671-681.
291. Tebas P, Yang S, Boyer JD, et al. Safety and immunogenicity of INO-4800 DNA vaccine against SARS-CoV-2: A preliminary report of an open-label, Phase I clinical trial. *EClinicalMedicine*. 2021;31:100689.
292. Somiari S, Glasspool-Malone J, Drabick JJ, et al. Theory and in vivo application of electroporative gene delivery. *Molecular Therapy*. 2000;2(3):178-187.
293. Dullaers M, Breckpot K, Van Meirvenne S, et al. Side-by-Side Comparison of Lentivirally Transduced and mRNA-Electroporated Dendritic Cells: Implications for Cancer Immunotherapy Protocols. *Molecular Therapy*. 2004/10/01/ 2004;10(4):768-779. doi:<https://doi.org/10.1016/j.ymthe.2004.07.017>
294. Singh N, Liu X, Hulitt J, et al. Nature of Tumor Control by Permanently and Transiently Modified GD2 Chimeric Antigen Receptor T Cells in Xenograft Models of Neuroblastoma. *Cancer Immunology Research*. 2014;2(11):1059-1070. doi:10.1158/2326-6066.Cir-14-0051
295. Batista Napotnik T, Polajžer T, Miklavčič D. Cell death due to electroporation – A review. *Bioelectrochemistry*. 2021/10/01/ 2021;141:107871. doi:<https://doi.org/10.1016/j.bioelechem.2021.107871>

296. Lino CA, Harper JC, Carney JP, Timlin JA. Delivering CRISPR: a review of the challenges and approaches. *Drug Delivery*. 2018/01/01 2018;25(1):1234-1257. doi:10.1080/10717544.2018.1474964
297. Reichenbach P, Giordano Attianese GMP, Ouchen K, et al. A lentiviral vector for the production of T cells with an inducible transgene and a constitutively expressed tumour-targeting receptor. *Nature Biomedical Engineering*. 2023:1-18.
298. Wellhausen N, Agarwal S, Rommel PC, Gill SI, June CH. Better living through chemistry: CRISPR/Cas engineered T cells for cancer immunotherapy. *Current Opinion in Immunology*. 2022/02/01/ 2022;74:76-84. doi:<https://doi.org/10.1016/j.coi.2021.10.008>
299. Dufait I, Liechtenstein T, Lanna A, et al. Retroviral and lentiviral vectors for the induction of immunological tolerance. *Scientifica (Cairo)*. Dec 2012;2012doi:10.6064/2012/694137
300. Poletti V, Mavilio F. Designing Lentiviral Vectors for Gene Therapy of Genetic Diseases. *Viruses*. Aug 2 2021;13(8)doi:10.3390/v13081526
301. Lundstrom K. Latest development in viral vectors for gene therapy. *Trends in Biotechnology*. 2003/03/01/ 2003;21(3):117-122. doi:[https://doi.org/10.1016/S0167-7799\(02\)00042-2](https://doi.org/10.1016/S0167-7799(02)00042-2)
302. García-Guerrero E, Sierro-Martínez B, Pérez-Simón JA. Overcoming Chimeric Antigen Receptor (CAR) Modified T-Cell Therapy Limitations in Multiple Myeloma. Review. *Frontiers in Immunology*. 2020-June-05 2020;11doi:10.3389/fimmu.2020.01128
303. Zheng K, Zheng X, Yang W. The Role of Metabolic Dysfunction in T-Cell Exhaustion During Chronic Viral Infection. *Front Immunol*. 2022;13:843242. doi:10.3389/fimmu.2022.843242
304. Chen L, Chen F, Niu H, et al. Chimeric Antigen Receptor (CAR)-T Cell Immunotherapy Against Thoracic Malignancies: Challenges and Opportunities. Systematic Review. *Frontiers in Immunology*. 2022-July-14 2022;13doi:10.3389/fimmu.2022.871661
305. Roma-Rodrigues C, Rivas-García L, Baptista PV, Fernandes AR. Gene Therapy in Cancer Treatment: Why Go Nano? *Pharmaceutics*. 2020;12(3):233.
306. Bulcha JT, Wang Y, Ma H, Tai PWL, Gao G. Viral vector platforms within the gene therapy landscape. *Signal Transduction and Targeted Therapy*. 2021/02/08 2021;6(1):53. doi:10.1038/s41392-021-00487-6
307. Ghaffari S, Khalili N, Rezaei N. CRISPR/Cas9 revitalizes adoptive T-cell therapy for cancer immunotherapy. *Journal of Experimental & Clinical Cancer Research*. 2021/08/26 2021;40(1):269. doi:10.1186/s13046-021-02076-5
308. Jackson AL, Linsley PS. Recognizing and avoiding siRNA off-target effects for target identification and therapeutic application. *Nature Reviews Drug Discovery*. 2010/01/01 2010;9(1):57-67. doi:10.1038/nrd3010
309. Ligtenberg MA, Pico de Coaña Y, Shmushkovich T, et al. Self-Delivering RNAi Targeting PD-1 Improves Tumor-Specific T Cell Functionality for Adoptive Cell Therapy of Malignant Melanoma. *Mol Ther*. Jun 6 2018;26(6):1482-1493. doi:10.1016/j.ymthe.2018.04.015
310. Lam JKW, Chow MYT, Zhang Y, Leung SWS. siRNA Versus miRNA as Therapeutics for Gene Silencing. *Molecular Therapy - Nucleic Acids*. 2015/01/01/ 2015;4:e252. doi:<https://doi.org/10.1038/mtna.2015.23>
311. Pushparaj PN, Aarthi JJ, Manikandan J, Kumar SD. siRNA, miRNA, and shRNA: in vivo Applications. *Journal of Dental Research*. 2008;87(11):992-1003. doi:10.1177/154405910808701109
312. Kim DH, Rossi JJ. Strategies for silencing human disease using RNA interference. *Nature Reviews Genetics*. 2007/03/01 2007;8(3):173-184. doi:10.1038/nrg2006
313. Tavazoie SF, Alarcón C, Oskarsson T, et al. Endogenous human microRNAs that suppress breast cancer metastasis. *Nature*. Jan 10 2008;451(7175):147-52. doi:10.1038/nature06487
314. Khatrı N, Rathı MN, Baradıa D, Trehan S, Misra A. In vivo delivery aspects of miRNA, shRNA and siRNA. *Critical Reviews™ in Therapeutic Drug Carrier Systems*. 2012;29(6)
315. Samelson LE, Patel MD, Weissman AM, Harford JB, Klausner RD. Antigen activation of murine T cells induces tyrosine phosphorylation of a polypeptide associated with the T cell antigen receptor. *Cell*. Sep 26 1986;46(7):1083-90. doi:10.1016/0092-8674(86)90708-7
316. Malissen M, Minard K, Mjolsness S, et al. Mouse T cell antigen receptor: structure and organization of constant and joining gene segments encoding the beta polypeptide. *Cell*. Jul 1984;37(3):1101-10. doi:10.1016/0092-8674(84)90444-6
317. Letourneur F, Klausner RD. Activation of T Cells by a Tyrosine Kinase Activation Domain in the Cytoplasmic Tail of CD3 ε. *Science*. 1992;255(5040):79-82. doi:doi:10.1126/science.1532456

318. Krishna S, Zhong X. Role of diacylglycerol kinases in T cell development and function. *Crit Rev Immunol*. 2013;33(2):97-118. doi:10.1615/critrevimmunol.2013006696
319. Wang D, Matsumoto R, You Y, et al. CD3/CD28 costimulation-induced NF-kappaB activation is mediated by recruitment of protein kinase C-theta, Bcl10, and IkappaB kinase beta to the immunological synapse through CARMA1. *Mol Cell Biol*. Jan 2004;24(1):164-71. doi:10.1128/mcb.24.1.164-171.2003
320. Gwack Y, Feske S, Srikanth S, Hogan PG, Rao A. Signalling to transcription: store-operated Ca²⁺ entry and NFAT activation in lymphocytes. *Cell Calcium*. Aug 2007;42(2):145-56. doi:10.1016/j.ceca.2007.03.007
321. Mérida I, Arranz-Nicolás J, Rodríguez-Rodríguez C, Ávila-Flores A. Diacylglycerol kinase control of protein kinase C. *Biochem J*. Apr 18 2019;476(8):1205-1219. doi:10.1042/bcj20180620
322. Kong KF, Yokosuka T, Canonigo-Balancio AJ, Isakov N, Saito T, Altman A. A motif in the V3 domain of the kinase PKC- θ determines its localization in the immunological synapse and functions in T cells via association with CD28. *Nat Immunol*. Oct 2 2011;12(11):1105-12. doi:10.1038/ni.2120
323. Hogan PG, Chen L, Nardone J, Rao A. Transcriptional regulation by calcium, calcineurin, and NFAT. *Genes Dev*. Sep 15 2003;17(18):2205-32. doi:10.1101/gad.1102703
324. Zhong XP, Hainey EA, Olenchok BA, et al. Enhanced T cell responses due to diacylglycerol kinase zeta deficiency. *Nat Immunol*. Sep 2003;4(9):882-90. doi:10.1038/ni958
325. Acuto O, Di Bartolo V, Michel F. Tailoring T-cell receptor signals by proximal negative feedback mechanisms. *Nat Rev Immunol*. Sep 2008;8(9):699-712. doi:10.1038/nri2397
326. De Sousa Linhares A, Leitner J, Grabmeier-Pfistershammer K, Steinberger P. Not All Immune Checkpoints Are Created Equal. *Front Immunol*. 2018;9:1909. doi:10.3389/fimmu.2018.01909
327. Smith-Garvin JE, Koretzky GA, Jordan MS. T cell activation. *Annu Rev Immunol*. 2009;27:591-619. doi:10.1146/annurev.immunol.021908.132706
328. Linsley PS, Greene JL, Brady W, Bajorath J, Ledbetter JA, Peach R. Human B7-1 (CD80) and B7-2 (CD86) bind with similar avidities but distinct kinetics to CD28 and CTLA-4 receptors. *Immunity*. Dec 1994;1(9):793-801. doi:10.1016/s1074-7613(94)80021-9
329. Linsley PS, Bradshaw J, Greene J, Peach R, Bennett KL, Mittler RS. Intracellular trafficking of CTLA-4 and focal localization toward sites of TCR engagement. *Immunity*. Jun 1996;4(6):535-43. doi:10.1016/s1074-7613(00)80480-x
330. Wei SC, Duffy CR, Allison JP. Fundamental Mechanisms of Immune Checkpoint Blockade Therapy. *Cancer Discov*. Sep 2018;8(9):1069-1086. doi:10.1158/2159-8290.Cd-18-0367
331. Qureshi OS, Zheng Y, Nakamura K, et al. Trans-endocytosis of CD80 and CD86: a molecular basis for the cell-extrinsic function of CTLA-4. *Science*. Apr 29 2011;332(6029):600-3. doi:10.1126/science.1202947
332. Guntermann C, Alexander DR. CTLA-4 suppresses proximal TCR signaling in resting human CD4(+) T cells by inhibiting ZAP-70 Tyr(319) phosphorylation: a potential role for tyrosine phosphatases. *J Immunol*. May 1 2002;168(9):4420-9. doi:10.4049/jimmunol.168.9.4420
333. Patsoukis N, Wang Q, Strauss L, Boussiotis VA. Revisiting the PD-1 pathway. *Sci Adv*. Sep 2020;6(38)doi:10.1126/sciadv.abd2712
334. Pedoem A, Azoulay-Alfaguter I, Strazza M, Silverman GJ, Mor A. Programmed death-1 pathway in cancer and autoimmunity. *Clin Immunol*. Jul 2014;153(1):145-52. doi:10.1016/j.clim.2014.04.010
335. Sheppard KA, Fitz LJ, Lee JM, et al. PD-1 inhibits T-cell receptor induced phosphorylation of the ZAP70/CD3zeta signalosome and downstream signaling to PKCtheta. *FEBS Lett*. Sep 10 2004;574(1-3):37-41. doi:10.1016/j.febslet.2004.07.083
336. Gautron AS, Dominguez-Villar M, de Marcken M, Hafler DA. Enhanced suppressor function of TIM-3+ FoxP3+ regulatory T cells. *Eur J Immunol*. Sep 2014;44(9):2703-2711. doi:10.1002/eji.201344392
337. Gabrilovich DI, Nagaraj S. Myeloid-derived suppressor cells as regulators of the immune system. *Nat Rev Immunol*. Mar 2009;9(3):162-74. doi:10.1038/nri2506
338. Chauvin JM, Zarour HM. TIGIT in cancer immunotherapy. *J Immunother Cancer*. Sep 2020;8(2)doi:10.1136/jitc-2020-000957
339. McNeill L, Salmond RJ, Cooper JC, et al. The differential regulation of Lck kinase phosphorylation sites by CD45 is critical for T cell receptor signaling responses. *Immunity*. Sep 2007;27(3):425-37. doi:10.1016/j.immuni.2007.07.015

340. Hou D, Cenciarelli C, Jensen JP, Nguyen HB, Weissman AM. Activation-dependent ubiquitination of a T cell antigen receptor subunit on multiple intracellular lysines. *J Biol Chem*. May 13 1994;269(19):14244-7.
341. Cenciarelli C, Hou D, Hsu KC, et al. Activation-induced ubiquitination of the T cell antigen receptor. *Science*. Aug 7 1992;257(5071):795-7. doi:10.1126/science.1323144
342. Schwartz RH. T cell anergy. *Annu Rev Immunol*. 2003;21:305-34. doi:10.1146/annurev.immunol.21.120601.141110
343. Wherry EJ, Kurachi M. Molecular and cellular insights into T cell exhaustion. *Nat Rev Immunol*. Aug 2015;15(8):486-99. doi:10.1038/nri3862
344. Yi JS, Cox MA, Zajac AJ. T-cell exhaustion: characteristics, causes and conversion. *Immunology*. Apr 2010;129(4):474-81. doi:10.1111/j.1365-2567.2010.03255.x
345. Chou JP, Effros RB. T cell replicative senescence in human aging. *Curr Pharm Des*. 2013;19(9):1680-98. doi:10.2174/138161213805219711
346. Wongjitrat C, Sukwit S, Chuenchitra T, et al. CTLA-4 and its ligands on the surface of T- and B-lymphocyte subsets in chronic hepatitis B virus infection. *J Med Assoc Thai*. Jan 2013;96 Suppl 1:S54-9.
347. Weng NP, Akbar AN, Goronzy J. CD28(-) T cells: their role in the age-associated decline of immune function. *Trends Immunol*. Jul 2009;30(7):306-12. doi:10.1016/j.it.2009.03.013
348. Dong Y, Li X, Zhang L, et al. CD4(+) T cell exhaustion revealed by high PD-1 and LAG-3 expression and the loss of helper T cell function in chronic hepatitis B. *BMC Immunol*. Aug 7 2019;20(1):27. doi:10.1186/s12865-019-0309-9
349. Liu W, Stachura P, Xu HC, et al. Senescent Tumor CD8(+) T Cells: Mechanisms of Induction and Challenges to Immunotherapy. *Cancers (Basel)*. Sep 30 2020;12(10)doi:10.3390/cancers12102828
350. Kasakovski D, Xu L, Li Y. T cell senescence and CAR-T cell exhaustion in hematological malignancies. *J Hematol Oncol*. Jul 4 2018;11(1):91. doi:10.1186/s13045-018-0629-x
351. Palmer DC, Guittard GC, Franco Z, et al. Cish actively silences TCR signaling in CD8+ T cells to maintain tumor tolerance. *J Exp Med*. Nov 16 2015;212(12):2095-113. doi:10.1084/jem.20150304
352. Jung IY, Kim YY, Yu HS, Lee M, Kim S, Lee J. CRISPR/Cas9-Mediated Knockout of DGK Improves Antitumor Activities of Human T Cells. *Cancer Res*. Aug 15 2018;78(16):4692-4703. doi:10.1158/0008-5472.Can-18-0030
353. Kumar J, Kumar R, Kumar Singh A, et al. Deletion of Cbl-b inhibits CD8(+) T-cell exhaustion and promotes CAR T-cell function. *J Immunother Cancer*. Jan 2021;9(1)doi:10.1136/jitc-2020-001688
354. Si J, Shi X, Sun S, et al. Hematopoietic Progenitor Kinase1 (HPK1) Mediates T Cell Dysfunction and Is a Druggable Target for T Cell-Based Immunotherapies. *Cancer Cell*. Oct 12 2020;38(4):551-566.e11. doi:10.1016/j.ccell.2020.08.001
355. Whiteside TL. Immune suppression in cancer: effects on immune cells, mechanisms and future therapeutic intervention. *Semin Cancer Biol*. Feb 2006;16(1):3-15. doi:10.1016/j.semcancer.2005.07.008
356. Khalaf K, Hana D, Chou JT, Singh C, Mackiewicz A, Kaczmarek M. Aspects of the Tumor Microenvironment Involved in Immune Resistance and Drug Resistance. *Front Immunol*. 2021;12:656364. doi:10.3389/fimmu.2021.656364
357. Dyck L, Mills KHG. Immune checkpoints and their inhibition in cancer and infectious diseases. *Eur J Immunol*. May 2017;47(5):765-779. doi:10.1002/eji.201646875
358. Lorenz U. SHP-1 and SHP-2 in T cells: two phosphatases functioning at many levels. *Immunol Rev*. Mar 2009;228(1):342-59. doi:10.1111/j.1600-065X.2008.00760.x
359. Liu J, Curtin J, You D, et al. Critical role of kinase activity of hematopoietic progenitor kinase 1 in anti-tumor immune surveillance. *PLoS One*. 2019;14(3):e0212670. doi:10.1371/journal.pone.0212670
360. Shui JW, Boomer JS, Han J, et al. Hematopoietic progenitor kinase 1 negatively regulates T cell receptor signaling and T cell-mediated immune responses. *Nat Immunol*. Jan 2007;8(1):84-91. doi:10.1038/ni1416
361. Kiefer F, Tibbles LA, Anafi M, et al. HPK1, a hematopoietic protein kinase activating the SAPK/JNK pathway. *EMBO J*. Dec 16 1996;15(24):7013-25.
362. Arnold R, Patzak IM, Neuhaus B, et al. Activation of hematopoietic progenitor kinase 1 involves relocation, autophosphorylation, and transphosphorylation by protein kinase D1. *Mol Cell Biol*. Mar 2005;25(6):2364-83. doi:10.1128/MCB.25.6.2364-2383.2005
363. Ling P, Meyer CF, Redmond LP, et al. Involvement of hematopoietic progenitor kinase 1 in T cell receptor signaling. *J Biol Chem*. Jun 1 2001;276(22):18908-14. doi:10.1074/jbc.M101485200

364. Liou J, Kiefer F, Dang A, et al. HPK1 is activated by lymphocyte antigen receptors and negatively regulates AP-1. *Immunity*. Apr 2000;12(4):399-408. doi:10.1016/s1074-7613(00)80192-2
365. Hernandez S, Qing J, Thibodeau RH, et al. The Kinase Activity of Hematopoietic Progenitor Kinase 1 Is Essential for the Regulation of T Cell Function. *Cell Rep*. Oct 2 2018;25(1):80-94. doi:10.1016/j.celrep.2018.09.012
366. Di Bartolo V, Montagne B, Salek M, et al. A novel pathway down-modulating T cell activation involves HPK-1-dependent recruitment of 14-3-3 proteins on SLP-76. *J Exp Med*. Mar 19 2007;204(3):681-91. doi:10.1084/jem.20062066
367. Lasserre R, Cuche C, Blecher-Gonen R, et al. Release of serine/threonine-phosphorylated adaptors from signaling microclusters down-regulates T cell activation. *J Cell Biol*. Nov 28 2011;195(5):839-53. doi:10.1083/jcb.201103105
368. Patzak IM, Königsberger S, Suzuki A, Mak TW, Kiefer F. HPK1 competes with ADAP for SLP-76 binding and via Rap1 negatively affects T-cell adhesion. *Eur J Immunol*. Nov 2010;40(11):3220-5. doi:10.1002/eji.201040313
369. Alzabin S, Pyarajan S, Yee H, et al. Hematopoietic progenitor kinase 1 is a critical component of prostaglandin E2-mediated suppression of the anti-tumor immune response. *Cancer Immunol Immunother*. Mar 2010;59(3):419-29. doi:10.1007/s00262-009-0761-0
370. Sawadikosol S, Russo KM, Burakoff SJ. Hematopoietic progenitor kinase 1 (HPK1) negatively regulates prostaglandin E2-induced fos gene transcription. *Blood*. May 1 2003;101(9):3687-9. doi:10.1182/blood-2002-07-2316
371. Sawadikosol S, Pyarajan S, Alzabin S, Matejovic G, Burakoff SJ. Prostaglandin E2 activates HPK1 kinase activity via a PKA-dependent pathway. *J Biol Chem*. Nov 30 2007;282(48):34693-9. doi:10.1074/jbc.M707425200
372. Linney ID, Kaila N. Inhibitors of immuno-oncology target HPK1 - a patent review (2016 to 2020). *Expert Opin Ther Pat*. Oct 2021;31(10):893-910. doi:10.1080/13543776.2021.1924671
373. Brdicka T, Pavlistová D, Leo A, et al. Phosphoprotein associated with glycosphingolipid-enriched microdomains (PAG), a novel ubiquitously expressed transmembrane adaptor protein, binds the protein tyrosine kinase csk and is involved in regulation of T cell activation. *J Exp Med*. May 1 2000;191(9):1591-604. doi:10.1084/jem.191.9.1591
374. Wallis AM, Wallace EC, Hostager BS, Yi Z, Houtman JCD, Bishop GA. TRAF3 enhances TCR signaling by regulating the inhibitors Csk and PTPN22. *Sci Rep*. May 18 2017;7(1):2081. doi:10.1038/s41598-017-02280-4
375. Davidson D, Bakinowski M, Thomas ML, Horejsi V, Veillette A. Phosphorylation-dependent regulation of T-cell activation by PAG/Cbp, a lipid raft-associated transmembrane adaptor. *Mol Cell Biol*. Mar 2003;23(6):2017-28. doi:10.1128/mcb.23.6.2017-2028.2003
376. Torgersen KM, Vang T, Abrahamsen H, et al. Release from tonic inhibition of T cell activation through transient displacement of C-terminal Src kinase (Csk) from lipid rafts. *J Biol Chem*. Aug 3 2001;276(31):29313-8. doi:10.1074/jbc.C100014200
377. Wallis AM, Bishop GA. TRAF3 regulation of inhibitory signaling pathways in B and T lymphocytes by kinase and phosphatase localization. *J Leukoc Biol*. Jan 17 2018;doi:10.1002/jlb.2mir0817-339rr
378. Chow LM, Fournel M, Davidson D, Veillette A. Negative regulation of T-cell receptor signalling by tyrosine protein kinase p50csk. *Nature*. Sep 9 1993;365(6442):156-60. doi:10.1038/365156a0
379. Manz BN, Tan YX, Courtney AH, et al. Small molecule inhibition of Csk alters affinity recognition by T cells. *Elife*. Aug 24 2015;4doi:10.7554/eLife.08088
380. Tan YX, Manz BN, Freedman TS, Zhang C, Shokat KM, Weiss A. Inhibition of the kinase Csk in thymocytes reveals a requirement for actin remodeling in the initiation of full TCR signaling. *Nat Immunol*. Feb 2014;15(2):186-94. doi:10.1038/ni.2772
381. Dobenecker MW, Schmedt C, Okada M, Tarakhovsky A. The ubiquitously expressed Csk adaptor protein Cbp is dispensable for embryogenesis and T-cell development and function. *Mol Cell Biol*. Dec 2005;25(23):10533-42. doi:10.1128/mcb.25.23.10533-10542.2005
382. Xu S, Huo J, Tan JE, Lam KP. Cbp deficiency alters Csk localization in lipid rafts but does not affect T-cell development. *Mol Cell Biol*. Oct 2005;25(19):8486-95. doi:10.1128/mcb.25.19.8486-8495.2005
383. Schmedt C, Saijo K, Niidome T, Kühn R, Aizawa S, Tarakhovsky A. Csk controls antigen receptor-mediated development and selection of T-lineage cells. *Nature*. Aug 27 1998;394(6696):901-4. doi:10.1038/29802

384. Eichmann TO, Lass A. DAG tales: the multiple faces of diacylglycerol--stereochemistry, metabolism, and signaling. *Cell Mol Life Sci*. Oct 2015;72(20):3931-52. doi:10.1007/s00018-015-1982-3
385. Riese MJ, Grewal J, Das J, et al. Decreased diacylglycerol metabolism enhances ERK activation and augments CD8+ T cell functional responses. *J Biol Chem*. Feb 18 2011;286(7):5254-65. doi:10.1074/jbc.M110.171884
386. Joshi RP, Koretzky GA. Diacylglycerol kinases: regulated controllers of T cell activation, function, and development. *Int J Mol Sci*. Mar 26 2013;14(4):6649-73. doi:10.3390/ijms14046649
387. Singh BK, Kambayashi T. The Immunomodulatory Functions of Diacylglycerol Kinase ζ . *Front Cell Dev Biol*. 2016;4:96. doi:10.3389/fcell.2016.00096
388. Baldanzi G, Bettio V, Malacarne V, Graziani A. Diacylglycerol Kinases: Shaping Diacylglycerol and Phosphatidic Acid Gradients to Control Cell Polarity. *Front Cell Dev Biol*. 2016;4:140. doi:10.3389/fcell.2016.00140
389. Mérida I, Andrada E, Gharbi SI, Ávila-Flores A. Redundant and specialized roles for diacylglycerol kinases α and ζ in the control of T cell functions. *Sci Signal*. Apr 28 2015;8(374):re6. doi:10.1126/scisignal.aaa0974
390. Mérida I, Torres-Ayuso P, Ávila-Flores A, et al. Diacylglycerol kinases in cancer. *Adv Biol Regul*. Jan 2017;63:22-31. doi:10.1016/j.jbior.2016.09.005
391. Prinz PU, Mandler AN, Masouris I, Durner L, Oberneder R, Noessner E. High DGK- α and disabled MAPK pathways cause dysfunction of human tumor-infiltrating CD8+ T cells that is reversible by pharmacologic intervention. *J Immunol*. Jun 15 2012;188(12):5990-6000. doi:10.4049/jimmunol.1103028
392. Ávila-Flores A, Arranz-Nicolás J, Andrada E, Soutar D, Mérida I. Predominant contribution of DGK ζ over DGK α in the control of PKC/PDK-1-regulated functions in T cells. *Immunol Cell Biol*. Jul 2017;95(6):549-563. doi:10.1038/icb.2017.7
393. Joshi RP, Schmidt AM, Das J, et al. The ζ isoform of diacylglycerol kinase plays a predominant role in regulatory T cell development and TCR-mediated ras signaling. *Sci Signal*. Nov 26 2013;6(303):ra102. doi:10.1126/scisignal.2004373
394. Guo R, Wan CK, Carpenter JH, et al. Synergistic control of T cell development and tumor suppression by diacylglycerol kinase alpha and zeta. *Proc Natl Acad Sci U S A*. Aug 19 2008;105(33):11909-14. doi:10.1073/pnas.0711856105
395. Riese MJ, Wang LC, Moon EK, et al. Enhanced effector responses in activated CD8+ T cells deficient in diacylglycerol kinases. *Cancer Res*. Jun 15 2013;73(12):3566-77. doi:10.1158/0008-5472.Can-12-3874
396. Fischer EH, Charbonneau H, Tonks NK. Protein tyrosine phosphatases: a diverse family of intracellular and transmembrane enzymes. *Science*. Jul 26 1991;253(5018):401-6. doi:10.1126/science.1650499
397. Stanford SM, Rapini N, Bottini N. Regulation of TCR signalling by tyrosine phosphatases: from immune homeostasis to autoimmunity. *Immunology*. Sep 2012;137(1):1-19. doi:10.1111/j.1365-2567.2012.03591.x
398. Tiganis T, Bennett AM. Protein tyrosine phosphatase function: the substrate perspective. *Biochem J*. Feb 15 2007;402(1):1-15. doi:10.1042/bj20061548
399. Wiede F, Shields BJ, Chew SH, et al. T cell protein tyrosine phosphatase attenuates T cell signaling to maintain tolerance in mice. *J Clin Invest*. Dec 2011;121(12):4758-74. doi:10.1172/jci59492
400. Wiede F, Lu KH, Du X, et al. PTPN2 phosphatase deletion in T cells promotes anti-tumour immunity and CAR T-cell efficacy in solid tumours. *Embo j*. Jan 15 2020;39(2):e103637. doi:10.15252/embj.2019103637
401. Goh PK, Wiede F, Zeissig MN, et al. PTPN2 elicits cell autonomous and non-cell autonomous effects on antitumor immunity in triple-negative breast cancer. *Sci Adv*. Feb 25 2022;8(8):eabk3338. doi:10.1126/sciadv.abk3338
402. Zhao Q, Weiss A. Enhancement of lymphocyte responsiveness by a gain-of-function mutation of ZAP-70. *Mol Cell Biol*. Dec 1996;16(12):6765-74. doi:10.1128/mcb.16.12.6765
403. Binstadt BA, Billadeau DD, Jevremović D, et al. SLP-76 is a direct substrate of SHP-1 recruited to killer cell inhibitory receptors. *J Biol Chem*. Oct 16 1998;273(42):27518-23. doi:10.1074/jbc.273.42.27518
404. Brockdorff J, Williams S, Couture C, Mustelin T. Dephosphorylation of ZAP-70 and inhibition of T cell activation by activated SHP1. *Eur J Immunol*. Aug 1999;29(8):2539-50. doi:10.1002/(sici)1521-4141(199908)29:08<2539::Aid-immu2539>3.0.Co;2-m

405. Cuevas B, Lu Y, Watt S, et al. SHP-1 regulates Lck-induced phosphatidylinositol 3-kinase phosphorylation and activity. *J Biol Chem*. Sep 24 1999;274(39):27583-9. doi:10.1074/jbc.274.39.27583
406. Kon-Kozlowski M, Pani G, Pawson T, Siminovitch KA. The tyrosine phosphatase PTP1C associates with Vav, Grb2, and mSos1 in hematopoietic cells. *J Biol Chem*. Feb 16 1996;271(7):3856-62. doi:10.1074/jbc.271.7.3856
407. Plas DR, Johnson R, Pingel JT, et al. Direct regulation of ZAP-70 by SHP-1 in T cell antigen receptor signaling. *Science*. May 24 1996;272(5265):1173-6. doi:10.1126/science.272.5265.1173
408. Sozio MS, Mathis MA, Young JA, et al. PTPH1 is a predominant protein-tyrosine phosphatase capable of interacting with and dephosphorylating the T cell receptor zeta subunit. *J Biol Chem*. Feb 27 2004;279(9):7760-9. doi:10.1074/jbc.M309994200
409. Stefanová I, Hemmer B, Vergelli M, Martin R, Biddison WE, Germain RN. TCR ligand discrimination is enforced by competing ERK positive and SHP-1 negative feedback pathways. *Nat Immunol*. Mar 2003;4(3):248-54. doi:10.1038/ni895
410. Carter JD, Neel BG, Lorenz U. The tyrosine phosphatase SHP-1 influences thymocyte selection by setting TCR signaling thresholds. *Int Immunol*. Dec 1999;11(12):1999-2014. doi:10.1093/intimm/11.12.1999
411. Lorenz U, Bergemann AD, Steinberg HN, et al. Genetic analysis reveals cell type-specific regulation of receptor tyrosine kinase c-Kit by the protein tyrosine phosphatase SHP1. *J Exp Med*. Sep 1 1996;184(3):1111-26. doi:10.1084/jem.184.3.1111
412. Dempke WCM, Uciechowski P, Fenchel K, Chevassut T. Targeting SHP-1, 2 and SHIP Pathways: A Novel Strategy for Cancer Treatment? *Oncology*. 2018;95(5):257-269. doi:10.1159/000490106
413. Watson HA, Wehenkel S, Matthews J, Ager A. SHP-1: the next checkpoint target for cancer immunotherapy? *Biochemical Society Transactions*. 2016;44(2):356-362. doi:10.1042/bst20150251
414. Xiao Y, Qiao G, Tang J, et al. Protein Tyrosine Phosphatase SHP-1 Modulates T Cell Responses by Controlling Cbl-b Degradation. *J Immunol*. Nov 1 2015;195(9):4218-27. doi:10.4049/jimmunol.1501200
415. Stromnes IM, Fowler C, Casamina CC, et al. Abrogation of SRC homology region 2 domain-containing phosphatase 1 in tumor-specific T cells improves efficacy of adoptive immunotherapy by enhancing the effector function and accumulation of short-lived effector T cells in vivo. *J Immunol*. Aug 15 2012;189(4):1812-25. doi:10.4049/jimmunol.1200552
416. Sathish JG, Dolton G, Leroy FG, Matthews RJ. Loss of Src homology region 2 domain-containing protein tyrosine phosphatase-1 increases CD8+ T cell-APC conjugate formation and is associated with enhanced in vivo CTL function. *J Immunol*. Jan 1 2007;178(1):330-7. doi:10.4049/jimmunol.178.1.330
417. Fowler CC, Pao LI, Blattman JN, Greenberg PD. SHP-1 in T cells limits the production of CD8 effector cells without impacting the formation of long-lived central memory cells. *J Immunol*. Sep 15 2010;185(6):3256-67. doi:10.4049/jimmunol.1001362
418. Chemnitz JM, Parry RV, Nichols KE, June CH, Riley JL. SHP-1 and SHP-2 associate with immunoreceptor tyrosine-based switch motif of programmed death 1 upon primary human T cell stimulation, but only receptor ligation prevents T cell activation. *J Immunol*. Jul 15 2004;173(2):945-54. doi:10.4049/jimmunol.173.2.945
419. Hebeisen M, Baitsch L, Presotto D, et al. SHP-1 phosphatase activity counteracts increased T cell receptor affinity. *J Clin Invest*. Mar 2013;123(3):1044-56. doi:10.1172/jci65325
420. Snook JP, Soedel AJ, Ekiz HA, O'Connell RM, Williams MA. Inhibition of SHP-1 Expands the Repertoire of Antitumor T Cells Available to Respond to Immune Checkpoint Blockade. *Cancer Immunol Res*. Apr 2020;8(4):506-517. doi:10.1158/2326-6066.Cir-19-0690
421. Mustelin T, Taskén K. Positive and negative regulation of T-cell activation through kinases and phosphatases. *Biochem J*. Apr 1 2003;371(Pt 1):15-27. doi:10.1042/bj20021637
422. Cloutier JF, Veillette A. Association of inhibitory tyrosine protein kinase p50csk with protein tyrosine phosphatase PEP in T cells and other hemopoietic cells. *Embo j*. Sep 16 1996;15(18):4909-18.
423. Cloutier JF, Veillette A. Cooperative inhibition of T-cell antigen receptor signaling by a complex between a kinase and a phosphatase. *J Exp Med*. Jan 4 1999;189(1):111-21. doi:10.1084/jem.189.1.111
424. Gjörlöf-Wingren A, Saxena M, Williams S, Hammi D, Mustelin T. Characterization of TCR-induced receptor-proximal signaling events negatively regulated by the protein tyrosine phosphatase PEP. *Eur J Immunol*. Dec 1999;29(12):3845-54. doi:10.1002/(sici)1521-4141(199912)29:12<3845::Aid-immu3845>3.0.Co;2-u

425. Gauthier J, Yakoub-Agha I. Chimeric antigen-receptor T-cell therapy for hematological malignancies and solid tumors: Clinical data to date, current limitations and perspectives. *Curr Res Transl Med*. Sep 2017;65(3):93-102. doi:10.1016/j.retram.2017.08.003
426. Alcázar I, Cortés I, Zaballos A, et al. p85beta phosphoinositide 3-kinase regulates CD28 coreceptor function. *Blood*. Apr 2 2009;113(14):3198-208. doi:10.1182/blood-2008-04-152942
427. Chung SA, Criswell LA. PTPN22: its role in SLE and autoimmunity. *Autoimmunity*. Dec 2007;40(8):582-90. doi:10.1080/08916930701510848
428. Bottini N, Musumeci L, Alonso A, et al. A functional variant of lymphoid tyrosine phosphatase is associated with type I diabetes. *Nat Genet*. Apr 2004;36(4):337-8. doi:10.1038/ng1323
429. Gregersen PK, Lee HS, Batliwalla F, Begovich AB. PTPN22: setting thresholds for autoimmunity. *Semin Immunol*. Aug 2006;18(4):214-23. doi:10.1016/j.smim.2006.03.009
430. Zheng J, Ibrahim S, Petersen F, Yu X. Meta-analysis reveals an association of PTPN22 C1858T with autoimmune diseases, which depends on the localization of the affected tissue. *Genes Immun*. Dec 2012;13(8):641-52. doi:10.1038/gene.2012.46
431. Zheng J, Petersen F, Yu X. The role of PTPN22 in autoimmunity: learning from mice. *Autoimmun Rev*. Mar 2014;13(3):266-71. doi:10.1016/j.autrev.2013.10.011
432. Brownlie RJ, Garcia C, Ravasz M, Zehn D, Salmond RJ, Zamoyska R. Resistance to TGF β suppression and improved anti-tumor responses in CD8(+) T cells lacking PTPN22. *Nat Commun*. Nov 7 2017;8(1):1343. doi:10.1038/s41467-017-01427-1
433. Brownlie RJ, Zamoyska R, Salmond RJ. Regulation of autoimmune and anti-tumour T-cell responses by PTPN22. *Immunology*. Jul 2018;154(3):377-382. doi:10.1111/imm.12919
434. Brownlie RJ, Wright D, Zamoyska R, Salmond RJ. Deletion of PTPN22 improves effector and memory CD8+ T cell responses to tumors. *JCI Insight*. Jul 23 2019;5(16)doi:10.1172/jci.insight.127847
435. Li K, Hou X, Li R, et al. Identification and structure-function analyses of an allosteric inhibitor of the tyrosine phosphatase PTPN22. *J Biol Chem*. May 24 2019;294(21):8653-8663. doi:10.1074/jbc.RA118.007129
436. Vang T, Liu WH, Delacroix L, et al. LYP inhibits T-cell activation when dissociated from CSK. *Nat Chem Biol*. Mar 18 2012;8(5):437-46. doi:10.1038/nchembio.916
437. Wu S, Bottini M, Rickert RC, Mustelin T, Tautz L. In silico screening for PTPN22 inhibitors: active hits from an inactive phosphatase conformation. *ChemMedChem*. Mar 2009;4(3):440-4. doi:10.1002/cmcd.200800375
438. Yu X, Sun JP, He Y, et al. Structure, inhibitor, and regulatory mechanism of Lyp, a lymphoid-specific tyrosine phosphatase implicated in autoimmune diseases. *Proc Natl Acad Sci U S A*. Dec 11 2007;104(50):19767-72. doi:10.1073/pnas.0706233104
439. Yang Q, Co D, Sommercorn J, Tonks NK. Cloning and expression of PTP-PEST. A novel, human, nontransmembrane protein tyrosine phosphatase. *J Biol Chem*. Aug 15 1993;268(23):17650.
440. Davidson D, Cloutier JF, Gregorieff A, Veillette A. Inhibitory tyrosine protein kinase p50csk is associated with protein-tyrosine phosphatase PTP-PEST in hemopoietic and non-hemopoietic cells. *J Biol Chem*. Sep 12 1997;272(37):23455-62. doi:10.1074/jbc.272.37.23455
441. Garton AJ, Flint AJ, Tonks NK. Identification of p130(cas) as a substrate for the cytosolic protein tyrosine phosphatase PTP-PEST. *Mol Cell Biol*. Nov 1996;16(11):6408-18. doi:10.1128/mcb.16.11.6408
442. Davidson D, Shi X, Zhong MC, Rhee I, Veillette A. The phosphatase PTP-PEST promotes secondary T cell responses by dephosphorylating the protein tyrosine kinase Pyk2. *Immunity*. Aug 27 2010;33(2):167-80. doi:10.1016/j.immuni.2010.08.001
443. Côté JF, Chung PL, Théberge JF, et al. PSTPIP is a substrate of PTP-PEST and serves as a scaffold guiding PTP-PEST toward a specific dephosphorylation of WASP. *J Biol Chem*. Jan 25 2002;277(4):2973-86. doi:10.1074/jbc.M106428200
444. Lee C, Rhee I. Important roles of protein tyrosine phosphatase PTPN12 in tumor progression. *Pharmacol Res*. Jun 2019;144:73-78. doi:10.1016/j.phrs.2019.04.011
445. Bonnevier JL, Zhang R, Mueller DL. E3 ubiquitin ligases and their control of T cell autoreactivity. *Arthritis Res Ther*. 2005;7(6):233-42. doi:10.1186/ar1842
446. Petroski MD, Deshaies RJ. Function and regulation of cullin-RING ubiquitin ligases. *Nat Rev Mol Cell Biol*. Jan 2005;6(1):9-20. doi:10.1038/nrm1547
447. Johnston JA. Are SOCS suppressors, regulators, and degraders? *J Leukoc Biol*. May 2004;75(5):743-8. doi:10.1189/jlb.1003507

448. Yu CR, Mahdi RM, Ebong S, Vistica BP, Gery I, Egwuagu CE. Suppressor of cytokine signaling 3 regulates proliferation and activation of T-helper cells. *J Biol Chem.* Aug 8 2003;278(32):29752-9. doi:10.1074/jbc.M300489200
449. Choi YB, Son M, Park M, Shin J, Yun Y. SOCS-6 negatively regulates T cell activation through targeting p56lck to proteasomal degradation. *J Biol Chem.* Mar 5 2010;285(10):7271-80. doi:10.1074/jbc.M109.073726
450. Guittard G, Dios-Esponera A, Palmer DC, et al. The Cish SH2 domain is essential for PLC- γ 1 regulation in TCR stimulated CD8(+) T cells. *Sci Rep.* Mar 28 2018;8(1):5336. doi:10.1038/s41598-018-23549-2
451. Palmer DC, Webber BR, Patel Y, et al. Internal checkpoint regulates T cell neoantigen reactivity and susceptibility to PD1 blockade. *Med.* Oct 14 2022;3(10):682-704.e8. doi:10.1016/j.medj.2022.07.008
452. Delconte RB, Kolesnik TB, Dagley LF, et al. CIS is a potent checkpoint in NK cell-mediated tumor immunity. *Nature Immunology.* 2016/07/01 2016;17(7):816-824. doi:10.1038/ni.3470
453. Putz EM, Guillerey C, Kos K, et al. Targeting cytokine signaling checkpoint CIS activates NK cells to protect from tumor initiation and metastasis. *Oncoimmunology.* 2017;6(2):e1267892. doi:10.1080/2162402x.2016.1267892
454. Wang D, Huang XF, Hong B, et al. Efficacy of intracellular immune checkpoint-silenced DC vaccine. *JCI Insight.* Feb 8 2018;3(3)doi:10.1172/jci.insight.98368
455. Miah MA, Yoon C-H, Kim J, Jang J, Seong Y-R, Bae Y-S. CISH is induced during DC development and regulates DC-mediated CTL activation. *European Journal of Immunology.* 2012;42(1):58-68. doi:<https://doi.org/10.1002/eji.201141846>
456. Burton JC, Grimsey NJ. Ubiquitination as a Key Regulator of Endosomal Signaling by GPCRs. *Front Cell Dev Biol.* 2019;7:43. doi:10.3389/fcell.2019.00043
457. Kar G, Keskin O, Nussinov R, Gursoy A. Human proteome-scale structural modeling of E2-E3 interactions exploiting interface motifs. *J Proteome Res.* Feb 3 2012;11(2):1196-207. doi:10.1021/pr2009143
458. Keane MM, Ettenberg SA, Nau MM, et al. cbl-3: a new mammalian cbl family protein. *Oncogene.* Jun 3 1999;18(22):3365-75. doi:10.1038/sj.onc.1202753
459. Kim M, Tezuka T, Suziki Y, Sugano S, Hirai M, Yamamoto T. Molecular cloning and characterization of a novel cbl-family gene, cbl-c. *Gene.* Oct 18 1999;239(1):145-54. doi:10.1016/s0378-1119(99)00356-x
460. Keane MM, Rivero-Lezcano OM, Mitchell JA, Robbins KC, Lipkowitz S. Cloning and characterization of cbl-b: a SH3 binding protein with homology to the c-cbl proto-oncogene. *Oncogene.* Jun 15 1995;10(12):2367-77.
461. Paolino M, Penninger JM. Cbl-b in T-cell activation. *Semin Immunopathol.* Jun 2010;32(2):137-48. doi:10.1007/s00281-010-0197-9
462. Jafari D, Mousavi MJ, Keshavarz Shahbaz S, et al. E3 ubiquitin ligase Casitas B lineage lymphoma-b and its potential therapeutic implications for immunotherapy. *Clin Exp Immunol.* Apr 2021;204(1):14-31. doi:10.1111/cei.13560
463. Liu YC. Ubiquitin ligases and the immune response. *Annu Rev Immunol.* 2004;22:81-127. doi:10.1146/annurev.immunol.22.012703.104813
464. Thien CB, Langdon WY. c-Cbl and Cbl-b ubiquitin ligases: substrate diversity and the negative regulation of signalling responses. *Biochem J.* Oct 15 2005;391(Pt 2):153-66. doi:10.1042/bj20050892
465. Wang HY, Altman Y, Fang D, et al. Cbl promotes ubiquitination of the T cell receptor zeta through an adaptor function of Zap-70. *J Biol Chem.* Jul 13 2001;276(28):26004-11. doi:10.1074/jbc.M010738200
466. Rao N, Miyake S, Reddi AL, et al. Negative regulation of Lck by Cbl ubiquitin ligase. *Proc Natl Acad Sci U S A.* Mar 19 2002;99(6):3794-9. doi:10.1073/pnas.062055999
467. Naramura M, Kole HK, Hu RJ, Gu H. Altered thymic positive selection and intracellular signals in Cbl-deficient mice. *Proc Natl Acad Sci U S A.* Dec 22 1998;95(26):15547-52. doi:10.1073/pnas.95.26.15547
468. Hicke L. A new ticket for entry into budding vesicles-ubiquitin. *Cell.* Sep 7 2001;106(5):527-30. doi:10.1016/s0092-8674(01)00485-8
469. Liu YC, Gu H. Cbl and Cbl-b in T-cell regulation. *Trends Immunol.* Mar 2002;23(3):140-3. doi:10.1016/s1471-4906(01)02157-3
470. Balagopalan L, Barr VA, Sommers CL, et al. c-Cbl-mediated regulation of LAT-nucleated signaling complexes. *Mol Cell Biol.* Dec 2007;27(24):8622-36. doi:10.1128/mcb.00467-07
471. Lyle C, Richards S, Yasuda K, et al. c-Cbl targets PD-1 in immune cells for proteasomal degradation and modulates colorectal tumor growth. *Sci Rep.* Dec 27 2019;9(1):20257. doi:10.1038/s41598-019-56208-1

472. Gonzalez H, Hagerling C, Werb Z. Roles of the immune system in cancer: from tumor initiation to metastatic progression. *Genes Dev.* Oct 1 2018;32(19-20):1267-1284. doi:10.1101/gad.314617.118
473. Liu Q, Zhou H, Langdon WY, Zhang J. E3 ubiquitin ligase Cbl-b in innate and adaptive immunity. *Cell Cycle.* 2014;13(12):1875-84. doi:10.4161/cc.29213
474. Wiedemann A, Müller S, Favier B, et al. T-cell activation is accompanied by an ubiquitination process occurring at the immunological synapse. *Immunol Lett.* Apr 15 2005;98(1):57-61. doi:10.1016/j.imlet.2004.10.014
475. Krawczyk C, Bachmaier K, Sasaki T, et al. Cbl-b is a negative regulator of receptor clustering and raft aggregation in T cells. *Immunity.* Oct 2000;13(4):463-73. doi:10.1016/s1074-7613(00)00046-7
476. Bachmaier K, Krawczyk C, Kozieradzki I, et al. Negative regulation of lymphocyte activation and autoimmunity by the molecular adaptor Cbl-b. *Nature.* Jan 13 2000;403(6766):211-6. doi:10.1038/35003228
477. Zhang R, Zhang N, Mueller DL. Casitas B-lineage lymphoma b inhibits antigen recognition and slows cell cycle progression at late times during CD4+ T cell clonal expansion. *J Immunol.* Oct 15 2008;181(8):5331-9. doi:10.4049/jimmunol.181.8.5331
478. Fang D, Wang HY, Fang N, Altman Y, Elly C, Liu YC. Cbl-b, a RING-type E3 ubiquitin ligase, targets phosphatidylinositol 3-kinase for ubiquitination in T cells. *J Biol Chem.* Feb 16 2001;276(7):4872-8. doi:10.1074/jbc.M008901200
479. Fang D, Liu YC. Proteolysis-independent regulation of PI3K by Cbl-b-mediated ubiquitination in T cells. *Nat Immunol.* Sep 2001;2(9):870-5. doi:10.1038/ni0901-870
480. Chiang YJ, Kole HK, Brown K, et al. Cbl-b regulates the CD28 dependence of T-cell activation. *Nature.* Jan 13 2000;403(6766):216-20. doi:10.1038/35003235
481. Chiang JY, Jang IK, Hodes R, Gu H. Ablation of Cbl-b provides protection against transplanted and spontaneous tumors. *J Clin Invest.* Apr 2007;117(4):1029-36. doi:10.1172/jci29472
482. Gruber T, Hermann-Kleiter N, Hinterleitner R, et al. PKC-theta modulates the strength of T cell responses by targeting Cbl-b for ubiquitination and degradation. *Sci Signal.* Jun 23 2009;2(76):ra30. doi:10.1126/scisignal.2000046
483. Zhang J, Bárdos T, Li D, et al. Cutting edge: regulation of T cell activation threshold by CD28 costimulation through targeting Cbl-b for ubiquitination. *J Immunol.* Sep 1 2002;169(5):2236-40. doi:10.4049/jimmunol.169.5.2236
484. Yang B, Gay DL, MacLeod MK, et al. Nedd4 augments the adaptive immune response by promoting ubiquitin-mediated degradation of Cbl-b in activated T cells. *Nat Immunol.* Dec 2008;9(12):1356-63. doi:10.1038/ni.1670
485. Li D, Gál I, Vermes C, et al. Cutting edge: Cbl-b: one of the key molecules tuning CD28- and CTLA-4-mediated T cell costimulation. *J Immunol.* Dec 15 2004;173(12):7135-9. doi:10.4049/jimmunol.173.12.7135
486. Guo H, Qiao G, Ying H, et al. E3 ubiquitin ligase Cbl-b regulates Pten via Nedd4 in T cells independently of its ubiquitin ligase activity. *Cell Rep.* May 31 2012;1(5):472-82. doi:10.1016/j.celrep.2012.04.008
487. Venuprasad K, Huang H, Harada Y, et al. The E3 ubiquitin ligase Itch regulates expression of transcription factor Foxp3 and airway inflammation by enhancing the function of transcription factor TIEG1. *Nat Immunol.* Mar 2008;9(3):245-53. doi:10.1038/ni1564
488. Hoyne GF, Flening E, Yabas M, et al. Visualizing the role of Cbl-b in control of islet-reactive CD4 T cells and susceptibility to type 1 diabetes. *J Immunol.* Feb 15 2011;186(4):2024-32. doi:10.4049/jimmunol.1002296
489. Wohlfert EA, Gorelik L, Mittler R, Flavell RA, Clark RB. Cutting edge: deficiency in the E3 ubiquitin ligase Cbl-b results in a multifunctional defect in T cell TGF-beta sensitivity in vitro and in vivo. *J Immunol.* Feb 1 2006;176(3):1316-20. doi:10.4049/jimmunol.176.3.1316
490. Harada Y, Harada Y, Elly C, et al. Transcription factors Foxo3a and Foxo1 couple the E3 ligase Cbl-b to the induction of Foxp3 expression in induced regulatory T cells. *J Exp Med.* Jul 5 2010;207(7):1381-91. doi:10.1084/jem.20100004
491. Loeser S, Loser K, Bijker MS, et al. Spontaneous tumor rejection by cbl-b-deficient CD8+ T cells. *J Exp Med.* Apr 16 2007;204(4):879-91. doi:10.1084/jem.20061699
492. Schanz O, Cornez I, Yajnanarayana SP, et al. Tumor rejection in Cblb(-/-) mice depends on IL-9 and Th9 cells. *J Immunother Cancer.* Jul 2021;9(7)doi:10.1136/jitc-2021-002889

493. Peer S, Baier G, Gruber T. Cblb-deficient T cells are less susceptible to PD-L1-mediated inhibition. *Oncotarget*. Jun 27 2017;8(26):41841-41853. doi:10.18632/oncotarget.18360
494. Stromnes IM, Blattman JN, Tan X, Jeevanjee S, Gu H, Greenberg PD. Abrogating Cbl-b in effector CD8(+) T cells improves the efficacy of adoptive therapy of leukemia in mice. *J Clin Invest*. Oct 2010;120(10):3722-34. doi:10.1172/jci41991
495. Zhou SK, Chen WH, Shi ZD, et al. Silencing the expression of Cbl-b enhances the immune activation of T lymphocytes against RM-1 prostate cancer cells in vitro. *J Chin Med Assoc*. Dec 2014;77(12):630-6. doi:10.1016/j.jcma.2014.03.008
496. Fujiwara M, Anstadt EJ, Clark RB. Cbl-b Deficiency Mediates Resistance to Programmed Death-Ligand 1/Programmed Death-1 Regulation. *Front Immunol*. 2017;8:42. doi:10.3389/fimmu.2017.00042
497. Han S, Chung DC, St Paul M, et al. Overproduction of IL-2 by Cbl-b deficient CD4(+) T cells provides resistance against regulatory T cells. *Oncoimmunology*. 2020;9(1):1737368. doi:10.1080/2162402x.2020.1737368
498. Paolino M, Choidas A, Wallner S, et al. The E3 ligase Cbl-b and TAM receptors regulate cancer metastasis via natural killer cells. *Nature*. Mar 27 2014;507(7493):508-12. doi:10.1038/nature12998
499. Jeon MS, Atfield A, Venuprasad K, et al. Essential role of the E3 ubiquitin ligase Cbl-b in T cell anergy induction. *Immunity*. Aug 2004;21(2):167-77. doi:10.1016/j.immuni.2004.07.013
500. Gronski MA, Boulter JM, Moskophidis D, et al. TCR affinity and negative regulation limit autoimmunity. *Nat Med*. Nov 2004;10(11):1234-9. doi:10.1038/nm1114
501. Paolino M, Thien CB, Gruber T, et al. Essential role of E3 ubiquitin ligase activity in Cbl-b-regulated T cell functions. *J Immunol*. Feb 15 2011;186(4):2138-47. doi:10.4049/jimmunol.1003390
502. Hinterleitner R, Gruber T, Pfeifhofer-Obermair C, et al. Adoptive transfer of siRNA Cblb-silenced CD8+ T lymphocytes augments tumor vaccine efficacy in a B16 melanoma model. *PLoS One*. 2012;7(9):e44295. doi:10.1371/journal.pone.0044295
503. Nurieva RI, Zheng S, Jin W, et al. The E3 ubiquitin ligase GRAIL regulates T cell tolerance and regulatory T cell function by mediating T cell receptor-CD3 degradation. *Immunity*. May 28 2010;32(5):670-80. doi:10.1016/j.immuni.2010.05.002
504. Ichikawa D, Mizuno M, Yamamura T, Miyake S. GRAIL (gene related to anergy in lymphocytes) regulates cytoskeletal reorganization through ubiquitination and degradation of Arp2/3 subunit 5 and coronin 1A. *J Biol Chem*. Dec 16 2011;286(50):43465-74. doi:10.1074/jbc.M111.222711
505. Su L, Lineberry N, Huh Y, Soares L, Fathman CG. A novel E3 ubiquitin ligase substrate screen identifies Rho guanine dissociation inhibitor as a substrate of gene related to anergy in lymphocytes. *J Immunol*. Dec 1 2006;177(11):7559-66. doi:10.4049/jimmunol.177.11.7559
506. Czyzyk J, Chen HC, Bottomly K, Flavell RA. p21 Ras/impedes mitogenic signal propagation regulates cytokine production and migration in CD4 T cells. *J Biol Chem*. Aug 22 2008;283(34):23004-15. doi:10.1074/jbc.M804084200
507. Kriegl MA, Rathinam C, Flavell RA. E3 ubiquitin ligase GRAIL controls primary T cell activation and oral tolerance. *Proc Natl Acad Sci U S A*. Sep 29 2009;106(39):16770-5. doi:10.1073/pnas.0908957106
508. Grewal IS, Flavell RA. CD40 and CD154 in cell-mediated immunity. *Annu Rev Immunol*. 1998;16:111-35. doi:10.1146/annurev.immunol.16.1.111
509. Reinwald S, Wiethe C, Westendorf AM, et al. CD83 expression in CD4+ T cells modulates inflammation and autoimmunity. *J Immunol*. May 1 2008;180(9):5890-7. doi:10.4049/jimmunol.180.9.5890
510. Lineberry NB, Su LL, Lin JT, Coffey GP, Seroogy CM, Fathman CG. Cutting edge: The transmembrane E3 ligase GRAIL ubiquitinates the costimulatory molecule CD40 ligand during the induction of T cell anergy. *J Immunol*. Aug 1 2008;181(3):1622-6. doi:10.4049/jimmunol.181.3.1622
511. Lineberry N, Su L, Soares L, Fathman CG. The single subunit transmembrane E3 ligase gene related to anergy in lymphocytes (GRAIL) captures and then ubiquitinates transmembrane proteins across the cell membrane. *J Biol Chem*. Oct 17 2008;283(42):28497-505. doi:10.1074/jbc.M805092200
512. Su LL, Iwai H, Lin JT, Fathman CG. The transmembrane E3 ligase GRAIL ubiquitinates and degrades CD83 on CD4 T cells. *J Immunol*. Jul 1 2009;183(1):438-44. doi:10.4049/jimmunol.0900204
513. Haymaker C, Yang Y, Wang J, et al. Absence of Grail promotes CD8(+) T cell anti-tumour activity. *Nat Commun*. Aug 10 2017;8(1):239. doi:10.1038/s41467-017-00252-w
514. Nurieva RI, Zheng S, Jin W, et al. The E3 Ubiquitin Ligase GRAIL Regulates T Cell Tolerance and Regulatory T Cell Function by Mediating T Cell Receptor-CD3 Degradation. *Immunity*. 2010/05/28/2010;32(5):670-680. doi:<https://doi.org/10.1016/j.immuni.2010.05.002>

515. Athanasopoulos V, Barker A, Yu D, et al. The ROQUIN family of proteins localizes to stress granules via the ROQ domain and binds target mRNAs. *Febs j.* May 2010;277(9):2109-27. doi:10.1111/j.1742-4658.2010.07628.x
516. Glasmacher E, Hoefig KP, Vogel KU, et al. Roquin binds inducible costimulator mRNA and effectors of mRNA decay to induce microRNA-independent post-transcriptional repression. *Nat Immunol.* Aug 2010;11(8):725-33. doi:10.1038/ni.1902
517. Vogel KU, Edelmann SL, Jeltsch KM, et al. Roquin paralogs 1 and 2 redundantly repress the Icos and Ox40 costimulator mRNAs and control follicular helper T cell differentiation. *Immunity.* Apr 18 2013;38(4):655-68. doi:10.1016/j.immuni.2012.12.004
518. Linterman MA, Rigby RJ, Wong R, et al. Roquin differentiates the specialized functions of duplicated T cell costimulatory receptor genes CD28 and ICOS. *Immunity.* Feb 20 2009;30(2):228-41. doi:10.1016/j.immuni.2008.12.015
519. Yang M, Chen T, Li X, et al. K33-linked polyubiquitination of Zap70 by Nrdp1 controls CD8(+) T cell activation. *Nat Immunol.* Dec 2015;16(12):1253-62. doi:10.1038/ni.3258
520. Hu H, Wang H, Xiao Y, et al. Otud7b facilitates T cell activation and inflammatory responses by regulating Zap70 ubiquitination. *J Exp Med.* Mar 7 2016;213(3):399-414. doi:10.1084/jem.20151426
521. Jahan AS, Lestra M, Swee LK, et al. Usp12 stabilizes the T-cell receptor complex at the cell surface during signaling. *Proc Natl Acad Sci U S A.* Feb 9 2016;113(6):E705-14. doi:10.1073/pnas.1521763113
522. Liu WH, Kang SG, Huang Z, et al. A miR-155-Peli1-c-Rel pathway controls the generation and function of T follicular helper cells. *J Exp Med.* Aug 22 2016;213(9):1901-19. doi:10.1084/jem.20160204
523. Huang X, Hao S, Liu J, et al. The ubiquitin ligase Peli1 inhibits ICOS and thereby Tfh-mediated immunity. *Cell Mol Immunol.* Apr 2021;18(4):969-978. doi:10.1038/s41423-021-00660-5
524. Ko CJ, Zhang L, Jie Z, et al. The E3 ubiquitin ligase Peli1 regulates the metabolic actions of mTORC1 to suppress antitumor T cell responses. *Embo j.* Jan 15 2021;40(2):e104532. doi:10.15252/emboj.2020104532
525. Chang M, Jin W, Chang JH, et al. The ubiquitin ligase Peli1 negatively regulates T cell activation and prevents autoimmunity. *Nat Immunol.* Aug 28 2011;12(10):1002-9. doi:10.1038/ni.2090
526. Scharschmidt E, Wegener E, Heissmeyer V, Rao A, Krappmann D. Degradation of Bcl10 induced by T-cell activation negatively regulates NF-kappa B signaling. *Mol Cell Biol.* May 2004;24(9):3860-73. doi:10.1128/mcb.24.9.3860-3873.2004
527. Heissmeyer V, Rao A. E3 ligases in T cell anergy--turning immune responses into tolerance. *Sci STKE.* Jul 6 2004;2004(241):pe29. doi:10.1126/stke.2412004pe29
528. Guo Y, Yang L, Lei S, Tan W, Long J. NEDD4 Negatively Regulates GITR via Ubiquitination in Immune Microenvironment of Melanoma. *Oncotargets Ther.* 2019;12:10629-10637. doi:10.2147/ott.S212317
529. Fang D, Elly C, Gao B, et al. Dysregulation of T lymphocyte function in itchy mice: a role for Itch in TH2 differentiation. *Nat Immunol.* Mar 2002;3(3):281-7. doi:10.1038/ni763
530. Venuprasad K, Elly C, Gao M, et al. Convergence of Itch-induced ubiquitination with MEKK1-JNK signaling in Th2 tolerance and airway inflammation. *J Clin Invest.* Apr 2006;116(4):1117-26. doi:10.1172/jci26858
531. Gao M, Labuda T, Xia Y, et al. Jun turnover is controlled through JNK-dependent phosphorylation of the E3 ligase Itch. *Science.* Oct 8 2004;306(5694):271-5. doi:10.1126/science.1099414
532. Kathania M, Khare P, Zeng M, et al. Itch inhibits IL-17-mediated colon inflammation and tumorigenesis by ROR- γ t ubiquitination. *Nat Immunol.* Aug 2016;17(8):997-1004. doi:10.1038/ni.3488
533. Kleine-Eggebrecht N, Staufner C, Kathemann S, et al. Mutation in ITCH Gene Can Cause Syndromic Multisystem Autoimmune Disease With Acute Liver Failure. *Pediatrics.* Feb 2019;143(2)doi:10.1542/peds.2018-1554
534. Perry WL, Hustad CM, Swing DA, O'Sullivan TN, Jenkins NA, Copeland NG. The itchy locus encodes a novel ubiquitin protein ligase that is disrupted in a18H mice. *Nat Genet.* Feb 1998;18(2):143-6. doi:10.1038/ng0298-143
535. Jin HS, Park Y, Elly C, Liu YC. Itch expression by Treg cells controls Th2 inflammatory responses. *J Clin Invest.* Nov 2013;123(11):4923-34. doi:10.1172/jci69355
536. Aki D, Li H, Zhang W, et al. The E3 ligases Itch and WWP2 cooperate to limit T(H)2 differentiation by enhancing signaling through the TCR. *Nat Immunol.* Jul 2018;19(7):766-775. doi:10.1038/s41590-018-0137-8

537. Huang H, Jeon MS, Liao L, et al. K33-linked polyubiquitination of T cell receptor-zeta regulates proteolysis-independent T cell signaling. *Immunity*. Jul 23 2010;33(1):60-70. doi:10.1016/j.immuni.2010.07.002
538. Deftos ML, He YW, Ojala EW, Bevan MJ. Correlating notch signaling with thymocyte maturation. *Immunity*. Dec 1998;9(6):777-86. doi:10.1016/s1074-7613(00)80643-3
539. Liu WH, Lai MZ. Deltex regulates T-cell activation by targeted degradation of active MEKK1. *Mol Cell Biol*. Feb 2005;25(4):1367-78. doi:10.1128/mcb.25.4.1367-1378.2005
540. Hsiao HW, Liu WH, Wang CJ, et al. Deltex1 is a target of the transcription factor NFAT that promotes T cell anergy. *Immunity*. Jul 17 2009;31(1):72-83. doi:10.1016/j.immuni.2009.04.017
541. Safford M, Collins S, Lutz MA, et al. Egr-2 and Egr-3 are negative regulators of T cell activation. *Nat Immunol*. May 2005;6(5):472-80. doi:10.1038/ni1193
542. Hsu TS, Hsiao HW, Wu PJ, Liu WH, Lai MZ. Deltex1 promotes protein kinase C θ degradation and sustains Casitas B-lineage lymphoma expression. *J Immunol*. Aug 15 2014;193(4):1672-80. doi:10.4049/jimmunol.1301416
543. Zou Q, Jin J, Hu H, et al. USP15 stabilizes MDM2 to mediate cancer-cell survival and inhibit antitumor T cell responses. *Nat Immunol*. Jun 2014;15(6):562-70. doi:10.1038/ni.2885
544. Li Q, Lozano G. Molecular pathways: targeting Mdm2 and Mdm4 in cancer therapy. *Clin Cancer Res*. Jan 1 2013;19(1):34-41. doi:10.1158/1078-0432.Ccr-12-0053
545. Zhou J, Kryczek I, Li S, et al. The ubiquitin ligase MDM2 sustains STAT5 stability to control T cell-mediated antitumor immunity. *Nature Immunology*. 2021/04/01 2021;22(4):460-470. doi:10.1038/s41590-021-00888-3
546. Dan L, Liu L, Sun Y, et al. The phosphatase PAC1 acts as a T cell suppressor and attenuates host antitumor immunity. *Nat Immunol*. Mar 2020;21(3):287-297. doi:10.1038/s41590-019-0577-9
547. Düwel M, Welteke V, Oeckinghaus A, et al. A20 negatively regulates T cell receptor signaling to NF-kappaB by cleaving Malt1 ubiquitin chains. *J Immunol*. Jun 15 2009;182(12):7718-28. doi:10.4049/jimmunol.0803313
548. Harhaj EW, Dixit VM. Deubiquitinases in the regulation of NF-kB signaling. *Cell Res*. Jan 2011;21(1):22-39. doi:10.1038/cr.2010.166
549. Giordano M, Roncagalli R, Bourdely P, et al. The tumor necrosis factor alpha-induced protein 3 (TNFAIP3, A20) imposes a brake on antitumor activity of CD8 T cells. *Proc Natl Acad Sci U S A*. Jul 29 2014;111(30):11115-20. doi:10.1073/pnas.1406259111
550. Thome M, Charton JE, Pelzer C, Hailfinger S. Antigen receptor signaling to NF-kappaB via CARMA1, BCL10, and MALT1. *Cold Spring Harb Perspect Biol*. Sep 2010;2(9):a003004. doi:10.1101/cshperspect.a003004
551. Verdeil G, Schmitt-Verhulst AM. Unleashing antitumor T-cell activation without ensuing autoimmunity: the case for A20-deletion in adoptive CD8(+) T-cell therapy. *Oncoimmunology*. Oct 2014;3(10):e958951. doi:10.4161/21624011.2014.958951
552. Reiley WW, Jin W, Lee AJ, et al. Deubiquitinating enzyme CYLD negatively regulates the ubiquitin-dependent kinase Tak1 and prevents abnormal T cell responses. *J Exp Med*. Jun 11 2007;204(6):1475-85. doi:10.1084/jem.20062694
553. Shifrut E, Carnevale J, Tobin V, et al. Genome-wide CRISPR Screens in Primary Human T Cells Reveal Key Regulators of Immune Function. *Cell*. Dec 13 2018;175(7):1958-1971.e15. doi:10.1016/j.cell.2018.10.024
554. Gérard A, Favre C, Garçon F, et al. Functional interaction of RasGAP-binding proteins Dok-1 and Dok-2 with the Tec protein tyrosine kinase. *Oncogene*. Feb 26 2004;23(8):1594-8. doi:10.1038/sj.onc.1207283
555. Gérard A, Ghiotto M, Fos C, et al. Dok-4 is a novel negative regulator of T cell activation. *J Immunol*. Jun 15 2009;182(12):7681-9. doi:10.4049/jimmunol.0802203
556. Carnevale J, Shifrut E, Kale N, et al. RASA2 ablation in T cells boosts antigen sensitivity and long-term function. *Nature*. Sep 2022;609(7925):174-182. doi:10.1038/s41586-022-05126-w
557. Deshaies RJ, Joazeiro CA. RING domain E3 ubiquitin ligases. *Annu Rev Biochem*. 2009;78:399-434. doi:10.1146/annurev.biochem.78.101807.093809
558. Metzger MB, Pruneda JN, Klevit RE, Weissman AM. RING-type E3 ligases: master manipulators of E2 ubiquitin-conjugating enzymes and ubiquitination. *Biochim Biophys Acta*. Jan 2014;1843(1):47-60. doi:10.1016/j.bbamcr.2013.05.026

559. Sitaram P, Uyemura B, Malarkannan S, Riese MJ. Beyond the Cell Surface: Targeting Intracellular Negative Regulators to Enhance T cell Anti-Tumor Activity. *Int J Mol Sci*. Nov 20 2019;20(23)doi:10.3390/ijms20235821
560. Laletin V, Bernard PL, Costa da Silva C, Guittard G, Nunes JA. Negative intracellular regulators of T-cell receptor (TCR) signaling as potential antitumor immunotherapy targets. *J Immunother Cancer*. May 2023;11(5)doi:10.1136/jitc-2022-005845
561. Zhao M, Kiernan CH, Stairiker CJ, et al. Rapid in vitro generation of bona fide exhausted CD8+ T cells is accompanied by Tcf7 promoter methylation. *PLoS Pathog*. Jun 2020;16(6):e1008555. doi:10.1371/journal.ppat.1008555
562. Chmielewski M, Kopecky C, Hombach AA, Abken H. IL-12 release by engineered T cells expressing chimeric antigen receptors can effectively Muster an antigen-independent macrophage response on tumor cells that have shut down tumor antigen expression. *Cancer Res*. Sep 1 2011;71(17):5697-706. doi:10.1158/0008-5472.CAN-11-0103
563. Yeku OO, Brentjens RJ. Armored CAR T-cells: utilizing cytokines and pro-inflammatory ligands to enhance CAR T-cell anti-tumour efficacy. *Biochem Soc Trans*. Apr 15 2016;44(2):412-8. doi:10.1042/BST20150291
564. David RM, Doherty AT. Viral Vectors: The Road to Reducing Genotoxicity. *Toxicol Sci*. Feb 2017;155(2):315-325. doi:10.1093/toxsci/kfw220
565. Zimmermann K, Kuehle J, Dragon AC, et al. Design and Characterization of an "All-in-One" Lentiviral Vector System Combining Constitutive Anti-GD2 CAR Expression and Inducible Cytokines. *Cancers (Basel)*. Feb 6 2020;12(2)doi:10.3390/cancers12020375
566. Liu Y, Di S, Shi B, et al. Armored Inducible Expression of IL-12 Enhances Antitumor Activity of Glypican-3-Targeted Chimeric Antigen Receptor-Engineered T Cells in Hepatocellular Carcinoma. *J Immunol*. Jul 1 2019;203(1):198-207. doi:10.4049/jimmunol.1800033
567. Leisegang M, Engels B, Meyerhuber P, et al. Enhanced functionality of T cell receptor-redirectioned T cells is defined by the transgene cassette. *J Mol Med (Berl)*. May 2008;86(5):573-83. doi:10.1007/s00109-008-0317-3
568. de Felipe P, Martin V, Cortes ML, Ryan M, Izquierdo M. Use of the 2A sequence from foot-and-mouth disease virus in the generation of retroviral vectors for gene therapy. *Gene Ther*. Feb 1999;6(2):198-208. doi:10.1038/sj.gt.3300811
569. Mizuguchi H, Xu Z, Ishii-Watabe A, Uchida E, Hayakawa T. IRES-dependent second gene expression is significantly lower than cap-dependent first gene expression in a bicistronic vector. *Mol Ther*. Apr 2000;1(4):376-82. doi:10.1006/mthe.2000.0050
570. Irving M, Zoete V, Hebeisen M, et al. Interplay between T cell receptor binding kinetics and the level of cognate peptide presented by major histocompatibility complexes governs CD8+ T cell responsiveness. *J Biol Chem*. Jun 29 2012;287(27):23068-78. doi:10.1074/jbc.M112.357673
571. Wang B, Wang M, Zhang W, et al. Integrative analysis of pooled CRISPR genetic screens using MAGeCKFlute. *Nature Protocols*. 2019/03/01 2019;14(3):756-780. doi:10.1038/s41596-018-0113-7
572. Pelosof R, Fairchild L, Huang C-H, et al. Prediction of potent shRNAs with a sequential classification algorithm. *Nature Biotechnology*. 2017/04/01 2017;35(4):350-353. doi:10.1038/nbt.3807
573. Doench JG, Fusi N, Sullender M, et al. Optimized sgRNA design to maximize activity and minimize off-target effects of CRISPR-Cas9. *Nature Biotechnology*. 2016/02/01 2016;34(2):184-191. doi:10.1038/nbt.3437
574. Campillo-Davo D, Flumens D, Lion E. The Quest for the Best: How TCR Affinity, Avidity, and Functional Avidity Affect TCR-Engineered T-Cell Antitumor Responses. *Cells*. Jul 18 2020;9(7)doi:10.3390/cells9071720
575. Bos R, Marquardt KL, Cheung J, Sherman LA. Functional differences between low- and high-affinity CD8(+) T cells in the tumor environment. *Oncoimmunology*. Nov 1 2012;1(8):1239-1247. doi:10.4161/onci.21285
576. Tan MP, Dolton GM, Gerry AB, et al. Human leucocyte antigen class I-redirectioned anti-tumour CD4+ T cells require a higher T cell receptor binding affinity for optimal activity than CD8+ T cells. *Clinical and Experimental Immunology*. 2016;187(1):124-137. doi:10.1111/cei.12828
577. Stone J, Kranz D. Role of T Cell Receptor Affinity in the Efficacy and Specificity of Adoptive T Cell Therapies. Review. *Frontiers in Immunology*. 2013-August-21 2013;4doi:10.3389/fimmu.2013.00244

578. Knudson Karin M, Goplen Nicholas P, Cunningham Cody A, Daniels Mark A, Teixeira E. Low-Affinity T Cells Are Programmed to Maintain Normal Primary Responses but Are Impaired in Their Recall to Low-Affinity Ligands. *Cell Reports*. 2013/08/15/ 2013;4(3):554-565. doi:<https://doi.org/10.1016/j.celrep.2013.07.008>
579. Duong MN, Erdes E, Hebeisen M, Rufer N. Chronic TCR-MHC (self)-interactions limit the functional potential of TCR affinity-increased CD8 T lymphocytes. *Journal for ImmunoTherapy of Cancer*. 2019/11/05 2019;7(1):284. doi:10.1186/s40425-019-0773-z
580. Holler PD, Chlewicki LK, Kranz DM. TCRs with high affinity for foreign pMHC show self-reactivity. *Nature Immunology*. 2003/01/01 2003;4(1):55-62. doi:10.1038/ni863
581. Weber KS, Donermeyer DL, Allen PM, Kranz DM. Class II-restricted T cell receptor engineered *in vitro* for higher affinity retains peptide specificity and function. *Proceedings of the National Academy of Sciences*. 2005;102(52):19033-19038. doi:10.1073/pnas.0507554102
582. Ventura PMO, Gakovic M, Fischer BA, et al. Concomitant deletion of Ptpn6 and Ptpn11 in T cells fails to improve anticancer responses. *EMBO Rep*. Nov 7 2022;23(11):e55399. doi:10.15252/embr.202255399